Intelligent Control and Optimization for Power Frequency Balance in Multi-Generation System

THESIS

Submitted in partial fulfilment
of the requirements for the degree of

DOCTOR OF PHILOSOPHY

by

YOGESH KRISHAN BHATESHVAR

2011PHXF003P

Under the Supervision of

Dr. Hitesh Datt Mathur

BIRLA INSTITUTE OF TECHNOLOGY AND SCIENCE, PILANI

2016

BIRLA INSTITUTE OF TECHNOLOGY AND SCIENCE

PILANI -333031(RAJASTHAN) INDIA

CERTIFICATE

This is to certify that the thesis entitled **"Intelligent Control and Optimization for Power Frequency Balance in Multi-Generation System**" and submitted by **YOGESH KRISHAN BHATESHVAR** ID No **2011PHXF003P** for award of Ph.D. of the Institute embodies original work done by him under my supervision.

Date: _____ Signature: _____

Dr. H.D. Mathur

Associate Professor
BITS-Pilani, Pilani Campus

Acknowledgements

I wish to express deep sense of gratitude and sincere thanks to my thesis supervisor Dr. H.D. Mathur, Associate Professor, Department of Electrical & Electronics Engineering for his able guidance, encouragement and suggestions throughout the period of this research work. It has been a privilege for me to work under his guidance.

Gratitude is also accorded to B.I.T.S., Pilani for providing all the necessary facilities to complete the research work. Special thanks are due to Prof V. S. Rao, Vice Chancellor, Prof. A. K. Sarkar, Director-Pilani campus, Prof. S. K. Verma, Dean, Academic Research Division, and Dr. Hemant R. Jadhav, Associate Dean, Academic Research Division for giving me an opportunity to undertake research in my area of interest.

My Thanks are also due to Prof. Surekha Bhanot and Dr. Dheerendra Singh who are the members of Doctoral Advisory Committee and Doctoral Research Committee members, for their valuable suggestions and moral support, which helped me improve the quality of the manuscript.

I also express my gratitude for the kind and affectionate enquiries about the work and the encouragement given by Academic Research Division staff. A special thanks to Mr. Ravinder Yadav, Mr. Ashok Saini and Mr. Tulsiram for their support especially in the laboratory setup operation.

Special thanks are also extended to all of faculties of Department of EEE and my colleagues for their kind inspiration. I wish to offer my special thanks to friends and research colleagues Mr. V. Balaji, Mr. Vikrant Bhakar, Mr. Tridev Mishra, Mr. Narpat Sangwa, Mr. Surender Pratap, Mr. Fani Mani, Mr. Satish Mohanty, Mr. Sanjeev Jakhar, Mr. Ravi Trivedi and Mr. Nikhil Gakkhar

for their kind support and cooperation. I heartily thank my friend Dr. Ashish Sharma, Assistant Professor, VSS University of Technology Burla, Sambalpur, Odisha, for his kind cooperation.

I would like to acknowledge the love-filled and unfailing encouragement provided in the task by my wife Kiran. She has been a constant source of strength and inspiration. I can honestly say that it was only her determination and constant encouragement that ultimately made it possible for me to see this project through to the end. I am indebted to my daughter Tejasvi, who never complained about my inability to share time with her, during my period of study. Finally a very special expression of appreciation is extended to my parents, without their encouragement, patience, and understanding this endeavor would not have been possible.

Last but not the least I am thankful to everyone who was involved directly or in-directly throughout the journey of my Ph.D. research work.

Finally, I thank the Almighty for giving me the strength and patience to work through all these years.

Pilani Yogesh Krishan Bhateshvar

12.05.2015

Abstract

Electric power systems are continuously growing in size and complexity. The gap between electrical power demand and generation is also escalating day by day and often it is a challenge to meet the demand of large consumers. In interconnected power system, the load consumptions are varying abruptly and a wide fluctuation in load causes variation in the frequency and voltage of the system. These variations in frequency and voltage may hamper power balance and stability of the system. Tie-line power interchange may also vary with load variation. In this case, automatic generation control (AGC) plays a vital role as it is a centralized operation in a control area with the objectives to minimize the transient deviations in these variables (area frequency and tie-line power interchange) and to make their steady state errors zero.

A control area in a power system is defined as a system or a combination of sub systems to which a common generation control scheme is applied to meet load demand. Electrical interconnections are made between neighboring control areas as well as within a control area where later is stronger. All the generators in a control area swing in unison and each control area is characterized by a single frequency. To achieve steady state operation, each control area adjusts generation to meet its load demand and also participate in regulating the frequency.

Modern power system has been restructured to make it open for increasing competition whenever possible and profitable. This progression is termed as deregulation where generation, transmission and distribution are managed by independent companies. This has posed more challenges on AGC as distribution companies are free to purchase power from generating companies within interconnected power system. Another factor that further complicated the

AGC issue is integration of non-conventional energy sources into the control area as they do not contribute in system inertia. A two area deregulated interconnected power system has been studied in this thesis where different types of generating units are considered while modeling the system. When dealing with the AGC in power systems, unexpected external disturbances, parameter uncertainties and the model uncertainties of the power system pose serious challenges for controller design. These complexities of large interconnected power system and its multi-variable nature of operation, render the classic methods of automatic control almost redundant. Limitations and problems, which appear when classic regulators are used, may be surpassed, if intelligent control schemes are applied. This work has emphasized on two major aspects of AGC, first is mathematical modeling of interconnected deregulated two area power system with thermal and hydro generating units. The system is further enhanced by integrating wind power generating system (WPGS) and superconducting magnetic energy storage (SMES). WPGS is providing short term active power by inertial support mechanism while SMES is suppressing oscillations by providing relatively large power output in fast reaction time at the time of sudden load demand. Second aspect is on controller part where a comprehensive study is performed using optimal intelligent controllers, where firstly, an objective function is determined out of nine objective functions based on their performance index and later the optimization technique is finalized based on best fitness value and convergence rate for all objective function. The optimization techniques used are genetic algorithm (GA), ant colony optimization (ACO) and particle swarm optimization (PSO) and further six different variants of PSO have been explored in this work. PSO with *success rate variant* is finally selected for all cases as it meets the requirement to minimize the selected objective function by achieving best fitness value. On controller part, fuzzy logic controller is chosen whose performance is compared with

conventional controllers and later fuzzy controller is also optimized in different strategies by same optimization technique in which its rule base, membership function parameter, scaling and gain factor and rule's weight are optimally selected. In addition to this, controller behavior is also analyzed by varying system parameters like frequency bias constant, synchronizing constant and power system time constant to $\pm$ 30 % from their nominal values.

Hardware implementation of fuzzy logic controller is also attempted where Arduino Mega 2560 microcontroller is used as controller and dSPACE 1104 is used for interfacing in MATLAB/Simulink environment. Results obtained by hardware setup are compared with simulated controller and found aligned. This justifies the controller design suitable for system under study.

In the end of thesis, the conclusions and future scope of this research work have been discussed. The investigations reported in this thesis will lead to further research in strengthening the control schemes for AGC.

TABLE OF CONTENTS

TABLE OF CONTENTS

Page No.

TABLE OF CONTENTS

Page No.

TABLE OF CONTENTS **Page No.**

TABLE OF CONTENTS

TABLE OF CONTENTS	Page No.

LIST OF TABLES

LIST OF FIGURES

List of Abbreviations

ACE	Area control error
AGC	Automatic generation control
ANN	Artificial neural network
BES	Battery energy storage
CHIL	Controller as hardware-in-loop
CPC	Control performance criteria
DCS	Disturbance control standard
DFIG	Doubly fed induction generator
DISCO	Distribution company
DPM	DISCO participation factor
FLC	Fuzzy logic controller
FFLC	Four step optimized fuzzy logic controller
GA	Genetic algorithm
GENCO	Generation company
GRC	Generation rate constraints
IPP	Independent power producer
ISO	Independent system operator
LFC	Load Frequency control
NERC	North American electric reliability council
MF	Membership function

PI	Proportional integrator
PID	Proportional integral derivative
PSO	Particle swarm optimization
PSO I	Particle swarm optimized integral controller
PSO PID	Particle swarm optimized proportional integral derivative controller
PWM	Pulse width modulation
SMES	Superconducting magnetic storage
TRANSCO	Transmission company
TFLC	Ranges and Scaling factors optimized FLC in two steps
T2FLC	MF's parameters and scaling factors optimized FLC in 2 steps
UART	Universal asynchronous receiver/transmitter
VIU	Vertically integrated utility
VSWT	Variable speed wind turbine
WPGS	Wind power generating system
ZN	Ziegler–Nichols tuning method
ZN PI	Ziegler–Nichols tuned proportional integral controller
ZN PID	Ziegler–Nichols tuned proportional integral derivative controller

List of Symbols

i	Subscript referring to area i (i = 1, 2)
H	Per unit inertia constant
Δf_i	Incremental change in frequency
ΔP_{tie}	Incremental change in tie-line power flowing out of area
D	Load frequency constant
ΔP_g	Incremental change in power generation
ΔP_d	Incremental change in load demand
T_g	Speed governor time constant
T_t	Turbine time constant
T_r	Reheater time constant
T_w	Hydro turbine time constant
R	Speed regulation parameter
P_r	Rated area power output
K_r	Reheat coefficient
T_p	Power system time constant
M	Effective rotary inertia
a_{12}	Area size ratio coefficient
B	Frequency bias constant
δ	Area power angle
T_{12}	Synchronizing coefficient

Chapter 1

Introduction

1.1 Background

The existing power system has been under immense pressure in order to meet the increasing energy demand. Recent *Conference of Parties* in Paris deliberated on increasing more energy production using non-conventional sources of energy. It is also critical to enhance the efficiency of existing fossil fuel dependent plants as it is impossible to get fully rid of their uses. There are many promises made by different countries to reduce greenhouse gases emission. Therefore, power system engineers are required to exploit all the available sources of energy with maximum possible efficiency and integrate more power from non-conventional sources, while maintaining a balance between power system parameters to achieve delivery of quality power to consumers.

To strengthen the power system operation and control, power system structure has been deregularised. The deregulation of the industry has provided electrical energy with a new dimension where it is being considered as a commodity. The 'commodity' status given to electrical power has attracted entry of private players in the sector. The private players make the whole business challenging from the system operator's point of view, as it now starts dealing with many players which are not under its direct control. This calls for the introduction of a fair and transparent set of rules for running the power business. The market design structure plays an important role in the successful deregulation of the power industry. This competition has given impetus to bring new reforms in different sectors of the power system and has also given tremendous relief to customers. It has been observed that economic efficiency of production and

use of electricity are improved in deregulated scenario [1]. Some of the significant benefits of power industry deregulation include:

1. Generation and distribution of electric power are made free from monopoly structure
2. Reduction of electricity price due to competitive environment
3. Development of innovative technologies in different sectors of power industry

In this structural transformation of the power system, many conventional industry segments have been replaced by new entities, which hold major responsibilities. The structural segments representing different components of this new power industry structure are:

- Generation companies (GENCOs)
- Transmission companies (TRANSCOs)
- Distribution companies (DISCOs)
- Independent System operator (ISO)
- Independent power producer (IPP)

Coordination and flow diagram of all components of deregulated (restructured) power system is shown in Fig. 1.1

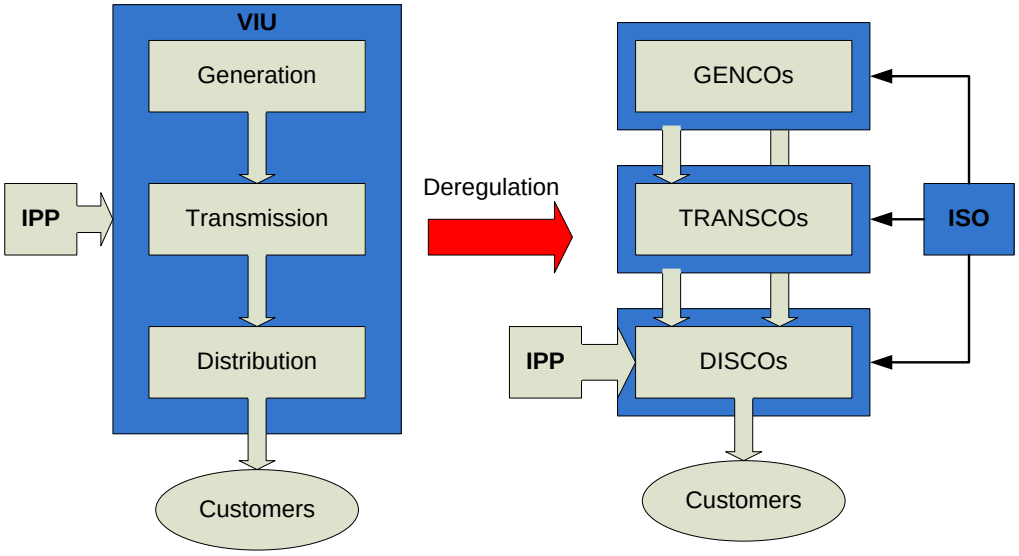

Fig. 1.1: Flow diagram of various components of deregulated power system

Deregulation of power industry has greatly increased power transfers between control areas and has changed the pattern of inter-area power transfers. In this deregulated power system, generated power from producer to the ultimate consumer is transmitted through three different utilities: GENCOs, TRANSCOs and DISCOs. Components of a deregulated power system are briefly discussed below.

GENCOs are the primary segment of deregulated power industry structure. These utilities are the producers and sellers of electrical energy. A GENCO may consist of a single generating unit or a group of generating units. TRANSCOs are the utilities which own the transmission lines and their primary duty is to transport electrical energy produced by GENCOs to DISCOs. DISCO is a distribution company which delivers electricity to the consumers after purchasing electricity through spot market or from GENCOs through direct contract. They own and operate the local distributing network.

An ISO is a central operator, responsible for the balance of the grid system by monitoring and controlling the whole power system without bias. The ISO, being an independent entity, does not participate in the electricity trading. It is mainly responsible for ensuring reliable and secure operation of power system. There are various services required to maintain the system security and reliability, such as the supply of frequency control services, control of spinning and non-spinning reserves and control of reactive power. These services are termed as "ancillary services" and all these ancillary services, including frequency control, remain under the control of ISO. The work in this thesis mainly emphasizes on frequency control ancillary service. In a competitive market, there are many transactions which take place in frequency regulation such as Poolco, bilateral and mixed transactions [2].

In Poolco based transaction, the DISCOs and GENCOs of the same area participate in the frequency regulation through the ISO. The ISO accepts bids from different GENCOs within a control area, who are willing to increase or decrease their level of production. Similarly, DISCOs also submit bids to the ISO for increasing or decreasing their level of consumption. Finally, the ISO activates the most favorable bid and GENCO participation is determined by utilizing the bids submitted by the GENCOs.

In bilateral transaction, GENCOs and DISCOs make an agreement for bilateral contracts between each other and submit their contractual agreements to ISO. In such a transaction agreement, the GENCO does not exceed production level from the contracted value. The DISCOs have to monitor its consumption continuously to ensure the loads are as per the contractual agreement but demand of local load will be fulfilled by the Poolco transaction. While in mixed or hybrid model combines various features of the previous two models. In the hybrid model, the utilization of a Poolco is not obligatory, and any customer would be allowed to

negotiate a power supply agreement directly with suppliers or choose to accept power at the spot market price. In this model, Poolco would serve all participants (buyers and sellers) who choose not to sign bilateral contracts [3], [4].

Power exchange scenario in these transactions occurs in such a way that in case of Poolco transaction, tie-line power between two control areas is settled at zero value whereas in the case of bilateral transaction, the tie-line power is not settled at zero value but is settled to a scheduled value (which is decided by the bilateral contract between GENCOs of one area and DISCOs of other areas) [5].

The probability of system blackouts can be decreased by increasing power exchange between different systems inside the large interconnected power system through expanding the interconnection between power system networks. In a large-scale power system where several control areas are interconnected, it is necessary to keep the system frequency and the inter-area tie line power as close as possible to the scheduled values. Frequency, as well as scheduled power exchange between the control areas, can be regulated by changing mechanical input power to the generators. A well designed power system should be able to cope up with system disturbances as well as changes in the load. In addition to this, it should also provide good quality of power while maintaining both voltage and frequency within tolerable limits.

The frequency of a system is dependent on active power balance. As frequency is a common factor throughout the system, a change in active power demand at one point is reflected throughout the system by a change in frequency. A speed governor on each generating unit provides the primary speed control function, while supplementary control, originates at a central control center [6]. This power frequency balance is addressed by automatic generation control (AGC). AGC in a power system needs to accomplish the critical objectives of regulating

frequency to the specified nominal value and to maintain the interchange power between control areas at the scheduled values, by adjusting the output of selected generators. Undesired frequency deviations have a direct impact on power system operation and system reliability. A large frequency deviation can damage equipment, degrade load performance, cause the transmission lines to be overloaded and can interfere with system protection schemes, ultimately leading to an unstable condition of the power system. These objectives are met by measuring a control error signal, called the area control error (ACE), which represents the real power imbalance between generation and load, and is a linear combination of net interchange of tie-line power and frequency deviation [7].

1.2 Motivation

Keeping in view the recent advances and focus on generating companies to provide clean and green power, wind power generating system (WPGS) is a feasible alternative to integrate in existing conventional interconnected power system with intention to support short-term active power when system is subjected to a sudden load perturbation. Doubly fed induction generator (DFIG) is suited most as a wind power generation system with following objectives:

- To facilitate a frequency control support function that extracts kinetic energy from DFIG to provide short term active power support
- To analyze impact of different levels of wind power penetration by DFIG with and without frequency control support function.

With the advent of smart grid technologies in the modern power system era, energy storage solutions may provide quick and active power support to strengthen smooth operation when the system is subjected to load perturbations. The energy storage systems such as redox flow batteries [8], Superconducting magnetic energy storage (SMES) [9]–[11], ultra capacitor [12],

[13] are being considered for immediate active power support. SMES, in particular, is seen as a viable option whenever demand arises. Therefore, adding additional source of clean energy i.e., SMES with an idea to provide quick support to frequency regulation ancillary service may improve frequency regulation profile significantly. Since a SMES unit with a self-commutated converter is capable of controlling both the active and reactive power simultaneously and quickly, increasing attention is being given to power system stabilization by SMES control.

The increasing numbers of major power grid blackouts that have been experienced in recent years show the requirement of a good and accurate power system controller. Therefore, it becomes essential to design a properly tuned AGC system that controls the power generation and tie-line power transfer. Researchers have emphasized on different control techniques for the secondary control part in AGC. These controllers have shown good results in terms of achieving frequency control in lesser time. Some of the techniques that have been independently tried and presented in the literature include intelligent controllers using neural network [14]–[16] and fuzzy logic [17]–[20]. Optimization of PID controller with GA, PSO, and differential evolution have also been researched [21]–[26].

Again this interconnection of the power systems results in higher order system and increased number of tuning controller parameters. As a result, while modeling such complex high-order power systems, the model and parameter approximations cannot be avoided. Therefore, there is a requirement for an intelligent AGC controller that is able to handle these system uncertainties and system variations of system parameters in reality. It has been observed that literature lacks in suggesting a composite controller i.e. an efficient optimized intelligent controller for two-area multi-generation integrated power system.

1.3 Problem description

For power frequency balance i.e., the AGC problem it is necessary that the regulation of frequency should be in minimum possible time. In interconnected power networks, with deregulated markets in two or more areas, the generation within each area has to be controlled in order to maintain scheduled power interchange. The control schemes have two main control loops for primary and secondary control. The primary control action is realized by using a turbine-governor system in the plant. In the primary control level, only active power is balanced, therefore, steady state frequency error can occur. Hence, this primary level of control is not enough for interconnected systems. In interconnected power systems, frequency must be equal in all areas. So, second level of generation control, called as secondary or supplementary control, is provided in large power systems which include two or more areas. Active power is controlled in the tie line between neighboring areas with central and local load controllers. The complexity of secondary control is increased when more sources of energy, mainly renewable sources are integrated. Emphasis is required to be given on WPGS and SMES, for providing short-term active power support, in order to balance frequency and tie-line power transfer. Conventional control strategies are insufficient to achieve this balance. Therefore, different intelligent control schemes with optimized parameters are needed to be explored.

1.4 Proposed work

In this thesis, three different two area deregulated power system models with (a) thermal and hydro units, (b) thermal, hydro and WPGS units and (c) thermal, hydro, WPGS and SMES units, are simulated with different control strategies in order to achieve faster settlement of frequency and tie-line oscillations. The design of AGC controller incorporates system parameter uncertainties, system parameters variations, load characteristics and excitation control. Fuzzy

logic based controllers have been widely accepted for different engineering and industrial applications, as they are an appropriate choice for linear, non-linear, complex or ill-defined systems. In this work, an intelligent optimized controller is designed to achieve these defined objectives of AGC. The fuzzy logic based controller, as an intelligent controller has been optimized in various design stages e.g. optimization of scaling and gain factor, membership functions, rule base and rule weight. Different dynamic parameters mainly settling time, peak overshoot and peak undershoot are considered for performance analysis. MATLAB/Simulink is used for all simulation purpose.

The control schemes used in this thesis are classified into two categories. First includes conventional controllers, where I, PI, and PID controllers are used and in second fuzzy logic controller. Both types of controllers are optimized by different optimization techniques namely ZN, GA, PSO and ACO and a comprehensive comparative analysis is carried out. Fuzzy logic controller is also optimized in different steps by PSO technique where the gain factor, scaling factor, membership function's parameters and rule base are optimized. In the last part of the thesis, controller as hardware-in-loop (CHIL) is also tested on these models. Hardware controller has been developed with Arduino Mega 2560 board and interfaced with Simulink model using dSPACE 1104 ACE board. The fuzzy logic controller is embedded into CHIL and results are compared with Simulink results.

1.4.1 Objective of the Proposed Research

1. To develop mathematical models for multi-area power system with AGC in a deregulated environment.
2. To develop mathematical models of multi-area power system with WPGS and SMES.
3. To develop optimized intelligent control schemes for faster settlement of frequency and tie-line oscillations.
4. To validate control scheme with CHIL for developed models.

The flow diagram of the proposed approach in the present work is shown in Fig. 1.2.

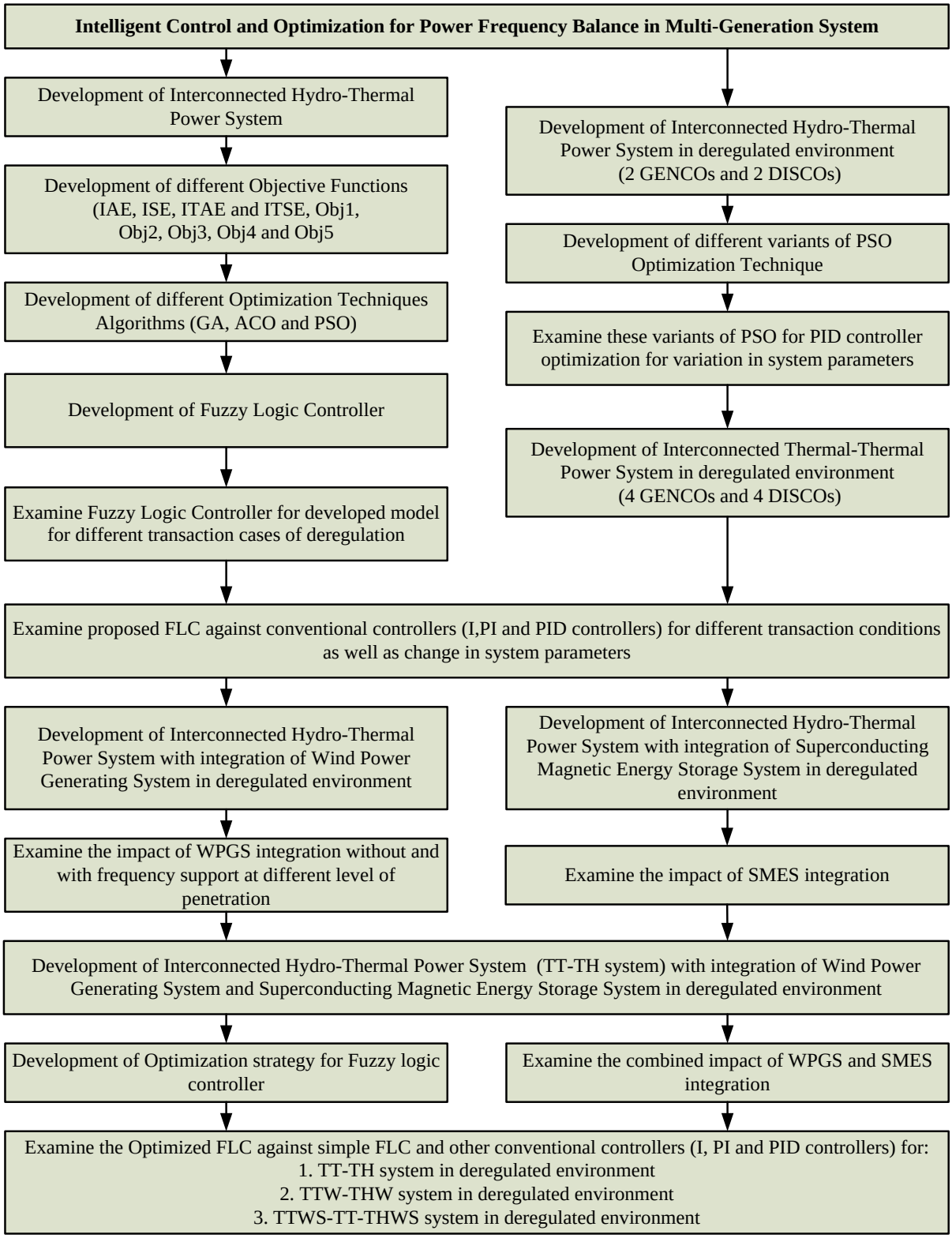

Fig.1.2: Flow diagram of proposed work

1.5 Thesis organization

The work in this thesis is divided in seven chapters as follows:

Chapter 1 deals with a brief description of the AGC problem. It also describes different system models and different proposed control techniques used in this thesis.

Chapter 2 consists of a literature review of AGC problem of power system. The different controlling techniques are classified in different categories.

Chapter 3 presents the modeling of different types of power plants for AGC problem. Linearized models of power plants are developed for thermal and hydro in a deregulated environment. These plants models are combined to get linear multi-area power system models.

Chapter 4 presents different types of control strategies and optimization methods for AGC problem. A comprehensive comparative analysis has been carried out to find best dynamic performance for all developed power system models. In this chapter, fuzzy logic controller is also designed for two area interconnected power system model in deregulated environment. Later on, same fuzzy logic controller is optimized using different strategies.

Chapter 5 presents the impact of integration of WPGS and SMES to AGC for two area power system model. The performance of optimized fuzzy logic controller is also determined for two area power system with integrated WPGS and SMES.

Chapter 6 presents the proposed control scheme with CHIL for developed models. A comparison is also carried out for simulation and CHIL results.

Chapter 7 concludes the entire work and discusses the scope of future studies.

References:

[1] Loi Lei Lai, *Power System Restructuring and Deregulation: Trading , Performance &*

Information Technology. John Wiley & Sons Ltd., 2001.

[2] P. Z. Grossman and D. H. Cole, *The End of a natural monoploy: Deregulation and Competition in the electric power industry*. Elsvier Science Ltd., 2003.

[3] R. D. Christie and A. Bose, "Load Frequency Control Issues In Power System Operations After Deregulation," *IEEE Trans. power Syst.*, vol. 11, no. 3, pp. 1191–1200, 1996.

[4] R. D. Christie, B. F. Wollenberg, and I. Wangensteen, "Transmission Management in the Deregulated Environment," *Proc. IEEE*, vol. 88, no. 2, pp. 170–195, 2000.

[5] S. K. Jain, S. Chakrabarti, and S. N. Singh, "Review of Load Frequency Control methods, Part-II: Post-deregulation scenario and case studies," in *International Conference on Control, Automation, Robotics and Embedded Systems*, 2013, pp. 1–7.

[6] P. Kundur, *Power System Stability and Control*. New York: McGraw-Hill, 2006.

[7] O. I.Elgerd and E. Fosha, "Optimum Megawatt-Frequency Control of Multiarea Electric Energy Systems," *IEEE Trans. Power Appar. Syst.*, vol. PAS-89, no. 4, pp. 556–563, 1970.

[8] T. Sasaki, T. Kadoya, and K. Enomoto, "Study on Load Frequency Control Using Redox Flow Batteries," *IEEE Trans. power Syst.*, vol. 19, no. 1, pp. 660–667, 2004.

[9] S. Nomura, T. Shintomi, S. Akita, T. Nitta, R. Shimada, and S. Meguro, "Technical and Cost Evaluation on SMES for Electric Power Compensation," *IEEE Trans. Appl. Supercond.*, vol. 20, no. 3, pp. 1373–1378, 2010.

[10] D. Wu, K. T. Chau, C. Liu, S. Gao, and F. Li, "Transient stability analysis of SMES for smart grid with vehicle-to-grid operation," *IEEE Trans. Appl. Supercond.*, vol. 22, no. 3, p. 5701105, 2012.

[11] J. X. Jin and X. Y. Chen, "Study on the SMES Application Solutions for Smart Grid," *Phys. Procedia*, vol. 36, pp. 902–907, Jan. 2012.

[12] S. Manfredi, M. Pagano, and R. Raimo, "Ultracapacitor-based distributed energy resources to support time-varying smart-grid power flows," *Int. Symp. Power Electron. Power Electron. Electr. Drives, Autom. Motion*, pp. 1148–1153, Jun. 2012.

[13] R. Gupta, N. Nigam, and A. Gupta, "Application of energy storage devices in power systems," *Int. J. Eng. Sci. Technol.*, vol. 3, no. 1, pp. 289–297, 2011.

[14] H. Bevrani, S. Member, and P. R. Daneshmand, "Fuzzy Logic-Based Load-Frequency Control Concerning High Penetration of Wind Turbines," *IEEE Syst. J.*, vol. 6, no. 1, pp. 173–180, 2012.

[15] S. Panda and N. K. Yegireddy, "Automatic generation control of multi-area power system using multi-objective non-dominated sorting genetic algorithm-II," *Int. J. Electr. Power Energy Syst.*, vol. 53, pp. 54–63, 2013.

[16] A. Yazdizadeh, M. H. Ramezani, and E. Hamedrahmat, "Decentralized load frequency control using a new robust optimal MISO PID controller," *Int. J. Electr. Power Energy Syst.*, vol. 35, no. 1, pp. 57–65, Feb. 2012.

[17] S. P. Ghoshal, "Optimizations of PID gains by particle swarm optimizations in fuzzy based automatic generation control," *Electr. Power Syst. Res.*, vol. 72, no. 3, pp. 203–212, Dec. 2004.

[18] S. Prakash and S. K. Sinha, "Load frequency control of three area interconnected hydro-thermal reheat power system using artificial intelligence and PI controllers," *Int. J. Eng. Sci. Technol.*, vol. 4, no. 1, pp. 23–37, 2012.

[19] R. Farhangi, M. Boroushaki, S. H. Hosseini, and S. Hamid, "Load-frequency control of interconnected power system using emotional learning-based intelligent controller," *Int. J. Electr. Power Energy Syst.*, vol. 36, no. 1, pp. 76–83, Mar. 2012.

[20] X. Du and P. Li, "Fuzzy Logic Control Optimal Realization Using GA for Multi-Area AGC Systems," *Int. J. Inf. Technol.*, vol. 12, no. 7, pp. 63–72, 2006.

[21] S. P. Ghoshal and S. K. Goswami, "Application of GA based optimal integral gains in fuzzy based active power-frequency control of non-reheat and reheat thermal generating systems," *Electr. Power Syst. Res.*, vol. 67, no. 2, pp. 79–88, Nov. 2003.

[22] Z. M. Al-Hamouz and H. N. Al-Duwaish, "A new load frequency variable structure controller using genetic algorithms," *Electr. Power Components Syst.*, vol. 55, pp. 1–6, 2000.

[23] S. Panda, B. Mohanty, and P. K. Hota, "Hybrid BFOA–PSO algorithm for automatic generation control of linear and nonlinear interconnected power systems," *Appl. Soft Comput.*, vol. 13, no. 12, pp. 4718–4730, Dec. 2013.

[24] U. K. Rout, R. K. Sahu, and S. Panda, "Design and analysis of differential evolution algorithm based automatic generation control for interconnected power system," *Ain Shams Eng.*, vol. 4, no. 3, pp. 409–421, Sep. 2013.

[25] R. Roy, "Evolutionary Computation based Four-Area Automatic Generation Control in Restructured Environment," in *International Conference on Power Systems ICPS'09*, 2009, pp. 25–30.

[26] A. Sharifi, K. Sabahi, M. A. Shoorehdeli, M. A. Nekoui, and M. Teshnehlab, "Load Frequency Control in Interconnected Power System using Multi-Objective PID Controller," in *IEEE Conference on Soft Computing in Industrial Applications SMCia'08*, 2008, pp. 217–221.

Chapter 2

Literature Survey

2.1 Introduction

The AGC problem has been attempted by various researchers across the world with main aim to maintain the system frequency and tie line flow at their scheduled values at all times. In earlier times, control of frequency in a power system could be achieved via the flywheel governor of the synchronous machine and this governor action was called the primary control. However, this conventional technique was subsequently found to be inadequate, and a supplementary control was included in the governor for fine adjustment of the frequency by resetting the frequency error to zero through an integral action. This scheme constitutes the classical approach to the AGC of power systems.

Various components of power systems possess non-linear characteristics, which make finding optimum operating point tedious. The conventional proportional integrator (PI) control strategy using the operating point for tuning of parameters was found unsuitable for the AGC. Due to inherent characteristics of changing loads, the operating points of a power system may change very randomly during a daily cycle. As a result, a fixed parameter type conventional controller may not be capable of providing the desired performance for other operating points [1], [2]. Various aspects of power systems including linear/non-linear power system models, centralized/decentralized structure, as well as deregulation of power system have been investigated for the development of the AGC approach. Furthermore, different issues related to characteristics of load, excitation control and sensitivity features have also been studied. Significant research work has also

been done in AGC design for interconnected power systems, incorporating ac and dc links. Different control techniques e.g. classical, optimal and sub-optimal control techniques have been discussed. Apart from this adaptive control, robust control, self tuning control, variable structure control based controllers have been examined for AGC controller design. Recently, advancement in the area of artificial intelligence techniques like fuzzy logic, neural networks and bio-inspired algorithms have found their application into the design of AGC control strategies. Penetration of these AI techniques has been increasing sharply due to their ability to tackle difficulties associated with nonlinear models, along with insufficient knowledge about the system. The microprocessor-based AGC regulator has also been discussed in the literature. In addition to this, increasing penetration of renewable resources of energy like wind turbines and PV cells has further led to more complex power system structures. In mitigating oscillations, different energy storage options like ultra capacitor, SMES have also been considered for AGC studies.

2.2 AGC Schemes for different types of Power System Models

The major sources of generation to meet the power demand are from hydro and thermal units. AGC strategies for several different power system structures such as single area [3], [4], two-area [5]–[8] and multi-area power system [9]–[12] have been discussed by researchers. Nonlinearities such as governor dead band and practical limits on the rate of increase of turbine output are often neglected. But in the practical scenario, the maximum limit of the rate of change in generation power of a steam plant is predefined. The impact of generation rate constraints (GRC) has been shown in [9] on system performance. It has also been shown that governor dead band nonlinearity tends to produce a continuous oscillation in the frequency and tie-line power transient response [10]. With increasing

size and complexity, uncertainties in the control and operation of power systems are introduced. Considerable attention has been paid by researchers to study the system nonlinearities [11]–[13]. Sensitivity analysis has also been performed to study the robustness in the system to wide variations in the system parameters [14]. It has been established that developing the AGC strategy based on a linearized model, when, the system was nonlinear, did not necessarily ensure the stability of the system.

2.3 AGC Schemes in Deregulated Environment

In a traditional electric power system, vertically integrated utilities (VIU) owned generation, transmission as well as distribution networks and supplied power to the customers at regulated rates. Deregulating power systems transformed the VIU-dominated system into open energy market system and enhanced the economic efficiency. The market participants who provide energy services in this open energy market have become more competitive. This system consists of GENCOs, DISCOs, and TRANSCOs. Apart from these companies, Independent System Operator (ISO) have been introduced to implement a secure and economical operation of power systems in coordination with all other companies in a deregulated power system [15], [16].

In this newly emerged structure, DISCO has the freedom to purchase the power from any GENCO, located within or outside of control area. The ISO is independent and a disassociated agent for market participants. In the open energy market, all the transactions are done under the supervision of the ISO. There are various ancillary services which are controlled by the ISO to provide secure, reliable and economical power transmission. AGC is one of ancillary services of ISO where ACE is used as a

control input for AGC operation. Different issues and analysis on power system models based on deregulated environment have been addressed by researchers in [15]–[22].

The Emergence of the deregulation era in power system has focused research on different arms of it. Christie et al. [16] described several possible structures for AGC in an open market and also addressed technical issues in power system operation after deregulation. Two different approaches for AGC based on HVDC-link and ramp-following controller were introduced by Bakken et al. [20] for Norway and Sweden interconnected power system in a competitive environment. A detailed simulation and optimization has been carried out by Donde et al. [15] for AGC systems after liberalization. The concept of DISCO participation matrix has also been shown for different types of contracts and trajectory sensitivity has also been explored. Yao et al. [23] developed an AGC logic based on North American Electric Reliability Council's (NERC) new standards. In the old NERC standard, the Control Performance Criteria (CPC) was used to measure their control performance. But, due to the lack of technical justification, NERC replaced the CPC with the new CPS and Disturbance Control Standard (DCS). Simulation results indicate significant reductions in the number of pulses and pulse reversals sent to controlling units and it was found convenient for controlling the degree of compliance, while minimizing unit control.

Roy et al. [24] studied the four-area multi-units AGC in a restructured power system. A chaotic ant swarm optimization and real coded GA were used to obtain optimal gain parameters for optimal transient performances. Bhatt et al. [22] also proposed a model for AGC in the restructured power system with the concept of DISCO participation matrix to simulate the bilateral contracts in three and four areas. Hybrid particle swarm

optimization was used to obtain optimal gain parameters for optimal transient performance.

Literature on deregulated environment mostly considers thermal and hydro units with linearized models with classical control techniques. In most of the earlier works, AGC pertain to interconnected thermal-thermal systems, mostly with non-reheat type turbines. Relatively lesser attention has been devoted to the AGC with interconnected non-conventional sources but in recent years, several control techniques based on optimal, intelligent and robust approaches have been proposed for AGC in deregulated power systems.

2.4 Wind Power Generating System for Frequency Regulation

Recently, wind as a source of energy generation has received extensive attention and has become a popular topic for research. Increasing levels of wind power generation have resulted in an urgent need for the assessment of their impact on the frequency control of power systems. The increasing penetration of variable-speed wind power generating systems (WPGS) in the electricity grid will result in reduction of the number of connected conventional power plants, thus a reduction in total system inertia. However, WPGS does not have participation in frequency support mechanisms.

Conroy et al. [25] investigated frequency response capability of the converter of variable-speed, wind-turbine generator with permanent magnet (synchronous generator to improve the frequency control performance). Lalor et al. [26] discussed on additional inertia to contribution capability of doubly fed induction generator (DFIG) wind turbines for frequency control. In this frequency control strategy, inertial control was combined with a proportional control but when transient contribution from DFIG finishes, its rotor speed

differs from the optimal value, which requires an additional control action to recover it. Ullah et al. [27] assesses the capability of a commercial multi-megawatt variable-speed wind turbine for providing a short-term active power support. Apart from this, some of their possible applications have been identified in a hydro-dominated system. It was found that short-term active power support from a wind farm could be beneficial for a hydro dominated system in arresting the initial frequency fall. Sun et al. [28] reviewed control methods to support frequency control at wind turbine level, wind farm level and power system level.

Morren et al. [29] proposed a method to allow variable-speed wind turbines to emulate inertia and support primary frequency control. In order to make "hidden inertia" available to grid, an additional controller was proposed, which adapts the torque set point as a function of the deviation of the grid frequency and rate of the change of the grid frequency. The required additional power is obtained from the kinetic energy stored in the rotating mass of the turbine blades. Bhatt et al. [30] analyzed the dynamic participation of DFIG to system frequency responses of a two-area interconnected power system. A frequency control support function, responding proportionally to frequency deviation, was proposed to take out the kinetic energy of turbine blades and to improve the frequency response of the system. Impact of different wind power penetrations in the system as well as varying active power support from wind farm on frequency control have also been investigated. Mauricio et al. [31] presented a modified inertial control scheme method to increase the participation of variable-speed wind energy conversion systems in existing frequency regulation mechanisms. The proposed method provides a

fast response with electronically-controlled wind-energy conversion system by dissipating the kinetic energy stored in rotational masses.

2.5 Energy Storage Options for Frequency Regulation

In order to diminish the frequency oscillation, the storage system such as battery energy storage (BES) and superconducting magnetic energy storage (SMES) can be incorporated in multi-area interconnected power system.

Tripathy et al. [32] proposed a small rating capacitive energy storage unit for performance improvement of an AGC. Tripathy et al. [33] also developed a discrete state-space model of a two area interconnected power system with SMES. The effect of small capacity SMES system was studied and simulation results showed an improvement of transient response with SMES. Chatterjee [34] dealt with the concept of AGC in a deregulated power system by considering a BES system. The performance of the power system under realistic situations is investigated by including GRC and dead band as nonlinearity in the simulation studies. Using time domain simulations, Chatterjee [34] observed that the BES system is capable of improving the system dynamic performance. C. Lu et al. [35] used BES to improve the performance of AGC, effect of governor dead band and GRC was also considered for a realistic response, it demonstrating BES is very effective in damping the oscillations caused by load disturbances. Aditya et al. [36] considered BES for an AGC of an interconnected reheat thermal system. It was found that BES meets sudden requirements of real power load and was very effective in reducing the peak deviations of frequency and tie-power.

It is an understanding that wind energy has a variable and uncertain output due to the erratic behavior of winds at a given location. Due to uncertainty of availability, especially

during peak hours of demands, wind energy may not be able to meet load demands. To overcome this disadvantage, energy storage plays a very important role by storing renewable energy (generated during off-peak time periods) and supplying it back to grid, when renewable energy is not able to fulfill load demand. Alternatively Energy storage could also be used to smooth the output fluctuations from an individual wind farm, thus, improving the quality of power being delivered. Depending on the capacity of the energy storage integrated WPGS, it can play an effective role in keeping the system frequency as well as tie-line power in a range of interest. With suitable technologies, wind energy along with energy storages, optimizes the potentiality of exiting grid.

Yoshimoto et al. [37] approached the smoothing out of a short-term fluctuation using a hybrid system of a battery energy storage system and a wind farm. In order to operate the hybrid system, the charging-level of the battery has to be regulated (it should not exceed its operable range). A control system based on state of charge feedback was developed to keep the charging level of the battery within its proper range. Jazaeri et al. [38] proposed an AGC of an isolated power system with a high wind penetration level equipped with a flywheel energy storage system. Simulation results obtained under various operating conditions were presented to evaluate the effectiveness of the control scheme. Senjyu et al. [39] proposed a methodology for controlling output of a wind power generator and battery energy storage system. The generated power fluctuation in low and high frequency domains were smoothened using pitch angle control and by battery charge or discharge.

2.6 Control Strategies for AGC

A number of control strategies have been employed in the design of AGC controllers. The advancement in hardware and software technologies has also transformed power system control. In any power system, performance of AGC depends upon proper design of the supplementary controller. Over the past few decades, in order to achieve an improved performance of the AGC, many control strategies, such as classical control, optimal state feedback control and variable structure control etc. were tried. All of these strategies have proved to be insufficient, due to the highly nonlinear nature of power system, increasing complexity, increasing rapid demand of load as well as increasing penetration of renewable energy.

2.6.1 Classical control

The AGC controller design techniques, using modern optimal control theory, enables the power engineers to design an optimal control system which meets the desired performance criteria. Among the various types of AGC controllers, the most widely employed is the conventional integral, proportional-integral (PI) and proportional-integral-derivative (PID) based controller. Fosha and Elgerd [40] used optimal control theory to develop an optimal AGC for two-area interconnected, non-reheat type thermal power system. Calovic [41] presented a linear regulator design for the AGC based on optimal linear regulator theory. An optimal tracking approach was proposed by Kwatny et al. [42], for AGC in which energy source dynamics and load following play a central role. In their work, it was also shown that load prediction and coordination of area generation in a multi-area interconnection can effectively improve inter-area power flow. In conventional control strategies, the integral of the control error is used as the control

signal for AGC. Initially, classical control methodologies were obtained using bode diagram, nyquist diagram and root locus to meet desired gain and phase margins. The design procedures of the classical methods for the AGC problem are straight forward and easy for practical implementation. Modern optimal theory based AGC controllers have also appeared in the literature. Tacker et. al [43] proposed optimal control for two-area interconnected power system for the existing operating policy as well as for improving system performance. The effect of plant response time on the closed loops roots had been investigated using linear optimal control theory by Barcelo [44]. Nanda et al. [45] proposed AGC of an interconnected hydrothermal system in continuous-discrete mode, using conventional integral and PI controllers. The effect of GRC as a non-linearity was studied for both hydro and thermal areas. In hydro areas, an electric or mechanical governor was considered, while in thermal areas, the single or double reheat turbine was considered. A selection of a suitable value of speed regulation parameter and sampling period has also been investigated. Saikia et al. [46] proposed integral plus double derivative controller for AGC with single reheat turbine and GRC. Most of the conventional AGC utilize an integral controller. The main drawback of integral controllers is that the dynamic performance of the system is limited by its integral gain. A high gain may cause large oscillations and may tend to instability. Thus, selection of integral gain is a compromise between a desirable transient recovery and low overshoot in the dynamic response.

2.6.2 Optimal control

Most of conventional AGC control strategies have used parameter adjustments based on heuristic approaches. Therefore, they are not appropriate to provide good dynamical

performance over a wide range of operating conditions. The Riccati-equation based robust controller was used by many researchers [47]–[52]. Goshaidas et al. [52] presented a robust control scheme for AGC of an interconnected power system with uncertain parameters. A combination of the singular-value decomposition technique and the Riccati equation approach was adopted to design a robust controller. The performance of this proposed robust controller has been studied with and without integral control action in the presence of parameter uncertainty in the plant. Goshaidas et al. [51] also presented a Riccati-equation based robust controller, for a two area interconnected power system. A combination of 'Matching conditions' and 'Lyapunov stability' theory had been adopted to implement a robust stabilizing controller. Ray et al. [49] presented a decentralized robust control scheme for the AGC of interconnected power systems with uncertain parameters. A singular value decomposition technique and Lyapunov stability theory were adopted to implement a decentralized robust controller. The effectiveness of the decentralized control algorithm was compared with a centralized robust one. In comparison, it was found that both control schemes have almost the same performance with integral control action, in the presence of parametric uncertainty in the plant.

Khodabakhshian and Edrisi [48] proposed a systematic tuning method to design a robust PID based AGC controller for multi machine power systems. This control strategy was based on a maximum peak resonance specification theory. The proposed controller had shown its robustness with a satisfactory response, even when parameters of the system changed in comparison to a conventional PI controller. Khodabakhshian and Hooshmand [47] further proposed a robust PID controller for AGC of hydro turbine power systems. This method was also based on a maximum peak resonance specification theory. It was

also concluded that by removing the transient droop compensator of the speed governor, a much faster dynamic performance could be achieved. Tan [53] had proposed PID tuning method of AGC for power systems. This tuning method was based on a two-degree-of-freedom internal model control method. In this method, two tuning parameters determined the performance of the resulting PID controller. An anti-GRC scheme was also proposed to overcome the GRC. Alomoush [54] proposed fractional-order PI and PID controllers for AGC, which performed better than conventional controllers, in terms of achieving better stability. Integral of the time-weighted absolute error, as a performance index, was utilized for the controller design.

A number of linear optimal control theories have been proposed to achieve better performance. Yet, fixed gain controllers, which are designed at nominal operating conditions, fail to provide best control performance over all operating conditions. In order to maintain the optimum system performance, it is required to track the operating conditions for updating controller parameters.

2.6.3 Adaptive control

Generally, as the operating point of the system gets altered, the fixed gain controller may not give optimal performance for the system. To keep the system performance near the optimal value, it is desirable to track the operating point. Adaptive control strategy is a control strategy which adjusts a controller's parameter in accordance to the system's varying parameters. A number of research works have been reported on adaptive control schemes [55]–[57] with self adjusting gain setting for AGC in the power system. Pan and Liaw [55] presented an adaptive PI controller for AGC, to satisfy the hyper-stability condition and to tackle variations in system parameters. Shoults et al. [57] developed a

multi-area adaptive AGC based on self tuning regulator for a comprehensive AGC simulator. A reduced-order adaptive control technique for AGC of interconnected hydrothermal power system was suggested by Liaw [56].

Adaptive control has been a topic of interest for researchers for the last few decades. Gozde et al. [58] suggested a gain scheduling PI control strategy for AGC of two area thermal power system with governor dead band non-linearity while [59], [60], discussed adaptive fuzzy gain scheduling for LFC schemes.

2.6.4 Robust control

Power system engineers are always concerned about the robustness of a controller with respect to plant perturbation and uncertainty. In electric power systems, on one hand, there are lot of uncertainties and disturbances due to variations in system parameters or improper modeling. On the other hand, the operating points of a power system may change very randomly during a daily cycle. Due to these factors, a classical and optimal control based AGC is certainly not suitable. Therefore, substantial attempts have been made to design AGC controllers with better performance to cope with uncertainties and disturbances using various robust methodologies. Various robust control based techniques such as robust pole assignment, loop shaping, H_∞, linear matrix inequality (LMI) have been adopted to tackle the AGC problems. Azzam [61] had proposed a robust pole assignment for AGC. This had a robust state feedback controller, based on optimum eigen values with minimum sensitivity to system parameter variation. Tan et al. [50] discussed a robust AGC based controller for power systems. Based on detailed robustness analysis of the control laws, it was concluded that more attention should be paid to the un-modeled dynamics, rather than parameter variation while designing robust automatic

generation control schemes. Al-Hamouz et al. [62] presented variable structure controller for AGC of single area power system, in which an optimal and systematic way of feedback gains selection proposed for variable structure controller. Franzè et al. [63] had presented a supervisory discrete-time predictive control strategy for AGC in networked multi-area power systems. Bevrani et al. [64] had proposed a decentralized robust approach for AGC in a deregulated environment, using a bilateral market scheme. It also included the effect of bilateral contracts in control area dynamical model, AGC problem was formulated as a multi-objective problem to cover robust performance and a mixed H_2/H_∞ was used to design the desired robust controllers.

2.6.5 Artificial intelligence based control and optimization strategies

With increased size and complexity of power system structures and due to the increasing penetration of renewable energy sources, the conventional control strategies for AGC are becoming infeasible. The intelligent control strategies, with use of soft computing techniques such as artificial neural network (ANN), fuzzy logic, genetic algorithm (GA), particle swarm optimization (PSO) algorithms, etc. have been explored for AGC problem for better performance.

2.6.5.1 Artificial neural network based control for frequency regulation

The ANN can be applied for frequency control to achieve better dynamic control, especially in a non-linear and highly complex power system. Birch et al. [65] had investigated the use of neural networks (NN) to act as the control intelligence, in conjunction with a standard adaptive AGC scheme. Demiroren et al. [66] investigated an application of layered ANN for AGC, while considering the effect of governor dead band and reheat into account for a two area interconnected power system. They used back

propagation-through-time algorithm as the neural network learning rule. Chaturvedi et al. [67] had developed a non-linear neural network controller, using a generalized neural network, to control the deviations in load frequency of a power system. Hemeida [68] explored the feasibility of applying a wavelet neural network (WNN) approach for the AGC, to damp the frequency oscillations of two area power systems. This intelligent control system trains the WNN controller on line with adaptive learning rates. The effects of governor dead zone were also considered for the system performance using the WNN controller.

2.6.5.2 Fuzzy logic controller for frequency regulation

Fuzzy logic control has been widely used in the power systems for solving different control related problems. Apart from effective controllability on linearized models, the fuzzy logic control can also efficiently control non-linear and highly complex models. FLC solves the problem based on experience and knowledge about the system, whereas conventional control strategies have constraints in addressing complex system problems like power frequency balance in multi area power system.

Mojtaba et al. [69] developed a fuzzy controller for AGC for multi area electric power system with variation in parametric uncertainties, GA was used for the optimization of the upper and lower bounds of the fuzzy membership functions. Simulation results showed that the designed controller was able to give a robust performance under wide range of uncertainty and load conditions. Mathur et al. [70] had developed a fuzzy logic controller for the AGC problem of electrical power system. The study had been designed for a three area interconnected power system with GRC as a non-linearity. Juang et al. [71] had proposed the GA based fuzzy gain scheduling approach for the AGC of a two

area interconnected power system. The fuzzy controller decided the integral or PI controller gain, according to area control error. Simulations were performed with different kinds of perturbation. Chang et al. [72] proposed a fuzzy gain scheduling based PI controller approach for AGC, designed for a four-area interconnected power system while considering dead band and GRC effect.

2.6.5.3 Genetic algorithm optimization in frequency regulation problem

Ghoshal et al. [73] determined GA based optimal gains for interconnected power system to get better optimal performance. Apart from this, sugeno fuzzy logic technique for on-line adaptive integral gain scheduling was also explored for AGC. Ghoshal [74] explored GA as well as hybrid genetic algorithm-simulated annealing techniques, to obtain optimal integral gains for integral controller, and gains for PID controller for interconnected power systems. Ghoshal [75] had also used various novel heuristic stochastic-search techniques for the optimization of PID controller gains. Classical particle swarm optimization, hybrid particle swarm optimizations and hybrid genetic algorithm simulated annealing were also explored to obtain optimal gains of PID controller. Al-Hamouz et al. [62] used GA for the selection of variable structure controller feedback gains, that was presented for AGC of a single area power system.

2.6.5.4 Particle swarm optimization in frequency regulation problem

The PSO is a population based stochastic nature inspired optimization technique, inspired from social behavior of bird flocking. Sharifi et al. [76] designed a multi-objective PID controller for AGC, based on adaptive weighted particle swarm optimization, for two area interconnected power system. In this approach, peak overshoot/undershoot and settling time were used as objective functions for multi-objective optimization. Similarly,

Bhatt et al. [77] explored the optimal PID gains for AGC using hybrid particle swarm optimization for interconnected power systems.

2.6.5.5 Other evolutionary optimization techniques

Some researchers used other evolutionary optimization technique to control frequency regulation. Naidu et al. [78] proposed multi-objective based optimization of artificial bee colony (ABC) algorithm for AGC on a two area interconnected reheat thermal power system, controller's gains had been selected to provide a compromise between the frequency response's settling time and maximum overshoot. Gozde et al. [79] examined ABC algorithm for AGC application, ABC algorithm was applied to the interconnected reheat thermal power system in order to tune the parameters of PI and PID controllers. Ali et al. [80] employed bacterial foraging optimization algorithm (BFOA) to find the parameters optimization of nonlinear AGC considering PID for a power system. Effectiveness of the proposed BFOA was validated over different operating conditions, and system parameters variations. Panda et al. [81] proposed hybrid bacteria foraging optimization algorithm and particle swarm optimization algorithm for AGC of an interconnected power system, PI controller was considered for AGC controller. Ibraheem et al. [82] proposed genetic algorithm-simulated annealing (GASA) optimization techniques for interconnected power system, in which gains of fuzzy logic based AGC tuned by GASA techniques.

2.7 Summary

A comprehensive literature survey on AGC was presented in this chapter. Deregulation and integration of renewable energy changed the structure of the power system thus, making most of the old era AGC control schemes and control techniques unsuitable in the

new regime. Various control techniques such as conventional, optimal, adaptive, robust, and artificial intelligence based control techniques have been thoroughly discussed. Literature survey shows that only a few investigations have been carried out using optimized fuzzy logic control strategies while addressing integration of renewable energy in deregulated scenario.

References

[1] O. P. Malik, A. Kumar, and G. S. Hope, "A load frequency control algorithm based on a generalized approach," *IEEE Trans. Power Syst.*, vol. 3, no. 2, pp. 375–382, 1988.

[2] R. K. Cavin, M. C. Budge, and P. Rasmussen, "An Optimal Linear Systems Approach to Load-Frequency Control," *IEEE Trans. Power Appar. Syst.*, vol. PAS-90, no. 6, 1971.

[3] Y. Wang, "New robust adaptive load-frequency control with system parametric uncertainties," *IEE Proc. - Gener. Transm. Distrib.*, vol. 141, no. 3, p. 184, 1994.

[4] P. H. Ashmole, D. R. Battlebury, and R. K. Bowdler, "Power-system model for large frequency disturbances," *Proc. Inst. Electr. Eng.*, vol. 121, no. 7, p. 601, 1974.

[5] E. Rakhshani, A. Luna, J. Sadeh, and P. Rodriguez, "PSO based optimal output feedback controller for two-area LFC system," *2012 20th Mediterr. Conf. Control Autom.*, pp. 1284–1289, Jul. 2012.

[6] B. V. Prasanth and SV Jayaram Kumar, "Load Frequency Control for a two area interconnected power system using robust genetic algorithm controller," *J. Theor. Appl. Inf. Technol.*, vol. 4, no. 12, pp. 1204–1212, 2008.

[7] A. E. Milani and B. Mozafari, "Genetic Algorithm Based Optimal Load Frequency Control in Two-Area Interconected Power Systems," *Trans. Power Syst. Optim.*, vol. 2, no. 1, pp. 6–10, 2011.

[8] A. Sreenath, Y. R. Atre, and D. R. Patil, "Two Area Load Frequency Control with Fuzzy Gain Scheduling of PI Controller," pp. 899–904, 2008.

[9] W.-C. Chan and Yuan-Yih Hsu, "Automatic generation control of interconnected power systems using variable-structure controllers," *IEE Proc. C Gener. Transm. Distrib.*, vol. 128, no. 5, pp. 269–279, 1981.

[10] S. C. Tripathy, G. S. Hope, and O. P. Malik, "Optimisation of load-frequency control parameters for power systems with reheat steam turbines and governor deadband nonlinearity," in *IEE Proceedings C Generation, Transmission and Distribution*, 1982, vol. 129, no. 1, pp. 10–16.

[11] K. R. Sudha and R. Vijaya Santhi, "Robust decentralized load frequency control of interconnected power system with Generation Rate Constraint using Type-2 fuzzy approach," *Int. J. Electr. Power Energy Syst.*, vol. 33, no. 3, pp. 699–707, Mar. 2011.

[12] R. K. Sahu, S. Panda, and U. K. Rout, "DE optimized parallel 2-DOF PID controller for load frequency control of power system with governor dead-band nonlinearity," *Int. J. Electr. Power Energy Syst.*, vol. 49, no. 1, pp. 19–33, 2013.

[13] K. P. S. Parmar, S. Majhi, and D. P. Kothari, "Load frequency control of a realistic power system with multi-source power generation," *Int. J. Electr. Power Energy Syst.*, vol. 42, no. 1, pp. 426–433, Nov. 2012.

[14] R. K. Sahu, S. Panda, and U. K. Rout, "DE optimized parallel 2-DOF PID controller for load frequency control of power system with governor dead-band nonlinearity," *Int. J. Electr. Power Energy Syst.*, vol. 49, pp. 19–33, Jul. 2013.

[15] V. Donde, M. A. Pai, and I. A. Hiskens, "Simulation and Optimization in an AGC System after Deregulation," *IEEE Trans. Power Syst.*, vol. 16, no. 3, pp. 481–489, 2001.

[16] R. D. Christie and A. Bose, "Load Frequency Control Issues In Power System Operations After Deregulation," *IEEE Trans. power Syst.*, vol. 11, no. 3, pp. 1191–1200, 1995.

[17] R. J. Abraham, D. Das, and A. Patra, "Load following in a bilateral market with local controllers," *Int. J. Electr. Power Energy Syst.*, vol. 33, no. 10, pp. 1648–1657, 2011.

[18] J. Kumar, K.-H. Ng, and G. Sheble, "AGC Simulator for Price-Based Operation-Part II: Case Study Results," *IEEE Trans. power Syst.*, vol. 12, no. 2, pp. 533–538, 1997.

[19] J. Kumar, K. Ng, and G. Sheblt, "AGC Simulator for Price-Based Operation Part I: A Model," *IEEE Trans. power Syst.*, vol. 12, no. 2, pp. 527–532, 1997.

[20] B. H. Bakken and O. S. Grande, "Automatic Generation Control in a Deregulated Power System," *IEEE Trans. power Syst.*, vol. 13, no. 4, pp. 1401–1406, 1998.

[21] R. Roy, P. Bhatt, and S. P. Ghoshal, "Evolutionary computation based three-area automatic generation control," *Expert Syst. Appl.*, vol. 37, no. 8, pp. 5913–5924, 2010.

[22] P. Bhatt, R. Roy, and S. P. Ghoshal, "Optimized multi area AGC simulation in restructured power systems," *Int. J. Electr. Power Energy Syst.*, vol. 32, no. 4, pp. 311–322, May 2010.

[23] M. Yao, R. R. Shoults, and R. Kelm, "AGC logic based on NERC's new control performance standard and disturbance control standard," *IEEE Trans. power Syst.*, vol. 15, no. 2, pp. 852–857, 2000.

[24] R. Roy, P. Bhatt, and S. Ghoshal, "Evolutionary computation based three-area automatic generation control," *Expert Syst. Appl.*, vol. 37, no. 8, pp. 5913–5924, 2010.

[25] J. F. Conroy and R. Watson, "Frequency response capability of full converter wind turbine generators in comparison to conventional generation," *IEEE Trans. Power Syst.*, vol. 23, no. 2, pp. 649–656, 2008.

[26] G. Lalor, a. Mullane, and M. O'Malley, "Frequency Control and Wind Turbine Technologies," *IEEE Trans. Power Syst.*, vol. 20, no. 4, pp. 1905–1913, 2005.

[27] N. R. Ullah, T. Thiringer, and D. Karlsson, "Temporary Primary Frequency Control Support by Variable Speed Wind Turbines— Potential and Applications," *IEEE Trans. Power Syst.*, vol. 23, no. 2, pp. 601–612, 2008.

[28] Y.-Z. Sun, Z.-S. Zhang, G. Li, and J. Lin, "Review on frequency control of power systems with wind power penetration," in *2010 International Conference on Power System Technology (POWERCON)*, 2010, pp. 1–8.

[29] J. Morren, S. W. H. De Haan, W. L. Kling, and J. A. Ferreira, "Wind Turbines Emulating Inertia and Supporting Primary Frequency Control," *IEEE Trans. power Syst.*, vol. 21, no. 1, pp. 433–434, 2006.

[30] P. Bhatt, R. Roy, and S. P. Ghoshal, "Dynamic participation of doubly fed induction generator in automatic generation control Optimize," *Renew. Energy*, vol. 36, no. 4, pp. 1203–1213, 2011.

[31] J. M. Mauricio, A. Marano, A. Gómez-expósito, and José Luis Martínez Ramos, "Frequency Regulation Contribution Through Variable-SpeedWind Energy Conversion Systems," *IEEE Trans. power Syst.*, vol. 24, no. 1, pp. 173–180, 2009.

[32] S. C. Tripathy, R. Balasubramanian, and P. S. Chandramohanan Nair, "Small rating capacitive energy storage for dynamic performance improvement of automatic generation control," in *IEE Proceedings C Generation, Transmission and Distribution*, 1991, vol. 138, no. 1, pp. 103–111.

[33] S. C. Tripathy and B. Bak-Jensen, "Automatic generation control of multi-area power system with superconducting magnetic storage unit," in *2001 IEEE Porto Power Tech Proceedings*, 2001, vol. 3, pp. 1–6.

[34] K. Chatterjee, "Effect of Battery Energy Storage System on Load Frequency Control under Deregulation," *Int. J. Emerg. Electr. Power Syst.*, vol. 12, no. 3, pp. 1–23, 2011.

[35] C. Lu, C.-C. Liu, and C.-J. Wu, "Effect of battery energy storage system on load frequency control considering governor deadband and generation rate constraint," *IEEE Trans. Energy Convers.*, vol. 10, no. 3, pp. 555–561, 1995.

[36] S.K. Aditya and D. Das, "Battery energy storage for load frequency control of an interconnected power system," *Electr. Power Syst. Res.*, vol. 58, no. 3, pp. 179–185, Jul. 2001.

[37] K. Yoshimoto, N. Toshiya, G. Koshimizu, and Y. Uchida, "New control method for regulating State-of-Charge of a battery in hybrid wind power/battery energy storage system," in *IEEE PES Power Systems Conference and Exposition, PSCE 2006*, 2006, vol. 8165, pp. 1244–1251.

[38] M. Jazaeri and H. Chitsaz, "A new efficient scheme for frequency control in an isolated power system with a wind generator," *Electr. Power Components Syst.*, vol. 40, no. 1, pp. 21–40, 2011.

[39] T. Senjyu, S. S. Member, Y. Kikunaga, S. S. Member, A. Yona, H. Sekine, A. Y. Saber, and T. Funabashi, "Coordinate Control of Wind Turbine and Battery in Wind Power Generator System," in *IEEE Power and Energy Society General Meeting - Conversion and Delivery of Electrical Energy in the 21st Century*, 2008, pp. 1–7.

[40] O. I.Elgerd and E. Fosha, "Optimum Megawatt-Frequency Control of Multiarea Electric Energy Systems," *IEEE Trans. Power Appar. Syst.*, vol. PAS-89, no. 4, pp. 556–563, 1970.

[41] Milan Calovic, "Linear Regulator Design for a Load and Frequency Control," *IEEE Trans. Power Appar. Syst.*, vol. PAS-91, no. 6, pp. 2271–2285, 1972.

[42] H. G. Kwatny, K. C. Kalnitsky, and A. Bhatt, "An Optimal Tracking Approach to Load-Frequency Control," *IEEE Trans. Power Appar. Syst.*, vol. PAS-94, no. 5, pp. 1635–1643, 1975.

[43] E.C.Tacker, C.C.Lee, T.W.Reddoch, T.O.Tan, and P.M.Julich, "Optimal control of interconnected, electric energy systems—A new formulation," in *Proceedings of the IEEE*, 1972, vol. 60, no. 10, pp. 1239–1241.

[44] W. R. Barcelo, "Effect of Power Plant Response on Optimum Load Frequency Control System Design," *IEEE Trans. Power Appar. Syst.*, vol. PAS-92, no. 1, pp. 254–258, 1973.

[45] J. Nanda, A. Mangla, and S. Suri, "Some New Findings on Automatic Generation Control of an Interconnected Hydrothermal System With Conventional Controllers," *IEEE Trans. Energy Convers.*, vol. 21, no. 1, pp. 187–194, 2006.

[46] L. Saikia, J. Nanda, and S. Mishra, "Performance comparison of several classical controllers in AGC for multi-area interconnected thermal system," *Electr. Power Energy Syst.*, vol. 33, no. 3, pp. 394–401, 2011.

[47] A. Khodabakhshian and R. Hooshmand, "A new PID controller design for automatic generation control of hydro power systems," *Electr. Power Energy Syst.*, vol. 32, no. 5, pp. 375–382, 2010.

[48] A. Khodabakhshian and M. Edrisi, "A new robust PID load frequency controller," *Control Eng. Pract.*, vol. 16, no. 9, pp. 1069–1080, 2008.

[49] G. Ray, a. N. Prasad, and T. K. Bhattacharyya, "Design of decentralized robust load-frequency controller based on SVD method," *Comput. Electr. Eng.*, vol. 25, no. 6, pp. 477–492, 1999.

[50] W. Tan and Z. Xu, "Robust analysis and design of load frequency controller for power systems," *Electr. Power Syst. Res.*, vol. 79, no. 5, pp. 846–853, 2009.

[51] G. Ray, a. N. Prasad, and G. D. Prasad, "A new approach to the design of robust load-frequency controller for large scale power systems," *Electr. Power Syst. Res.*, vol. 51, no. 1, pp. 13–22, 1999.

[52] G. Ray, A. N. Prasad, and G. Durga Prasad, "Design of a robust load—frequency controller for interconnected power systems based on the singular-value decomposition method," *Electr. Power Syst. Res.*, vol. 37, no. 3, pp. 209–219, 1996.

[53] W. Tan, "Tuning of PID load frequency controller for power systems," *Energy Convers. Manag.*, vol. 50, no. 6, pp. 1465–1472, 2009.

[54] M. I. Alomoush, "Load frequency control and automatic generation control using fractional-order controllers," *Electr. Eng.*, vol. 91, no. 7, pp. 357–368, Jan. 2010.

[55] C. T. Pan and C. M. Liaw, "Adaptive controller for power system load-frequency control," *IEEE Trans. Power Syst.*, vol. 4, no. 1, pp. 122–128, 1989.

[56] C. M. Liaw, "Design of a Reduced-Order Adaptive Load-Frequency Controller for an Interconnected Hydrothermal Power-System," *Int. J. Control*, vol. 60, no. 6, pp. 1051–1063, 1994.

[57] R. R. Shoults and J. A. J. Ibarra, "Multi-Area Adaptive LFC Developed for A Comprensive AGC Simulator," *IEEE Trans. Power Syst.*, vol. 8, no. 2, pp. 541–547, 1993.

[58] H. Gozde and M. C. Taplamacioglu, "Automatic generation control application with craziness based particle swarm optimization in a thermal power system," *Int. J. Electr. Power Energy Syst.*, vol. 33, no. 1, pp. 8–16, 2011.

[59] J. Talaq and F. Al-Basri, "Adaptive fuzzy gain scheduling for load frequency control," *IEEE Trans. Power Syst.*, vol. 14, no. 1, pp. 145–150, 1999.

[60] M. Masiala, M. Ghribi, and A. Kaddouri, "An adaptive fuzzy controller gain scheduling for power system load-frequency control," in *IEEE International Conference on Industrial Technology ICIT '04.*, 2004, vol. 3, pp. 1515–1520.

[61] M. Azzam, "Robust automatic generation control," *Energy Convers. Manag.*, vol. 40, no. 13, pp. 1413–1421, 1999.

[62] Z. M. Al-Hamouz and H. N. Al-Duwaish, "A new load frequency variable structure controller using genetic algorithms," *Electr. Power Components Syst.*, vol. 55, pp. 1–6, 2000.

[63] G. Franze and F. Tedesco, "Constrained load/frequency control problems in networked multi-area power systems," *J. Franklin Inst.*, vol. 348, pp. 832–852, 2011.

[64] H. Bevrani, Y. Mitani, and K. Tsuji, "Robust Decentralized LFC Design In a Deregulated Environment," *Proc. 2004 IEEE Int. Conf. Electr. Util. Deregulation, Restruct. Power Technol.*, no. April, pp. 326–331, 2004.

[65] A. P. Birch, A. T. Sapeluk, and C. S. Ozveren, "An Enhanced Neural Network Load Frequency Control Technique," in *International Conference on Control Control'94.*, 1994, vol. 1, pp. 409–415.

[66] A. Demiroren, N. S. Sengor, and A. H. L, "Automatic Generation Control by Using ANN Technique," *Electr. Power Components Syst.*, vol. 29, no. 10, pp. 883–896, 2001.

[67] D. K. Chaturvedi, P. S. Satsangi, and P. K. Kalra, "Load frequency control : a generalised neural network approach," *Electr. Power Energy Syst.*, vol. 21, pp. 405–415, 1999.

[68] A. M. Hemeida, "Wavelet neural network load frequency controller," *Energy Convers. Manag.*, vol. 46, no. 9–10, pp. 1613–1630, 2005.

[69] S. Mojtaba, S. Boroujeni, R. Hemmati, and H. F. Boroujeni, "Load frequency control in multi area electric power system using genetic scaled fuzzy logic," *Int. J. Phys. Sci.*, vol. 6, no. 3, pp. 377–385, 2011.

[70] H. D. Mathur and H. V. Manjunath, "Frequency stabilization using fuzzy logic based controller for multi-area power system," *South Pacific J. Nat. Sci.*, vol. 4, pp. 22–30, 2007.

[71] C.-F. Juang and C.-F. Lu, "Power System Load Frequency Control With Fuzzy Gain Scheduling," in *Proceedings of the 2002 IEEE International Conference on Fuzzy Systems, FUZZ-IEEE'02*, 2002, vol. 1, pp. 64–68.

[72] C. S. Chang and W. Fu, "Area load frequency control using fuzzy gain scheduling of PI controllers," *Electr. Power Components Syst.*, vol. 42, pp. 145–152, 1997.

[73] S. P. Ghoshal and S. K. Goswami, "Application of GA based optimal integral gains in fuzzy based active power-frequency control of non-reheat and reheat thermal generating systems," *Electr. Power Syst. Res.*, vol. 67, no. 2, pp. 79–88, 2003.

[74] S. P. Ghoshal, "Application of GA / GA-SA based fuzzy automatic generation control of a multi-area thermal generating system," *Electr. Power Syst. Res.*, vol. 70, pp. 115–127, 2004.

[75] S. P. Ghoshal, "Optimizations of PID gains by particle swarm optimizations in fuzzy based automatic generation control," *Electr. Power Syst. Res.*, vol. 72, no. 3, pp. 203–212, 2004.

[76] A. Sharifi, K. Sabahi, M. A. Shoorehdeli, M. A. Nekoui, and M. Teshnehlab, "Load Frequency Control in Interconnected Power System using Multi-Objective PID Controller," in *IEEE Conference on Soft Computing in Industrial Applications SMCia'08*, 2008, pp. 217–221.

[77] P. Bhatt, R. Roy, and S. Ghoshal, "GA/particle swarm intelligence based optimization of two specific varieties of controller devices applied to two-area multi-units automatic generation control," *Electr. Power Energy Syst. ...*, vol. 32, no. 4, pp. 299–310, 2010.

[78] K. Naidu, H. Mokhlis, and A. H. A. Bakar, "Multiobjective optimization using weighted sum Artificial Bee Colony algorithm for Load Frequency Control," *Int. J. Electr. Power Energy Syst.*, vol. 55, pp. 657–667, Feb. 2014.

[79] H. Gozde, M. Cengiz Taplamacioglu, and İ. Kocaarslan, "Comparative performance analysis of Artificial Bee Colony algorithm in automatic generation control for interconnected reheat thermal power system," *Int. J. Electr. Power Energy Syst.*, vol. 42, pp. 167–178, Nov. 2012.

[80] E. S. Ali and S. M. Abd-Elazim, "BFOA based design of PID controller for two area Load Frequency Control with nonlinearities," *Int. J. Electr. Power Energy Syst.*, vol. 51, pp. 224–231, Oct. 2013.

[81] S. Panda, B. Mohanty, and P. K. Hota, "Hybrid BFOA–PSO algorithm for automatic generation control of linear and nonlinear interconnected power systems," *Appl. Soft Comput.*, vol. 13, no. 12, pp. 4718–4730, Dec. 2013.

[82] N. Hasan and O. Singh, "GASA Tuned Optimal Fuzzy Regulator for AGC of an Interconnected Power System," *Int. J. Comput. Appl.*, vol. 20, no. 8, pp. 43–48, 2011.

Chapter 3

Modeling of Interconnected Power System

3.1 Introduction

The modeling of power system is necessary before entering into the design of AGC. In this chapter, the modeling of different components of power system is discussed. Detailed modeling of typical power generating system components, the tie-line modeling and the modeling of parallel operation of interconnected areas are introduced. In order to develop the transfer function of the interconnected power system, it is necessary to develop a linear model. A linear model can be developed by making suitable approximations and assumptions. A transfer function model as a mathematical model for different components is considered and detailed modeling of WPGS and SMES for system under study are also presented.

3.2 Modeling of Power Generating System

In the single area system, either one generating unit or bunch of generating units, is placed in close vicinity to distribute the electricity and these generating units present are responsible to maintain the desired frequency. In these generating units, synchronous generator is the principal source of electric energy. Electric frequency is related to the mechanical rotation of the synchronous generator's rotor and this electrical frequency depends on achieving a balance in the active power or a match between the electrical power output of the generator and the system load. In the next section, transfer function model of componets of power generating system are developed.

3.2.1 Generator-load model

In general, a synchronous generator is used in power systems. In an interconnected power system, all the generators run at the same speed. In a real time situation, electrical power storage in large amounts is not easy, so a balance must be maintained within the generated power and load demand.

To understand the speed control mechanism of an interconnected power system, the mechanism of an isolated generator needs to be understood. The isolated generator experiences two opposing torques; first is the mechanical torque (T_m) as input and another in the opposite direction of rotation electrical torque (T_e) as a load. In the steady state condition, both torques will be equal in magnitude and the speed will remain constant. When there is a variation in T_m or T_e, then the corresponding equilibrium is disturbed. This, in turn, results in frequency variation and the system will attain a new equilibrium point. Frequency is a direct function of the speed of the prime mover and it varies with any imbalance between electrical and mechanical torque [1]. When a small perturbation is applied to a synchronous machine, the relationship between the mechanical power (ΔP_m) and the electrical power (ΔP_L) is expressed by applying the swing equation:

$$\frac{2H}{\omega_s}\frac{d^2\Delta\delta}{dt^2} = \Delta P_m - \Delta P_L \tag{3.1}$$

Where H is inertia constant, $\Delta\delta$ is rotor angle deviation and $\boldsymbol{\omega}_s$ nominal rotational speed.

$$\frac{1}{\omega_s}\frac{d^2\Delta\delta}{dt^2} = \frac{1}{2H}\left(\Delta P_m - \Delta P_L\right) \tag{3.2}$$

The generator-load model is derived from (3.2) and given in (3.3). Input for this is the change in valve setting ΔP_v and output is the corresponding mechanical power output change ΔP_m, as shown below:

$$G_P = \frac{\Delta\omega}{(\Delta P_m - \Delta P_L)} = \frac{1}{2Hs+D} \tag{3.3}$$

Loads in power systems consist of a variety of electrical devices e.g. lighting equipment, rotating devices etc. Some of them are purely resistive and some of them are motor loads, which are a dominant part of electrical loads. Lighting equipment is basically resistive in nature and the rotating devices are composite of the resistive and inductive components. Generator model with load for AGC is shown in Fig. 3.1.

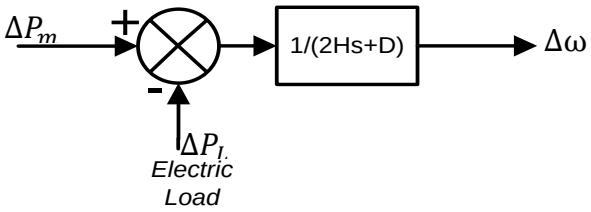

Fig. 3.1: Block diagram of generator for load damping effect

The frequency dependent load characteristic is given by:

$$(\Delta P_e = \Delta P_L + D\Delta\omega) \tag{3.4}$$

Where, ΔP_L is frequency insensitive load change $D\Delta\omega$ is frequency sensitive load change and D is load damping constant.

3.2.2 Modeling of governor

Governor is a device used to regulate the speed of a machine and to sense the frequency bias in a power system. Governors are also useful to regulate power, speed of the turbine

and help in frequency regulation. They not only regulate the speed, but also help in starting the turbine as well as protecting from hazard conditions. Input for governor is change in reference power and the change in compensated power $\Delta P_{err} = (\Delta P_{ref} - \Delta P_c)$ and output is the corresponding valve setting change ΔP_v, as shown below:

$$G_G = \frac{\Delta P_v}{\Delta P_{err}} = \frac{\Delta P_v}{(\Delta P_{ref} - \Delta P_c)} = \frac{1}{1+sT_g} \tag{3.5}$$

$$\Delta P_{err} = \Delta P_{ref} - \Delta P_c \tag{3.6}$$

$$\Delta P_c = \frac{1}{R}\Delta\omega \tag{3.7}$$

This is known as primary speed control. It does initial coarse readjustment of the speed or frequency. A coherent group of generators share load in proportion to their capacities. Depending upon the type and input of turbine, the primary control loop typically responds within 2–20s.

3.2.3 Modeling of turbine

Turbine is a rotary mechanical device that extracts natural energy from steam or water (depends on type of power plant) and converts it into mechanical power. The turbine drives the generator by this mechanical power. Generally in power plants, the types of turbines used are: reheat, hydraulic and non-reheat turbines. Input for turbine is the change in valve setting ΔP_v and output is the corresponding mechanical power output change ΔP_m. The transfer functions of non-reheat and reheat turbine are given in (3.8) and (3.9) respectively.

$$G_{T\_NR} = \frac{\Delta P_m}{\Delta P_v} = \frac{1}{1+sT_t} \tag{3.8}$$

Here, time constant T_t represents the time delay between switching the valve and producing the turbine torque. Reheat turbines are used for higher thermal efficiency and are modeled as second-order systems and they have two different stages of high and low steam pressure section. The transfer function can be represented as:

$$G_{T\_R} = \frac{\Delta P_m}{\Delta P_v} = \frac{F_h T_t s+1}{(1+sT_t)(1+sT_r)} \tag{3.9}$$

where, F_h is the reheat coefficient, which represents high pressure stage rating and T_r stands for low pressure reheat time constant.

Modeling of Hydraulic turbine depends on water pressure response or transitory response of water and this is deduced from dynamics of water in runway. The transfer function of the hydraulic turbine is in the form of:

$$G_{T\_Hy} = \frac{\Delta P_m}{\Delta P_v} = \frac{1-sT_w}{(1+s(T_w/2))} \tag{3.10}$$

$$T_w = {L.v}/{g.H_r} \tag{3.11}$$

Where, T_w is water starting time constant, L is length of raceway, v is water speed, g is acceleration of gravity and H_r is net headway of water in raceway.

Transient droop compensation is a part of the governor and is required for a hydraulic turbine. The transfer function of transient droop compensation is given by,

$$G_{T\_DCHy} = \frac{sT_R}{(1+s(R_T/R)T_R)} \tag{3.12}$$

Where, T_R is the reset time, R_T is the temporary droop and R is the permanent droop respectively [2].

3.2.4 Modeling of AGC in single area power system

A single area power system consists of a speed governor, a turbine and a generator with a primary controller as well as supplementary controller. The block diagram of system with these components connected is shown in Fig. 3.2.

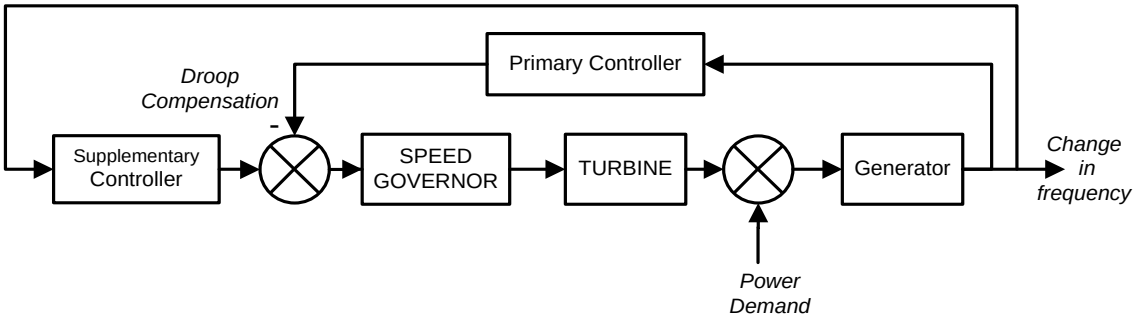

Fig. 3.2: Block diagram of single area control system

3.2.5 Modeling of control area

When a group of generators are closely coupled internally, they swing in unison. These power generating units operate in parallel and may be located at different places, to supply the power need of a control area. Such a group of generators characterized by a single frequency are said to be coherent and called the control area or control group. In this, various generators that are running coherently to track a load variation and load sharing is executed in proportion to their capacities.

For mathematical modeling, a coherent response of all generators for variation in the system load can be represented by an equivalent generator. The inertia constant (H_{eq}) of equivalent generator is equal to sum of inertia constants of all generators. Similarly, the effect of system load is lumped into a single damping constant (D_{eq}). The equivalent generator inertia constant (H_{eq}) and load damping constant (D_{eq}) can be represented for n generators running in parallel, as:

$$H_{eq} = H_1 + H_2 + \cdots + H_n \tag{3.13}$$

$$D_{eq} = D_1 + D_2 + \cdots + D_n \tag{3.14}$$

AGC takes account of the collective performance of all generators, as shown in Fig.3.3. The composite load-frequency characteristic of a power system depends on the combined effect of droop of all generator speed governors. So, when ΔP_L is applied then frequency change will be given by,

$$\Delta f_{steady\_state} = \frac{-\Delta P_L}{(1/R_{eq}+D_{eq})} \tag{3.15}$$

$$R_{eq} = \frac{1}{(1/R_1+1/R_2\ldots+1/R_n)} \tag{3.16}$$

Where R_{eq} is the equivalent droop value for n generators running coherently, and Δf_{steady_state} *is* the frequency deviation at steady state for applied load (ΔP_L).

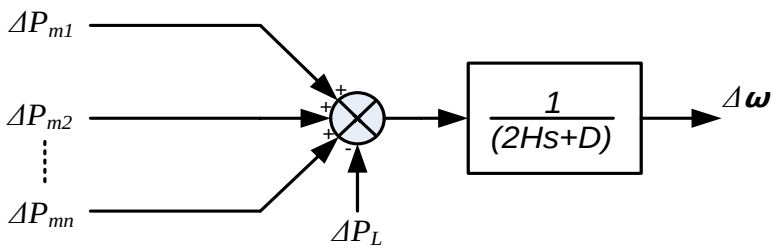

Fig. 3.3: Power system equivalent for AGC

Modeling of tie-line of interconnected power system

Interconnected power systems formed by different control areas are connected with each other via tie-lines, as shown in Fig. 3.4. The power exchange between two control areas occurs through the tie-line due to the difference of frequencies of control areas. In case of a two area power system, real power transferred over the tie line is given by,

$$P_{12} = \frac{|E_1||E_2|}{X_{12}} sin\delta_{12} \tag{3.17}$$

Where,

$$X_{12} = X_1 + X_{tie} + X_2 \tag{3.18}$$

and power angle is represented by:

$$\delta_{12} = \delta_1 - \delta_2 \tag{3.19}$$

For a small deviation in tie-line power flow,

$$\Delta P_{12} = \frac{dP_{12}}{d\delta_{12}} | \Delta\delta_{12}| \tag{3.20}$$

$$\Delta P_{12} = T_{12}\, \Delta\delta_{12} \tag{3.21}$$

Where, T_{12} is the synchronizing torque coefficient and tie-line power deviation takes the form,

$$\Delta P_{12} = T_{12}\,(\Delta\delta_1 - \Delta\delta_2) \tag{3.22}$$

$$T_{12} = \frac{|E_1||E_2|}{X_{12}} cos\delta_{12} \tag{3.23}$$

$$\Delta P_{12} = T_{12}\,(\int \Delta\omega_1 dt - \int \Delta\omega_2 dt) \tag{3.24}$$

$$\Delta P_{12} = 2\pi T_{12}\,(\int \Delta f_1 dt - \int \Delta f_2 dt) \tag{3.25}$$

$$\Delta P_{12}(s) = \frac{2\pi T_{12}}{s}(\Delta f_1(s) - \Delta f_2(s)) \tag{3.26}$$

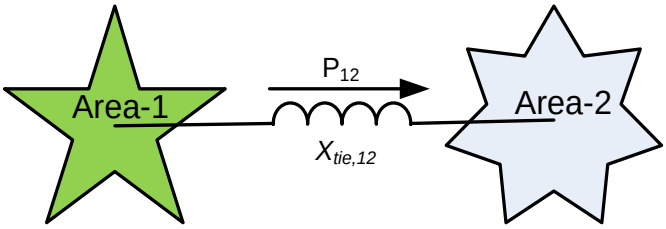

Fig. 3.4: Tie-line connecting control areas

Area control error (ACE)

In an interconnected power system, in addition to the regulating area frequency, net interchange power with neighboring control areas at scheduled values should be maintained. This is generally accomplished by the supplementary feedback control mechanism. ACE is the control error of a control area, which consists of a linear combination of frequency and tie line flows. The objective of AGC is to minimize the frequency error as well as to keep the tie-line error to scheduled values. Combining

frequency deviation as well as tie-line power deviation result in an error called *ACE*, defined as:

$$ACE_i = \beta_i \Delta f_i + \sum_{j=1}^{N} \Delta P_{tie,ij} \quad (3.27)$$

Where β_i is the frequency bias coefficient, $\Delta P_{tie,ij}$ is the tie-line power flow between i^{th} control area to j^{th} control area and N is the number of control areas interconnected together [3].

Each control area has its own supplementary controller and these controllers have the goal of controlling *ACE*. Using suitable control strategies, they minimize frequency deviation as well as tie-line power deviation.

3.2.6 Modeling of AGC in two area power system

A two area power system consists of two single area power systems, connected through a tie- line, as shown in the Fig. 3.5 where area-1 consists of thermal-reheat type generating unit and area-2 consists of hydro type generating unit. Each control area fulfills demand of their user pool and the tie-line allows electric power to flow between the control areas. Each control area is represented by an equivalent governor, turbine, generator and generator-load model in power system block.

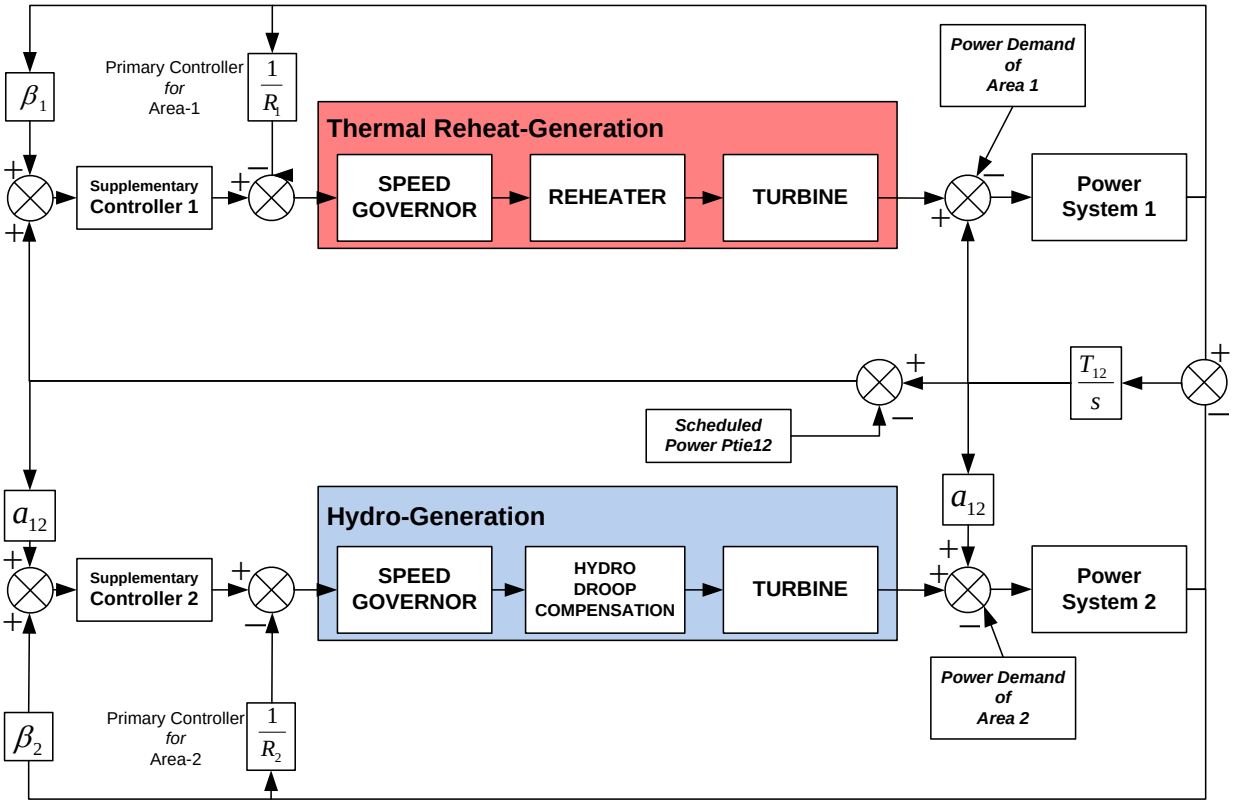

Fig. 3.5: Block diagram of two area power system

Vertical integrated utility (VIU)

For almost a century, all electric power utilities (Generation, Transmission and Distribution) were operated with a single organizational body i.e. Vertically Integrated Utility (VIU). In the traditional power system structure, VIUs had monopolies in generation, transmission and distribution in a certain geographic region. All these utilities were governed by VIU, under regulatory control of the government or public bodies. This meant that generation, transmission and distribution of electricity were under control of a single entity. There were also some Independent Power Producers (IPPs), which used to sell power to VIUs.

Fig.3.6 shows Traditional Power System Structure. In this structure, a VIU consisted of a group of generators and loads and all the generators were connected in parallel. Hence, the regulation of power imbalance in generation and supply was not a serious issue. The AGC role in such scenarios was limited to restore the system frequency to the specified nominal value.

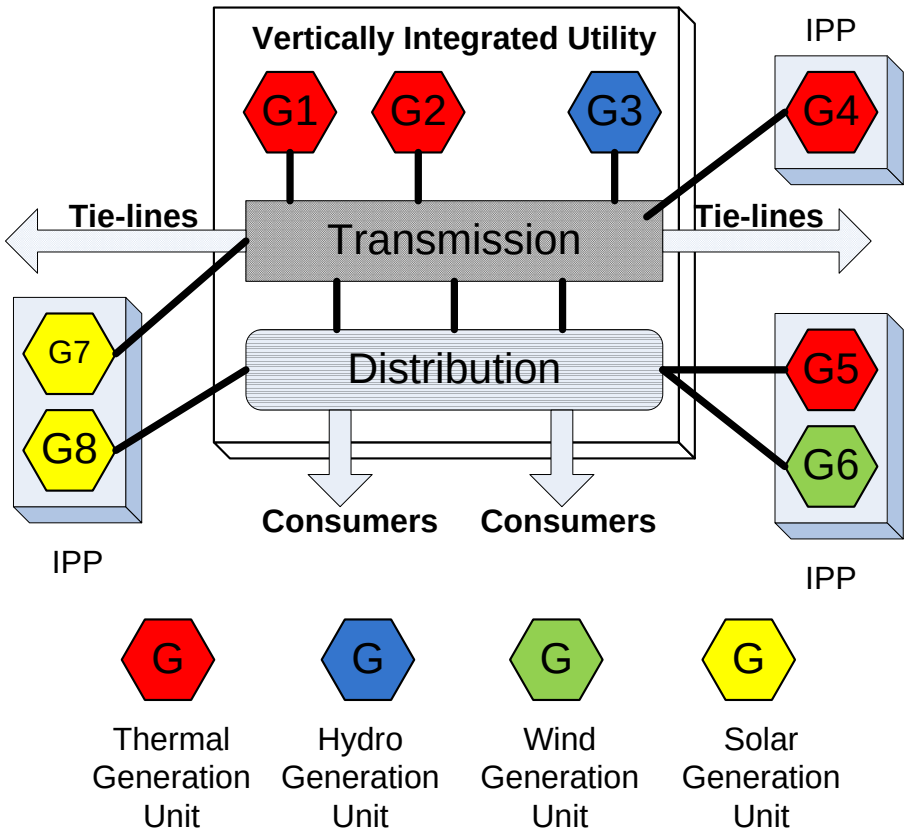

Fig. 3.6: Traditional power system structure

Deregulation of power industry

Deregulation of the power industry changed the way of operation of the power systems throughout the world. In this open market, electricity is sold like commodity. In a deregulated environment, the electric utility services are disaggregated into components. These utilities compete with each other for selling electricity as well as their services.

The AGC is treated like an ancillary service among various ancillary services. In a deregulated power system, management of such system becomes very complex. In the traditional power system structure, AGC was provided by VIUs in their territories but in deregulation however, different generation companies (GENCOs) and IPPs participate to provide this ancillary service, as shown in Fig. 3.7.

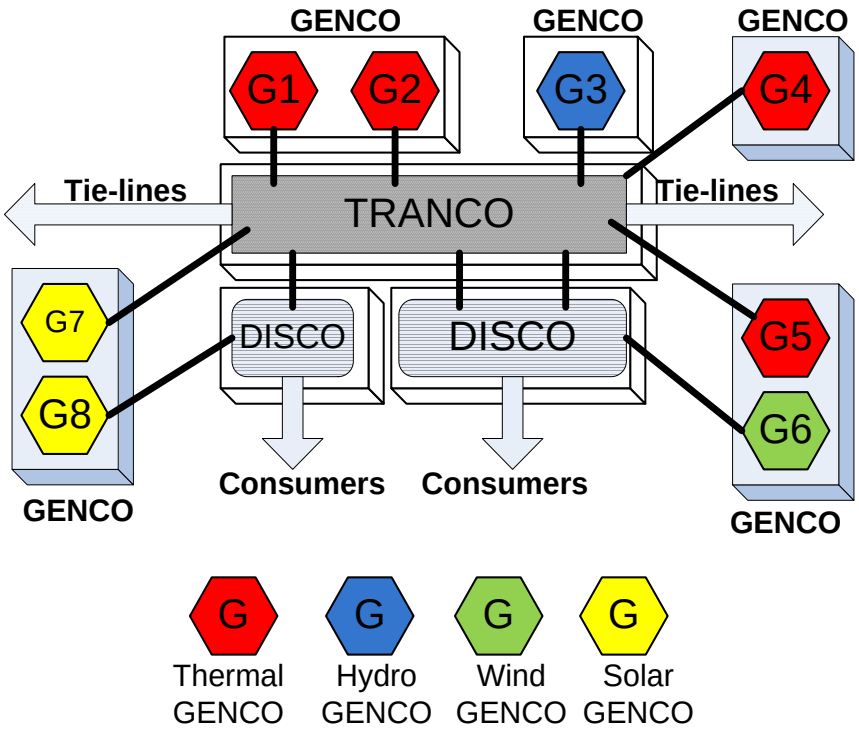

Fig. 3.7: Power system structure in deregulated environment

Christie et al. [4] described several possible scenarios of AGC under deregulation. A competitive power system provides a market within which these entities compete on the basis of price to sell electricity. In the deregulated scenario, GENCOs are no longer obliged to generate electricity; they can generate and sell their electricity when they find it profitable. As deregulation proceeds further, there are a number of players entering the system which is no longer centrally controlled. Thus, a central independent body is set up

for monitoring the bids for matching power exchange demand and to maintain the system reliability and security. The prime objective of the ISO is to maintain instantaneous balance for grid. An ISO also ensures unbiased access to the transmission system for all GENCOs [5]. For smooth operation of power system, the ISO operates several ancillary services. Ancillary Services are those services that are performed in support of basic services of generation, transmission and distribution. These services play a very significant role e.g. active power reserve, AGC, reactive power reserve.

In this scenario, while it is desirable to encourage competition to reduce cost and improve quality, it is more important to maintain system reliability. In power systems, reliability is measure of system security and it is the system ability to withstand disturbances.

After deregulation, Transmission Companies (TRANSCOs) are treated in an unbiased way for all users in the open access market and ISO is designated to operate TRANSCOs. ISO have to ensure sufficient quantity of on-line reserve capacity for maintaining reliability criteria. There reserve capacities must be procured by the ISO [5].

3.3 Two-Area Power System Model in Deregulated Environment

The system examined consists of two control areas, each having two GENCOs and two DISCOs. The Control area-1 is composed of two reheat-type thermal GENCOs of equal capacity and control area-2 is composed of two hydro GENCOs of equal capacity, as shown in Fig. 3.8.

The contract participation factor matrix (*cpf_matrix*) makes the visualization of contracts easy, rows indicate GENCOs and columns indicate DISCOs. The cpf_matrix is also known as DISCO participation matrix (DPM). Here, the ij^{th} entry corresponds to the

fraction of the total load power contracted by DISCO j from a GENCO i [6]. The cpf_matrix is:

$cpf\_matrix =$

Area-I		Area-I to Area-II		
cpf_{11}	cpf_{12}	cpf_{13}	cpf_{14}	G1
cpf_{21}	cpf_{22}	cpf_{23}	cpf_{24}	G2
cpf_{31}	cpf_{32}	cpf_{33}	cpf_{34}	G3
cpf_{41}	cpf_{42}	cpf_{43}	cpf_{44}	G4
Area-II to Area-I		Area-II		
D1	D2	D3	D4	

GENCO's

DISCO's

Where, in a column $\sum_j cpf_{ij}$ is equal to unity. The system output, which depends on the *ACE*, is

$$ACE_i = \Delta P_{tie,i} + b_i \Delta f_i \tag{3.28}$$

Coefficients that distribute *ACE* to several GENCOs are termed as *ACE* participation factors (*apf*s) as shown in *apf_matrix*:

$$apf\_matrix = \begin{bmatrix} apf_1 & 0 & 0 & 0 \\ 0 & apf_2 & 0 & 0 \\ 0 & 0 & apf_3 & 0 \\ 0 & 0 & 0 & apf_4 \end{bmatrix}$$

Where, within a control area $\sum_i apf_i$ is equal to unity.

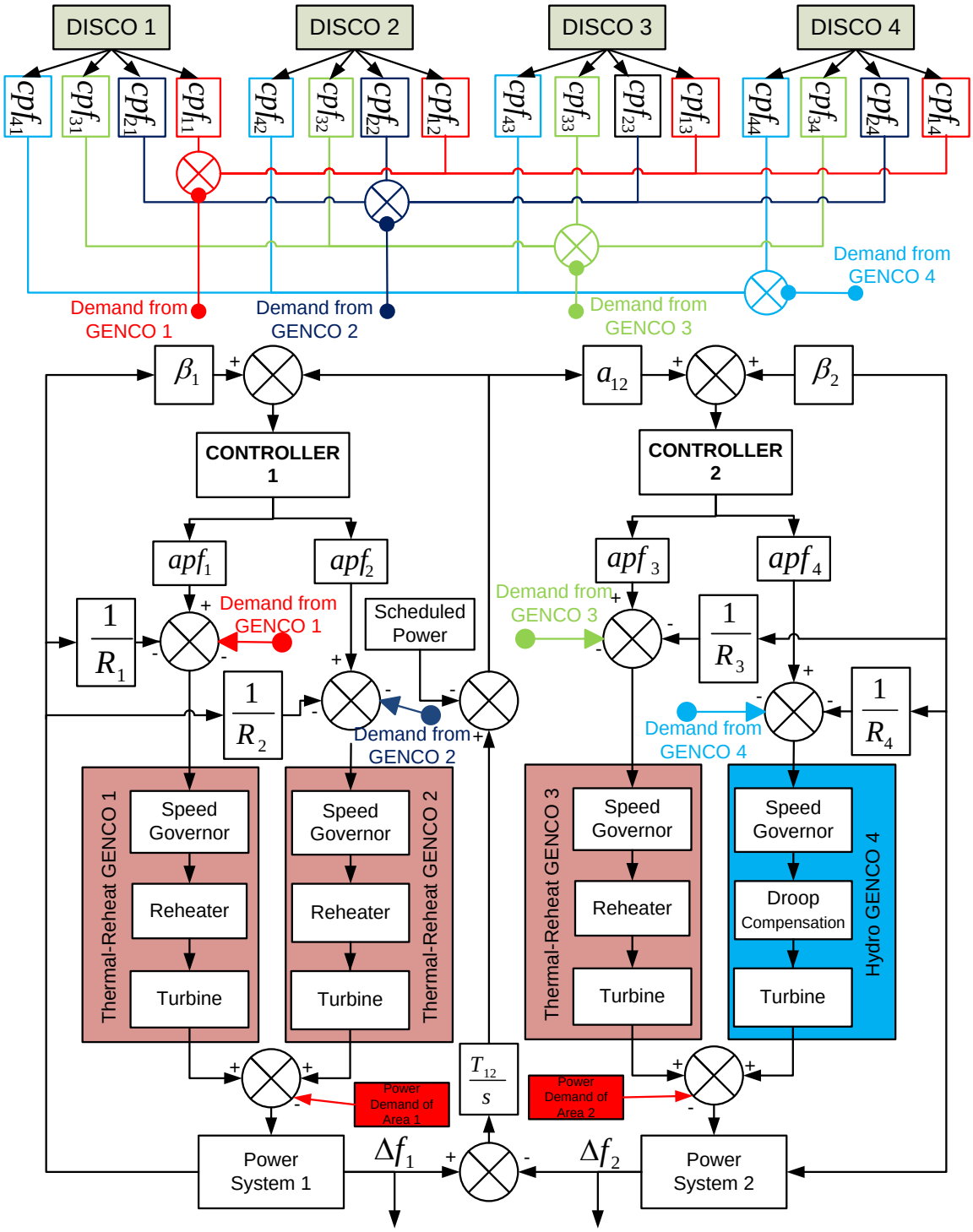

Fig. 3.8: System model of two area thermal-hydro power system in deregulated environment

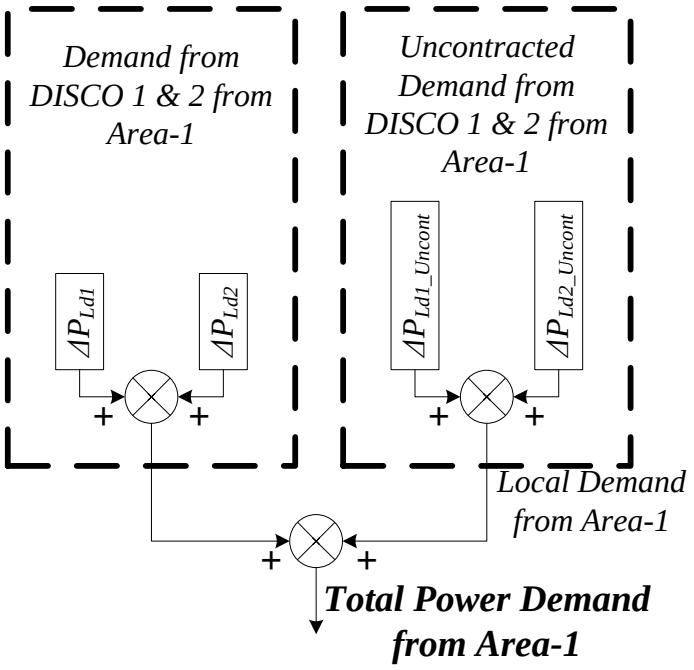

Fig. 3.9: Local power in control area-1

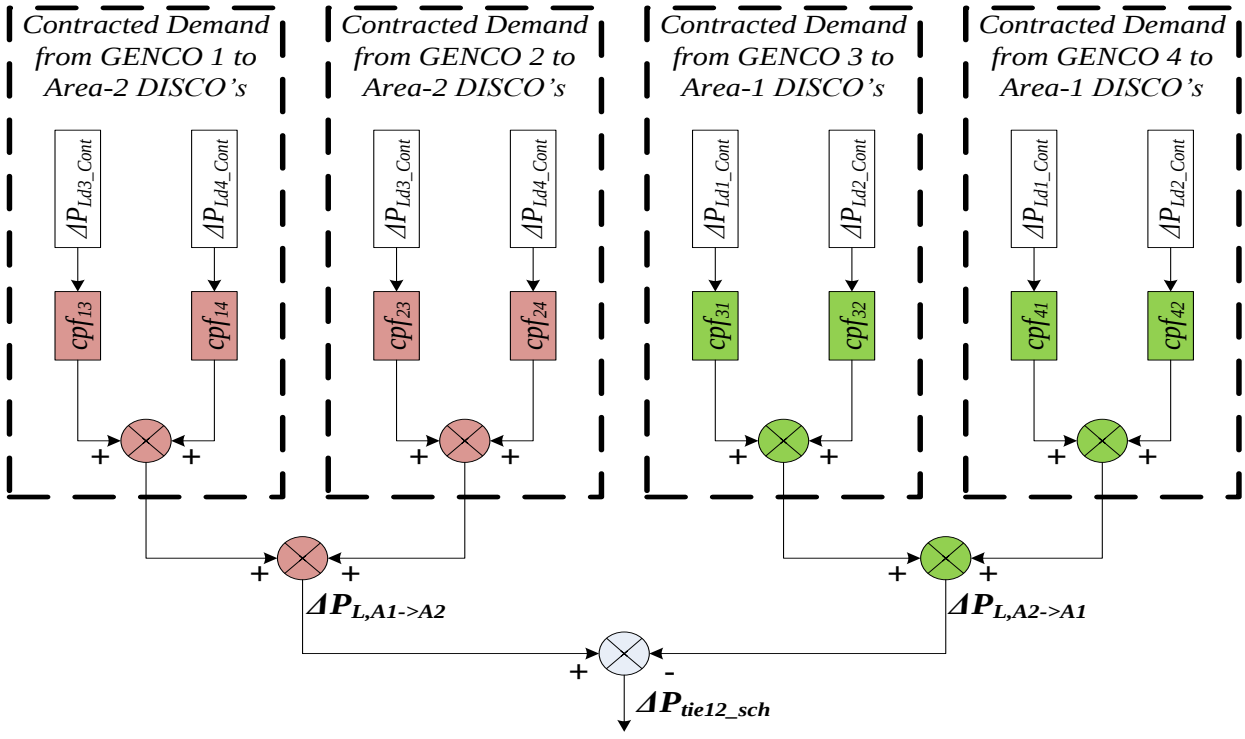

Fig. 3.10: Block diagram representation of scheduled_Ptie12

The contracted scheduled loads from area-1 DISCO's are ΔP_{Ld1_Cont} and ΔP_{Ld2_Cont} as well as from area-2 DISCOs are ΔP_{Ld3_Cont} and ΔP_{Ld4_Cont}. These contracted loads are shown in the ΔP_{LD_Cont} matrix. The uncontracted local loads from in area-1 DISCO's are ΔP_{Ld1_Uncont} andΔP_{Ld2_Uncont}. ΔP_{Ld3_Uncont} and ΔP_{Ld4_Uncont} are uncontracted loads from area-2 DISCO's. These uncontracted loads are shown in ΔP_{LD_Uncont} matrix [7].

$$\Delta P_{LD\_Cont} = \begin{bmatrix} \Delta P_{Ld1\_Cont} \\ \Delta P_{Ld2\_Cont} \\ \Delta P_{Ld3\_Cont} \\ \Delta P_{Ld4\_Cont} \end{bmatrix}; \Delta P_{LD\_Uncont} = \begin{bmatrix} \Delta P_{Ld1\_Uncont} \\ \Delta P_{Ld2\_Uncont} \\ \Delta P_{Ld3\_Uncont} \\ \Delta P_{Ld4\_Uncont} \end{bmatrix}$$

The total demanded power shown in matrix ΔP_{LD}, which included of contracted load and uncontracted load, as shown in:

$$\Delta P_{LD} = \Delta P_{LD\_Cont} + \Delta P_{LD\_Uncont} \tag{3.29}$$

Similarly, the total generated power through GENCOs from area-1 are ΔP_{g1} and ΔP_{g2} while the total generated power through GENCOs from area-2 are ΔP_{g3} and ΔP_{g4} at steady state. These generated powers are shown through the ΔP_G matrix.

The contracted generated powers from area-1 are ΔP_{g1_Cont} and ΔP_{g2_Cont} at steady state, and in the same way, from area-2 are ΔP_{g3_Cont} and ΔP_{g4_Cont}. This is represented by ΔP_{G_Cont} matrix. ΔP_{g1_Uncont} and ΔP_{g2_Uncont} are uncontracted required power from area-1 and ΔP_{g3_Uncont} and ΔP_{g4_Uncont} are uncontracted power from area-2 at steady state, as shown in ΔP_{G_Uncont} matrix.

$$\Delta P_{G\_Cont} = \begin{bmatrix} \Delta P_{g1\_Cont} \\ \Delta P_{g2\_Cont} \\ \Delta P_{g3\_Cont} \\ \Delta P_{g4\_Cont} \end{bmatrix}; \Delta P_{G\_Uncont} = \begin{bmatrix} \Delta P_{g1\_Uncont} \\ \Delta P_{g2\_Uncont} \\ \Delta P_{g3\_Uncont} \\ \Delta P_{g4\_Uncont} \end{bmatrix}$$

The un-contracted power demanded under contract violation from area-1 and area-2 are referred to as $\Delta P_{L1,LOC}$ and $\Delta P_{L2,LOC}$ respectively. It is total un-contracted power by local GENCOs only from the same control area. Fig. 3.9 show local power in Control Area-1.

$$\Delta P_{L(i),LOC} = \sum_j \Delta P_{g(j)\_Uncont} \tag{3.30}$$

In the matrix form, it is represented as:

$$\Delta P_{G\_Uncont} = apf\_matrix * P_{LD\_Uncont} \tag{3.31}$$

So, the total required generation power in the matrix form is represented as:

$$\Delta P_G = \Delta P_{G\_Cont} + \Delta P_{G\_Uncont} \tag{3.32}$$

$$\Delta P_G = cpf_{matrix} * \Delta P_{LD\_Cont} + apf_{matrix} * \Delta P_{LD\_Uncont} \tag{3.33}$$

The scheduled tie line power flow between areas *i* to *j* can be represented as:

$$\Delta P_{L,Ai\rightarrow Aj} = \sum_{m,n=1}^{M,N} (cpf\text{mn} * \Delta P_{Ld(n)\_Cont}) \tag{3.34}$$

Where *m* is m^{th} GENCO in control area A_i, and *n* is n^{th} DISCO in control area A_j. *M* is total number of GENCOs in area A_i, and *N* is total number of DISCOs in area A_j.

$$\Delta Ptieij, sch = \Delta P_{L,Ai\rightarrow Aj} - \Delta P_{L,Aj\rightarrow Ai} \tag{3.35}$$

Fig. 3.10 shows the block diagram representation of scheduled_Ptie12. For a two-area power system, scheduled tie line power flow between area-1 and area-2 can be represented as:

$$\Delta P_{L,A1\rightarrow A2} = (cpf13 * \Delta P_{Ld3_{Cont}} + cpf23 * \Delta P_{Ld3_{Cont}} + cpf14 * \Delta P_{Ld4_{Cont}} + cpf24 * \Delta P_{Ld4\_Cont}) \tag{3.36}$$

$$\Delta P_{L,A2\rightarrow A1} = (cpf31 * \Delta P_{Ld1\_Cont} + cpf41 * \Delta P_{Ld1\_Cont} + cpf32 * \Delta P_{Ld2\_Cont} + cpf42 * \Delta P_{Ld2\_Cont}) \quad (3.37)$$

$$\Delta Ptie12, sch = \Delta P_{L,A1\rightarrow A2} - \Delta P_{L,A2\rightarrow A1} \quad (3.38)$$

Governor dead-band

Governor dead-band or backslash is defined as the value of a sustained speed change within which, there is no change in valve position. The governor dead-band is important in case of a small disturbance, which affects stability. Therefore, the effect of governor dead-band is studied with AGC in a deregulated environment. The governor dead-band nonlinearity tends to produce a continuous sinusoidal oscillation [8].

The nonlinearity of hysteresis type can be expressed as, $y = F(x, \dot{x})$

The function *F* is evaluated as a fourier series and expressed as,

$$F(x, \dot{x}) = F_0 + N_1 x + \frac{N_2}{2\pi f_0}\dot{x} + \cdots \quad (3.39)$$

In above equation, as dead-band nonlinearity is symmetrical about the origin, the constant term F_0 is equal to zero.

$$F(x, \dot{x}) = N_1 x + \frac{N_2}{2\pi f_0}\dot{x} \quad (3.40)$$

Approximately, if sinusoidal oscillation frequency 0.5 and backslash 0.05% is considered, then Fourier coefficients N_1 and N_2 are obtained as 0.8 and -0.2 respectively [9]. Hence, dead band can be expressed in terms of transfer function DB(s),

$$DB(s) = N_1 + N_2 s \quad (3.41)$$

$$DB(s) = (0.8 - \frac{0.2}{\pi} s) \quad (3.42)$$

3.4 Modeling of Wind Power Generating System for Inertia Support

Reduction of fossil fuel-based energy sources has been among the top priority goals of regulatory agencies around the world. Therefore, there is an urgent need to exploit more sources of renewable energy. Wind energy, being one of the most promising options among renewable sources of energy, has witnessed a phenomenal growth in power generation. However, wind power generation is more challenging, compared to conventional sources of energy, since the availability of wind energy source is unpredictable and uncontrollable. This unpredictable nature of wind and wind turbine and its inability to participate in frequency regulation limits its grid penetration. An efficient integration of large amounts of wind turbines into the existing electrical networks can significantly impact grid stability. It has been noticed that without a suitable control strategy, integration of wind energy with high penetration would not be possible, particularly in ancillary services such as frequency regulation.

In this study, the role of WPGS for frequency and tie line power oscillation control with different levels of wind penetration has been considered. The varying active power support system is developed by WPGS for a two-area restructured interconnected system. Short term active power support responds proportionally to frequency deviation and this additional energy is extracted from the kinetic energy of turbine blades.

It has been observed that little emphasis has been given to the concept of inertial support by WPGS in order to minimize inter area oscillations in a restructured power system. The concept of releasing the kinetic energy of a WPGS when the frequency of the power system is reduced, in order to prevent the reduction of system inertia is presented in [10]. The experimental results of a Doubly Fed Induction Generator (DFIG)-based wind turbine using converters [11], modelling of a variable-speed wind turbine concepts in

power system dynamic simulations [12] and the impact assessment of high penetration of wind energy to the Irish network [13] are also available in literature. Frequency regulation and inertial support is also discussed in [14], [15].

3.4.1 Doubly fed induction generator as WPGS

DFIG is an electric machine that may be used as a motor or generator in which both the field windings and armature windings can be separately connected. DFIGs are widely used in wind turbines and have an additional feature that they can run slightly below or above to their synchronous speed, which makes them useful for variable speed wind turbine (VSWT) and VSWTs are more efficient than fixed speed wind turbines [16]. When DFIG is used as VSWT, the AC power with a varying frequency is produced that depends on the fluctuating wind speed. This is converted into DC which is then reconverted into AC power of desired frequency. Fig. 3.11 shows Schematic diagram of DFIG.

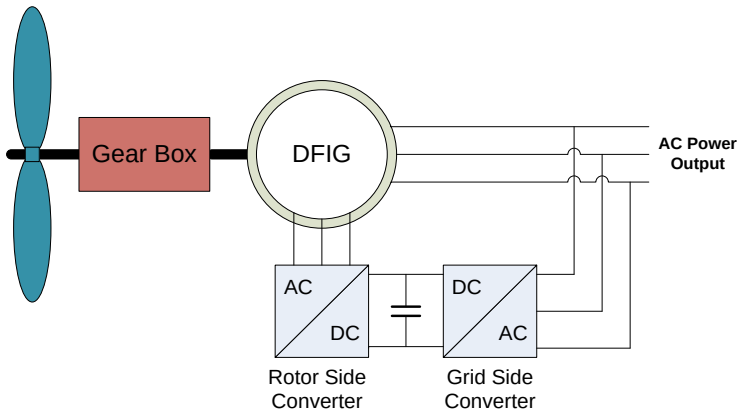

Fig. 3.11: Doubly fed induction generator

There are two windings in DFIG - one is stationary and another one is rotating. Both windings are used to give AC output, and therefore, this induction generator is called a doubly fed induction generator. Furthermore, the DFIG efficiency is also high, since

converters are only designed for a maximum of 35% of power being fed to grid. Rest of power is directly fed into grid without using converters [17]. A typical WPGS is shown in Fig. 3.12.

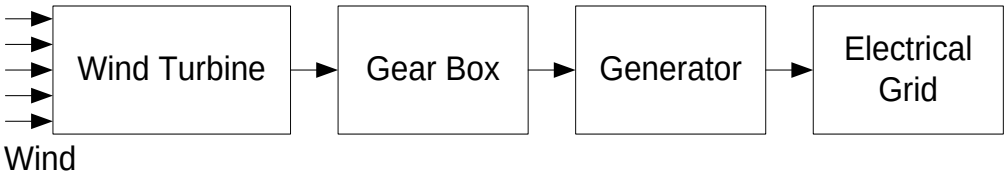

Fig. 3.12: Wind power generating system (WPGS)

3.4.2 Inertia support from WPGS for AGC

In an interconnected power system, when any disturbance arises, it causes frequency deviations, primarily characterized by the amount of system inertia. This initial response of the power system, which acts in response to a disturbance for bringing a balance between demand and supply, is called the inertial response of the system and this balancing phenomenon is a stabilizing effect which brings the power system back to the equilibrium condition. The inertial response occurs in power system due to the prevalence of synchronous generators but most of renewable energy resources, connected to grid through power electronic devices, result in decrement of overall system inertia. Renewable energy resources can provide an inertial response by different means and these have been discussed in [15], [18]–[23]. In this thesis, the concept of 'hidden inertia' has been explored in order to maintain the system inertia for maintaining power frequency balance.

Hidden inertia is an additional control for inertial response and can be realized for power electronics-based decoupled renewable energy systems. It reduces the maximum gradient of the frequency deviation, because the derivative of system frequency depends on total

system inertia. Hidden inertia is realized by means of releasing kinetic energy of rotating mass of wind turbines. Mechanism of releasing the hidden inertia actually involves an increment in the electrical power output. Therefore, additional control has to be applied, which is based on the derivative of the system frequency.

3.4.3 Wind turbine model for frequency regulation

The model developed in this study is based on a commercial WPGS model published by GE [24], and its simplified diagram is shown in Fig. 3.13. A one-mass model is considered for the mechanical drive of the turbine. The mechanical power developed by the turbine is given by:

$$P_{wind} = \frac{1}{2}\rho\pi R^2 v_{wind}{}^3 \tag{3.43}$$

$$P_M = C_p(\lambda,\beta) * P_{wind} \tag{3.44}$$

where R is the rotor radius, ρ is the air density, v is the wind speed and $C_p$is the power coefficient of the turbine which depends on the pitch angle β, and the tip-speed ratio λ, which is defined by:

$$\lambda = \frac{R\,\omega_e}{v} \tag{3.45}$$

Where, ω_e is the rotor speed of wind turbine.

The theoretical static upper limit of power coefficient is 16/27 (approximately 0.593), which is the maximum theoretically possible value (approximately 59%) that can be extracted from the kinetic energy of the wind (known as Betz's limit). The power coefficient is a characteristic of the wind turbine and it can be approximated by:

$$C_p(\lambda,\beta) = \sum_{i=0}^{4}\sum_{j=0}^{4}\alpha_{i,j}\beta^i\lambda^j \quad (3.46)$$

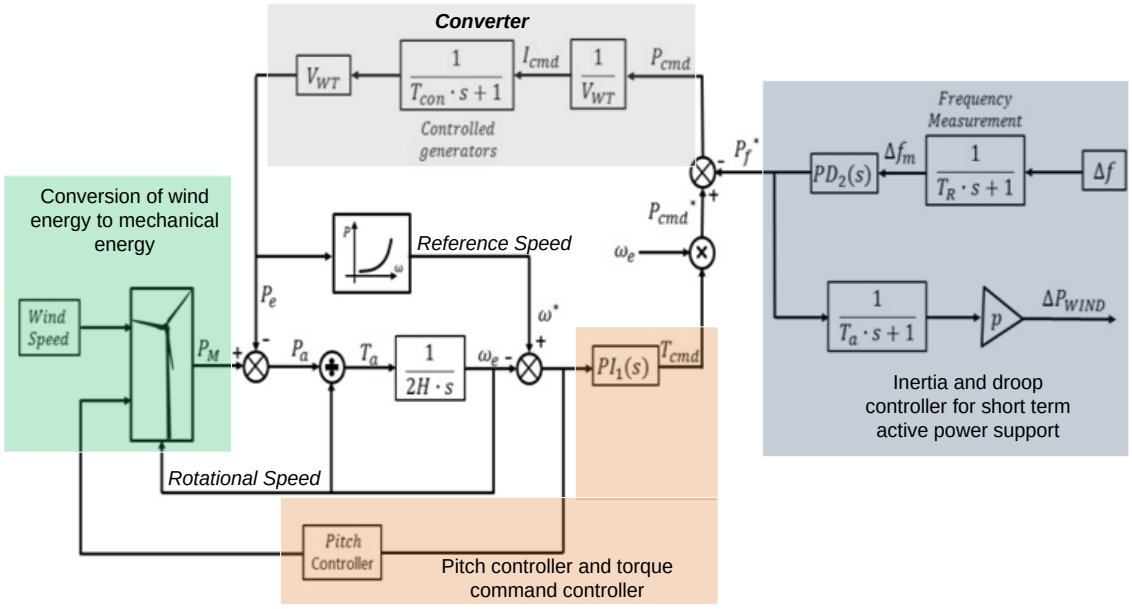

Fig. 3.13: Simplified block diagram of wind turbine

The Power coefficients for different values of pitch angles are shown in Fig. 3.14.

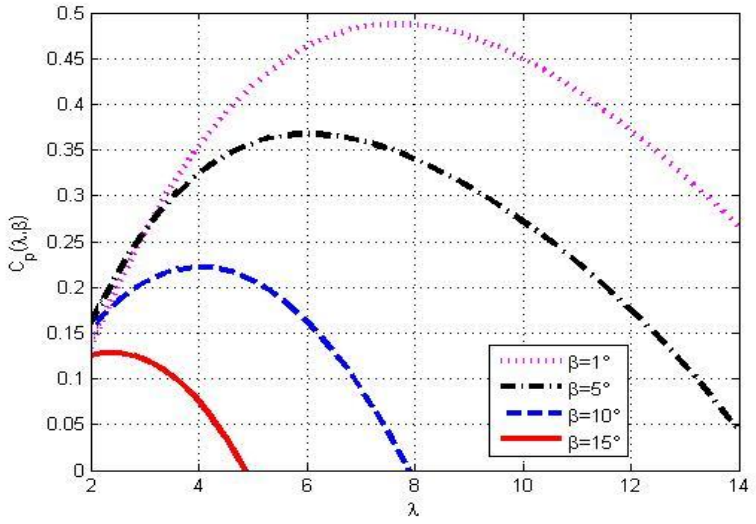

Fig. 3.14: Power coefficient vs tip speed ratio different values of pitch angle

Therefore, it can be concluded that to optimize the amount of power captured by wind turbine, the rotor speed and the pitch angle must be controlled. Thus, a reference speed

ω^* is generated based on the electric power P_e for maximum power tracking. The reference speed is generated by keeping the speed at 1.2 pu, when electric power is above 75% and when the power is reduced below 75% then it is expressed by:

$$\omega^* = -0.67\,P_e{}^2 + 1.42\,P_e + 0.51 \tag{3.47}$$

Then, the generator speed is controlled by a PI controller that has an output value P_ω^*, given by:

$$P_\omega^* = K_P(\omega^* - \omega_e) + K_I \int (\omega^* - \omega_e)\,dt \tag{3.48}$$

The frequency support to the grid, the so-called inertial control, must be added to system. Actually, this controller adds to the power reference output signal given by:

$$P_f^* = -K_{df}\frac{d\Delta f}{dt} - K_{pf}\Delta f \tag{3.49}$$

Where K_{df} & K_{pf} are constants and are chosen as weights to the frequency deviation derivative and frequency deviation respectively. By this inertial control mechanism, there is an extra increment in the system inertia, so it supports the frequency variation indirectly [25]. Thus, the total active power reference for wind turbine can be calculated as:

$$P_{f\omega}^* = P_\omega^* + P_f^* \tag{3.50}$$

3.5 Integration of Superconducting Magnetic Energy Storage in AGC

There are some operational constrains associated with the conventional thermal and hydro power plants, e.g. non-availability of required power in response to sudden and increased load demands (other than the energy stored in the generator rotors). The governor system may no longer be able to absorb the frequency oscillations, due to its

slow response. On the other hand, frequency oscillations in a power system can be effectively damped by fast-acting energy storage devices. Energy storage devices allocate the power requirement in response to the sudden changes in load. BES and SMES devices are active power sources with fast response. Few researchers have also explored BES units to improve the AGC in power systems [26], [27]. A fast acting feature of SMES units have led to their application as frequency stabilizers [28]–[33]. Fast acting energy storages can effectively dampen frequency oscillations in a power system, and consequently, they can share the sudden changes in the power requirement.

SMES as energy storage system can charge and discharge very rapidly with high quantities of power within a short span of time. During normal operation, the superconducting coil is charged to a set value from utility grid. When there is a sudden rise in the load demand, then most of the stored energy is released through the Power Conversion System (PCS). Alternatively, when there is a sudden release in the load, the coil immediately gets charged to its full value through the PCS, following which, excess energy is released as system returns to steady state. As soon as system returns to its steady state, the coil returns to its normal charged state [34], [35].

The SMES system includes four parts, i.e. superconducting coil, power conditioning system, refrigeration system and control unit. The power conditioning system incorporates the inverter/rectifier circuit for conversion of AC to DC and vice versa. The charging and discharging of SMES occur through the power conditioning system. Refrigeration system maintains superconducting coil to its critical temperature. Control unit is only responsible for the mode of operation. Schematic diagram of SMES unit is shown in Fig. 3.15.

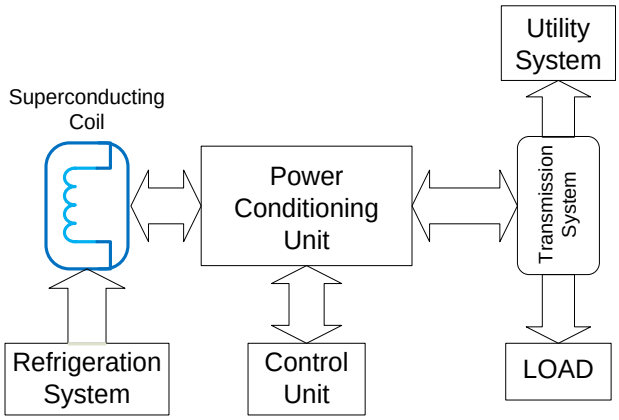

Fig. 3.15 Schematic diagram of SMES unit

3.5.1 SMES modeling for AGC

The block diagram of the SMES unit is shown in Fig. 3.16. SMES is ready to use for AGC, once the rated current is reached in the SMES coil. The ACE_i is the controller input of the SMES unit and U_{smi} is controller output. The controller output applied to the converter and in turn, the converter output is applied to the SMES coil, as described below:

$$\Delta V_{sm}(s) = \frac{1}{1+sT_{dc}} U_{smi}(s) - \frac{K_{sm}}{1+sT_{dc}} \Delta I_{sm}(s) \tag{3.51}$$

The deviation of coil current as voltage is applied to the SMES coil is given by:

$$\Delta I_{sm}(s) = \frac{1}{sL} \Delta V_{sm}(s) \tag{3.52}$$

Finally, the deviation of active power output (ΔP_{sm}) of the SMES unit is described as:

$$\Delta P_{sm} = (I_{sm0} + \Delta I_{sm}) \Delta V_{sm} \tag{3.53}$$

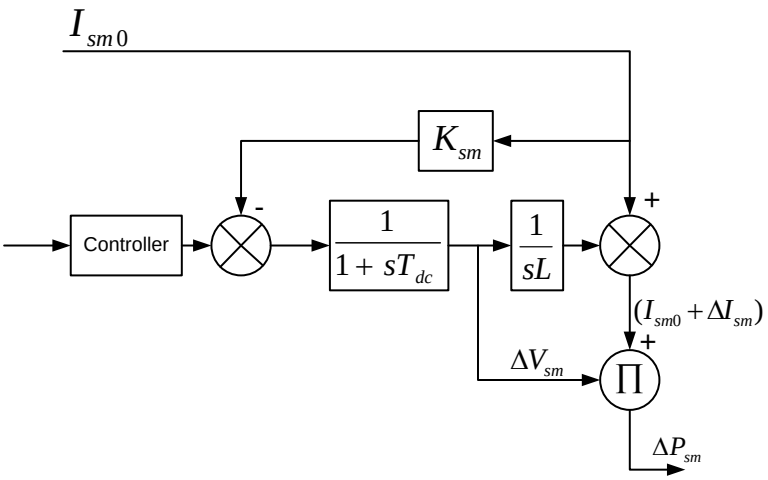

Fig. 3.16: Block diagram of SMES unit

Where,

ΔV_{sm}: Incremental change in SMES voltage

ΔI_{sm}: Incremental change in SMES dc current

T_{dc}: Controller's time constant

K_{sm}: Feedback gain

L: Inductance of SMES coil

I_{sm0}: Initial dc current flow through SMES coil

3.5.2 Operating modes of SMES

Operating mode selection is done by the controller based on inter-area oscillations. The SMES operates in three modes which are (1) charging, (2) discharging and (3) charge sustain mode. During the charging mode, superconducting coil is charged to a set value of charge from the utility grid. In the discharging mode, the stored energy is released. Whenever there is a sudden release in the load, the SMES comes into a charging mode

and it immediately gets charged to its full value. As soon as system returns to steady state, the SMES returns to a charge sustain mode [34], [35].

3.6 Summary

In this chapter, mathematical models of various power system components are discussed and later, these components are intergrated to form a closed loop single area system with primary as well as secondary control. Further, two area system models have been developed with and without deregulated environment. For a two-area power system, the area control error and scheduled tie line power flow equations are presented. Governor dead band has been considered as nonlinearity. The wind power generating system model and superconducting magnetic energy storage system for frequency regulation are also modeled with the intent to integrate with two area system for AGC. WPGS model is based on a commercial WPGS and considered a one-mass model for the mechanical drive of the turbine. The modeling of these elements is necessary before entering into the design of AGC.

References

[1] S. K. Jain, S. Chakrabarti, and S. N. Singh, "Review of load frequency control methods, Part-I: Introduction and pre-deregulation scenario," in *International Conference on Control, Automation, Robotics and Embedded Systems (CARE)*, 2013, pp. 1–5.

[2] P. Kundur, *Power System Stability and Control*. New York: McGraw-Hill, 2006.

[3] O. I.Elgerd and E. Fosha, "Optimum Megawatt-Frequency Control of Multiarea Electric Energy Systems," *IEEE Trans. Power Appar. Syst.*, vol. PAS-89, no. 4, pp. 556–563, 1970.

[4] R. D. Christie and A. Bose, "Load Frequency Control Issues In Power System Operations After Deregulation," *IEEE Trans. power Syst.*, vol. 11, no. 3, pp. 1191–1200, 1996.

[5] Loi Lei Lai, *Power System Restructuring and Deregulation: Trading , Performance & Information Technology*. John Wiley & Sons Ltd., 2001.

[6] M. Parida and J. Nanda, "Automatic Generation Control of a Hydro-Thermal System in Deregulated Environment," in *International Conference on Electrical Machines and Systems ICEMS 2005*, 2005, pp. 942–947.

[7] P. Bhatt, R. Roy, and S. P. Ghoshal, "Optimized multi area AGC simulation in restructured power systems," *Int. J. Electr. Power Energy Syst.*, vol. 32, no. 4, pp. 311–322, May 2010.

[8] H. Gozde and M. C. Taplamacioglu, "Automatic generation control application with craziness based particle swarm optimization in a thermal power system," *Int. J. Electr. Power Energy Syst.*, vol. 33, no. 1, pp. 8–16, Jan. 2011.

[9] S. C. Tripathy, G. S. Hope, and O. P. Malik, "Optimisation of load-frequency control parameters for power systems with reheat steam turbines and governor deadband nonlinearity," in *IEE Proceedings C Generation, Transmission and Distribution*, 1982, vol. 129, no. 1, pp. 10–16.

[10] J. Ekanayake and N. Jenkins, "Comparison of the Response of Doubly Fed and Fixed-Speed Induction Generator Wind Turbines to Changes in Network Frequency," *IEEE Trans. Energy Convers.*, vol. 19, no. 4, pp. 800–802, 2004.

[11] B. Rabelo and W. Hofmann, "Optimal active and reactive power control with the doubly-fed induction generator in the MW-class wind-turbines," in *Proceedings of 4th IEEE International Conference on Power Electronics and Drive Systems. IEEE PEDS 2001*, 2001, vol. 1, pp. 53–58.

[12] J. G. Slootweg, S. W. H. De Haan, H. Polinder, and W. L. Kling, "General Model for Representing Variable Speed Wind Turbines in Power System Dynamics Simulations," *IEEE Trans. power Syst.*, vol. 18, no. 1, pp. 144–151, 2003.

[13] G. Lalor, J. Ritchie, S. Rourke, D. Flynn, and M. J. O'Malley, "Dynamic frequency control with increasing wind generation," *IEEE Power Eng. Soc. Gen. Meet. 2004*, pp. 1–6, 2004.

[14] R. G. De Almeida and J. A. P. Lopes, "Participation of Doubly Fed Induction Wind Generators in System Frequency Regulation," *IEEE Trans. power Syst.*, vol. 22, no. 3, pp. 944–950, 2007.

[15] A. Mullane and M. O. Malley, "The Inertial Response of Induction-Machine-Based Wind Turbines," *IEEE Trans. Power Syst.*, vol. 20, no. 3, pp. 1496–1503, 2005.

[16] D. S. Zinger and E. Muljadi, "Annualized wind energy improvement using variable speeds," *IEEE Trans. Ind. Appl.*, vol. 33, no. 6, pp. 1444–1447, 1997.

[17] J. Fletcher and J. Yang, "Introduction to Doubly-Fed Induction Generator for Wind Power Applications," in *Paths to Sustainable Energy*, INTECH Open Access Publisher, 2010, pp. 259–278.

[18] Z. S. Zhang, Y.-Z.Sun, J.Lin, and G.-J.Li, "Coordinated frequency regulation by doubly fed induction generator-based wind power plants," *IET Renew. Power Gener. Receiv.*, vol. 6, no. 1, pp. 38–47, 2012.

[19] P. Bhatt, R. Roy, and S. P. Ghoshal, "Dynamic participation of doubly fed induction generator in automatic generation control," *Renew. Energy*, vol. 36, no.

4, pp. 1203–1213, 2011.

[20] N. R. Ullah, T. Thiringer, and D. Karlsson, "Temporary Primary Frequency Control Support by Variable Speed Wind Turbines— Potential and Applications," *IEEE Trans. Power Syst.*, vol. 23, no. 2, pp. 601–612, 2008.

[21] X. Yingcheng and T. Nengling, "Review of contribution to frequency control through variable speed wind turbine," *Renew. energy*, vol. 36, no. 6, pp. 1671–1677, 2011.

[22] F. Gonzalez-Longatt, "Impact of synthetic inertia from wind power on the protection/control schemes of future power systems: Simulation study," *11th Int. Conf. Dev. Power Syst. Prot. 2012. DPSP 2012*, pp. 1–6.

[23] M. Kayikçi and J. V. Milanović, "Dynamic contribution of DFIG-based wind plants to system frequency disturbances," *IEEE Trans. Power Syst.*, vol. 24, no. 2, pp. 859–867, 2009.

[24] N. W. Miller, J. J. Sanchez-gasca, W. W. Price, and R. W. Delmerico, "Dynamic modeling of GE 1.5 and 3.6 mw wind turbine-generators for stability simulations," *GE-Power Syst. energy Consult.*, no. July, pp. 1977–1983, 2003.

[25] A. Marano, A. Gomez-Exposito, J. L. Martinez Ramos, and J. M. Mauricio, "Frequency Regulation Contribution Through Variable-Speed Wind Energy Conversion Systems," *IEEE Transactions on Power Systems*, vol. 24. pp. 173–180, 2009.

[26] K. Chatterjee, "Effect of Battery Energy Storage System on Load Frequency Control under Deregulation," *Int. J. Emerg. Electr. Power Syst.*, vol. 12, no. 3, pp. 1–23, 2011.

[27] S. Banerjee, J. K. Chatterjee, and S. C. Tripathy, "Application of Magnetic Energy Storage unit as Load-Frequency Stabilizer," *IEEE Trans. Energy Convers.*, vol. 5, no. 1, pp. 46–51, 1990.

[28] K. R. Sudha and R. Vijaya Santhi, "Load Frequency Control of an Interconnected Reheat Thermal system using Type-2 fuzzy system including SMES units," *Int. J. Electr. Power Energy Syst.*, vol. 43, no. 1, pp. 1383–1392, Dec. 2012.

[29] P. Bhatt and R. Roy, "Dynamic Active Power Support by Doubly Fed Induction Generator for Frequency Control," in *International Conference on Probabilistic Methods Applied to Power Systems (PMAPS)*, 2010, pp. 131–136.

[30] S. C. Tripathy, R. Balasubramanian, and P. S. Chandramohanan Nair, "Small rating capacitive energy storage for dynamic performance improvement of automatic generation control," in *IEE Proceedings C Generation, Transmission and Distribution*, 1991, vol. 138, no. 1, pp. 103–111.

[31] M. Park, G.-H. Kim, A.-R. Kim, H.-M. Kim, I.-K. Yu, and S. Heo, "SMES application for frequency control during islanded microgrid operation," *Physica C: Superconductivity*, vol. 484. pp. 282–286, 2012.

[32] A. Demirören, H. L. Zeynelgil, and N. S. Sengor, "Automatic generation control for power system with SMES by using neural network controller," *Electr. Power Components Syst.*, vol. 31, no. 1, pp. 1–25, 2003.

[33] S. C. Tripathy and B. Bak-Jensen, "Automatic generation control of multi-area power system with superconducting magnetic storage unit," in *2001 IEEE Porto Power Tech Proceedings*, 2001, vol. 3, pp. 1–6.

[34] S. C. Tripathy and K. Juengst, "Sampled data automatic generation control with superconducting magnetic energy storage in power systems," *IEEE Trans. Energy Convers.*, vol. 12, no. 2, pp. 187–192, 1997.

[35] M. Sheikh, S. Muyeen, R. Takahashi, T. Murata, and J. Tamura, "Improvement of load frequency control with fuzzy gain scheduled SMES unit considering governor dead-band and GRC," in *5th International Conference on Electrical and Computer Engineering, 2008, Dhaka, Bangladesh*, 2008, pp. 1–6.

CHAPTER 4

Control and Optimization Strategies

4.1 Introduction

In the previous chapter, modeling of two area interconnected power system has been done for AGC. WPGA and SMES are also modeled for integrating with system. This chapter aims to develop control and optimization strategies for AGC of interconnected power system. Designing a supplementary controller based on intelligent techniques and control methodologies is a challenging task for power engineers. In order to design controller, objective function as well as optimization technique are needed to be selected.

4.2 Development of Supplementary Controller for Interconnected Power System

The increasing complexity and size of electric power system as well as increasing power demand has made the situation more complex and challenging. In each area, supplementary controller monitors the system frequency and tie-line power flows and based on these changes, the output of the generators within the area will be reset. As ACE is driven to zero, both frequency and tie-line power errors will be forced to zeros. This supplementary controller is viewed as a supervisory control function for matching the generation to the load demand.

Generally, supplementary controller comprises of a conventional controller such as, integral controller, PI controller and PID controller. Even when these controllers are employed in an interconnected power system, the system performance does not improve significantly. This is because fixed gain controllers are no longer suitable for frequently changing loads, especially when the numbers of interconnections are increased and non-

linearities are employed, the situation become worse. Different approaches used for supplementary control are as follows.

4.2.1 Classical controllers

Proportional Integral (PI) and proportional integral derivative (PID) controller are the classical controllers that are widely used in modern industrial control system [1]. The PI controllers are used to improve the dynamic response as well as to eliminate the steady state error while derivative controller adds to improve the transient response [2].

4.2.1.1 Proportional integral derivative controller

In the last few decades, the PID controller is utilized extensively for industrial processes because of their robustness and simplicity. The transfer function of the standard PID controller (is also known as the "three-term" controller) [3], is given by,

$$U(s) = K_p + \frac{K_i}{s} + K_d s \tag{4.1}$$

or

$$U(s) = K_p(1 + \frac{1}{T_i s} + T_d s) \tag{4.2}$$

where K_p is the proportional gain, K_i is the integral gain, K_d is the derivative gain, T_i is the integral time constant and T_d is the derivative time constant.

PID controller combines the effect of proportional, derivative and integral components on the closed loop response of system.

1. In case of the proportional term, while time response improves, there is an offset between the output response and desired response. This offset can be reduced by increasing the proportional gain, but this may lead towards oscillatory results.

2. When an integral term is considered, it reduces the steady state error to zero. Increasing the integral gain may tend to make system response more oscillatory and may even possibly become unstable.

3. The derivative term improves the transient response and reduces settling time. It also improves the stability of the system.

Suitable combinations of proportional, integral and derivative terms give the desired performances e.g. fast response, less peak overshoot, and undershoot elimination of steady state error. Controller parameters are tuned such that the closed-loop control system is stable and meets user defined objectives. There are different types of tuning methods for the PID controller based like analytical methods, heuristic methods, objective based optimization methods and frequency based methods. In this work, there are mainly two methods used for obtaining PID parameters first is classical approach where Ziegler-Nichols tuning method is used the second is different objective function based optimization technique.

Ziegler-Nichols tuning method

Most of conventional tuning methods are empirical based methods. Analytical methods are based on the mathematical model of system. But, accurate modeling of a system is a tedious task. The Ziegler–Nichols (ZN) tuning method for PI and PID controller is one of the most popular, methods. The ZN method is a heuristic approach to tune PI and PID

Controllers. This method is based on the selection of proper values of the proportional gain at which sustained oscillations occur, from which the ultimate gain K_u and oscillation period T_u are obtained [4]. The gain values of PI and PID controller, calculated from K_u and T_u, are obtained from Table 4.1

Table 4.1: Ziegler–Nichols (ZN) tuning method for PI and PID controller

PI Controller Gains		**PID Controller Gains**	
K_p	0.45 K_u	K_p	0.60 K_u
K_i	1.2 Kp/ T_u	K_i	2 Kp/ T_u
		K_d	$K_p T_u/8$

4.3 Selection of Objective Function and Optimization Techniques for AGC

Optimization techniques determine the best-suited solution for a defined problem. In mathematics, optimization may refer to finding either minimization or maximization of a mathematical function. Most of the real word problems cannot be solved using classical optimization methods. Hence, stochastic methodologies can become a favorable optimization method for finding near optimal solutions of complex or ill-defined optimization problems. These stochastic optimization methods are mostly based on the natural concepts. A stochastic approximation of a global optimum is, probably, more valuable than a deterministic local minimum provided by a classical method. Another advantage of these stochastic methods is that they are easy to implement. In this work, three different stochastic optimization methods are being considered, which are genetic algorithm (GA), ant colony optimization (ACO) and particle swarm optimization (PSO).

4.3.1 Objective function selection

When the system is complex and non-lineraties are added, then the classical methods like ZN methods may produce high oscillatory results. To overcome these difficulties, objective function based optimization methods have to be used. In this work, PID controller gains are selected in such a way that the closed loop systems give the desired response. The desired response should have a fast response and lesser overshoot, undershoot, steady state error, settling time. The PID controller gains can be obtained by minimizing one of the following standard error functions, where error e(t) is difference between the reference input and the measured variable.

$$J_{IAE} = \int_0^T (|e(t)|dt \tag{4.3}$$

$$J_{ISE} = \int_0^T (e(t)^2)dt \tag{4.4}$$

$$J_{ITAE} = \int_0^T t|e(t)|dt \tag{4.5}$$

$$J_{ITSE} = \int_0^T t(e(t)^2)dt \tag{4.6}$$

where T is simulation time.

Several other objective functions are also used to get the optimum performance of the two area interconnected power system in this thesis. These objective functions are based on either overshoot, undershoot or settling time and their combinations, these are given below:

$$J_{Obj1} = \int_0^T (PeakUndershoot(e(t))dt \tag{4.7}$$

$$J_{Obj2} = \int_0^T (SettlingTime(e(t))dt \tag{4.8}$$

$$J_{Obj3} = \int_0^T (PeakOvershoot(e(t) + a * PeakUndershoot(e(t))dt \tag{4.9}$$

$$J_{Obj4} = \int_0^T (PeakUndershoot(e(t) + a * SettlingTime(e(t))dt \quad (4.10)$$

$$J_{Obj5} =$$

$$\int_0^T (PeakOvershoot(e(t) + a * PeakUndershoot(e(t) + b * SettlingTime(e(t))dt \quad (4.11)$$

Implementation of these methods can be done by modern stochastic optimization techniques e.g. GA, ACO, and PSO. The formulation of the objective function is the critical part for finding the optimal solution, which is designed in such way that is desired to minimized or maximized.

4.3.2 Genetic algorithm

GA is an optimization algorithm based on the natural genetic mechanism, capable of finding optimal solutions. GA is a powerful optimization algorithm for the systematic tuning of controller. GA is an iterative procedure, where the size of the population is fixed in every iteration [5].

GA optimization process is explained by flow chart shown in Fig. 4.1. The GA optimization technique provides efficient and robust optimization, without realizing the mathematical model of system. Generally, it converges at a much faster rate, as compared to the conventional optimization techniques [6].

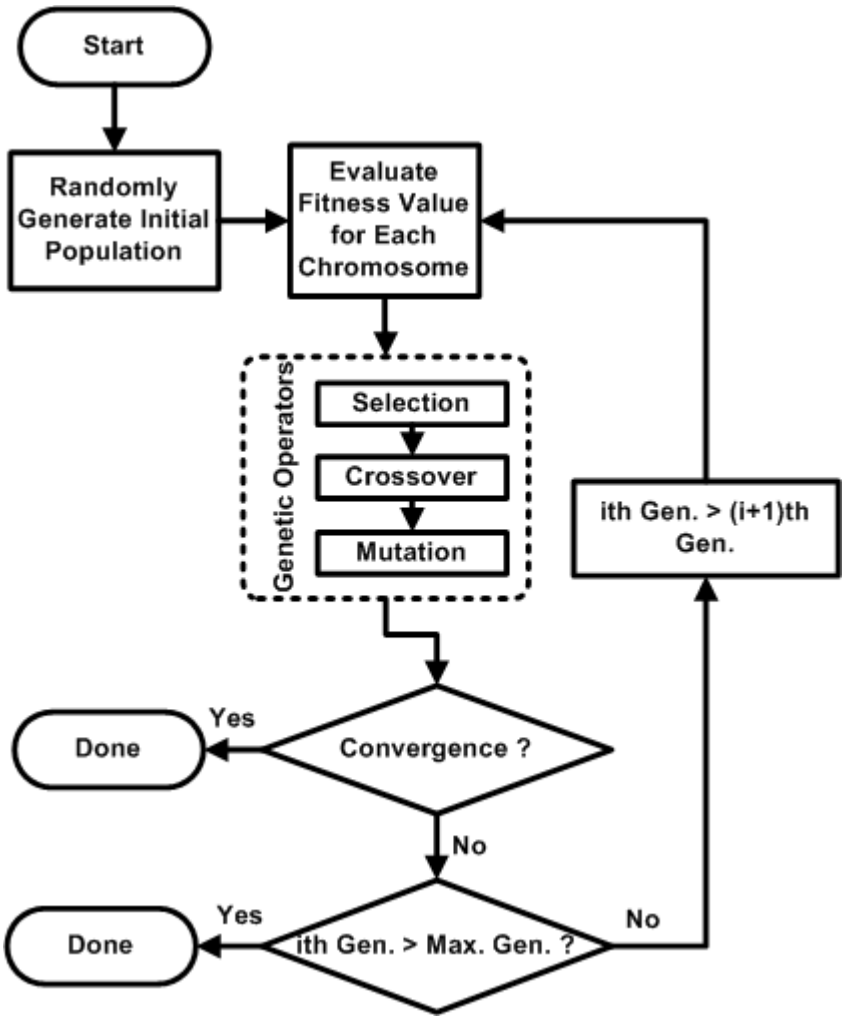

Fig. 4.1: Flowchart of GA

GA is an iterative procedure, where a constant population size is maintained in every iteration. GA utilizes the different genetic operators for the improvement of fitness of the individual population solution. These genetic operators are selection, crossover, mutation and elite, respectively. By utilizing these different genetic operators, GA improves the fitness of individual population solution. Initially a fixed number of random solutions are generated, than during the successive iterations by genetic operators, a new population, consisting of the same number of solutions with improved fitness, is generated. At the selection process, each solution of the population is evaluated by its fitness value, which is

provided by the user defined objective function. In the crossover process, pairs of selected solution are chosen by a defined method to generate new solutions. In the mutation process, the selected solution is randomly altered with a small probability, which helps to prevent the GA being trapped in a local optimal solution. In this work, GA optimization method is used for the optimization of a PID controller for an interconnected thermal-hydro power system models.

4.3.3 Ant colony optimization

ACO is a popular meta-heuristic optimization technique. It is inspired from the foraging behavior of ants, which are able to find the shortest route between their nest and a food source. This stigmergic behavior of ants allows them to communicate indirectly by depositing pheromone. Pheromone is an odorous chemical substance that ants deposit and smell while walking. After an ant has found a solution, it dies. The finest solution is found by a global cooperation among ants in a colony. They complete the tour by selecting nodes according to the state transition rule. Ants prefer those paths which are short and have high quantities of pheromone [7].

ACO is efficiently able to search the finest solution. Self organizing behavior of ants converges to one path. As ants move from one node to another node, the amount of pheromone deposit is proportional to the quality of solution as per the local pheromone updating rule. Once a tour is finished, the amount of pheromone is updated again as per the global updating rule. In this rule, the quantity of pheromone deposited on those nodes provides the available best solution up to the current iteration. To find optimum solution of any problem, search space is needed to be broken in discrete search space, where search space of each candidate solution represented by one cave and all potential solutions

represented by different caves, e.g. for PID controller optimization there will be three caves, cave 1 is for K_p, cave 2 for K_i and cave 3 for K_d gains respectively. Within cave these will be different nodes, each ant chose only one node in each cave to complete its path, as shown in Fig. 4.2.

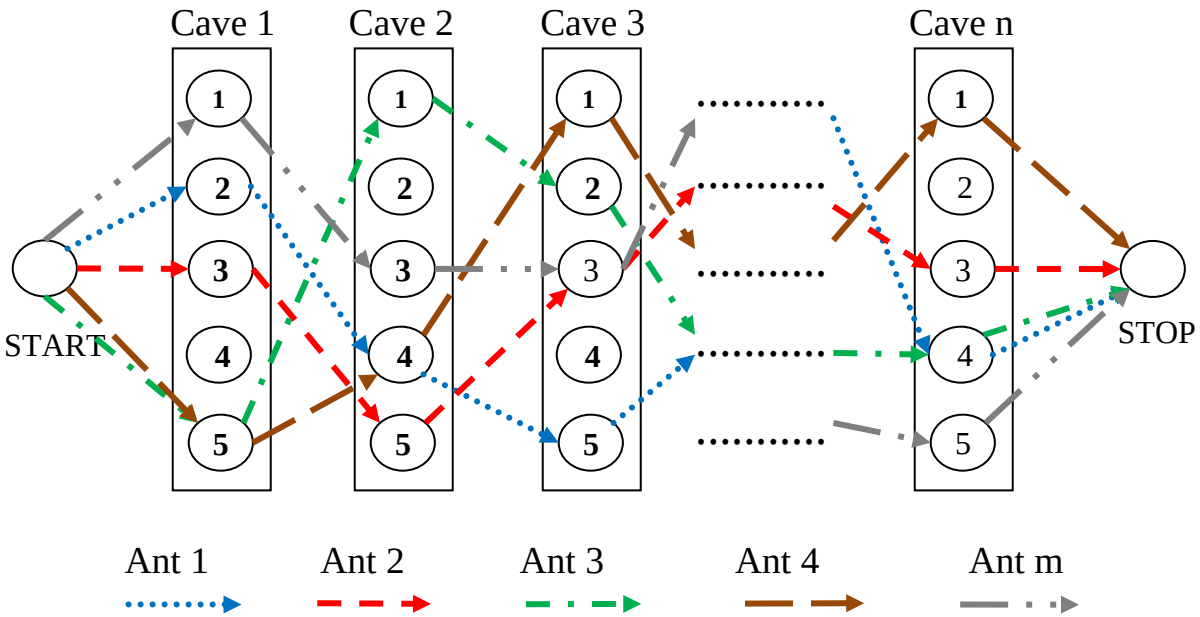

Fig. 4.2: Selection of nodes from different caves to complete path

When ants complete the global pheromone updating rule, a fraction of pheromone evaporates and each ant further deposits a quantity of pheromone proportional to fitness value. This complete process is iterated up to convergence. Local pheromone updating rule avoids early stagnation [8].

ACO optimization process is explained by pseudo code, as shown below:

Pseudo Code for ACO

```
1: Initialize no. of iterations, no. of ants and set up ACO parameters;
2:      Do while (stopping criteria is not met)
3:              Set ants on initial node
4:                      Place these ants to nodes selected based on probabilistically
5:              Complete tour
6:              Evaluate fitness value of all ant by fitness function
7:              Update pheromone
8:              Evaporate pheromone
9:      End Do
```

ACO optimization is also explained by flowchart in Fig. 4.3.

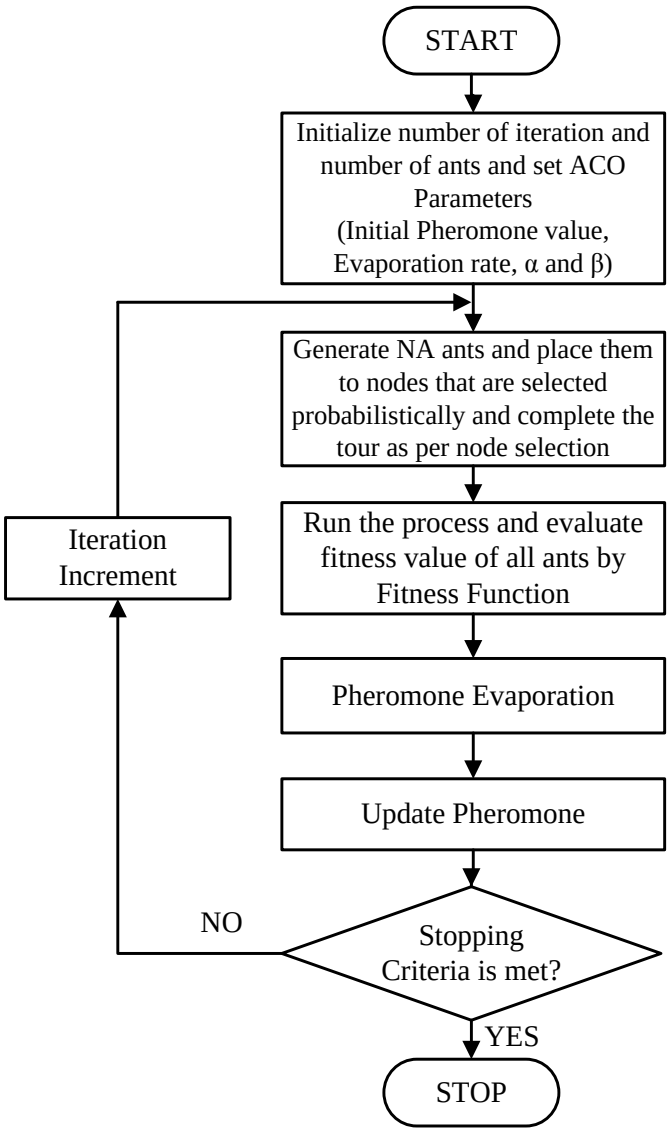

Fig. 4.3: ACO flowchart

The Selection of nodes is based on random proportional rule. Probability determines which adjacent node an ant situates at time *(t),* as shown in (4.13). Where factor α and β determine the relative influence of pheromone value and heuristic value on the selection of next node. η_{ij} is the inverse of the difference of objective function that ant *k* in node *i* choose node *j* to move to, which is defined by,

$$\eta_{ij} = \frac{1}{(f(x_j) - f(x_i))} \tag{4.12}$$

$$p_{ij}^{a}(t) = \begin{Bmatrix} \frac{[\tau_{ij}]^{\alpha}[\eta_{ij}]^{\beta}}{\sum_{n \epsilon N^a}[\tau_{in}]^{\alpha}[\eta_{in}]^{\beta}}; & if\ j \epsilon N^a \\ 0; & otherwise \end{Bmatrix} \tag{4.13}$$

τ_{ij}^{a}: Pheromone amount deposited at *ij* edge
α: Parameter to control influence of pheromone trace
β: Parameter to control influence of visibility value
N^a: All feasible nodes in neighborhood for *a* ant
When η_{ij} is ignored for selection of next node than (4.13) modified, as shown below:

$$p_{ij}^{a}(t) = \begin{Bmatrix} \frac{[\tau_{ij}^{a}]}{\sum_{n \epsilon N^a}[\tau_{in}^{a}]}; & if\ j \epsilon\ N^a \\ 0; & otherwise \end{Bmatrix} \tag{4.14}$$

Ants make the next move according to this possibility equation. After every move, amount of pheromone trace is updated, as:

$$\tau_{ij}(t+1) = (1-\rho)\ \tau_{ij}(t) \tag{4.15}$$

ρ: Evaporation rate (*0<ρ<1*)

$$\tau_{ij}(t+1) = \tau_{ij}(t) + \sum_{a=1}^{NA} \Delta\tau_{ij}^{a} \tag{4.16}$$

$\Delta\tau_{ij}^{a}$ shows the amount of pheromone trace left by a^{th} ant at *ij* edge

$$\Delta\tau_{ij}^{a} = \begin{Bmatrix} \frac{L^{min}}{L^{a}}; & \\ 0; & otherwise \end{Bmatrix} \tag{4.17}$$

L^{min} : Best Fitness value found up to last iteration

L^a: Fitness value found by a^{th} ant
$\Delta\tau_{ij}^a$: Amount of pheromone left by each a^{th} ant at ij edge
NA: Total numbers of ant

4.3.4 Particle swarm optimization

PSO algorithm was first given by Kennedy and Eberhart in 1995 [9], is a stochastic heuristic population based optimization method, which is based on swarm intelligence. It originated from the idea coming from research on birds and fish flock movement behavior. This algorithm is widely used for many applications because of its easy implementation and the fact that only few parameters need to be tuned. It converges to a global solution within a faster time in comparison to other stochastic optimization methods like GA and simulated annealing.

The basic idea of the PSO is that when birds are moving in search of food from one place to another, there is always one bird that moves very close to the food or has information about good food. Then, other birds eventually flock to the place where food can be found and their movement is inspired by their own best known position as well as the best known position of the flock. As far as the PSO algorithm is concerned, each bird position is compared to the best known position of the swarm and also to its own best known position. The birds' next move from place to place is root for development of the solution and a good position is equal to the most optimized solution.

PSO algorithm consists of 'n' particles that represent potential solutions. Each particle is represented by its current position 'x' and current velocity 'v' in an 'm' dimensional space. Wherever there is an iterative process, the position gets updated based on the following rules:

1. Inertia
2. Best known individual position
3. Best known swarm position

$$v_i^m(iter+1) = w * v_i^m(iter) + c_1 * R_1 * \left(pbest_i^m(iter) - x_i^m(iter)\right) + c_2 * R_2 * \left(gbest^m(iter) - x_i^m(iter)\right) \quad (4.18)$$

$$x_i^m(iter+1) = x_i^m(iter) + v_i^m(iter+1) \quad (4.19)$$

Where,

$iter$	Iteration number
i	Particle index
m	Dimension
v_i^m	Velocity of i^{th} particle in m^{th} dimension
x_i^m	i^{th} particle position in m^{th} dimension
$gbest^d$	Swarm global best position in m^{th} dimension
$pbest_i^d$	Particle best position of i^{th} particle in m^{th} dimension
w	Momentum
c_1, c_2	Acceleration constants
R_1, R_2	Random numbers with uniform distribution [0, 1]

Flowchart of PSO optimization is presented in Fig. 4.4.

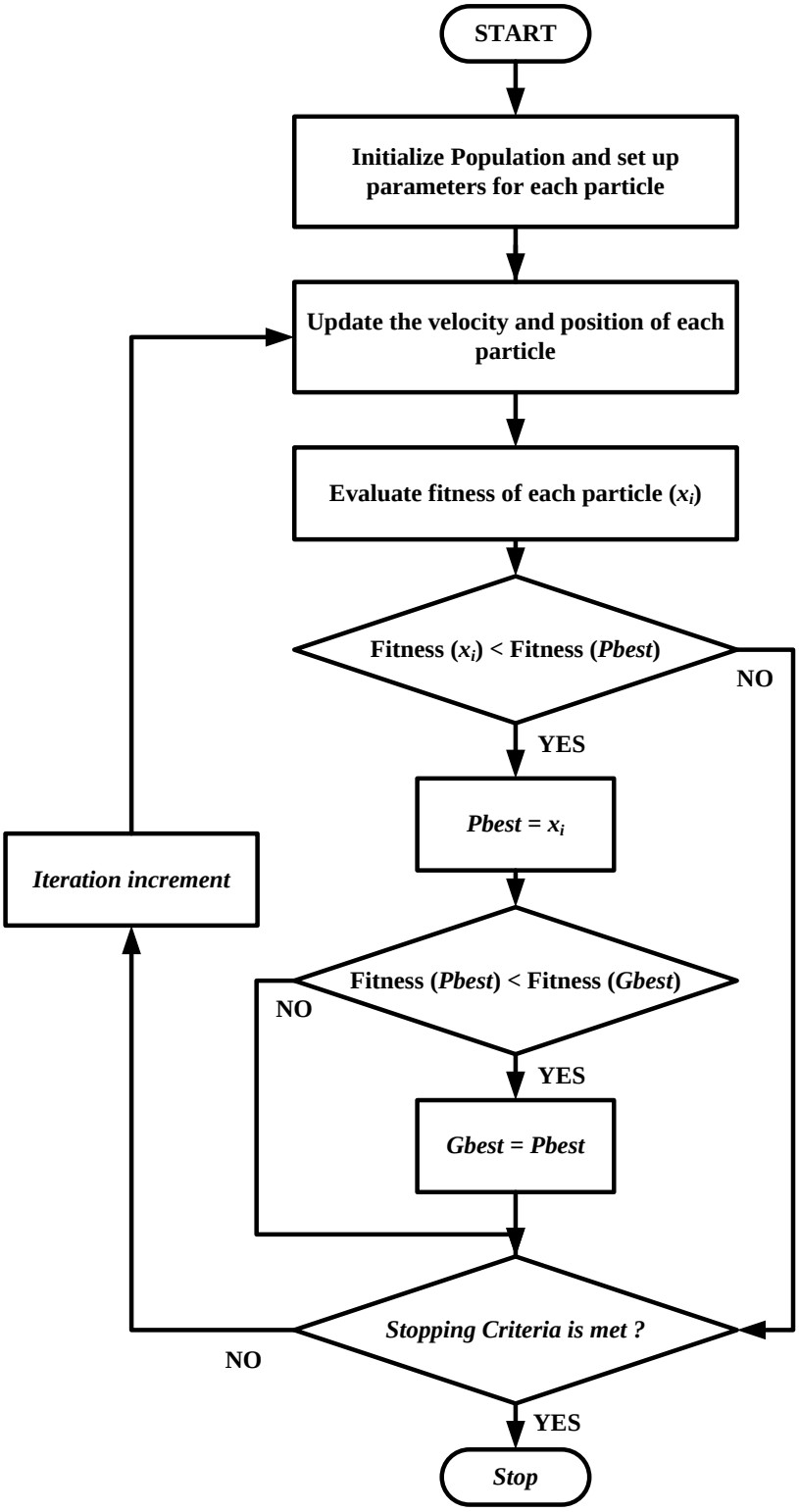

Fig. 4.4 PSO flowchart

Pseudo code for PSO

```
1: Initialize population and set up parameters for each particle;
2: while iter < max_iteration do
3:       for each particle i do
4:             Update the velocity v_i and position x_i using (4.18) & (4.19) respectively;
5:             Evaluate the fitness on the updated x_i of particle i;
6:             if f(x_i) < f(P_best) then
7:                   P_best = x_i ;
8:                   if f(P_best) < f(G_best) then
9:                         G_best = P_best ;
10:                  end if
11:            end if
12:      end for
13:      iter = iter + 1;
14: end while
```

4.3.5 Different variants for PSO

After the initial development of the PSO by Kennedy and Eberhart, several variants of the PSO algorithm have been proposed by researchers [10]–[18]. Various inertia weighting strategies as well as acceleration-constant weighting strategies have been developed. These strategies monitor the situation of the particles in the search space and based on a feedback parameter, weights are adjusted.

For all the algorithms, upper and lower bounds of the PID controller gain values have been set by keeping 1.5 times and 0.1 times of Zeigler Nichols method based gain values. This step is essential because if the gain values of PID controller are out of bounds, it would lead to instability of the system. In this work, the swarm size has been taken as 20 and the number of iterations has been taken as 200. Accelerating constant C_1 and C_2 were taken as 1.2 and 0.12 respectively and positions and velocities were randomly initialized.

4.3.5.1 Algorithm 1 – success rate

Nickabadi, Ebadzadeh and Safabakhsh [10] first delineated two situations occurring during the course of a PSO. Both cases initially consider two particles, but can be extrapolated for many particles. The first situation is where both the particles are far from the optimum but close to each other. This necessitates a larger velocity to ensure fast convergence to the optimum. In the second situation, the two particles are near the optimum, but are far from each other. A large inertia weight in later case would lead to oscillations about the optimum without convergence, requiring a smaller velocity of particles. With these two cases, they have described 'near' and 'far' from optimum differently from what is used conventionally. A particle close to the optimum but with high velocity will take time in reaching optimum point and hence, is considered to be far [10]. Not considering the particles' fitness value as a direct feedback factor in determining inertia weight, they instead proposed a percentage success method for evaluating inertia weight. A high success rate is an implication that the particles have converged at one point and are moving towards the global optimum together. This falls under the first scenario and requires a larger velocity and hence, a larger inertia weight. A low success rate means that the particles are moving about the optimum but not converging at it. A smaller velocity would help in faster convergence. As a result, the inertia weight is varied as a direct factor of the success percentage '$S(i,t)$' for each particle.

$$S(i,t) = \begin{cases} 1 & if\ F\left(pbest_{i,(t)}\right) < F\left(pbest_{i,(t-1)}\right) \\ 0 & otherwise \end{cases} \quad (4.20)$$

$$Ps = \frac{\sum_{i=1}^{n} S(i,t)}{n} \quad (4.21)$$

'*Ps*' is the percentage of particles that have a fitness values better than the previous iterations. The inertia weight is then updated as a linear function of '*Ps*'.

$$w = (w_{\max -} w_{\min})Ps + w_{\min} \quad (4.22)$$

In this work, w_{max} and w_{min} have been taken 0.9 and 0.4 respectively.

4.3.5.2 Algorithm 2– evolution speed and aggregation degree factors

Yang et al. [11] proposed an adaptive weight strategy using the evolution speed factor and aggregation. Bergh et al. [12] discussed two definitions of convergence was that all the particles assume the same value as time tends to infinity and the second was that global best values of iterations tend to a final overall global best value at infinite time. They further said that the classical PSO follows the first definition and to satisfy it, the velocity of particles becomes zero which leads to the optimization process being stuck in the local optima. The motivation behind the new adaptive method is to ensure that when the optimum solution is close by, it is vital to slow down the particles and allow them to perform an intensive search. If the particles do not near the optimum solution, they need to spread out and cover larger areas of the search space. The evolutionary speed and the aggregation degree factor as follows were proposed to include this.

Evolutionary speed factor:

$$h_{it} = \left| \frac{\min(F(pbest_{i,(t-1)}, pbest_{i,(t)})}{\max (F(pbest_{i,(t-1)}, pbest_{i,(t)}))} \right| \quad (4.23)$$

where $\mathrm{pbest}_{\mathrm{i,(t)}}$ is the local best fitness of the i^{th} particle till the t^{th} iteration. For every dimension, the value of 'h_{it}' remains the same because the fitness values are common across all dimensions. This factor keeps into account the previous runs of each particle. A smaller value of 'h_{it}' would imply that the particles' new velocity is greatly different from its previous velocity, so the particles move faster, in this case. For the purpose of our paper, the fitness values are of the same sign, so, the modulus sign can be discarded.

The aggregation degree factor:

$$s_{(t)} = \left| \frac{\min (Fbest_{(t)}, Favg_{(t)})}{\max (Fbest_{(t)}, Favg_{(t)})} \right| \quad (4.24)$$

Where $\mathrm{Favg}_{\mathrm{(t)}}$ is the average of all the fitness values in the t^{th} iteration and $\mathrm{Fbest}_{\mathrm{(t)}}$ is the best fitness value (minimum fitness value) among all the fitness values in that iteration. Note that this value is different from the global best fitness value because the latter is applicable from the first to the t^{th} iteration, but the former applies only to the t^{th} iteration. If this value is nearing one, it means the average fitness values are nearing the minimum of that particular iteration, and there is a risk of having particles stuck in local optima. As a result, a higher value of $s_{(t)}$ would necessitate a larger value of velocity to prevent local trapping. If this value is smaller, it is necessary to slow down the particles and perform a more intensive search in a smaller area.

With these two factors, Yang et al. [11] was proposed to modify the inertia weight as a function of evolutionary speed factor 'h_{it}' and aggregation degree factor '$s_{(t)}$' is:

$$w_{i,(t)} = win_i - \propto \left(1 - h_{i,(t)}\right) + \beta s_{(t)} \quad (4.25)$$

Where ∝ and β are two constants, in the range of [0,1] in our work a fixed value 0.2 have been taken for both.

4.3.5.3 Algorithm 3– global-local best inertia weight

Kennedy and Eberhart discussed the five principles of swarm intelligence, are proximity principle, the quality principle, the principle of diverse response, the principle of stability and the principle of adaptability [13]. Arumugam and Rao [14] compared the constant inertia weight strategy and linearly decreasing inertia weight strategy with their proposed method. Then, they proposed an algorithm that takes global and local best fitness values into account, satisfying the above principles also. The modification is

$$w = 1.1 \ - \frac{F(gbest)}{F(avg(pbest_i))} \quad (4.26)$$

$$F(avg(pbest_i\ )) = \frac{\sum_{i=1}^{n} F(pbest_i)}{n} \quad (4.27)$$

This inertia weight is used for all the particles in a single iteration and gets updated with the global best and local best fitness values. A greater difference in global and local fitness values will imply that particles are not close to the global best and it will result in a larger value of inertia weight. This will facilitate a larger search space to be searched due to an increase in velocity. When the average of the fitness values of the particles is near the global best fitness value, the search becomes more concentrated and the inertia weight is lowered. Having the ratio subtracted from 1.1 ensures that the inertia weight never becomes zero, even in case when the global best fitness value equals the average value. This inertia weight is then incorporated in the velocity equation. However, there

could be a possible problem that arises by adopting this method. This method does not have a way of jumping out of the local optima, in case the particles get stagnated. This is evident from the formula where once the particles achieve a fitness value similar to the global best, the inertia weight ceases to change drastically. This can lead to premature convergence if the global optimum is not actually the minimum value of the objective function.

4.3.5.4 Algorithm 4 – distance from global best

An adaptive inertia weight strategy along with a modification in the position-updating equation is proposed in [15] by Suresh et al. In order for particles to not lose explorative ability, it is important to not let them get stuck in the local optima. If the velocity of a particle is small, and the fitness value difference between global best, local best and a particle's current value is not significantly different, then the new velocity updated would change slightly compared to the previous one and this can lead to that particle being stuck in local optima. This can especially happen with the global best particle where the social and cognitive factors of the velocity update equation reduce to zero and inertia weight and velocity get damped quickly, without yet attaining a minimum fitness value. To prevent this from happening, the strategy proposed in the work, is

$$w = w_0\left(1 - \frac{distance_i}{maxdistance}\right) \tag{4.28}$$

$$distance_i = \sqrt{\sum_{d=1}^{D}(gbest_d - x_{i,d})^2} \tag{4.29}$$

$$maxdistance = \max\left(distance_i\right) \tag{4.30}$$

w_0 is a random value in between 0.5 and 1. This ensures that the attraction to the global best will dominate when the particles move farther away from it.

The velocity update equation is given by:

$$x_i = (1 - \rho) x_{i\,(t-1)} + v_i \tag{4.31}$$

ρ is a random value between the range of -0.25 to 0.25. This method prevents loss of diversity by enabling the particles to not lose their explorative ability.

4.3.5.5 Algorithm 5 – fixed inertia weight

In this standard method, a fixed inertia weight parameter introduces into the original PSO method. This algorithm is proposed by Shi and Eberhart in [16].

$$v_{ij(t+1)} = w * v_{ij,t} + c_1\, r_{1ij} \left(pbest_{ij} - x_{ij,t}\right) + c_2\, r_{ij}\, (gbest_j - x_{ij,t}) \tag{4.32}$$

$$x_{ij(t+1)} = x_{ij,t} + v_{ij(t+1)} \tag{4.33}$$

Here, the inertia weight is kept at a constant value 0.9.

4.3.5.6 Algorithm 6 – varying acceleration coefficients

So far, we have seen the inertia weights are being adapted according to different conditions. In [17], Ratnaweera et al. have emphasized on the variation of acceleration coefficients to ensure good explorative and exploitative capabilities. This method has been used in other applications such as congestion management in power systems [18]. As mentioned in the introductory paragraph, c_1 is the cognitive factor and is a representation of particles to its own best solution while c_2 is a social factor which represents a particle's attraction to the global best of the entire swarm. As Kennedy and

Eberhart have discussed in [13], a high cognitive learning factor leads to individual particles moving about randomly in the search space while a high social learning factor can lead to a premature convergence to local optimum. Particles need to explore extensively first and then exploit intensively later. A large cognitive coefficient and a small social factor initially will allow particles to fly about the search space. Lowering the former and increasing the latter over iterations will allow convergence to the optimum solution. For this, c_1 and c_2 are varied in a linear fashion.

$$c_1 = ((c_{1f} - c_{1i}) * iter\ no.\frac{1}{totaliteration}) + c_{1i} \quad (4.34)$$

$$c_2 = ((c_{2f} - c_{2i}) * iter\ no.\frac{1}{totaliteration}) + c_{2i} \quad (4.35)$$

Since c_1 is linearly decreased and c_2 is linearly increased, taking c_{1i} = 2.5, c_{2i} = 0.5, c_{1f} = 0.5 and c_{2f} = 2.5 accomplishes this, together with a constant inertia weight of 0.9.

4.4 Simulation results for different objective functions for different optimization technique

Three different evolutionary algorithms selected for analysis in present study are GA, ACO and PSO. Nine different objective functions are considered with above mentioned optimization techniques to optimize PID controllers for two area interconnected power system. Simulink model of the same is shown in Fig. 4.5. For comparison purposes, the system is simulated for a 0.01 p.u. load disturbance in both areas.

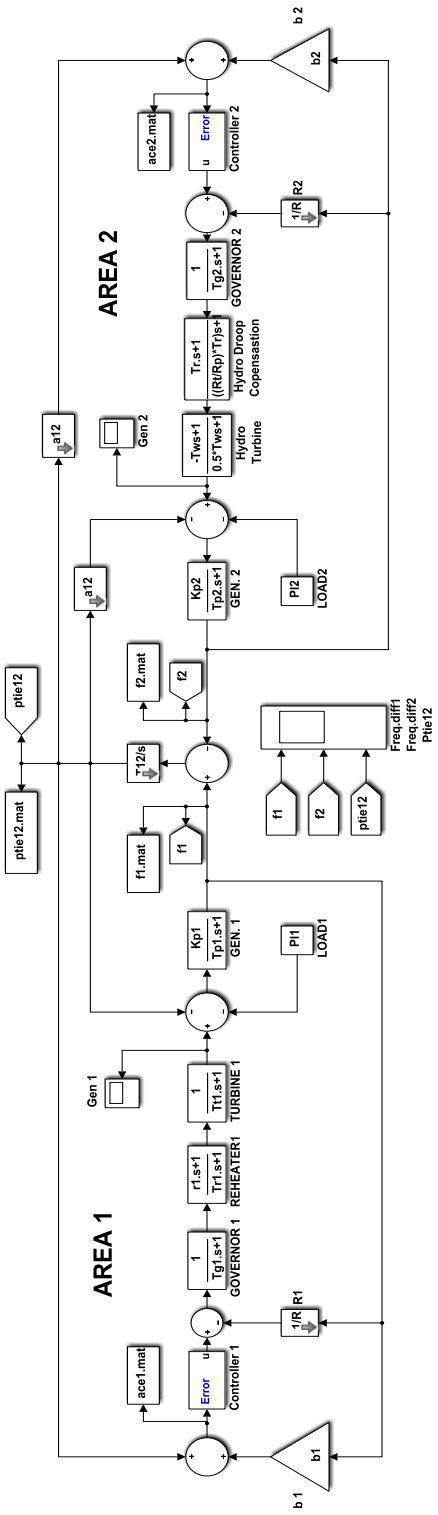

Fig 4.5: Simulink model of AGC for two area hydro-thermal power system

4.4. 1 Simulation results for different objective functions

In order to decide on the objective function, a detailed analysis of different objective functions are carried out based on different performance indices of deviation of frequency of area-1, area-2 and tie-line power. Fig. 4.6, 4.7 and 4.8 show three main performance indices (peak undershoot, peak overshoot and settling time) for deviation in frequency of area-1, area-2 and tie-line power.

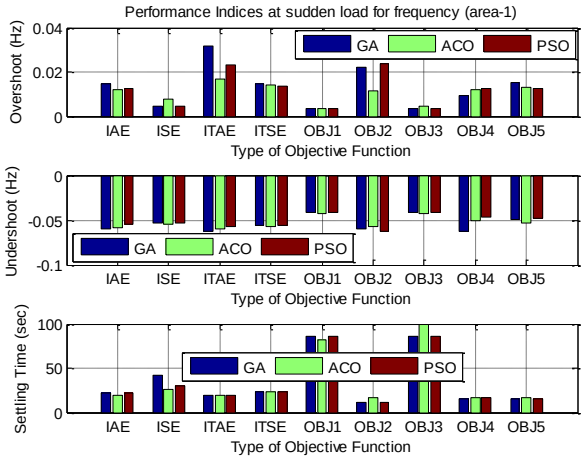

Fig. 4.6: Different performance indices of deviation in frequency of area-1 for different objective functions

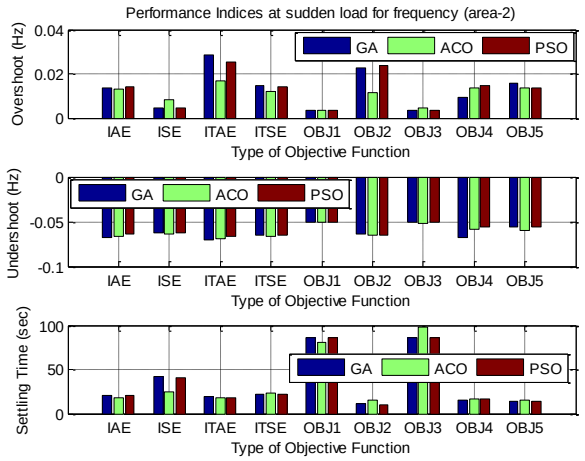

Fig. 4.7: Different performance indices of deviation in frequency of area-2 for different objective functions

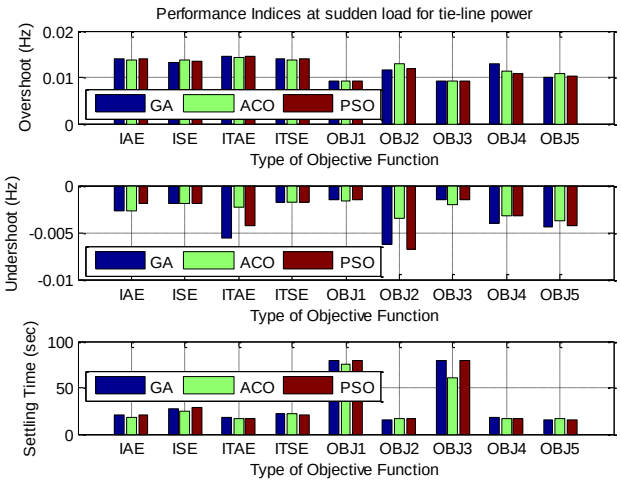

Fig. 4.8: Different performance indices of deviation in tie-line power for different objective functions

In these figures, it is observed that all performance indices are best optimized by OBJ5 objective function. In other objective functions all performance indices are optimized but are not significantly better as compared to proposed OBJ5 objective function. Thus it can be concluded based on these results that proposed OBJ5 objective function is best objective function for optimization.

Table 4.2: Integral based error functions for different objective functions for different optimization techniques

	IAE			**ISE**			**ITAE**			**ITSE**		
	GA	**ACO**	**PSO**	**GA**	**ACO**	**PSO**	**GA**	**ACO**	**PSO**	**GA**	**ACO**	**PSO**
IAE	**2.717722**	**2.729765**	2.642584	0.04583	0.046335	0.042628	14.26161	13.08518	14.55555	0.085913	0.088664	0.082372
ISE	2.895855	2.804775	2.840809	**0.040667**	**0.043162**	**0.040561**	25.1782	19.49448	25.03644	0.097459	0.08949	0.095477
ITAE	2.840031	3.201129	2.676748	0.053095	0.058201	0.04774	**11.26692**	**12.6982**	**11.12938**	0.097268	0.1003	0.089431
ITSE	2.670605	2.821921	**2.64044**	0.043058	0.046129	0.042478	15.28869	15.77973	15.22221	**0.082385**	**0.085899**	**0.081848**
OBJ 1	8.702252	8.478149	8.720647	0.09151	0.089196	0.091602	166.6438	159.7344	167.1653	0.624654	0.595491	0.626657
OBJ 2	4.072025	3.605259	3.664661	0.071151	0.06181	0.064372	18.72061	15.33625	17.98826	0.180987	0.118443	0.172196
OBJ 3	8.697746	7.80773	8.720647	0.091483	0.082132	0.091602	166.5456	140.9006	167.1653	0.624135	0.484248	0.626657
OBJ 4	3.446687	3.974079	4.051631	0.05944	0.061179	0.060193	16.42562	16.13152	16.64284	0.115455	0.116619	0.117579
OBJ 5	4.587036	4.451561	4.361613	0.068917	0.068101	0.065132	19.54165	20.30583	18.79797	0.15364	0.14575	0.141688

Table 4.3: Peak undershoot for different objective functions for different optimization techniques

	Δf1			*Δf2*			*Δptie12*		
	GA	**ACO**	**PSO**	**GA**	**ACO**	**PSO**	**GA**	**ACO**	**PSO**
IAE	-0.05972	-0.05825	-0.05495	-0.068	-0.06619	-0.06437	-0.00266	-0.00274	-0.0019
ISE	-0.0528	-0.05502	-0.05331	-0.06204	-0.06441	-0.06274	-0.00193	-0.00185	-0.00184
ITAE	-0.06184	-0.05998	-0.05702	-0.07104	-0.06927	-0.06669	-0.00562	-0.00233	-0.00429
ITSE	-0.05601	-0.05771	-0.05534	-0.06563	-0.06667	-0.06496	-0.00177	-0.00182	-0.00183
OBJ 1	-0.04201	-0.04232	-0.04201	-0.05086	-0.0512	-0.05086	-0.0015	-0.00161	-0.0015
OBJ 2	-0.0603	-0.05696	-0.06215	-0.06386	-0.0646	-0.06531	-0.0062	-0.00355	-0.00672
OBJ 3	-0.04201	-0.04332	**-0.04201**	-0.05086	**-0.05183**	**-0.05086**	-0.0015	-0.00198	**-0.0015**
OBJ 4	-0.06208	-0.05003	-0.04647	-0.06746	-0.05864	-0.05564	-0.00403	-0.00325	-0.00325
OBJ 5	-0.04972	-0.05324	**-0.04828**	-0.05608	-0.05983	-0.05572	-0.00437	-0.00376	-0.00429

Table 4.4: Peak overshoot for different objective functions for different optimization techniques

	Δf1			*Δf2*			*Δptie12*		
	GA	**ACO**	**PSO**	**GA**	**ACO**	**PSO**	**GA**	**ACO**	**PSO**
IAE	0.014785	0.012157	0.012679	0.013476	0.013157	0.013968	0.013936	0.013845	0.013892
ISE	0.004517	0.007632	0.004338	0.004705	0.008078	0.004471	0.013207	0.013712	0.013341
ITAE	0.031894	0.016986	0.023077	0.028404	0.016656	0.025497	0.014561	0.014236	0.01454
ITSE	0.014776	0.01393	0.013451	0.014878	0.012155	0.014324	0.01399	0.01376	0.013982
OBJ 1	**0.003454**	0.003709	0.003457	**0.003457**	0.003712	0.003459	**0.009157**	0.009254	0.009157
OBJ 2	0.022332	0.01123	0.023651	0.022657	0.01161	0.023852	0.011606	0.012889	0.011898
OBJ 3	0.003455	0.004472	0.003457	0.003456	0.004477	0.003459	0.009157	0.009317	0.009157
OBJ 4	0.009568	0.012148	0.012734	0.009539	0.013449	0.014805	0.01285	0.011239	0.010675
OBJ 5	0.015142	0.012958	**0.012776**	0.015999	0.013667	**0.013463**	0.010048	0.010741	**0.010376**

Table 4.5: Settling time for different objective functions for different optimization techniques

	Δf1			*Δf2*			*Δptie12*		
	GA	**ACO**	**PSO**	**GA**	**ACO**	**PSO**	**GA**	**ACO**	**PSO**
IAE	21.9979	19.30817	22.24425	20.99165	18.35523	21.28915	20.03976	17.82764	20.40873
ISE	42.2596	26.10162	30.37212	41.4519	25.15193	40.62654	27.43433	24.06251	28.08087
ITAE	19.7847	19.08837	19.12476	18.83403	18.07307	18.06076	17.37583	17.02879	17.03714
ITSE	23.49346	23.68225	23.29497	22.54084	22.73843	22.34107	21.44528	21.53893	21.32687
OBJ 1	86.55315	81.56145	86.55757	85.7382	80.74348	85.73256	78.88254	74.84738	78.87734
OBJ 2	11.6464	16.45857	**11.11314**	10.83597	15.42263	**10.46757**	**15.81337**	16.29782	16.06058
OBJ 3	86.54658	98.82054	86.55757	85.72553	98.04552	85.73256	78.87421	60.20836	78.87734
OBJ 4	15.90027	17.15111	17.30259	14.72614	16.04762	16.24475	17.42789	16.04762	16.19224
OBJ 5	**15.099**	16.95306	**15.17628**	**13.73813**	15.7729	**14.09432**	**15.34501**	16.89437	**15.50609**

In Table 4.2 values of different error functions have been shown for different objective functions. IAE index is best optimized in IAE based error based objective function and ISE, ITAE and ITSE indices are best optimized in ISE, ITAE and ITSE based error based objective functions respectively. But it has been observed that in these error functions based optimization, performance indices are not significantly improved. In OBJ4 objective function, error functions IAE, ISE, ITAE and ITSE show better results related to other proposed objective functions. But, Table 4.3, 4.4 and 4.5 show that different performance indices for OBJ5 objective function are found better than other objective functions. Therefore, in this thesis, further with different type of controller's parameters optimization, OBJ5 objective function has been used.

4.4. 2 Simulation results for different optimization techniques

In this work, three different optimization techniques are examined for performance analysis of two area hydro-thermal power system for different objective functions. These optimization techniques are GA, ACO and PSO.

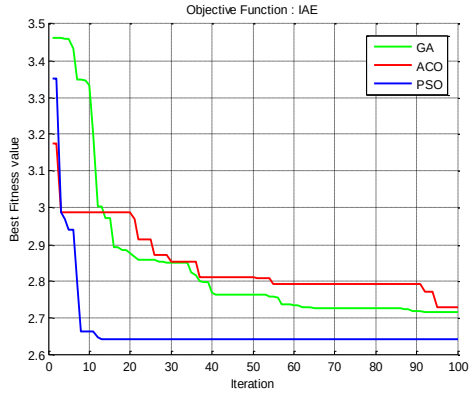

Fig. 4.9: Best fitness value with respect to iteration for different optimization techniques for IAE based objective function

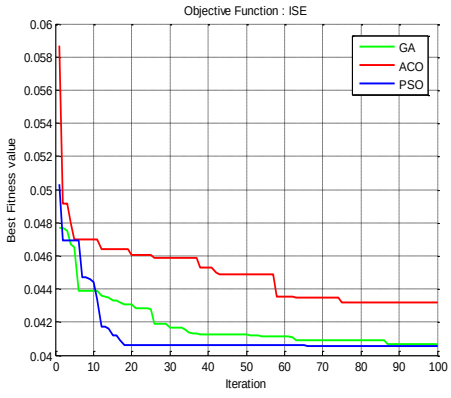

Fig. 4.10: Best fitness value with respect to iteration for different optimization techniques for ISE based objective function

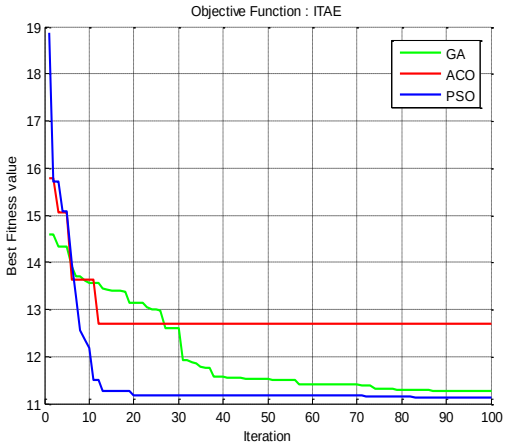

Fig. 4.11: Best fitness value with respect to iteration for different optimization techniques for ITAE based objective function

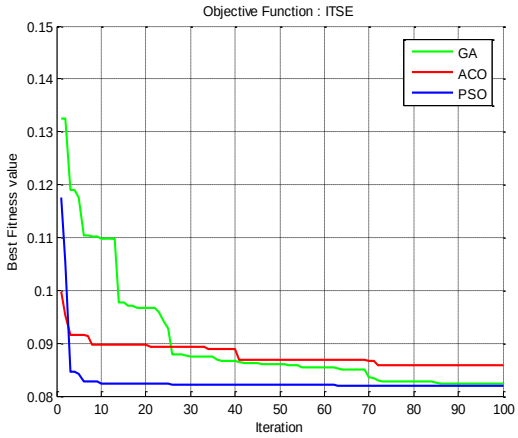

Fig. 4.12: Best fitness value with respect to iteration for different optimization techniques for ITSE based objective function

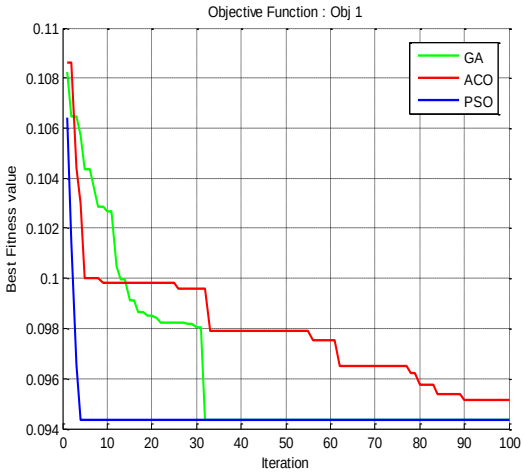

Fig. 4.13: Best fitness value with respect to iteration for different optimization techniques for objective function 1

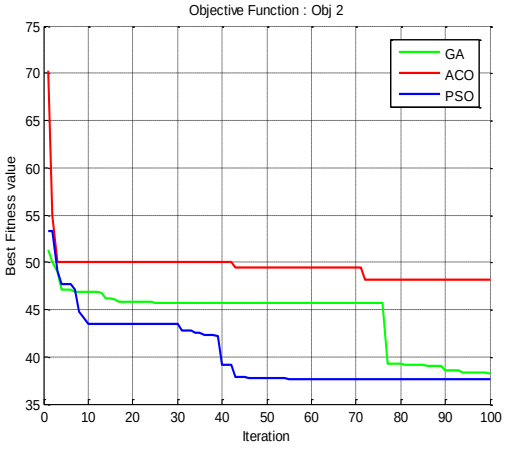

Fig. 4.14: Best fitness value with respect to iteration for different optimization techniques for objective function 2

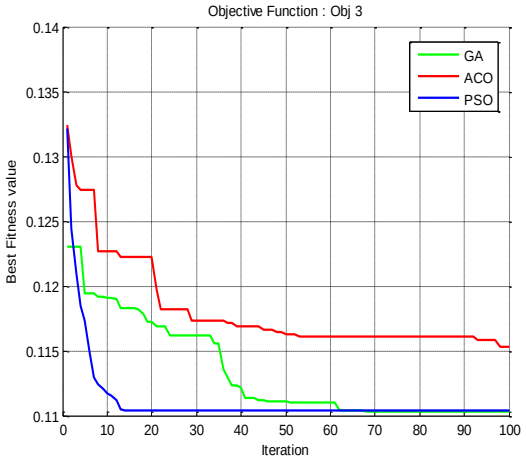

Fig. 4.15: Best fitness value with respect to iteration for different optimization techniques for objective function 3

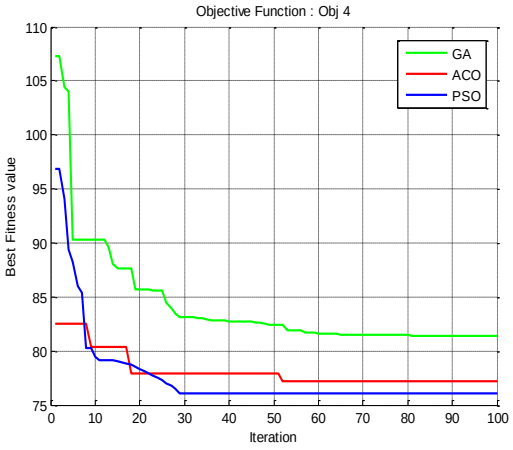

Fig. 4.16: Best fitness value with respect to iteration for different optimization techniques for objective function 4

Fig. 4.9, 4.10, 4.11 and 4.12 show the graph between best fitness value and iteration for IAE, ISE, ITAE and ITSE objective functions respectively for GA, ACO and PSO optimization techniques. Fig. 4.13, 4.14, 4.15, 4.16 and 4.17 show the same for OBJ1, OBJ2, OBJ3, OBJ4 and OBJ5 objective functions respectively. It is quite evident that PSO has shown superior results over GA and ACO techniques. While carrying out this comparison population size for GA, number of ants for ACO and swarm size for PSO have been considered same. Maximum iteration for optimization is also maintained same. Parameters of these different optimization techniques have been shown in appendix.

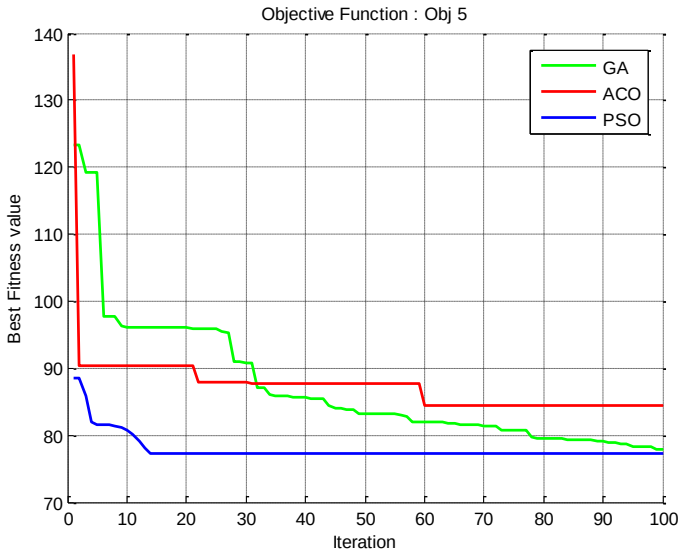

Fig. 4.17: Best fitness value with respect to iteration for different optimization techniques for objective function 5

Therefore, it justifies that PSO technique suits best for system under study as compared to other two techniques for different error based as well as performance indices based objective functions. It also converges in lesser time and effective enough to give better optimum results.

4.4.3 Simulation results for different PSO variants

In previous section, it is found that PSO is best optimization technique among GA, ACO and PSO. Now further, having chosen PSO, its six different variants are examined for performance analysis. In this thorough examination of PSO variants, PID controller is selected as AGC controller for two area interconnected power system and gains for PID controllers for both areas are being optimized. The test system Simulink model is shown in Fig. 4.18.

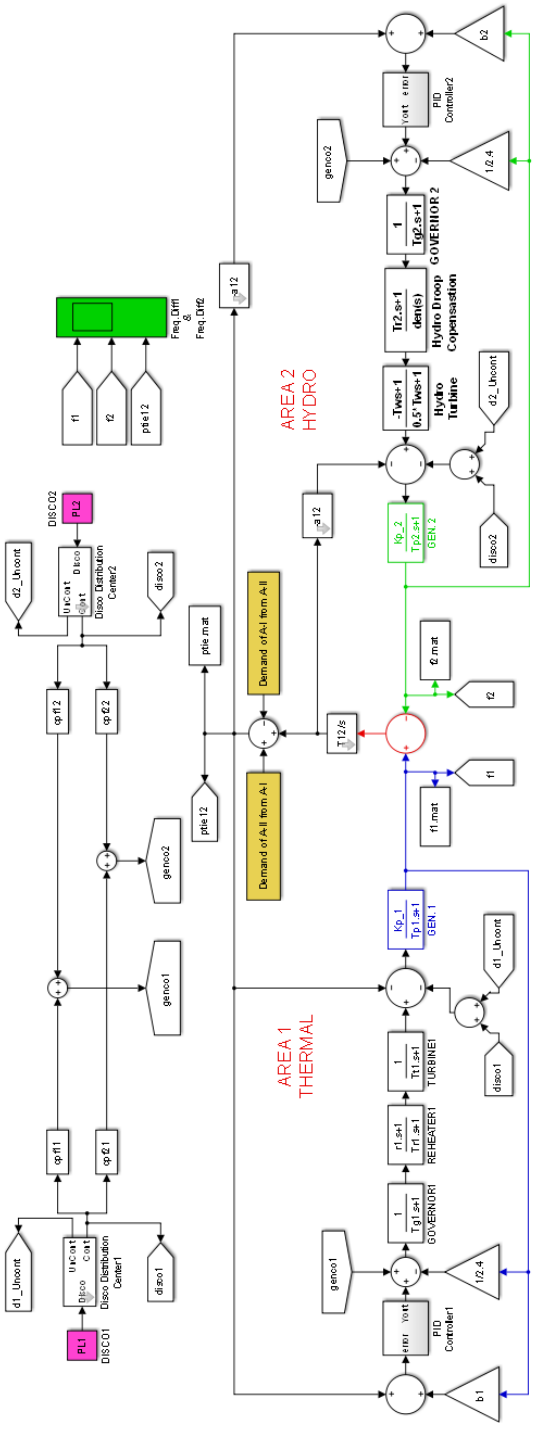

Fig. 4.18: Simulink model of AGC for two area thermal-hydro power system in deregulated environment

In order to inspect these different PSO variants five diverse cases have been considered, in which five different system parameters considered for variations, namely are frequency bias coefficient (β_1 and β_2) of each control area, generator's time constant (T_{p1} and T_{p2}) of each control area and synchronization coefficient (T_{12}). These cases are:

a. Standard Case (System parameters is equal to standard values)

b. N15 Case (System parameters are 15% less)

c. N30 Case (System parameters are 30% less)

d. P15 Case (System parameters are 15% more)

e. P30 Case (System parameters are 30% more)

In order to optimize the PID controllers' gains, each algorithm have been run for 200 iteration and swarm size is taken 5 times than no. of variables and other parameters values are given in appendix. Since PSO is a stochastic optimization technique, during every run it may not provide same global optimum solution. In order to examine this, for standard case these different PSO variants are made to run for 5 times and up to 200 iterations and out of these 5 runs only best run output is considered for comparison with other optimization algorithm. Different optimization curves for best fitness with respect to iteration are shown in Fig. 4.19 for standard case, it is found that algorithm 1 (Algo 1) converges faster than other algorithms and the best fitness value is also obtained in Algo 1.

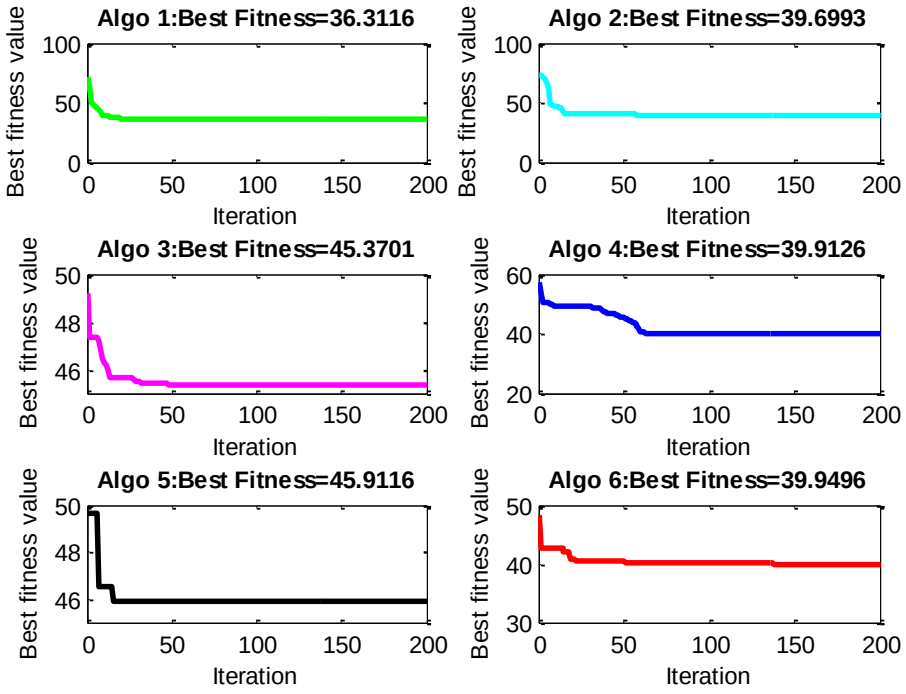

Fig. 4.19: Best fitness value with respect to iteration for different algorithm for standard case

For other four cases also, different PSO variants have been run for 5 times and for 200 iterations. Different optimization curves for best fitness with respect to iteration are shown in Fig. 4.20, 4.21, 4.22 and 4.23 for N15, N30, P15 and P30 case respectively. In these all cases, it is found that algorithm 1 (Algo 1) converges faster than other algorithms and the best fitness value among all these algorithms is also found better in Algo 1.

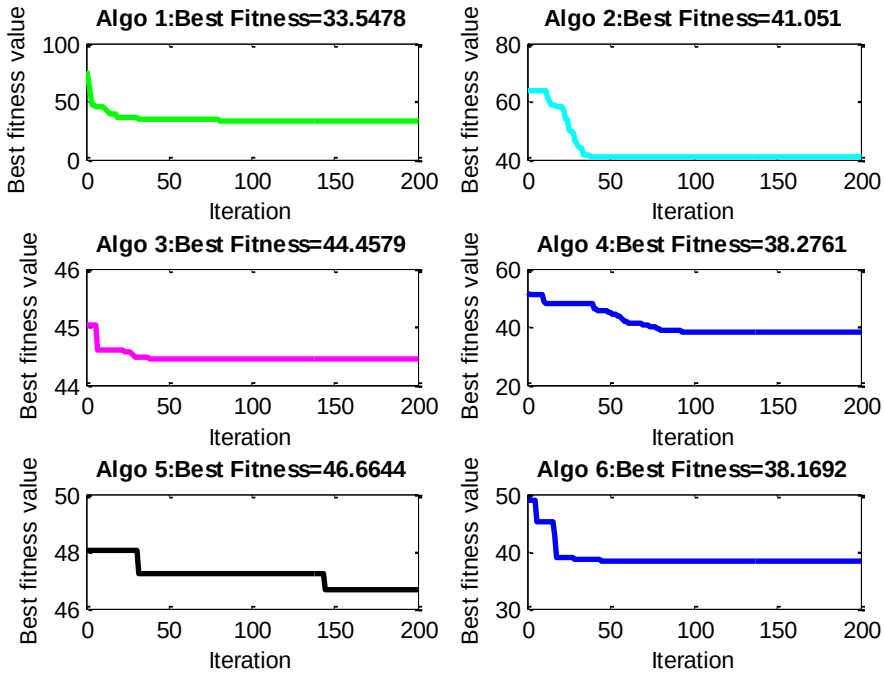

Fig. 4.20: Best fitness value with respect to iteration for different algorithm for N15 case

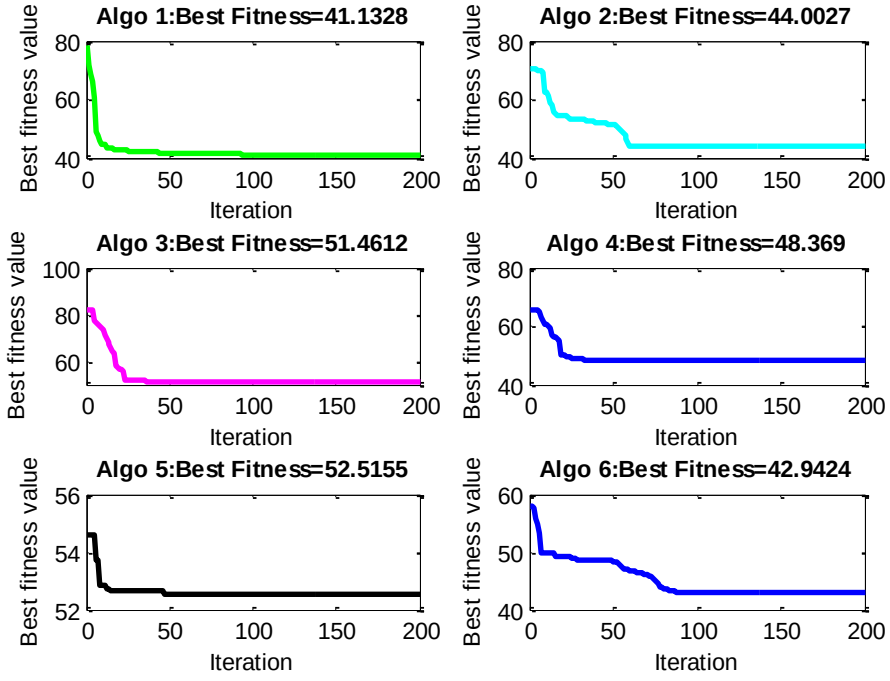

Fig. 4.21: Best fitness value with respect to iteration for different algorithm for N30 case

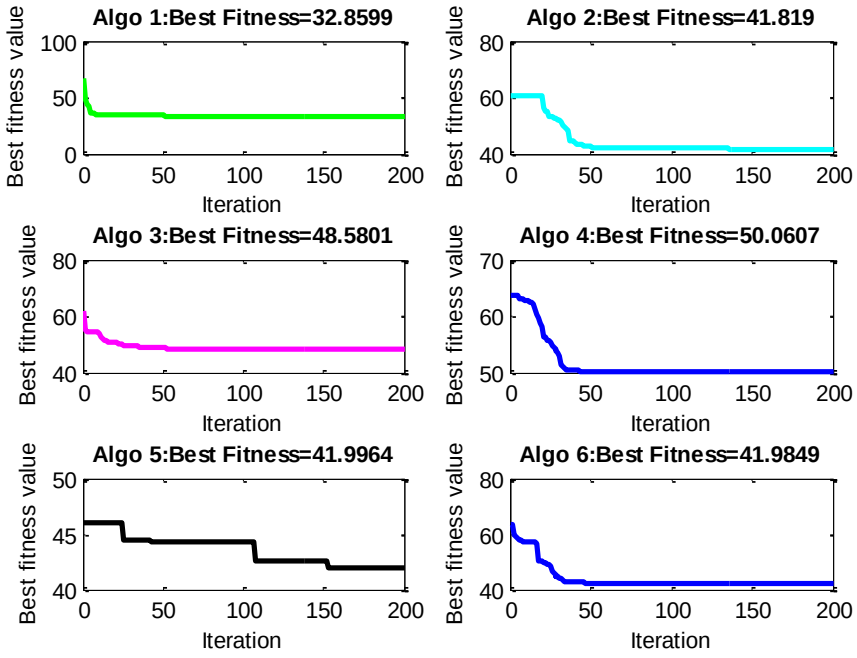

Fig. 4.22: Best fitness value with respect to iteration for different algorithm for P15 case

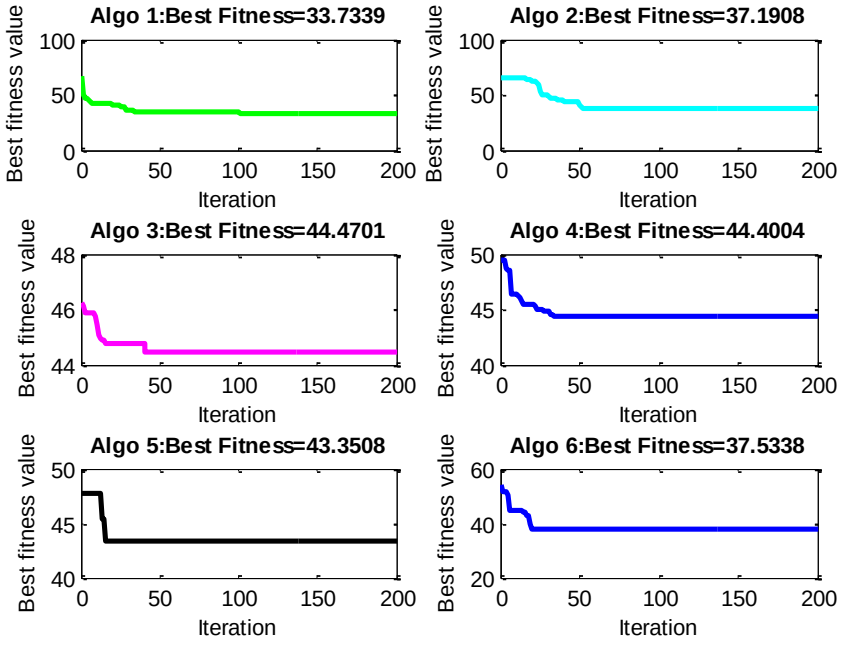

Fig. 4.23: Best fitness value with respect to iteration for different algorithm for P30 case

In order to justify effectiveness of these different PSO optimization techniques, different performance indices are examined for frequency deviation for both areas and tie-line power deviation at sudden load perturbation. Frequency deviation for area-1, area-2 and tie-line power deviation for standard case are shown for different algorithms in Fig. 4.24, 4.25 and 4.26 respectively. Different performance indices for frequency deviation in area-1, frequency deviation in area-2 and tie-line power deviation at sudden load perturbation for all stated cases are shown in Fig. 4.27, 4.28 and 4.29. These figures show that Algo 1 is best among all these different PSO variants. Table 4.6 shows best fitness value, mean fitness value and deviation of mean fitness and best fitness value for each algorithm while Table 4.7, 4.8 and 4.9 show numerical values in order to quantify results. Based on these results it is concluded that Algo 1 is better than other 5 variants in terms of faster convergence and best fitness value.

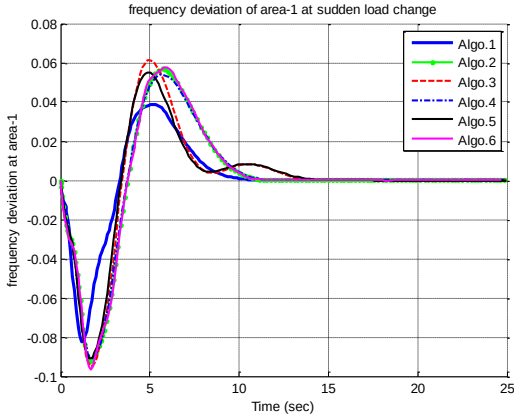

Fig. 4.24: frequency deviation for area-1 for different algorithm for standard case

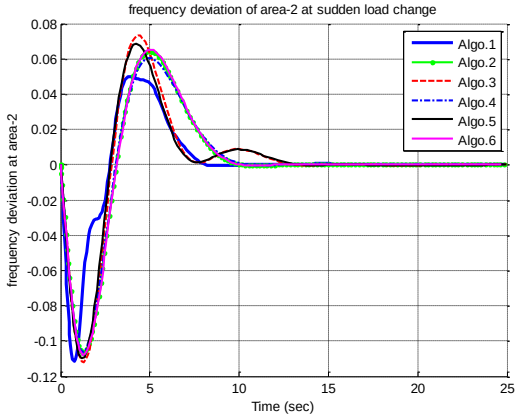

Fig. 4.25: frequency deviation for area-2 for different algorithm for standard case

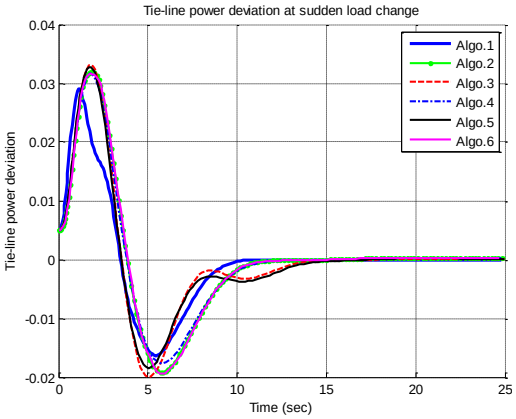

Fig. 4.26: tie-line power deviation for different algorithm for standard case

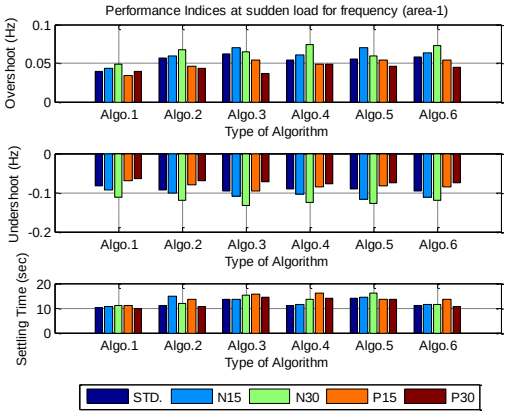

Fig. 4.27: Performance indices for deviation in frequency of area-1 for different algorithms for different cases of variation in system parameters

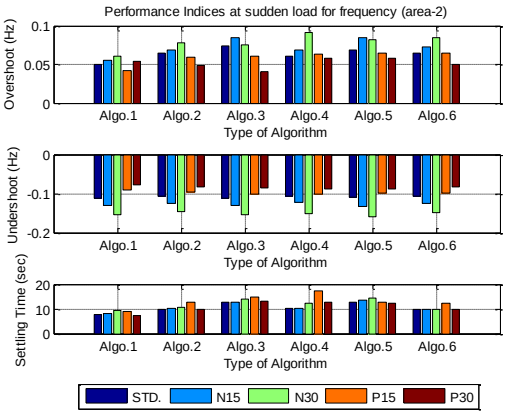

Fig. 4.28: Performance indices for deviation in frequency of area-2 for different algorithms for different cases of variation in system parameters

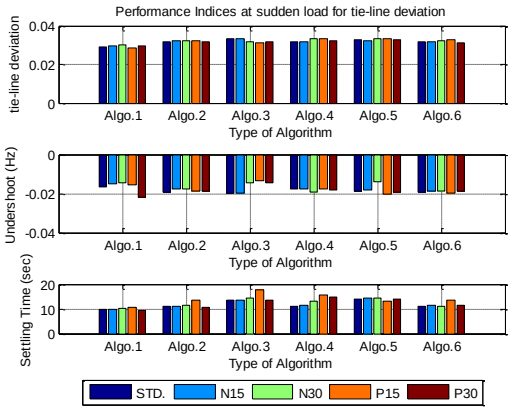

Fig. 4.29: Performance indices for deviation in tie-line power for different algorithms for different cases of variation in system parameters

Table 4.6: Best fitness, mean fitness and % deviation of best and mean fitness for different algorithms for different cases of variation in system parameters

Case:	Fitness	Algo-1	Algo-2	Algo-3	Algo-4	Algo-5	Algo-6
STD.	Best	**36.3116**	39.6993	45.3701	39.9126	45.9116	39.9496
	Mean	37.1192	43.206	51.8786	52.1634	51.8324	47.9752
	%dev	**2.18%**	**8.12%**	**12.55%**	**23.49%**	**11.42%**	**16.73%**
N15	Best	**33.5478**	41.051	44.4579	38.2761	46.6644	38.1692
	Mean	34.5069	42.9811	49.5311	52.8718	52.5112	48.157
	%dev	**2.78%**	**4.49%**	**10.24%**	**27.61%**	**11.13%**	**20.74%**
N30	Best	**41.1328**	43.285	51.4612	48.369	52.5155	42.9424
	Mean	41.4569	49.5969	55.5575	56.5051	58.5796	51.5287
	%dev	**0.78%**	**12.73%**	**7.37%**	**14.40%**	**10.35%**	**16.66%**
P15	Best	**30.5111**	34.6027	45.2416	37.8599	34.6144	34.8634
	Mean	32.9057	39.9461	48.5622	49.6308	46.7795	40.7753
	%dev	**7.28%**	**13.38%**	**6.84%**	**23.72%**	**26.01%**	**14.50%**
P30	Best	**33.7339**	37.1908	44.4701	44.4004	43.3508	37.5338
	Mean	35.9156	40.8986	48.1603	51.6316	46.8034	46.221
	%dev	**6.07%**	**9.07%**	**7.66%**	**14.01%**	**7.38%**	**18.79%**

Table 4.7: Performance indices for deviation in frequency of area-1 for different algorithms for different cases of variance in system parameters

Case	Performance Index	frequency deviation in area-1					
		Algo-1	**Algo-2**	**Algo-3**	**Algo-4**	**Algo-5**	**Algo-6**
STD.	Peak Overshoot	0.0389	0.0569	0.0614	0.054	0.055	0.0579
	Peak Undershoot	-0.0823	-0.0923	-0.0951	-0.0909	-0.091	-0.0965
	Settling Time (±5%)	10.3258	10.9772	13.3725	11.1397	13.9873	11.1095
N15	Peak Overshoot	0.0433	0.0592	0.0698	0.061	0.0705	0.0635
	Peak Undershoot	-0.0934	-0.1018	-0.1093	-0.1038	-0.1159	-0.1107
	Settling Time (±5%)	10.549	14.6272	13.6096	11.533	14.3143	11.3712
N30	Peak Overshoot	0.0486	0.0672	0.0648	0.0742	0.0598	0.0731
	Peak Undershoot	-0.1125	-0.119	-0.1316	-0.1243	-0.1278	-0.1209
	Settling Time (±5%)	10.9512	11.9187	15.4029	13.7107	16.0907	11.3457
P15	Peak Overshoot	0.0346	0.0465	0.0539	0.0492	0.0544	0.0543
	Peak Undershoot	-0.0694	-0.0802	-0.0948	-0.0854	-0.083	-0.0848
	Settling Time (±5%)	11.0674	13.7017	15.6878	15.882	13.524	13.4647
P30	Peak Overshoot	0.0389	0.0433	0.0365	0.0481	0.0466	0.0449
	Peak Undershoot	-0.0641	-0.0704	-0.0728	-0.0789	-0.0739	-0.0748
	Settling Time (±5%)	9.6465	10.6586	14.3357	13.877	13.511	10.7519

Table 4.8: Performance indices for deviation in frequency of area-2 for different algorithms for different cases of variance in system parameters

Case	Performance Index	frequency deviation in area-2					
		Algo-1	Algo-2	Algo-3	Algo-4	Algo-5	Algo-6
	Peak Overshoot	0.0498	0.0644	0.0734	0.0605	0.0685	0.0652
	Peak Undershoot	-0.1115	-0.1071	-0.1119	-0.1063	-0.11	-0.1077
STD.	Settling Time (±5%)	7.8309	9.7819	12.567	10.0281	12.89	9.7154
	Peak Overshoot	0.0552	0.0682	0.0841	0.0691	0.0844	0.0733
	Peak Undershoot	-0.13	-0.1237	-0.1296	-0.1233	-0.132	-0.1252
N15	Settling Time (±5%)	8.2727	10.3035	12.5507	10.3852	13.3584	9.9018
	Peak Overshoot	0.0603	0.078	0.0757	0.0917	0.0825	0.0849
	Peak Undershoot	-0.1549	-0.1473	-0.1527	-0.1526	-0.1596	-0.1479
N30	Settling Time (±5%)	9.3467	10.6057	14.104	12.4583	14.3415	9.7988
	Peak Overshoot	0.0424	0.0595	0.0603	0.064	0.0643	0.0651
	Peak Undershoot	-0.0903	-0.0958	-0.1007	-0.1004	-0.0976	-0.0986
P15	Settling Time (±5%)	8.9667	12.5973	14.7695	17.2353	12.7018	12.4812
	Peak Overshoot	0.0537	0.0485	0.0412	0.0577	0.0574	0.0504
	Peak Undershoot	-0.0787	-0.0827	-0.0844	-0.088	-0.087	-0.0836
P30	Settling Time (±5%)	7.455	9.5927	13.3293	12.888	12.4269	9.6093

Table 4.9: Performance indices for deviation in tie-line power for different algorithms for different cases of variance in system parameters

Case	Performance Index	tie-line power deviation					
		Algo-1	Algo-2	Algo-3	Algo-4	Algo-5	Algo-6
	Peak Overshoot	0.029	0.032	0.0331	0.0317	0.0328	0.0316
	Peak Undershoot	-0.0163	-0.0192	-0.02	-0.0176	-0.0184	-0.0195
STD.	Settling Time (±5%)	9.7073	10.9772	13.3725	11.1397	13.9873	10.9181
	Peak Overshoot	0.0296	0.0321	0.0332	0.0319	0.0325	0.0316
	Peak Undershoot	-0.0153	-0.0178	-0.02	-0.0177	-0.0184	-0.0185
N15	Settling Time (±5%)	9.7311	11.0554	13.4003	11.3393	14.3143	11.577
	Peak Overshoot	0.03	0.0322	0.0319	0.0333	0.0335	0.0324
	Peak Undershoot	-0.0142	-0.0174	-0.0144	-0.019	-0.0141	-0.0187
N30	Settling Time (±5%)	10.3008	11.359	14.5219	13.1177	14.5585	10.9404
	Peak Overshoot	0.0286	0.0324	0.0312	0.0332	0.0332	0.0328
	Peak Undershoot	-0.0158	-0.0184	-0.0136	-0.0177	-0.0202	-0.0195
P15	Settling Time (±5%)	10.7217	13.7017	17.7277	15.679	13.2922	13.6925
	Peak Overshoot	0.0295	0.032	0.0316	0.0323	0.0327	0.0313
	Peak Undershoot	-0.0216	-0.0185	-0.0145	-0.0183	-0.0191	-0.0188
P30	Settling Time (±5%)	9.3225	10.6586	13.7336	14.7142	14.1291	11.3485

4.5 Design of Fuzzy Logic Controller for Interconnected Power System AGC

Fuzzy logic controller is a popular and useful control technique for complex and nonlinear systems. It is a systematic and an easier way to implement the control algorithm for engineering problems. Conventional control methods give satisfactory solutions only on linear models. On the other hand, FLCs are more robust and more reliable in solving a wide range of control problems [19], [20]. Hence, FLCs is more suitable for nonlinear and complex power system models [21], [22].

A FLC maps crisp inputs into crisp outputs. The design of a FLC consists of four steps i.e. fuzzification, formation of fuzzy control rule base, fuzzy interference and defuzzification. The control actions of an FLC are described by some set of linguistic rules, obtained from experience. The FLC designed here is multiple input single output (MISO) type structure having two inputs and one output. The first input is ACE_i (area control error in i^{th} area) and another one is change in ACE_i.

Fuzzification

Fuzzification is the process of transforming a crisp or numerical quantity to a fuzzy set or linguistic variable. The fuzzification step involves measuring of the value of crisp variables, transferring the range of crisp variables into membership degrees corresponding membership functions.

Seven triangular membership functions are considered for inputs (ACE_i and $dACE_i/dt$) and output (u_i). These seven membership functions are named as Very Positive (VP), Medium Positive (MP), Small Positive (SP), Zero (Z), Small Negative (SN), Medium Negative (MN) and Very Negative (VN), as shown in Fig. 4.30.

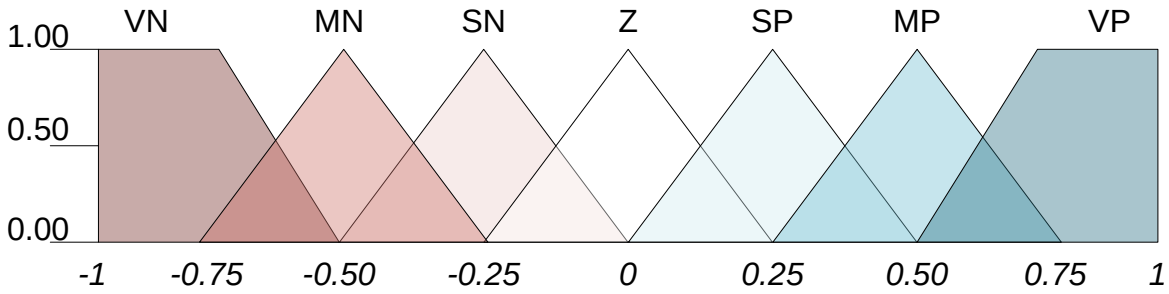

Fig. 4.30: Membership functions of inputs and output variables

Membership functions or fuzzy sets

Membership functions are the key components of FLC design. The difference between a crisp set and fuzzy set is that a crisp set is defined with adequate boundaries whereas fuzzy set is defined with imprecise bosundaries. Only trapezoidal and triangular types of membership function have been used for FLC design of the system under consideration.

Trapezoidal type of membership function is described as:

$$f(x; X_L, X_C, X_R) = max\ (min\left(\frac{x-X_L}{X_C-X_L}, \frac{X_R-x}{X_R-X_C}\right), 0) \quad (4.36)$$

Triangular type of membership function is described:

$$f(x; X_L, X_{CL}, X_{CR}, X_R) = max\ (min\left(\frac{x-X_L}{X_{CL}-X_L}, 1, \frac{X_R-x}{X_R-X_{CR}}\right), 0) \quad (4.37)$$

Table 4.10 gives details of membership functions of FLC.

Table 4.10: Details of membership functions of FLC

S.N.	MF's	MF's Type	Parameters	MF: *f(E)*	Centroid Value (β_{jk})
1	VVL	Trapezoidal	[-1.5R_x - R_x -0.75R_x - 0.5R_x]	*max(min(0.5λE+3,1,-2-λE),0)*	-0.811R_x
2	VL	Triangular	[-0.75R_x -0.5R_x - 0.25R_x]	*max(min(λE+3,- λE-1),0)*	-0.50R_x
3	L	Triangular	[-0.5R_x -0.25R_x 0]	*max(min(λE+2,- λE),0)*	-0.25R_x
4	Z	Triangular	[-0.25R_x 0 0.25R_x]	*max(min(λE+1,1- λE),0)*	0
5	H	Triangular	[0 0.25R_x 0.5R_x]	*max(min(λE,2- λE),0)*	0.25R_x
6	VH	Triangular	[0.25R_x 0.5R_x 0.75R_x]	*max(min(λE-1,3- λE),0)*	0.50R_x
7	VVH	Trapezoidal	[0.5R_x 0.75R_x R_x 1.5R_x]	*max(min(λE-2,1,3-0.5λE),0)*	0.811R_x

where $\lambda=4/R_x$, E= Variable *(as Error variable)*, R_x=Variable's MF's Range, x=ACE_i, $dACE_i$ and U_i

Fuzzy rules

A fuzzy system is characterized by the rule base and a set of fuzzy IF-THEN rules are based on expert knowledge. It is heart of the fuzzy system. The rule base contains the membership function of fuzzy subsets along with the set of rules [23]. Design of the rule base is based on the operator's understanding on the behavior of the process. The rules of the FLC are shown below:

R1. IF ACE_i = MF_ACE_1 **AND** $dACE_i$ = MF_dACE_1 **THEN** u= MF_U_{11}
R2. IF ACE_i = MF_ACE_2 **AND** $dACE_i$ = MF_dACE_1 **THEN** u= MF_U_{21}

IF ACE_i = MF_ACE_j **AND** $dACE_i$ = MF_dACE_7 **THEN** u= MF_U_{j7}

R8. IF ACE_i = MF_ACE_1 **AND** $dACE_i$ = MF_dACE_2 **THEN** u= MF_U_{12}

IF ACE_i = MF_ACE_7 **AND** $dACE_i$ = MF_dACE_k **THEN** u= MF_U_{7k}

R49. IF ACE_i = MF_ACE_j **AND** $dACE_i$ = MF_dACE_k **THEN** u= MF_U_{jk}

Table 4.11 provides rules for FLC controller, complete rule base represents in 7x7 matrix.

Table 4.11: FLC rulebase

Change in Error \ Error	VVL	VL	L	Z	H	VH	VVH
VVH	ZE	L	L	VL	VL	VVL	VVL
VH	H	ZE	L	L	VL	VL	VVL
H	H	H	ZE	L	L	VL	VL
Z	VH	H	H	ZE	L	L	VL
L	VH	VH	H	H	ZE	L	L
VL	VVH	VH	VH	H	H	ZE	L
VVL	VVH	VVH	VH	VH	H	H	ZE

Fuzzy inference

In the fuzzy inference mechanism, fuzzy logic principles are used to combines fuzzy rules from the fuzzy rule base to map fuzzy input sets to fuzzy output sets. It is responsible for combining and evaluating all the defined fuzzy rules for FLC. Mamdani inference mechanism and Takagi-Sugeno inference mechanism are two widely used inference mechanisms. The Mamdani fuzzy theory is advantageous in power system control problem because of its intuitive nature and its property of handling nonlinear and complex system. It minimize the implication method and maximizes the aggregation method [24]. Hence, we use the Mamdani-type fuzzy inference system for FLC modeling. The generic rule of the fuzzy inference system is written as,

$$\textbf{RULE (j x k)} = \sum_{j=1}^{7}\sum_{k=1}^{7} \textbf{IF } ACE_i = MF\_ACE_j \textbf{ AND } dACE_i = MF\_dACE_k \textbf{ THEN } U_i = MF\_U_{jk}$$

Mathematical equations for these methods are express as:

$$\mu_{MF\_Ujk}(ACEi, dACEi) = \min[\mu_{MF\_ACEj}(K_e * ACEi), \mu_{MF\_dACEk}(K_{ce} * dACEi)] \quad (4.38)$$

$$[\mu_{MF\_ACEj}(K_e*ACEi)\ \mathbf{AND}\ \mu_{MF\_dACEk}(K_{ce}*dACEi)] \rightarrow \mu_{MF\_Ujk}(u) \quad (4.39)$$

$$Aggregation\{R_1, R_2, .., R_{49}\} = max\{R_1, R_2, .., R_{49}\} \quad (4.40)$$

Defuzzification

Defuzzification is the last step of FLC for converting fuzzy control action to numerical or crisp control action. Generally, center average and center of gravity defuzzifiers are widely used in defuzzification techniques, but in this work, the center of gravity or centroid method is selected as a defuzzification method, expressed as,

$$U = \frac{\sum_k \sum_j \beta_{jk} \int \mu_{MF\_Ujk}}{\sum_k \sum_j \int \mu_{MF\_Ujk}} \quad (4.41)$$

PID type FLC structure

PID type FLC structure has the advantages of both PID controllers as well as the nonlinear structure of FLC. When PD type FLC is used for a system, there exists a steady-state error. This steady-state error can be eliminated using the integration control action with the fuzzy controller. On the other hand if PI type FLC is implemented with low selected gains, then it gives a slow response and if the gains are high, then it results in a large overshoot. Thus, to improve the control performance, integral control action along with derivative control action is required with FLC. Designing a FLC with three inputs i.e., error, the change rate of error and the integration of error is a difficult approach due to its complex structure and difficulty in computation. Apart from this, constructing rules for integral action is an unrealistic approach; since it is an unusual practice for the operator to observe the integration of error. Thus, we need to design a FLC that has characteristics of PID controller only by using the error and the rate of change of error as its inputs. In this approach, the integrator is serially connected to the

output of the PD type FLC, as shown in Fig. 4.31. This FLC composed of proportional, integration and derivative control action is called PID type FLC [25], [26].

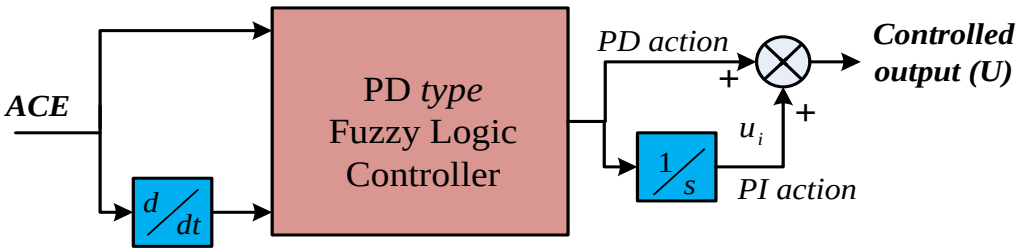

Fig. 4.31: PID type fuzzy logic controller

Performance of PID type FLC depends on the proper selection of its scaling parameters. In this chapter, further different optimization strategies for PID type FLC have been discussed.

4.5.1 Simulation results for comparing different controllers for AGC in deregulated environment

Intelligent control strategies such as fuzzy logic based controllers have emerged to tackle nonlinear and complex problems. Simulation results presented deals with design of FLC for AGC of interconnected power system based model and its effectiveness over conventional controllers. In this work three different conventional controllers are considered and these are integral controller, PI controller and PID controller, where integral controller is optimized using PSO technique (PSO I), PI controller tuned with ZN method (ZN PI) and PID controller gains are also obtained from ZN method (ZN PID) and PSO optimization technique (PSO PID). Two-area thermal reheat based model in deregulated environment are having two GENCOs and two DISCOs in each control area in this test case. AGC controller employed using a suitable control strategy provides optimum results with variation in parameters as well as in different transaction for

deregulation. Three different transaction conditions have been considered for deregulated environment, these are Poolco based transactions, combination of Poolco & bilateral based transactions and contract violation. These different controllers performance thoroughly have been examined for different conditions of system parameter variations (as given in section 4.4.3) and transactions cases. Simulink model for for comparing different controllers for AGC in deregulated environment is shown in Fig. 4.32 and Simulink model of DISCO distribution center is shown in Fig. 4.33 and Fig. 4.34.

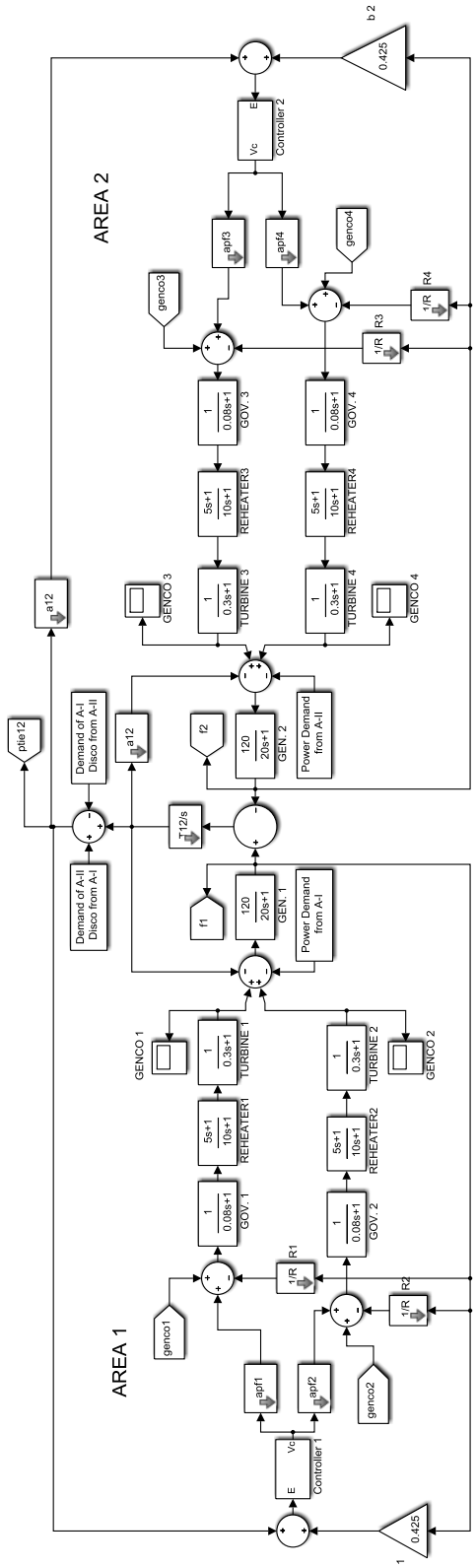

Fig. 4.32: Simulink model of AGC for two area thermal reheat based power system

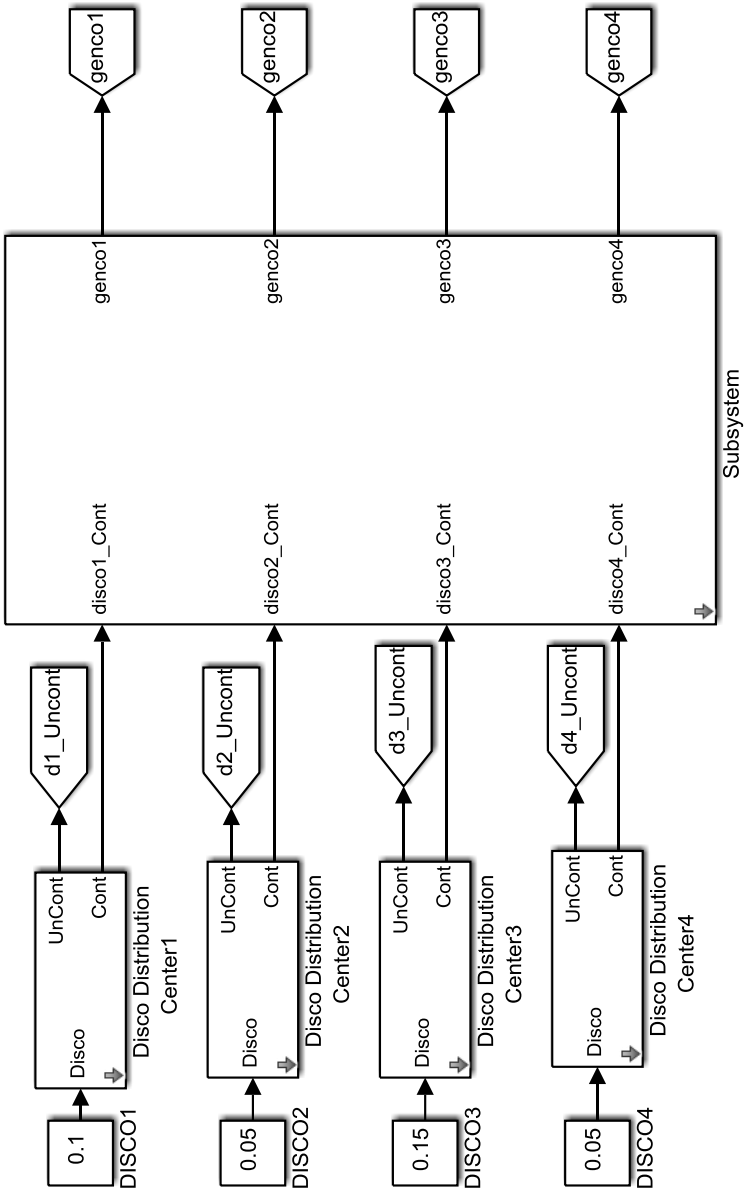

Fig. 4.33: DISCO distribution center Simulink model

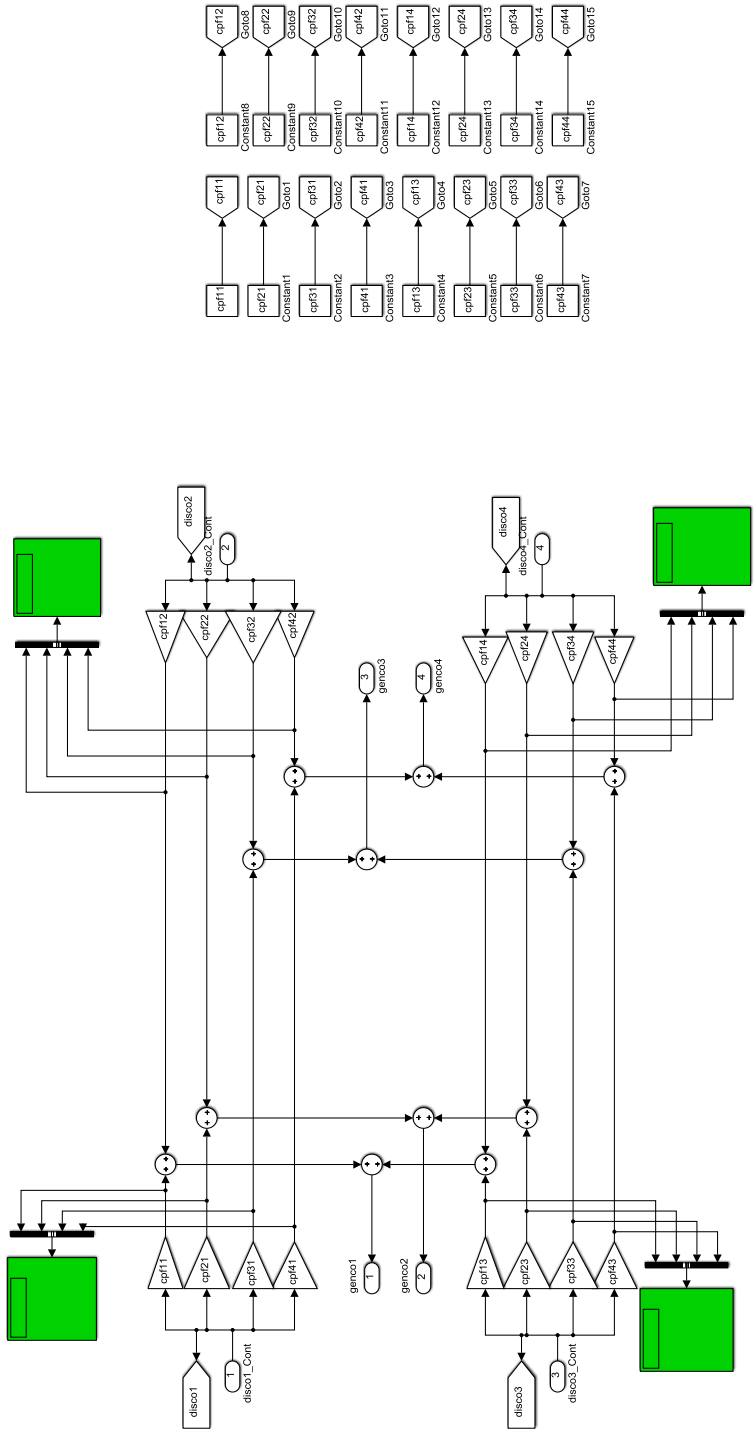

Fig. 4.34: Inside view of DISCO distribution center Simulink model

Proposed FLC controller performance examined against conventional controllers for two area thermal reheat based power system for nine different cases as shown in Table 4.12, where these cases differ from each other by different transaction and variation in system parameters. Details of cpf_matix and load matrix for different cases had shown in Table 4.13.

Table 4.12 Cases for different transactions and with corresponding variation in system parameters

Case	Transaction	System parameters
1.1	Poolco based transactions	standard value
1.2	Poolco based transactions	+30%
1.3	Poolco based transactions	-30%
2.1	Combination of Poolco & bilateral based transactions	standard value
2.2	Combination of Poolco & bilateral based transactions	+30%
2.3	Combination of Poolco & bilateral based transactions	-30%
3.1	Contract violation	standard value
3.2	Contract violation	+30%
3.3	Contract violation	-30%

Table 4.13 cpf_matrix and load for different test cases for proposed system

Test Cases:	**cpf_matrix**	**Contracted Load (p.u.) (ΔP_{LD_Cont})**	**Uncontracted Load (p.u.) ($\Delta P_{LD_{Uncont}}$)**	**Load (p.u.) ΔP_{LD}**
Case 1.1, 1.2 and 1.3: (PoolCo based transactions)	$\begin{bmatrix} 0.5 & 0.5 & 0 & 0 \\ 0.5 & 0.5 & 0 & 0 \\ 0 & 0 & 0.5 & 0.5 \\ 0 & 0 & 0.5 & 0.5 \end{bmatrix}$	$\begin{bmatrix} 0.10 \\ 0.05 \\ 0.15 \\ 0.05 \end{bmatrix}$	$\begin{bmatrix} 0.00 \\ 0.00 \\ 0.00 \\ 0.00 \end{bmatrix}$	$\begin{bmatrix} 0.10 \\ 0.05 \\ 0.15 \\ 0.05 \end{bmatrix}$
Case 2.1, 2.2 and 2.3: (Combination of Poolco and bilateral based transactions)	$\begin{bmatrix} 0.25 & 0.2 & 0.15 & 0.15 \\ 0.25 & 0.25 & 0.15 & 0.2 \\ 0.3 & 0.25 & 0.35 & 0.35 \\ 0.2 & 0.3 & 0.35 & 0.3 \end{bmatrix}$	$\begin{bmatrix} 0.10 \\ 0.05 \\ 0.15 \\ 0.05 \end{bmatrix}$	$\begin{bmatrix} 0.00 \\ 0.00 \\ 0.00 \\ 0.00 \end{bmatrix}$	$\begin{bmatrix} 0.10 \\ 0.05 \\ 0.15 \\ 0.05 \end{bmatrix}$
Case 3.1, 3.2 and 3.3: (Contract violation)	$\begin{bmatrix} 0.25 & 0.2 & 0.15 & 0.15 \\ 0.25 & 0.25 & 0.15 & 0.2 \\ 0.3 & 0.25 & 0.35 & 0.35 \\ 0.2 & 0.3 & 0.35 & 0.3 \end{bmatrix}$	$\begin{bmatrix} 0.10 \\ 0.05 \\ 0.15 \\ 0.05 \end{bmatrix}$	$\begin{bmatrix} 0.025 \\ 0.000 \\ 0.075 \\ 0.000 \end{bmatrix}$	$\begin{bmatrix} 0.010 \\ 0.050 \\ 0.150 \\ 0.050 \end{bmatrix}$

Different controllers' performance for case 1.1:

Fig. 4.35 and Fig. 4.36 show deviation in frequency for area-1 and deviation in frequency for area-2 respectively, whereas Fig. 4.37 shows deviation in tie-line power for case 1.1.

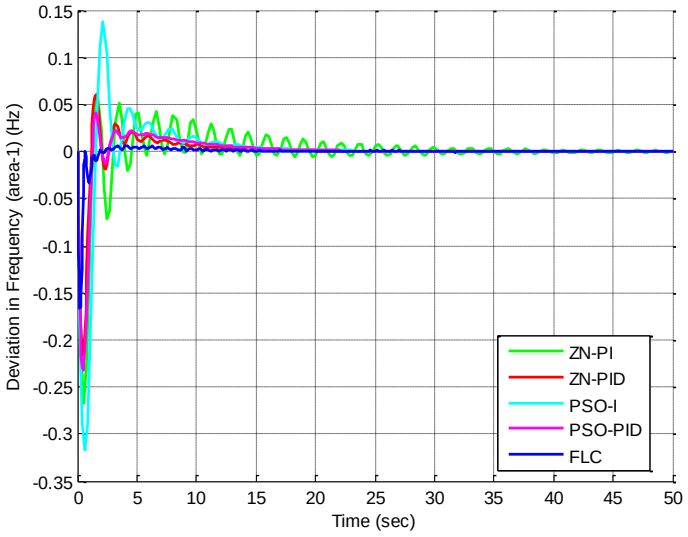

Fig. 4.35: Deviation in frequency of area-1 for different controllers for case 1.1

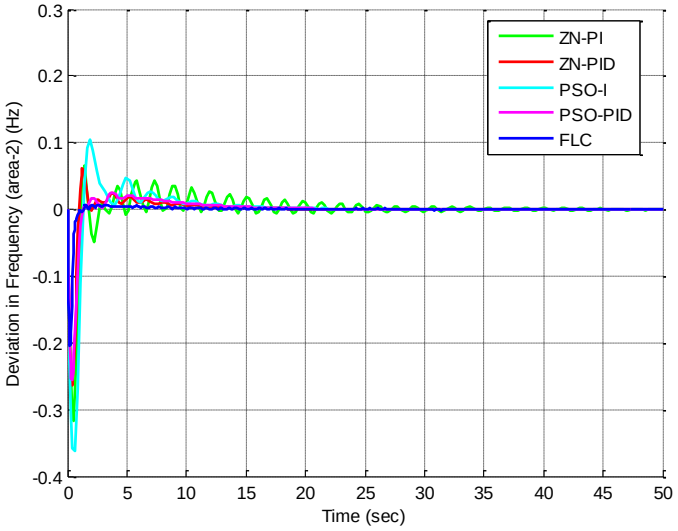

Fig. 4.36: Deviation in frequency of area-2 for different controllers for case 1.1

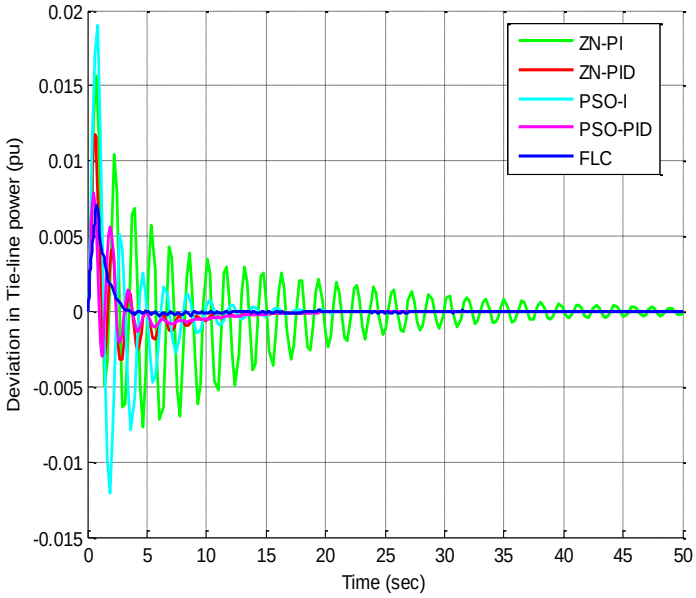

Fig. 4.37: Deviation in tie-line power for different controllers for case 1.1

It is observed from these figures that FLC gives better performance than other conventional controllers in terms of faster settling and lesser deviations.

In order to detail examination of FLC performance, simulation has been carried out for different cases and based on simulation results three different performance indices are obtained.

Table 4.14: Peak undershoot for different cases

Parameters	Case	ZN PI	ZN PID	PSO I	PSO PID	FLC
deviation in frequency of area-1	**1.1**	-0.26708	-0.21628	-0.31758	-0.23247	-0.11879
	1.2	-0.33961	-0.28682	-0.39162	-0.3066	-0.16624
	1.3	-0.21584	-0.17369	-0.27036	-0.18894	-0.09503
	2.1	-0.25744	-0.20214	-0.32984	-0.22811	-0.11233
	2.2	-0.33392	-0.27243	-0.41613	-0.30218	-0.15791
	2.3	-0.20895	-0.1626	-0.28718	-0.18518	-0.08552
	3.1	-0.27357	-0.21058	-0.35962	-0.24082	-0.11322
	3.2	-0.35313	-0.28148	-0.4407	-0.3161	-0.15882
	3.3	-0.22226	-0.16943	-0.31579	-0.19597	-0.08886
deviation in frequency of area-2	**1.1**	-0.31663	-0.26305	-0.36257	-0.25547	-0.14568
	1.2	-0.42468	-0.35711	-0.4735	-0.34661	-0.20527
	1.3	-0.25966	-0.20916	-0.30503	-0.20414	-0.11347
	2.1	-0.32877	-0.27527	-0.35255	-0.26555	-0.15624
	2.2	-0.41936	-0.37092	-0.45103	-0.3556	-0.21837
	2.3	-0.26296	-0.22035	-0.28908	-0.21153	-0.12028
	3.1	-0.36475	-0.30519	-0.39837	-0.29278	-0.16416
	3.2	-0.47323	-0.40293	-0.50077	-0.38901	-0.23048
	3.3	-0.29647	-0.24372	-0.32735	-0.23506	-0.12773
deviation in tie-line power	**1.1**	-0.0077	-0.00317	-0.01204	-0.00294	-0.00044
	1.2	-0.00545	-0.00264	-0.00609	-0.00189	-0.00029
	1.3	-0.01195	-0.00449	-0.01738	-0.00472	-0.00037
	2.1	-0.0425	-0.0425	-0.04596	-0.0425	-0.04250
	2.2	-0.0425	-0.0425	-0.0451	-0.0425	-0.04250
	2.3	-0.0425	-0.0425	-0.04758	-0.0425	-0.04250
	3.1	-0.04875	-0.04875	-0.04875	-0.04875	-0.04875
	3.2	-0.04875	-0.04875	-0.04875	-0.04875	-0.04875
	3.3	-0.04875	-0.04875	-0.04875	-0.04875	-0.04875

Table 4.15: Peak overshoot for different cases

Parameters	Cases	ZN PI	ZN PID	PSO I	PSO PID	FLC
deviation in frequency of area-1	**1.1**	0.061642	0.059662	0.136994	0.040862	0.005584
	1.2	0.076251	0.065746	0.107349	0.048375	0.006666
	1.3	0.05836	0.059732	0.164198	0.04056	0.004551
	2.1	0.066282	0.065181	0.150761	0.049134	0.024043
	2.2	0.086327	0.079188	0.133664	0.061882	0.035252
	2.3	0.059534	0.060976	0.16189	0.044815	0.014376
	3.1	0.042008	0.044935	0.127821	0.024065	0.025293
	3.2	0.044691	0.048443	0.102719	0.028213	0.030886
	3.3	0.044378	0.04824	0.151227	0.027259	0.009889
deviation in frequency of area-2	**1.1**	0.065698	0.061177	0.105333	0.024984	0.005617
	1.2	0.117898	0.091056	0.124882	0.025236	0.006733
	1.3	0.045908	0.047203	0.105165	0.030093	0.004720
	2.1	0.061776	0.050558	0.064207	0.020005	0.005486
	2.2	0.090775	0.068506	0.070077	0.022362	0.006602
	2.3	0.042881	0.042779	0.104852	0.021174	0.003234
	3.1	0.036495	0.035011	0.05342	0.017479	0.003926
	3.2	0.056178	0.045045	0.031862	0.019352	0.005286
	3.3	0.04352	0.032725	0.103037	0.017143	0.002922
deviation in tie-line power	**1.1**	0.015651	0.011722	0.019039	0.007894	0.008689
	1.2	0.0137	0.011153	0.017229	0.007719	0.007103
	1.3	0.016824	0.012482	0.021135	0.00838	0.008451
	2.1	0.004443	0.00114	0.004992	0.001351	0.000185
	2.2	0.002818	0.001284	0.004165	0.001563	0.000453
	2.3	0.009696	0.001372	0.007756	0.001271	0.000209
	3.1	0.005156	0.001479	0.004939	0.00166	0.000290
	3.2	0.003393	0.00166	0.004162	0.001904	0.000401
	3.3	0.011009	0.001872	0.006948	0.001539	0.000278

Table 4.16: Settling time for different cases

Parameters	Cases	ZN PI	ZN PID	PSO I	PSO PID	FLC
deviation in frequency of area-1	**1.1**	>50	22.52587	25.17658	24.88668	27.7504
	1.2	40.14577	24.51903	28.18193	27.58768	31.7759
	1.3	>50	20.95452	28.32464	22.95769	26.25187
	2.1	55.6931	22.38654	25.35075	24.73466	21.79341
	2.2	38.9376	24.65795	28.30013	27.3525	35.73497
	2.3	>50	20.9365	27.91722	22.94984	16.71158
	3.1	>50	22.46479	25.41195	24.85241	20.67424
	3.2	41.65574	24.76528	28.41388	27.3217	39.46482
	3.3	>50	21.03955	27.96822	23.07112	16.64430
deviation in frequency of area-2	**1.1**	>50	22.29212	25.74674	24.88668	37.47064
	1.2	40.89676	24.51903	28.18193	27.39388	35.50720
	1.3	>50	21.22245	28.99765	22.95769	27.01390
	2.1	>50	22.38654	25.87983	24.92514	32.13141
	2.2	39.56957	24.90986	28.30013	27.3525	35.85930
	2.3	>50	21.34361	28.87739	22.94984	35.42242
	3.1	>50	22.46479	25.89621	25.37187	27.85617
	3.2	39.71591	24.76528	28.41388	28.03346	43.50653
	3.3	>50	21.4503	27.02756	23.35049	16.12956
deviation in tie-line power	**1.1**	39.6139	10.00507	12.94905	9.940239	2.813297
	1.2	24.2227	10.37291	9.814486	9.455948	2.739189
	1.3	>50	11.6321	21.68346	10.28163	3.027106
	2.1	37.27394	10.81516	15.83152	14.37647	3.712205
	2.2	24.86176	11.00964	16.06829	14.26536	3.219711
	2.3	>50	11.22956	20.51662	14.13679	3.422609
	3.1	38.94625	12.07599	16.15147	14.74475	3.315993
	3.2	24.98597	11.3646	16.39373	14.70404	3.111799
	3.3	>50	12.68649	20.67385	14.68795	3.133259

Table 4.14, 4.15 and 4.16 show peak undershoot, peak overshoot and settling time respectively for deviation in frequency of area-1, deviation in frequency of area-2 and deviation in tie-line power. Results obtained by FLC show less peak undershoot, peak overshoot for different cases than other conventional controllers while in only few cases FLC obtained slightly large settling time than PID controller, but in these cases peak undershoot and peak overshoot are significantly reduced. Therefore, it can be concluded that FLC is appropriate controller for AGC and this controller is able to give optimum results even in case of change in transaction or variations in system parameters.

4.6 Optimization of Fuzzy Logic Controller

The design of FLC is fully based on operator experience and understanding about a process. Sometimes the optimum performance is far-off from the operator's understanding and it is here that FLC optimization requirement originates. In this research work, four different optimization strategies are used for FLC optimization as shown in Fig. 4.38.

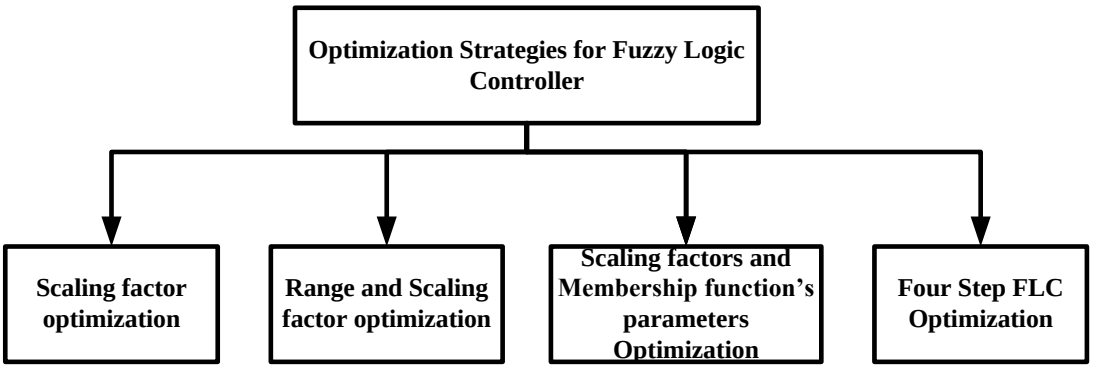

Fig. 4.38: Different optimization strategies for FLC

4.6.1 Scaling factor optimized FLC

In this method, scaling factor of FLC is optimized. As per Fig. 4.39, there are four tunable parameters that need to be optimized for improved performance of FLC. These parameters are scaling parameters (K_e *and* K_{ce}) and gain parameters (K_{pu} *and* K_{iu}) for FLC.

4.6.2 Range and scaling factor optimized FLC

In this method, range and scaling factor of FLC are optimized in the following two steps. As per Fig. 4.39, there are seven tunable parameters that need to be optimized for

improved performance of FLC. These parameters are range parameters (R_e, R_{ce} *and* R_u), scaling parameters (K_e *and* K_{ce}) and gain parameters (K_{pu} *and* K_{iu}) for FLC.

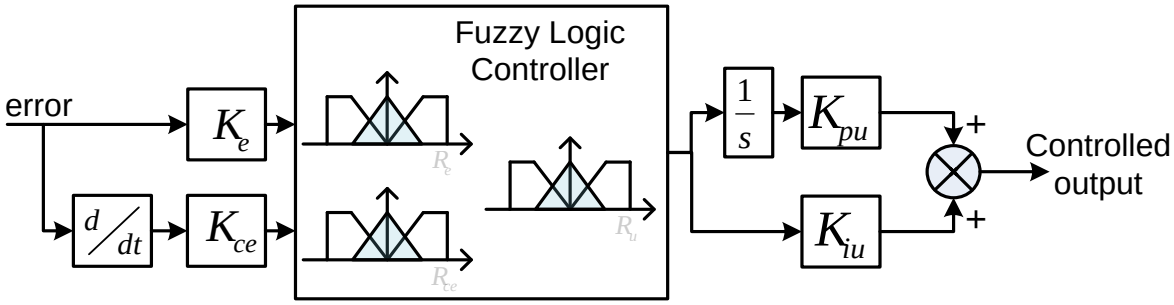

Fig. 4.39: MISO type FLC

In this FLC optimization process, all seven MF's for each variables are equally distributed in a ratio mentioned in Fig. 4.40. Both of these steps are optimized by PSO optimization techniques.

1) *Range optimization with constant scale of MF's:* In this first step, membership functions range of input and output variables of FLC controller are optimized.

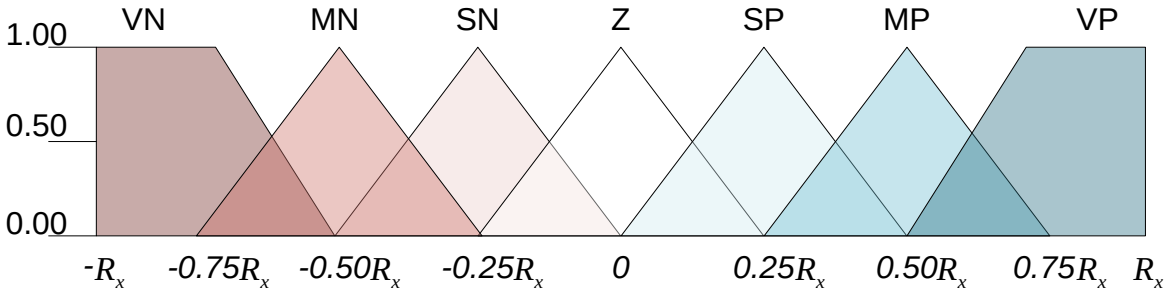

Fig. 4.40: MF distribution across range of variable of FLC

$$R_{e\_min} \leq R_e \leq R_{e\_max}$$

$$R_{ce\_min} \leq R_{ce} \leq R_{ce\_max}$$

$$R_{u\_min} \leq R_u \leq R_{u\_max}$$

Variable Range for input variable ACE_i and $dACE_i$, range R_x is R_e and R_{ce} respectively and for output variable U_i, range R_x is R_u.

2) *Scaling factor & gain optimization:* In this second step, optimum value of scaling factors (K_e *and* K_{ce}) and gain parameters (K_{pu} and K_{iu}) for FLC are to be found out. Objective function selected for this step is same as that in the previous step.

$$K_{e\_min} \leq K_e \leq K_{e\_max}$$

$$K_{ce\_min} \leq K_{ce} \leq K_{ce\_max}$$

$$K_{pu\_min} \leq K_{pu} \leq K_{pu\_max}$$

$$K_{iu\_min} \leq K_{iu} \leq K_{iu\_max}$$

4.6.3 Scaling factors and membership function's parameters optimized FLC

Initialize a nominal FLC with 2 inputs and single output as (Multiple input and single output) MISO type FLC. Each input and output has 7 Membership function with linear distribution across range (Fig.4.30).

1) *Scaling factor & gain optimization:* In this first step, optimum value of two scaling factors (K_e *and* K_{ce}) and two gain parameters (K_{pu} and K_{iu}) need to be optimized.
2) *MF's parameters optimization:* Membership Function specifies the degree to which a given input belongs to set or a function, which defines how each point in the input space, is mapped to a degree of membership between 0 and 1. Here for 7 MFs of trapezoidal and triangular type are used each input as well as output, corresponding to each variable, there are 9 parameters selected for optimization, as shown in Fig. 4.41. Initially MF's distribution of each variable is symmetrical

around zero, so either positive side parameters can be chosen or negative side parameters can be chosen for optimization, but due to symmetrical structure all 18 parameters will be optimized.

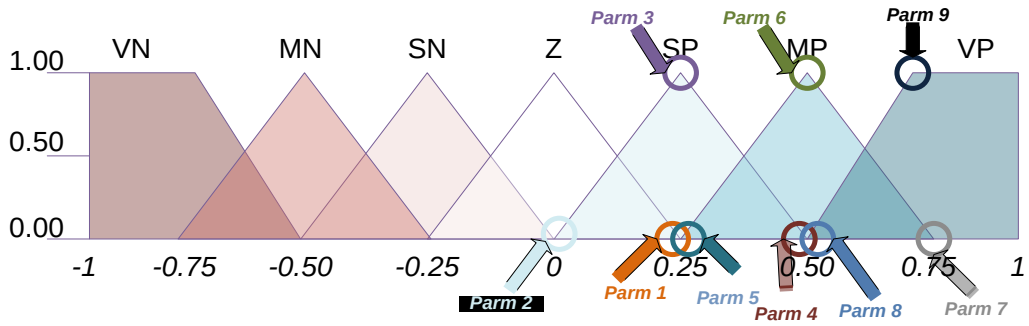

Fig. 4.41: Each variable's MF's parameters for optimization

4.6.4 Four step optimized FLC

Four step optimization of FLC comprises of rule base optimization, scaling factors optimization, membership functions parameters optimization and rules weight optimization, respectively. A PSO success rate variant optimization technique with proposed objective function 5 is used to find out optimum values in each step.

1) *Rule base optimization:* Good rule base is a major concern, when no human expert is available. Rule base is a collection of logic rules in the form of IF-THEN statements, where the IF part is called the "antecedent" and the THEN part is called the "consequent". Rule Base optimization is to find the best possible consequent part corresponding to antecedent part. Optimum values of consequent parts of rule base need to be found out for all possible combinations of antecedent parts. In this step, apart from center rule, all other rules need to be optimized. For example in case of two input and single output, with each of 7 MF's, having 49 rules, 48 rules need to be optimized, as shown in Fig. 4.42.

Change in Error \ Error	VVL	VL	L	Z	H	VH	VVH
VVH							
VH							
H							
Z				ZE			
L							
VL							
VVL							

Fig. 4.42: Rule base optimization for 48 rules

2) *Scaling factors and gain parameters optimization*: Similar to Rule Base and Scaling factor optimized FLC, this step is used to obtain the optimum value of scaling and gain factors. Fig. 4. 43 show FLC with different tunable scaling and gain factors with their ranges.

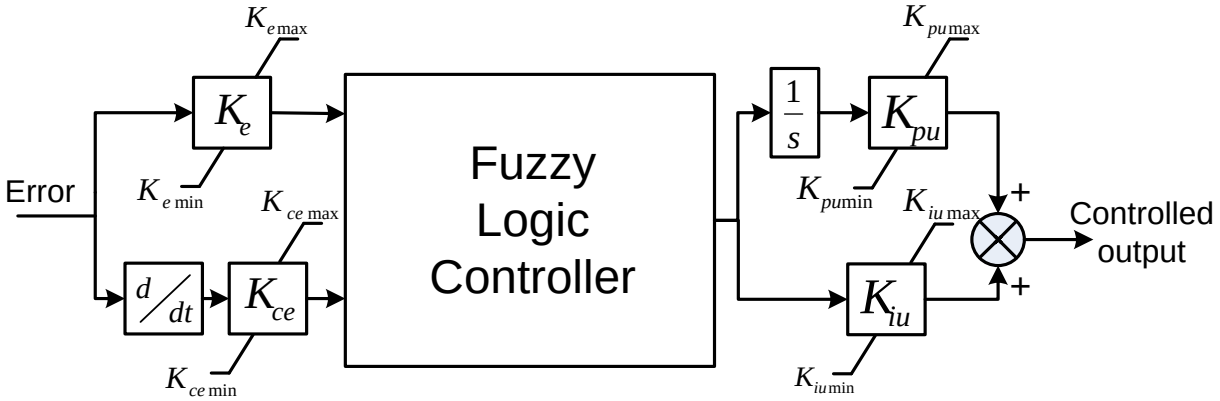

Fig. 4.43: Scaling and gain parameters optimization

3) *MF's parameters optimization: In* this step, MF's parameters being optimized as discussed earlier.

4) *Rules weight optimization:* This fourth step of optimization is selecting the appropriate weight for individual rules in the rule base. Default rule weights for all rules in FLC controller design are selected as 1, but for a complex system putting all rules with unity gain is inappropriate. So, rule weights for all rules are selected between 0.01 and 1.

4.6.5 Simulation results for optimized FLC for interconnected power system in deregulated environment:-

A dual input and single output type PID-type-FLC is designed for AGC. Seven triangular type membership functions are considered for both inputs as well as for single output. Four different type of optimization approach examined for FLC optimization. These are:

a. Scaling factors optimized FLC
b. Ranges and Scaling factors optimized FLC in two steps (TFLC)
c. Membership function's parameters and Scaling factors optimized FLC in two steps (T2FLC)
d. Four step optimized FLC (FFLC)

The simulation model for AGC of TT-TH system used for evaluting optimized FLC performance is shown in Fig. 4.44. The optimized controllers are examined againest conventional controllers (Integral, PI and PID controller).

In this system following controllers examined,

i. PI Controller (Zigler-Nichols tuned)

ii. PID Controller (Zigler-Nichols tuned)

iii. Integral controller (PSO optimized)

iv. PID Controller (PSO optimized)

v. FLC (scaling factor optimized by PSO)

vi. TFLC (ranges and scaling factor optimized by PSO in two steps)

vii. T2FLC (scaling factor and membership functions optimized by PSO in two steps)

viii. FFLC (rule base, membership functions, scaling factor and rules weight optimized by PSO in four steps)

The *cpf_matrix* and DISCO demand matrix used for following cases are:

$$cpf\_matrix = \begin{bmatrix} 0.25 & 0.2 & 0.15 & 0.15 \\ 0.25 & 0.25 & 0.15 & 0.2 \\ 0.3 & 0.25 & 0.35 & 0.35 \\ 0.2 & 0.3 & 0.35 & 0.3 \end{bmatrix} \text{ and } \Delta P_L = \begin{bmatrix} 0.10 \\ 0.05 \\ 0.15 \\ 0.05 \end{bmatrix}$$

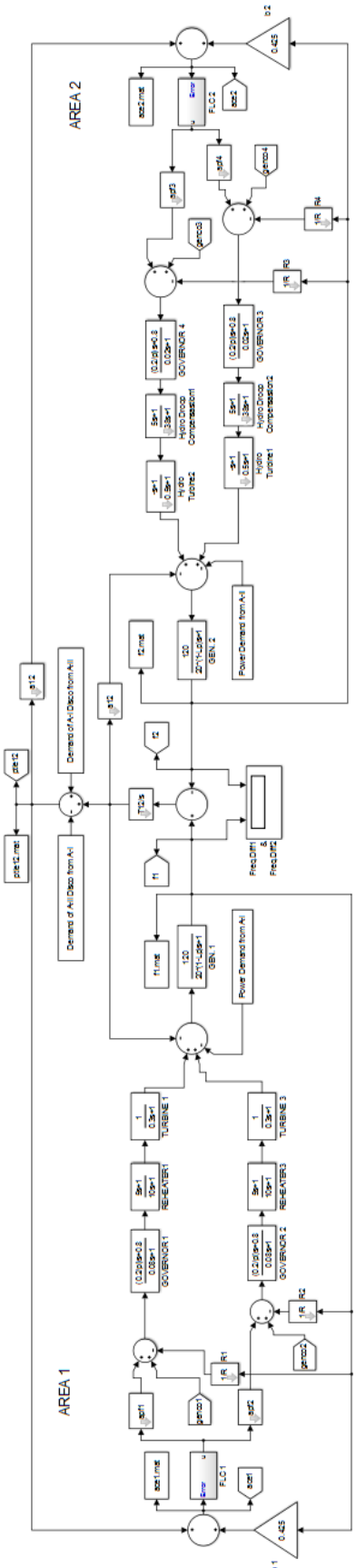

Fig. 4.44: Simulink model for TT-TH system

Scaling factors optimized FLC:-

In Fig. 4.45, K_e & K_{ce} are scaling factors for both the input variables (ACE_i,$dACE_i$) respectively and K_{pu} & K_{iu} are the proportional and integral gains respectively. Therefore, U_i is a crisp value obtained after defuzzification and u_i is a final output signal from controller.

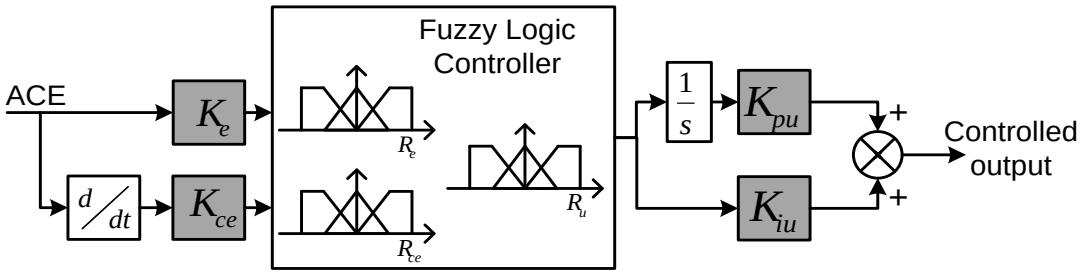

Fig. 4.45: Scaling factors optimized FLC

Fig. 4.46 shows best fitness value with respect to iteration for scaling factor optimization for Scaling factors optimized FLC.

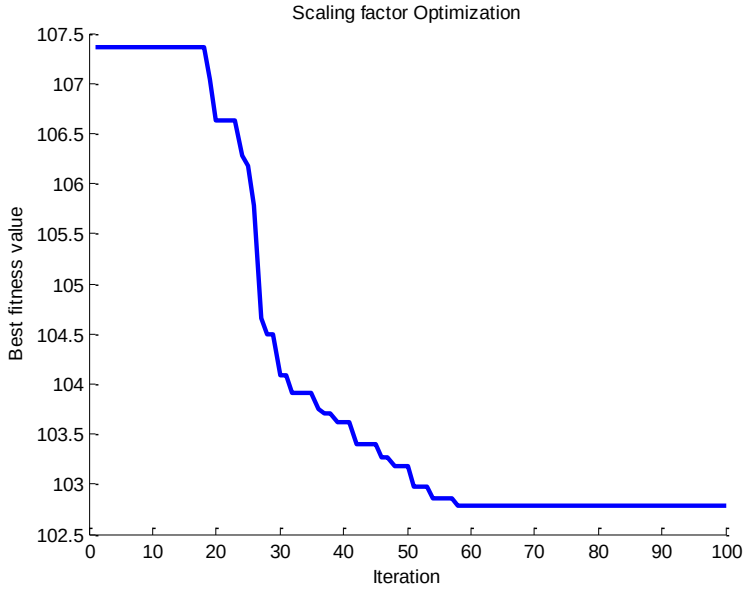

Fig. 4.46: Scaling factor optimization for FLC

Ranges and scaling factors optimized FLC in two steps (TFLC):-

In Fig. 4.47, seven different parameters have shown for ranges and scaling factors optimization for FLC, which are optimized in two steps, in which four are scaling factors (K_e, K_{ce}, K_{pu} & K_{iu}) and three are range parameters (R_e, R_{ce} & R_u).

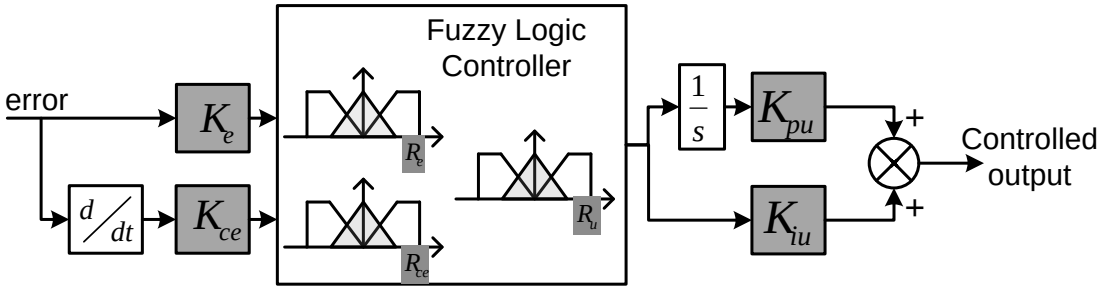

Fig. 4.47: Ranges and scaling factors optimized FLC in two steps (TFLC)

Fig. 4.48 shows best fitness value with respect to iteration for range and scaling factor optimization for TFLC.

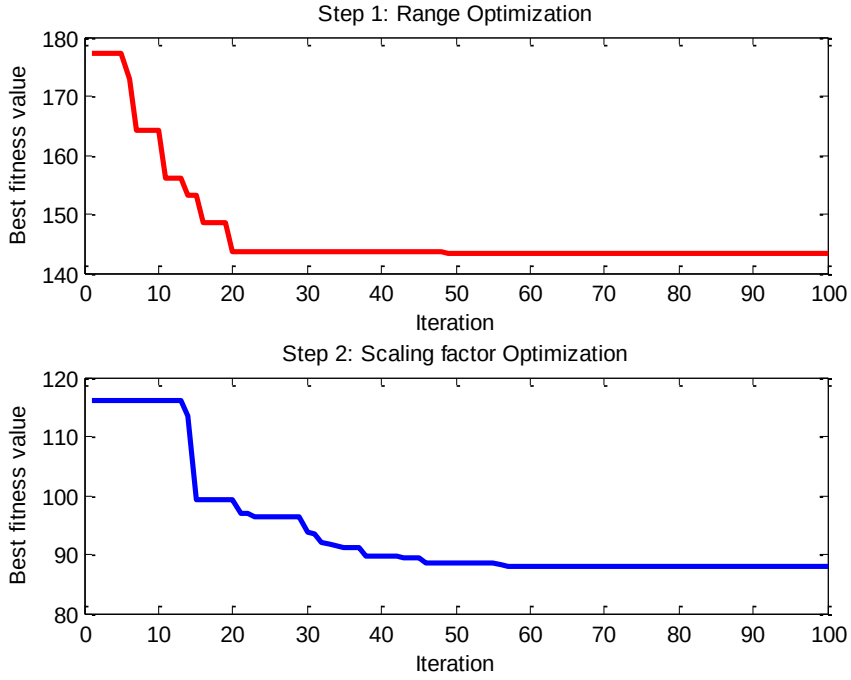

Fig. 4.48: Optimized parameters for TFLC

Membership function's parameters and scaling factors optimized FLC in two steps (T2FLC):-

Fig. 4.49 shows T2FLC, in 4 scaling factors and 27 membership function parameters is optimized for two inputs and one output variable in two steps.

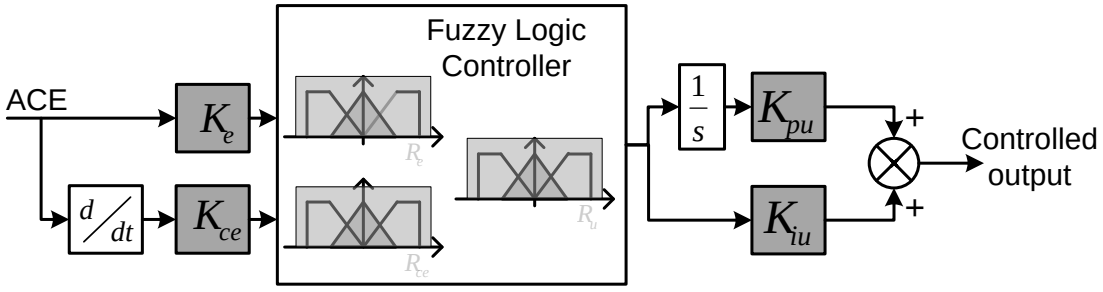

Fig. 4.49: Membership function's parameters and scaling factors optimized FLC in two steps (T2FLC)

Fig. 4.50 shows best fitness value with respect to iteration for scaling factor and membership function's parameters optimization for T2FLC.

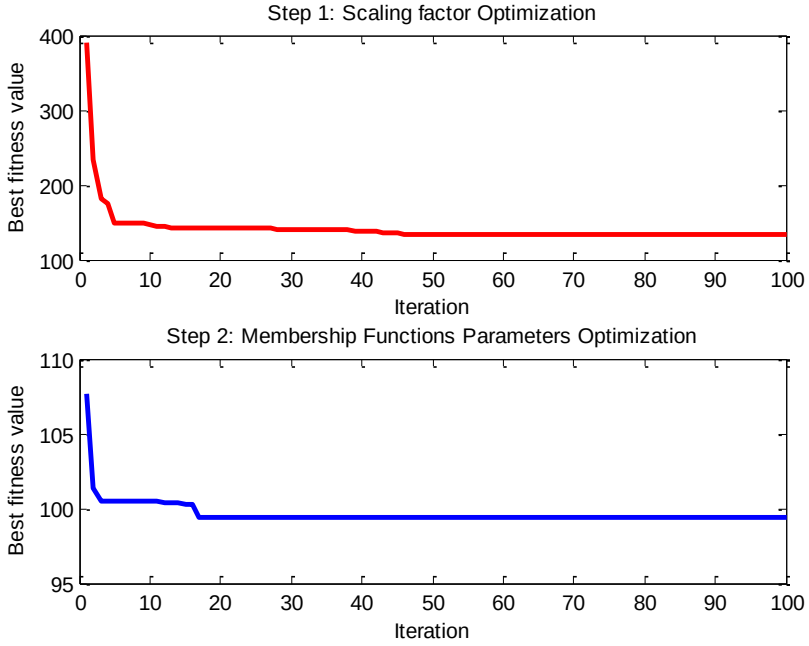

Fig. 4.50: Optimized parameters for T2FLC

Four step optimized FLC:-

Fig. 4.51 shows four steps optimized FLC, in which rule base is optimized in step 1, membership function parameters are optimized in step 2, scaling factors are optimized in step 3 and rule weights are optimized in step 4.

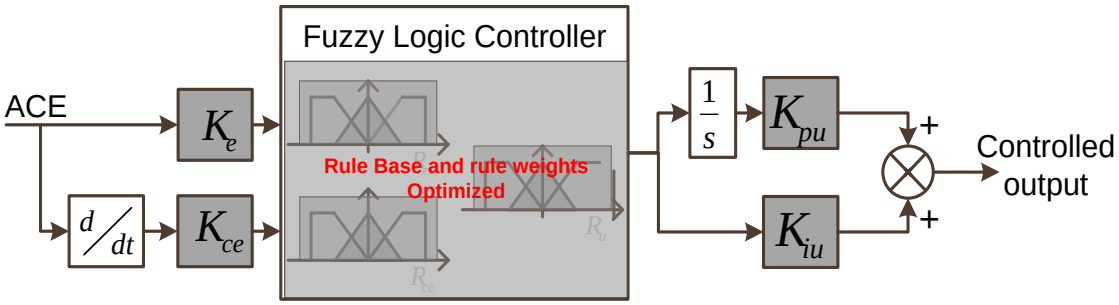

Fig. 4.51: Four step optimized FLC

Fig. 4.52 shows best fitness value with respect to iteration for different steps of optimization.

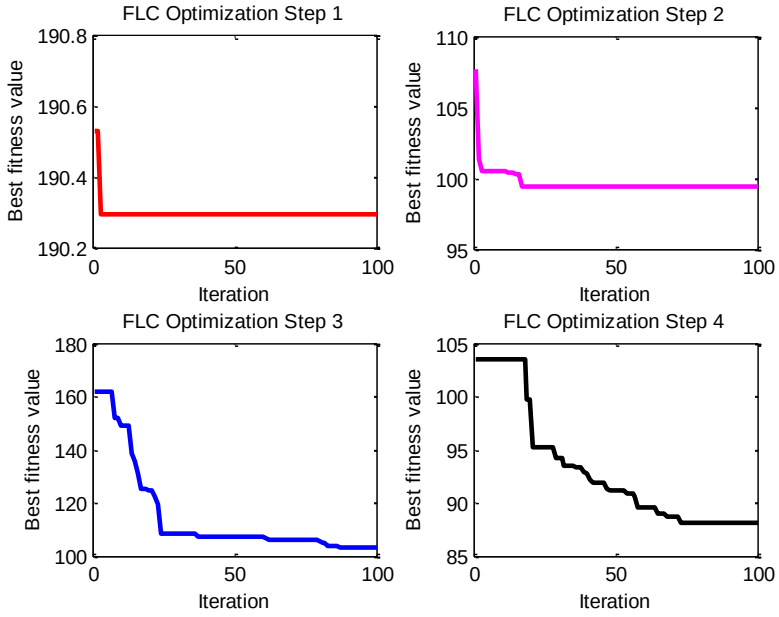

Fig. 4.52: Optimized parameters for FFLC

Rule base and rules weight of area 1 FFLC controller: -

1. If (E is VVL) and (CE is VVL) then (u is VVL)	(0.26813)
2. If (E is VVL) and (CE is VL) then (u is VVL)	(0.60042)
3. If (E is VVL) and (CE is L) then (u is VL)	(0.39729)
4. If (E is VVL) and (CE is Z) then (u is VL)	(0.38126)
5. If (E is VVL) and (CE is H) then (u is L)	(0.58340)
6. If (E is VVL) and (CE is VH) then (u is L)	(0.06562)
7. If (E is VVL) and (CE is VVH) then (u is Z)	(0.43036)
8. If (E is VL) and (CE is VVL) then (u is VVL)	(0.07569)
9. If (E is VL) and (CE is VL) then (u is VL)	(0.35730)
10. If (E is VL) and (CE is L) then (u is VL)	(0.09441)
11. If (E is VL) and (CE is Z) then (u is L)	(0.51140)
12. If (E is VL) and (CE is H) then (u is L)	(0.70374)
13. If (E is VL) and (CE is VH) then (u is Z)	(0.42155)
14. If (E is VL) and (CE is VVH) then (u is H)	(0.09758)
15. If (E is L) and (CE is VVL) then (u is VL)	(0.29840)
16. If (E is L) and (CE is VL) then (u is VL)	(0.45279)
17. If (E is L) and (CE is L) then (u is L)	(0.29053)
18. If (E is L) and (CE is Z) then (u is L)	(0.79907)
19. If (E is L) and (CE is H) then (u is Z)	(0.55694)
20. If (E is L) and (CE is VH) then (u is H)	(0.43832)
21. If (E is L) and (CE is VVH) then (u is H)	(0.99901)
22. If (E is Z) and (CE is VVL) then (u is VL)	(0.43709)
23. If (E is Z) and (CE is VL) then (u is L)	(0.48095)
24. If (E is Z) and (CE is L) then (u is L)	(0.28965)
25. If (E is Z) and (CE is Z) then (u is Z)	(0.04951)
26. If (E is Z) and (CE is H) then (u is H)	(0.28965)
27. If (E is Z) and (CE is VH) then (u is H)	(0.48095)
28. If (E is Z) and (CE is VVH) then (u is VH)	(0.43709)
29. If (E is H) and (CE is VVL) then (u is L)	(0.99899)
30. If (E is H) and (CE is VL) then (u is L)	(0.43832)
31. If (E is H) and (CE is L) then (u is Z)	(0.55694)
32. If (E is H) and (CE is Z) then (u is H)	(0.79907)
33. If (E is H) and (CE is H) then (u is H)	(0.29053)
34. If (E is H) and (CE is VH) then (u is VH)	(0.45279)
35. If (E is H) and (CE is VVH) then (u is VH)	(0.29838)
36. If (E is VH) and (CE is VVL) then (u is L)	(0.09758)
37. If (E is VH) and (CE is VL) then (u is Z)	(0.42155)
38. If (E is VH) and (CE is L) then (u is H)	(0.70374)
39. If (E is VH) and (CE is Z) then (u is H)	(0.51141)
40. If (E is VH) and (CE is H) then (u is VH)	(0.09441)
41. If (E is VH) and (CE is VH) then (u is VH)	(0.35731)
42. If (E is VH) and (CE is VVH) then (u is VVH)	(0.07569)
43. If (E is VVH) and (CE is VVL) then (u is Z)	(0.43036)
44. If (E is VVH) and (CE is VL) then (u is H)	(0.06562)
45. If (E is VVH) and (CE is L) then (u is H)	(0.58340)
46. If (E is VVH) and (CE is Z) then (u is VH)	(0.38126)
47. If (E is VVH) and (CE is H) then (u is VH)	(0.39729)
48. If (E is VVH) and (CE is VH) then (u is VVH)	(0.60042)
49. If (E is VVH) and (CE is VVH) then (u is VVH)	(0.26813)

Rule base and rules weight of area 2 FFLC controller: -

1. If (E is VVL) and (CE is VVL) then (u is VVL)	(0.74027)
2. If (E is VVL) and (CE is VL) then (u is VVL)	(0.63942)
3. If (E is VVL) and (CE is L) then (u is VL)	(0.44391)
4. If (E is VVL) and (CE is Z) then (u is VL)	(0.64860)
5. If (E is VVL) and (CE is H) then (u is L)	(0.74991)
6. If (E is VVL) and (CE is VH) then (u is L)	(0.63165)
7. If (E is VVL) and (CE is VVH) then (u is Z)	(0.07199)
8. If (E is VL) and (CE is VVL) then (u is VVL)	(0.21175)
9. If (E is VL) and (CE is VL) then (u is VL)	(0.69855)
10. If (E is VL) and (CE is L) then (u is VL)	(0.32976)
11. If (E is VL) and (CE is Z) then (u is L)	(0.82635)
12. If (E is VL) and (CE is H) then (u is L)	(0.35286)
13. If (E is VL) and (CE is VH) then (u is Z)	(0.78919)
14. If (E is VL) and (CE is VVH) then (u is H)	(0.59271)
15. If (E is L) and (CE is VVL) then (u is VL)	(0.44320)
16. If (E is L) and (CE is VL) then (u is VL)	(0.65462)
17. If (E is L) and (CE is L) then (u is L)	(0.70293)
18. If (E is L) and (CE is Z) then (u is L)	(0.84476)
19. If (E is L) and (CE is H) then (u is Z)	(0.51820)
20. If (E is L) and (CE is VH) then (u is H)	(0.49518)
21. If (E is L) and (CE is VVH) then (u is H)	(0.46083)
22. If (E is Z) and (CE is VVL) then (u is VL)	(0.54640)
23. If (E is Z) and (CE is VL) then (u is L)	(0.82628)
24. If (E is Z) and (CE is L) then (u is L)	(0.64377)
25. If (E is Z) and (CE is Z) then (u is Z)	(0.08635)
26. If (E is Z) and (CE is H) then (u is H)	(0.64377)
27. If (E is Z) and (CE is VH) then (u is H)	(0.82628)
28. If (E is Z) and (CE is VVH) then (u is VH)	(0.54640)
29. If (E is H) and (CE is VVL) then (u is L)	(0.46083)
30. If (E is H) and (CE is VL) then (u is L)	(0.49518)
31. If (E is H) and (CE is L) then (u is Z)	(0.51820)
32. If (E is H) and (CE is Z) then (u is H)	(0.84476)
33. If (E is H) and (CE is H) then (u is H)	(0.70293)
34. If (E is H) and (CE is VH) then (u is VH)	(0.65462)
35. If (E is H) and (CE is VVH) then (u is VH)	(0.44320)
36. If (E is VH) and (CE is VVL) then (u is L)	(0.59271)
37. If (E is VH) and (CE is VL) then (u is Z)	(0.78919)
38. If (E is VH) and (CE is L) then (u is H)	(0.35286)
39. If (E is VH) and (CE is Z) then (u is H)	(0.82635)
40. If (E is VH) and (CE is H) then (u is VH)	(0.32976)
41. If (E is VH) and (CE is VH) then (u is VH)	(0.69855)
42. If (E is VH) and (CE is VVH) then (u is VVH)	(0.21175)
43. If (E is VVH) and (CE is VVL) then (u is Z)	(0.07199)
44. If (E is VVH) and (CE is VL) then (u is H)	(0.63165)
45. If (E is VVH) and (CE is L) then (u is H)	(0.74991)
46. If (E is VVH) and (CE is Z) then (u is VH)	(0.64860)
47. If (E is VVH) and (CE is H) then (u is VH)	(0.44391)
48. If (E is VVH) and (CE is VH) then (u is VVH)	(0.63942)
49. If (E is VVH) and (CE is VVH) then (u is VVH)	(0.74027)

Table 4.17 shows gains for different type AGC controller's of two area power system.

Table 4.17: Different type of AGC controller's gains for two area power system

	Area-1 Controller				Area-2 Controller			
ZN tuned PI Controller	K_{p1}	K_{i1}			K_{p1}	K_{i2}		
	1.1861	0.8180			1.1861	0.8180		
ZN tuned PID Controller	K_{p1}	K_{i1}	K_{d1}		K_{p1}	K_{i2}	K_{d2}	
	1.5814	1.8177	0.3440		1.5814	1.8177	0.3440	
PSO optimized Integral Controller		K_{i1}				K_{i2}		
		0.7603				2.4586		
PSO optimized PID Controller	K_{p1}	K_{i1}	K_{d1}		K_{p1}	K_{i2}	K_{d2}	
	0.6346	1.2537	0.1366		0.6704	2.3843	0.4779	
Fuzzy Logic Controller	K_{e1}	K_{ce1}	K_{p1}	K_{i1}	K_{e2}	K_{ce2}	K_{p2}	K_{i2}
	0.0812	0.0392	26.6234	36.5911	0.0404	0.0539	17.7500	52.5939
Scaling factor and range optimized FLC	K_{e1}	K_{ce1}	K_{p1}	K_{i1}	K_{e2}	K_{ce2}	K_{p2}	K_{i2}
	0.1563	0.0857	36.7550	13.9749	0.0529	0.1778	8.5650	12.1155
Scaling factor and MF's parameter optimized FLC	K_{e1}	K_{ce1}	K_{p1}	K_{i1}	K_{e2}	K_{ce2}	K_{p2}	K_{i2}
	0.0812	0.0392	26.6234	36.5911	0.0404	0.0539	17.7500	52.5939
Four step optimized FLC	K_{e1}	K_{ce1}	K_{p1}	K_{i1}	K_{e2}	K_{ce2}	K_{p2}	K_{i2}
	0.0241	0.0350	4.4968	18.2482	0.0191	0.0213	7.6416	14.6433

Table 4.18 and 4.19 show optimized FFLC MF's parameters for area 1 and area 2 respectively.

Table 4.18: Optimized FFLC MF's parameters for area 1

MF's Name	Input 1 (ACE_1) MF's Parameters			Input 2 ($dACE_1$) MF's Parameters			Output (U_1)MF's Parameters		
	Left	**Mid**	**Right**	**Left**	**Mid**	**Right**	**Left**	**Mid**	**Right**
VVL	-15.00	-9.79	-7.04	-15.00	-9.68	-6.49	-15.00	-9.68	-6.39
VL	-9.66	-6.57	-3.25	-9.65	-6.25	-3.56	-9.71	-6.26	-3.21
L	-6.75	-3.19	0	-6.31	-2.99	0	-6.92	-3.72	0
Z	-3.62	0	3.62	-3.32	0	3.32	-3.08	0	3.08
H	0	3.19	6.75	0	2.99	6.31	0	3.72	6.92
VH	3.25	6.57	9.66	3.56	6.25	9.65	3.21	6.26	9.71
VVH	7.04	9.79	15.00	6.49	9.68	15.00	6.39	9.68	15.00

Table 4.19: Optimized FFLC MF's parameters for area 2

MF's Name	Input 1 (ACE_2) MF's Parameters			Input 2 ($dACE_2$) MF's Parameters			Output (U_2)MF's Parameters		
	Left	Mid	Right	Left	Mid	Right	Left	Mid	Right
VVL	-15.00	-9.63	-6.87	-15.00	-9.61	-6.59	-15.00	-9.65	-6.23
VL	-9.77	-6.21	-3.72	-9.80	-6.38	-3.38	-9.78	-6.51	-3.45
L	-6.51	-2.94	0	-6.78	-3.37	0	-7.01	-3.59	0
Z	-3.46	0	3.46	-3.31	0	3.31	-3.55	0	3.55
H	0	2.94	6.51	0	3.37	6.78	0	3.59	7.01
VH	3.72	6.21	9.77	3.38	6.38	9.80	3.45	6.51	9.78
VVH	6.87	9.63	15.00	6.59	9.61	15.00	6.23	9.65	15.00

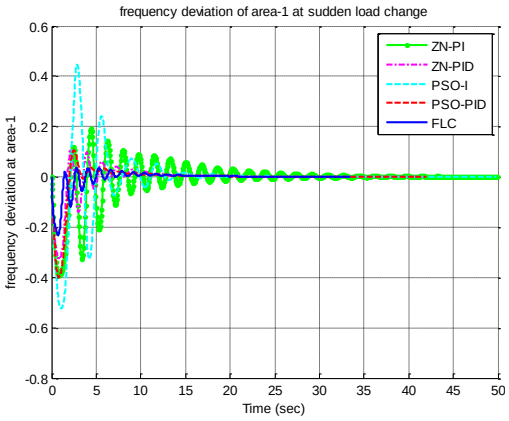

Fig. 4.53: Deviation in frequency of area-1 for FLC against different conventional controllers

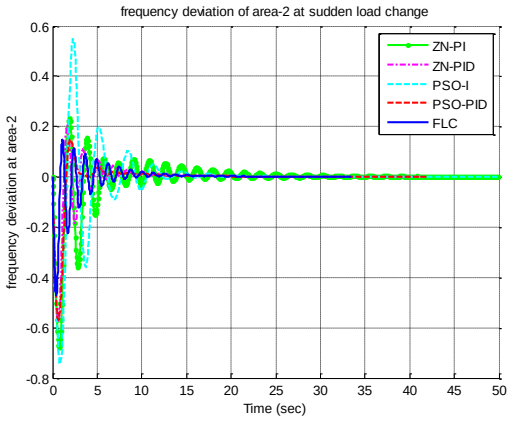

Fig. 4.54: Deviation in frequency of area-2 for FLC against different conventional controllers

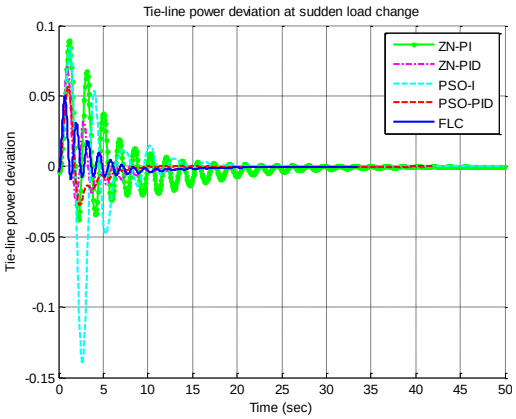

Fig. 4.55: Deviation in tie-line power for FLC against different conventional controllers

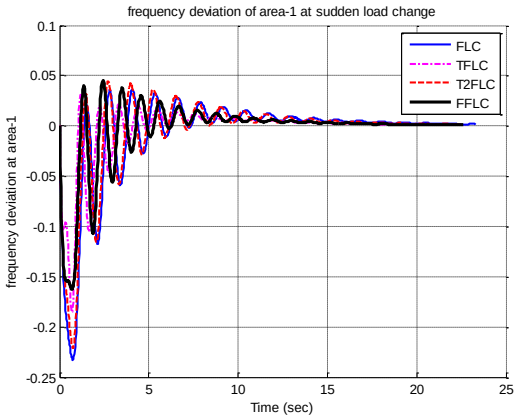

Fig. 4.56: Deviation in frequency of area-1 for different optimized FLC controllers

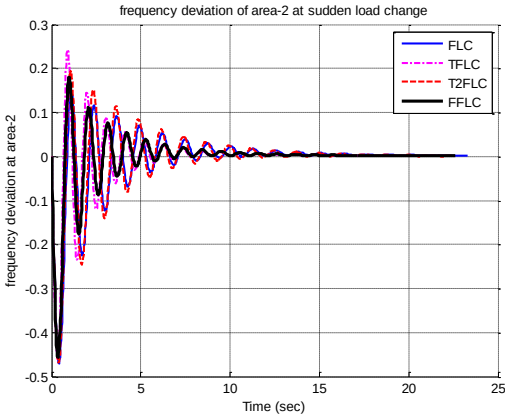

Fig. 4.57: Deviation in frequency of area-2 for different optimized FLC controllers

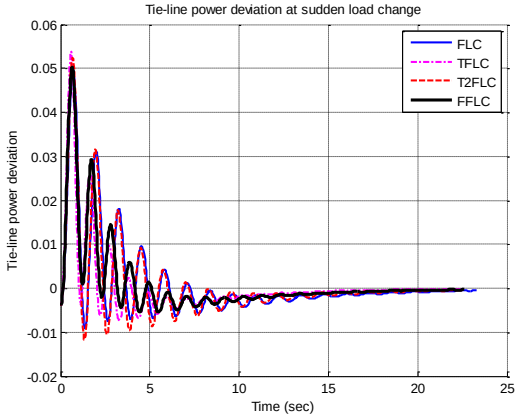

Fig. 4.58: Deviation in tie-line power for different optimized FLC controllers

There are 8 different controllers being examined for above system, out of 8 controllers, there are 4 conventional controllers. Responses of conventional controllers compared against FLC controller in one plot and in another plot different optimized FLC have been compared. Fig. 4.53 and 4.56 show frequency deviation in area-1 for different controllers and Fig. 4.54 and 4.57 show frequency deviations in area-2 for different controllers. Fig. 4.55 and 4.58 show tie-line deviation for TT-TH system. It is observed from these six plots that FLC gives better response than conventional controllers and among all controllers, FFLC shows better performance.

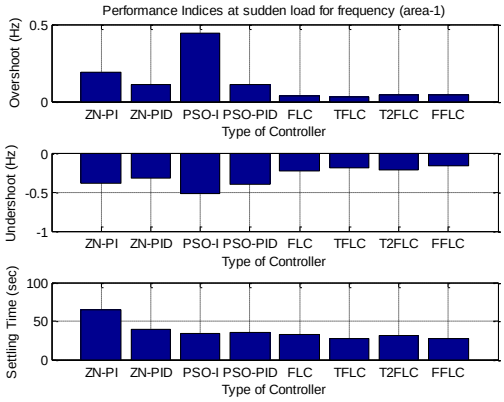

Fig. 4.59: Performance indices for different controllers for deviation in frequency of area-1

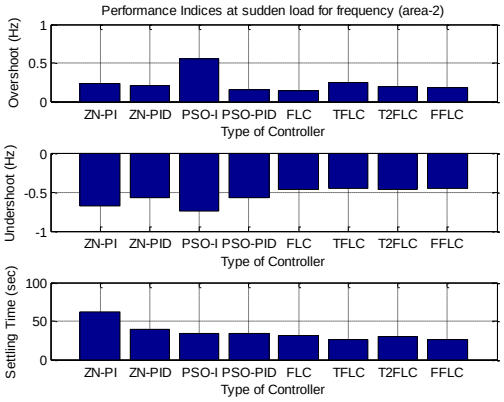

Fig. 4.60: Performance indices for different controllers for deviation in frequency of area-2

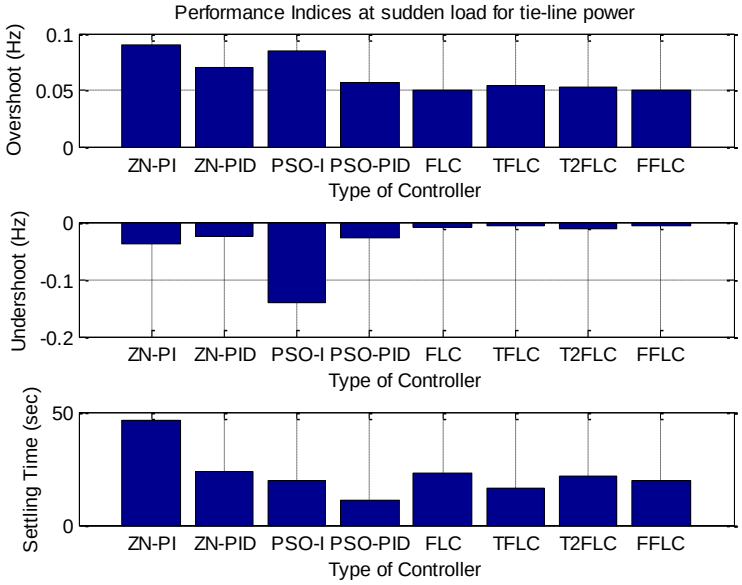

Fig. 4.61: Performance indices for different controllers for deviation in tie-line power deviation

Further these results are represented in terms of peak undershoot, peak overshoot and settling time as Fig. 4.59, 4.60 and 4.61, which shows bar chart for these performance indices for frequency deviation of area-1, frequency deviation of area-2 and tie-line power deviation.

Table 4.20: Performance indices of Δf1, Δf2 and Δptie12 at sudden load for different controllers

	ZN PI	ZN PID	PSO I	PSO PID	FLC	TFLC	T2FLC	FFLC
Peak Undershoot								
Δf1	-0.39223	-0.32367	-0.52407	-0.40066	-0.23285	-0.18525	-0.22116	-0.16247
Δf2	-0.67892	-0.57361	-0.74587	-0.56979	-0.47016	-0.45977	-0.46935	-0.45582
Δptie12	-0.03769	-0.02528	-0.14017	-0.02749	-0.00913	-0.00729	-0.01175	-0.00542
Peak Overshoot								
Δf1	0.192766	0.10903	0.445695	0.108625	0.036266	0.031286	0.044249	0.045647
Δf2	0.235671	0.204848	0.547588	0.148994	0.145693	0.242522	0.192791	0.180608
Δptie12	0.089528	0.070646	0.084106	0.05622	0.049582	0.053816	0.052455	0.050356
Settling Time								
Δf1	64.60568	39.89337	34.07402	34.9962	32.55599	26.95173	30.73199	27.11018
Δf2	62.24771	39.06753	33.73327	34.29838	31.97447	26.40513	30.35117	26.64072
Δptie12	46.52841	23.48263	19.65757	11.01491	23.31172	16.40705	21.80819	19.44155

Apart from these figures Table 4.20 shows numerical values of these performance indices. From these results, it is observed FFLC shows better performance from all considered controllers for present system. It is concluded that FFLC is an effective controller in terms of providing lesser deviation and faster settling for two area thermal hydro interconnected power system.

4.7 Summary

In this chapter, different objective functions have been considered. Out of these, four objective functions are error-based functions and the rest five are based on performance indices. Apart from these, three basic optimization techniques are explored for interconnected hydro thermal system namely GA, ACO and PSO. Further different variants of PSO are also analyzed to introduce adaptiveness. Then fuzzy logic based AGC controller was designed for interconnected two area power system and later FLC is optimized with different strategies. Finally four step optimized FLC found better compared to other controllers on the basis of dynamic performance.

References

[1] C. Knospe, "PID control," *IEEE Control Syst. Mag.*, vol. 26, no. 1, pp. 30–31, 2006.

[2] K. H. Ang, G. Chong, and Y. Li, "PID control system analysis, design, and technology," *IEEE Trans. Control Syst. Technol.*, vol. 13, no. 4, pp. 559–576, 2005.

[3] K. H. Ang, G. Chong, and Y. Li, "PID Control System Analysis , Design , and Technology," *IEEE Trans. Control Syst. Technol.*, vol. 13, no. 4, pp. 559–576, 2005.

[4] J. G. Ziegler, N. B. Nichols, and N. Y. ROCHESTER, "Optimum Settings for Automatic Controllers," *Trans. A.S.M.E.*, vol. 65, no. 5, pp. 433–444, 1942.

[5] L. Renhou and Z. Yi, "Fuzzy logic controller based on genetic algorithms," *Fuzzy sets Syst.*, vol. 83, pp. 1–10, 1996.

[6] D. Goldberg, *Genetic Algorithms in Search, Optimization, and Machine Learning*. Pearson Education India, 1989.

[7] M. Dorigo and T. Stützle, *Ant Colony Optimization*. London, England: MIT Press Cambridge, Massachusetts, 2004.

[8] C. Juang and P. Chang, "Designing fuzzy-rule-based systems using continuous ant-colony optimization," *IEEE Trans. Fuzzy Syst.*, vol. 18, no. 1, pp. 138–149, 2010.

[9] J. Kennedy and R. Eberhart, "Particle swarm optimization," in *Proceedings of International Conference on Neural Networks ICNN'95*, 1995, pp. 1942–1948.

[10] A. Nickabadi, M. M. Ebadzadeh, and R. Safabakhsh, "A novel particle swarm optimization algorithm with adaptive inertia weight," *Appl. Soft Comput.*, vol. 11, pp. 3658–3670, 2011.

[11] X. Yang, J. Yuan, J. Yuan, and H. Mao, "A modified particle swarm optimizer with dynamic adaptation," *Appl. Math. Comput.*, vol. 189, no. 2, pp. 1205–1213, 2007.

[12] F. Van Den Bergh, "An analysis of particle swarm optimizers," University of Pretoria, Pretoria, 2006.

[13] J. Kennedy and R. Eberhart, "Particle swarm optimization," in *IEEE International conference on Neural Networks*, 1995, vol. 4, pp. 1942–1948.

[14] M. S. Arumugam and M. V. C. Rao, "On the improved performances of the particle swarm optimization algorithms with adaptive parameters, cross-over operators and root mean square (RMS) variants for computing optimal control of a class of hybrid systems," *Appl. Soft Comput.*, vol. 8, no. 1, pp. 324–336, 2008.

[15] K. Suresh, S. Ghosh, D. Kundu, A. Sen, S. Das, and A. Abraham, "Inertia-Adaptive Particle Swarm Optimizer for Improved Global Search," in *Intelligent Systems Design and Applications*, 2008, pp. 253–258.

[16] Y. Shi and R. Eberhart, "A modified particle swarm optimizer," in *IEEE World*

Congress on Computational Intelligence in Evolutionary Computation Proceedings, 1998, 1998, pp. 69–73.

[17] A. Ratnaweera, S. K. Halgamuge, and H. C. Watson, "Self-organizing hierarchical particle swarm optimizer with time-varying acceleration coefficients," *IEEE Trans. Evol. Comput.*, vol. 8, no. 3, pp. 240–255, 2004.

[18] E. Muneender and D. M. Vinodkumar, "Particle Swarm Optimization with Time Varying Acceleration Coefficients for Congestion Management," in *IEEE Conference on Sustainable Utilization and Development in Engineering and Technology*, 2012, pp. 92–96.

[19] G. Chown and R. Hartman, "Design and experience with a fuzzy logic controller for automatic generation control (AGC)," *IEEE Trans. power Syst.*, vol. 13, no. 3, pp. 965–970, 1998.

[20] R. C. Bansal, "Bibliography on the fuzzy set theory applications in power systems (1994-2001)," *IEEE Trans. Power Syst.*, vol. 18, no. 4, pp. 1291–1299, 2003.

[21] E. Cam and Ilhan Kocoaarslan, "Load frequency control in two area power systems using fuzzy logic controller," *Energy Convers. Manag.*, vol. 46, pp. 233–243, 2005.

[22] H. D. Mathur and H. V. Manjunath, "Frequency stabilization using fuzzy logic based controller for multi-area power system," *South Pacific J. Nat. Sci.*, vol. 4, pp. 22–30, 2007.

[23] L. X. Wang, *A course in fuzzy systems and control*. Prentice Hall International Inc., 1996.

[24] C. C. LEE, "Fuzzy Logic in Control Systems : Fuzzy Logic Controller-Part I," *IEEE Trans. Syst. Man. Cybern.*, vol. 20, no. 2, pp. 404–418, 1990.

[25] W. Zhi Qiao and M. Mizumoto, "PID type fuzzy controller and parameters adaptive method," *Fuzzy Sets Syst.*, vol. 78, pp. 23–35, 1996.

[26] Z.-W. Woo, H.-Y. Chung, and J.-J. Lin, "A PID type fuzzy controller with self-tuning scaling factors," *Fuzzy Sets Syst.*, vol. 115, no. 2, pp. 321–326, 2000.

Chapter 5

Simulation Test Cases and Results: Impact of Integration of WPGS and SMES

5.1 Introduction

The rising penetration level of wind power into power system has brought complexity into it. Therefore, it becomes important to understand the impact of it on a power system. In order to investigate the effect of a WPGS integration with inertial support for interconnected power system, different sets of simulations have been conducted in a two area thermal-hydro interconnected power system with integral controller as supplementary controller and in order to mitigate oscillation, impact of SMES integration is also examined. In this study, different types of combinations based on WPGS and SMES integration are taken. WPGS provides maximum of 0.1 p.u. short term active power support through inertial control mechanism for all different cases considered in this thesis.

5.2 Integration of WPGS in Interconnected Power System with different level of Penetration

In present study, combinations of generating units for interconnected power system model are in such a way that area-1 has thermal-thermal generating units and area-2 thermal-hydro generating units. WPGS with different level of penetration ranging from 0 to 30% is simulated and analyzed. The Simulink model of AGC with WPGS integration is shown in Fig. 5.1. Fig 5.2 shows Simulink model for WPGS and Fig. 5.3 shows Simulink model of wind power that convert the wind speed to mechanical power.

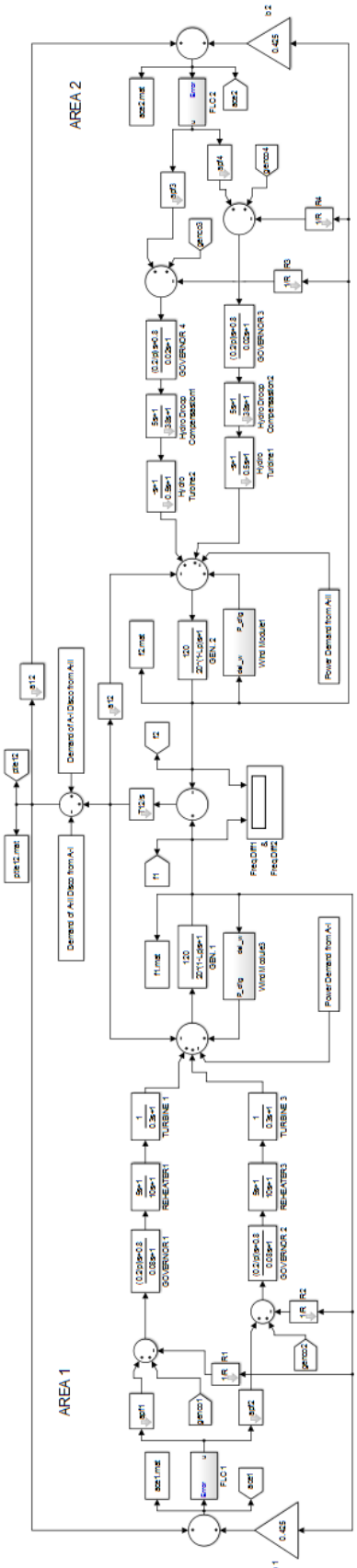

Fig. 5.1: Simulink model of AGC for two area hydro-thermal power system with WPGS integration

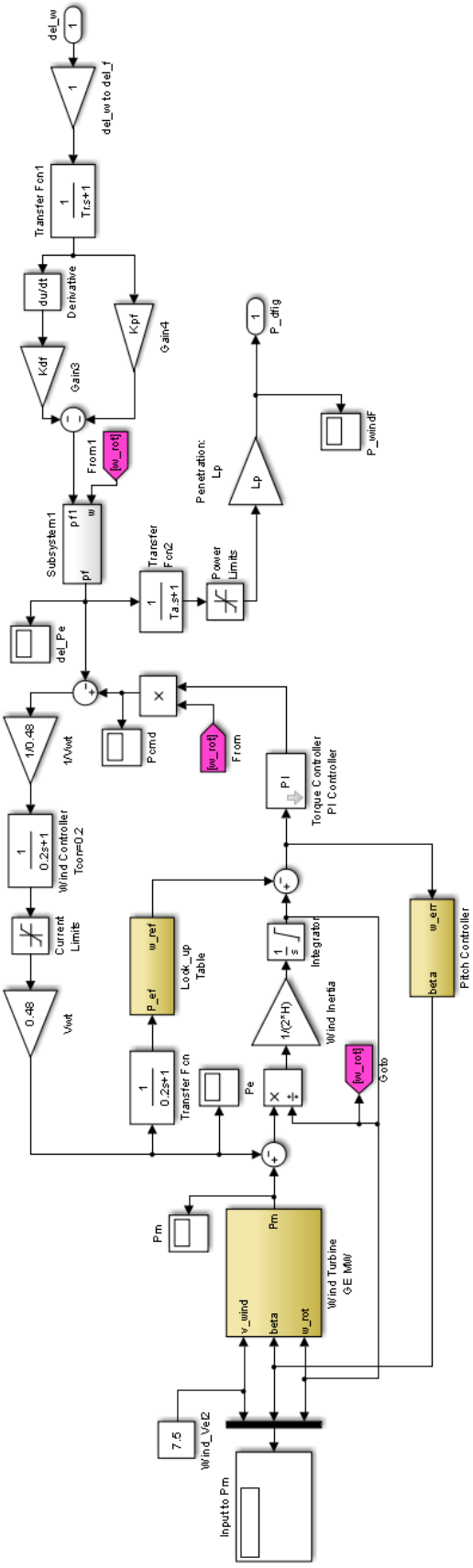

Fig. 5.2: Simulink model for WPGS

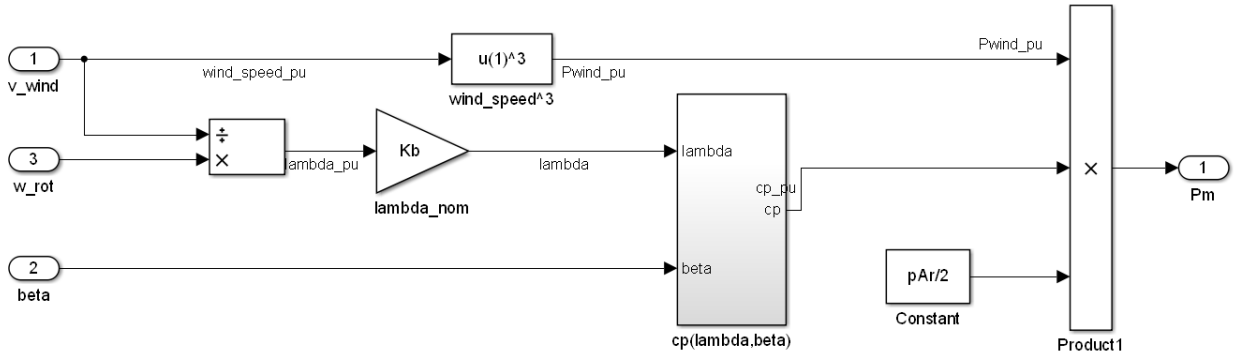

Fig. 5.3: Simulink model for wind power

5.2.1 Simulation results to examine impact of WPGS without frequency regulation support

When the generation and demand balance is lost, the system frequency will change at a rate initially determined by the total system inertia. In general, integration of wind power system will increase the installed power capacity but the effective system inertia will reduce because of WPGS units based on power converters create a decoupling effect [1], [2]. Increasing penetration level will make power grid weak because of intermittent nature of wind. This has forced power system engineers to limit it around 20-25%. In order to study the impact of WPGS integration without frequency support, the different levels of penetration 10%, 20% and 30% are considered.

Fig. 5.4, 5.5 and 5.6 shows deviation in frequency of area-1, deviation in frequency of area-2 and deviation in tie-line power respectively. Fig. 5.7, 5.8 and 5.9 shows the different performance indices for deviation in frequencies of both areas and deviation in tie-line power respectively. In these figures, it is observed from different performance indices that system response become poorer as penetration being increased.

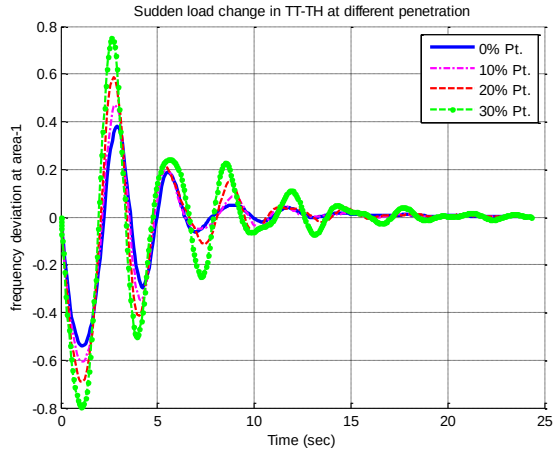

Fig. 5.4: Deviation in frequency of area-1 for different penetration level of WPGS

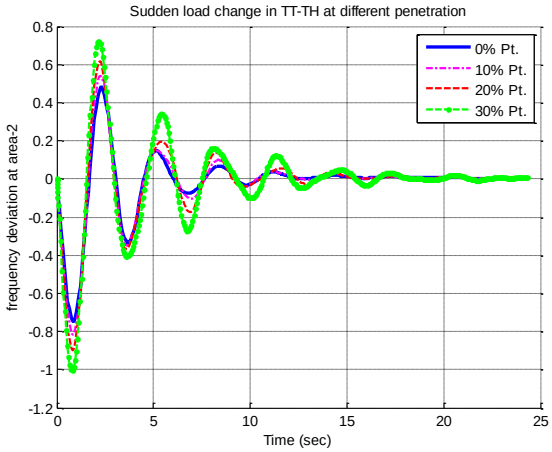

Fig. 5.5: Deviation in frequency of area-2 for different penetration level of WPGS

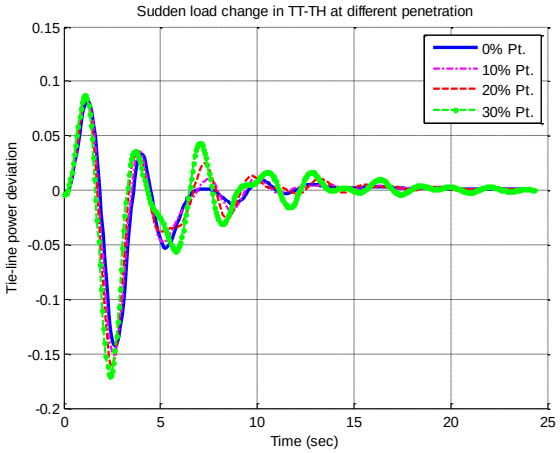

Fig. 5.6: Deviation in tie-line power for different penetration level of WPGS

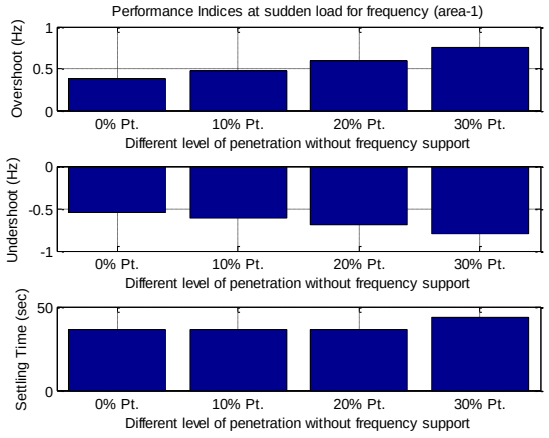

Fig. 5.7: Performance indices for deviation in frequency of area-1 for different penetration level of WPGS

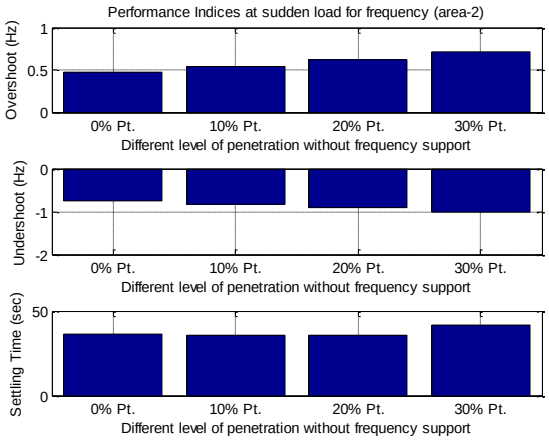

Fig. 5.8: Performance indices for deviation in frequency of area-2 for different penetration level of WPGS

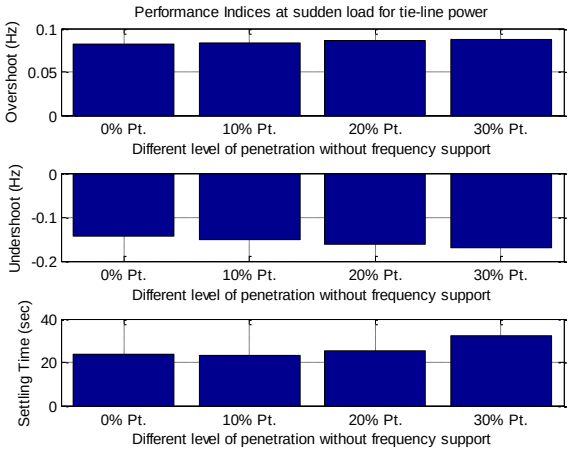

Fig. 5.9: Performance indices for deviation in tie-line power for different penetration level of WPGS

5.2.2 Simulation results to examine impact of WPGS with frequency regulation support

The study for impact of WPGS integration is simulated in different sets as marked below:

- **i.** Impact of WPGS integration in TTW-TH (area-1 Thermal-Thermal with WPGS and area-2 Thermal-Hydro) system at different level of penetration
- **ii.** Impact of WPGS integration in TT-THW (area-1 Thermal-Thermal and area-2 Thermal-Hydro with WPGS) system at different level of penetration
- **iii.** Impact of WPGS integration in TTW-THW (area-1 Thermal-Thermal with WPGS and area-2 Thermal-Hydro with WPGS) system at different level of penetration

5.2.2.1 Simulation results for TTW-TH system

In this case, the concept of inertial support by WPGS in order to minimize inter area oscillations have been examined. WPGS is integrated only in area-1, where both

GENCOs are thermal- reheat based generation units. The different level of penetration has been considered for study the impact of WPGS integration with inertial support in this (TTW-TH) system.

Fig. 5.10, 5.11 and 5.12 show deviation in frequency of area-1, deviation in frequency of area-2 and deviation in tie-line power respectively. It is observed that as penetration increases, the deviation also increases. These results of different performance indices for deviation in frequencies of both areas and deviation in tie-line power are obtained and given in Fig. 5.13, 5.14 and 5.15. It is observed that impact of penetration is more than inertial support by WPGS.

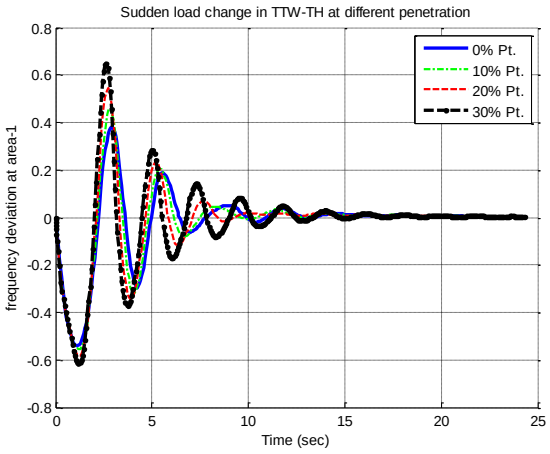

Fig. 5.10: Deviation in frequency of area-1 for TTW-TH system at different penetration level of WPGS

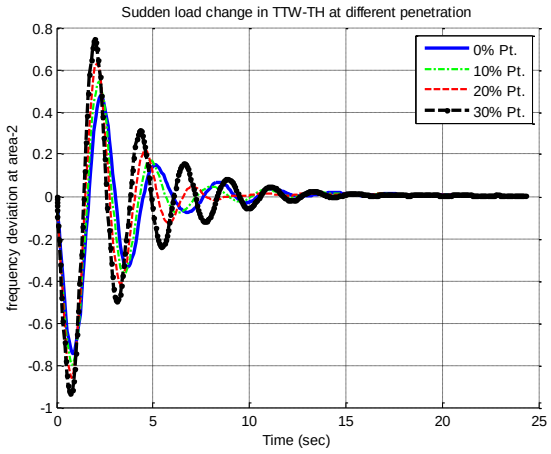

Fig. 5.11: Deviation in frequency of area-2 for TTW-TH system at different penetration level of WPGS

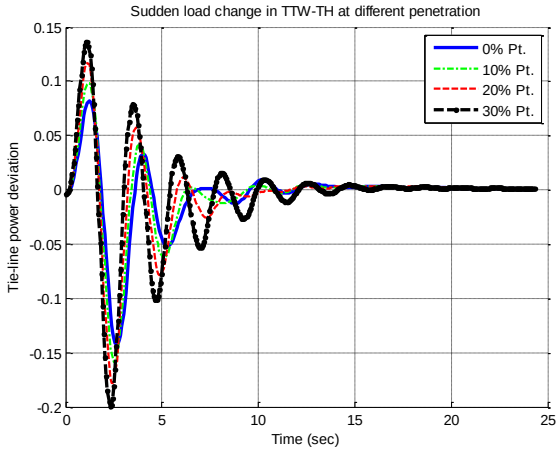

Fig. 5.12: Deviation in tie-line power for TTW-TH system at different penetration level of WPGS

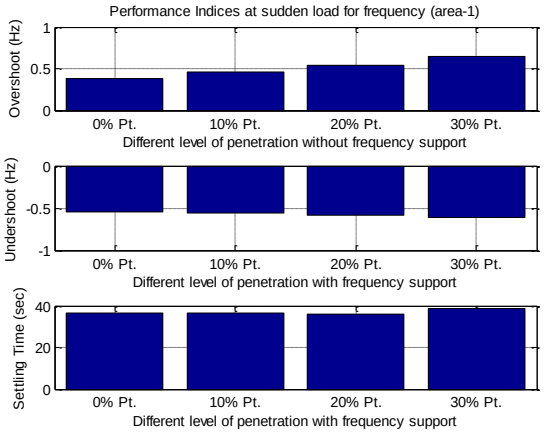

Fig. 5.13: Performance indices for deviation in frequency of area-1 for TTW-TH system

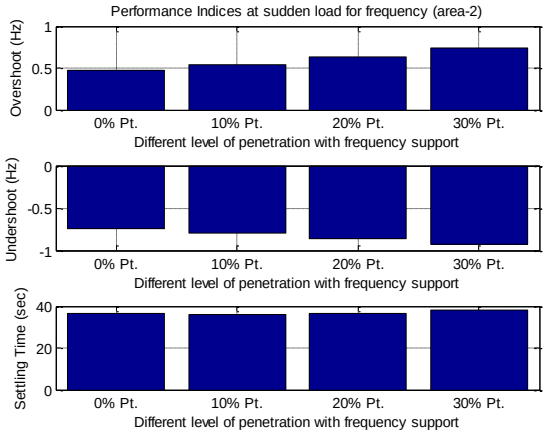

Fig. 5.14: Performance indices for deviation in frequency of area-2 for TTW-TH system

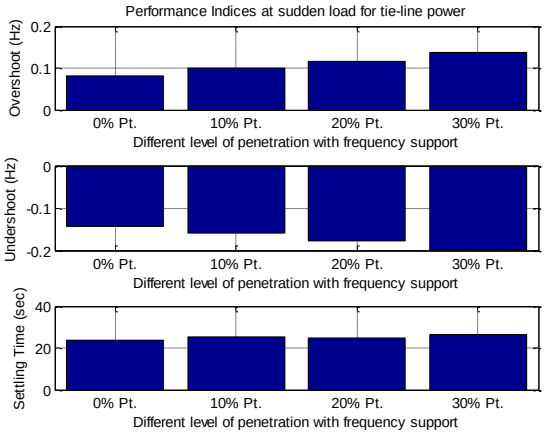

Fig. 5.15: Performance indices for deviation in tie-line power for TTW-TH system

5.2.2.2 Simulation results for TT-THW system

To observe the effect of inertial support by WPGS, two area interconnected system is considered where WPGS is integrated only in area-2. Fig. 5.16, 5.17 and 5.18 show deviation in frequency of area-1, deviation in frequency of area-2 and deviation in tie-line power respectively. These figures show that as penetration is increasing, the peak

deviations decrease. Performance indices for deviation in frequencies of both areas and deviation in tie-line power are shown in Fig. 5.19, 5.20 and 5.21. It is observed in present case, effect of inertial support by WPGS is more than the impact of penetration.

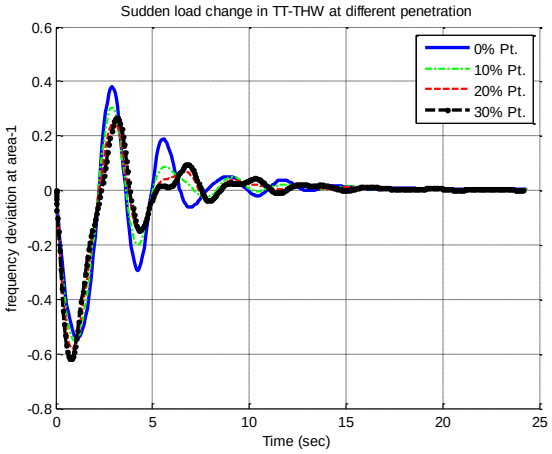

Fig. 5.16: Deviation in frequency of area-1 for TT-THW system at different penetration level of WPGS

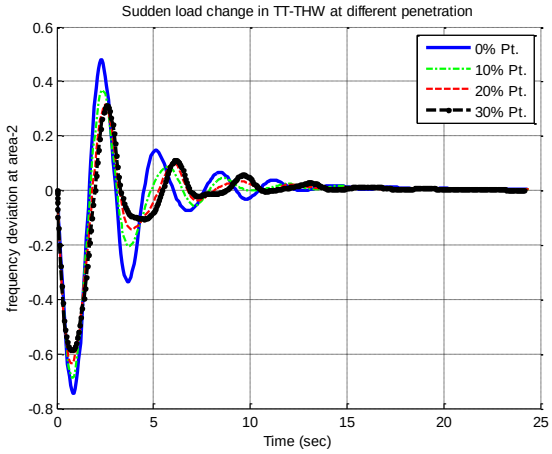

Fig. 5.17: Deviation in frequency of area-2 for TT-THW system at different penetration level of WPGS

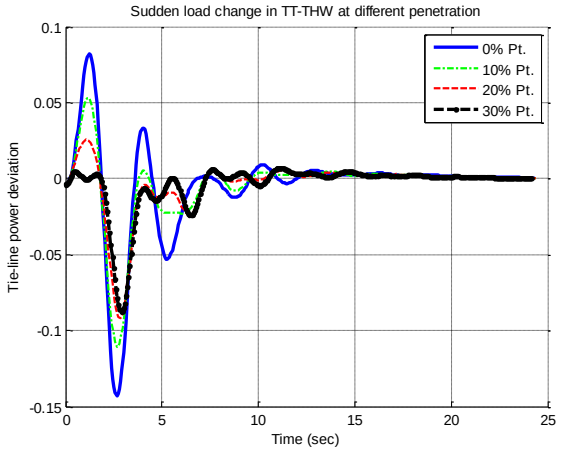

Fig. 5.18: Deviation in tie-line power for TT-THW system at different penetration level of WPGS

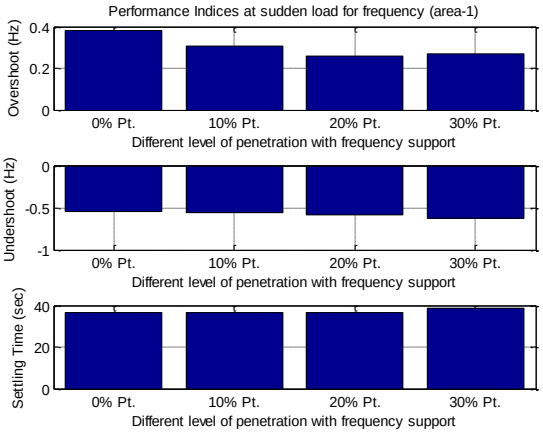

Fig. 5.19: Performance indices for deviation in frequency of area-1 for TT-THW system

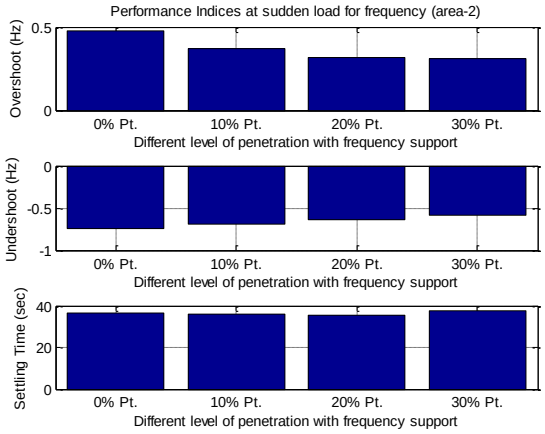

Fig. 5.20: Performance indices for deviation in frequency of area-2 for TT-THW system

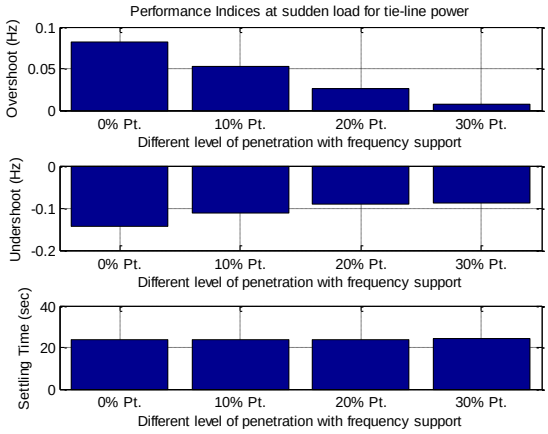

Fig. 5.21: Performance indices for deviation in tie-line power for TT-THW system

5.2.2.3 Simulation results for TTW-THW system

In this case, in order to examine the effect of inertial support by WPGS, WPGS is integrated in both areas. Fig. 5.22, 5.23 and 5.24 show deviation in frequency of area-1, deviation in frequency of area-2 and deviation in tie-line power respectively. It is observed from these figures that as penetration is increasing, the deviations are decreasing where Fig. 5.25, 5.26 and 5.27 show quantified presentation of different performance indices. It is observed that WPGS integration in both areas is very effective for oscillation mitigation.

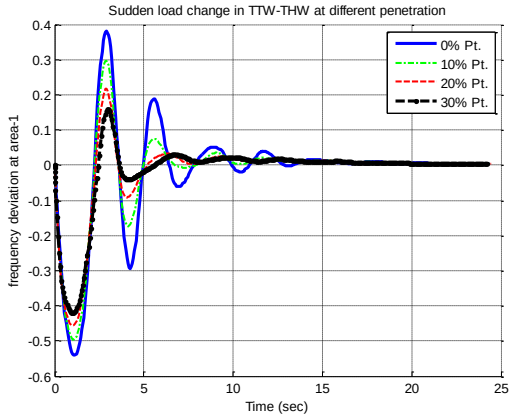

Fig. 5.22: Deviation in frequency of area-1 for TTW-THW system at different penetration level of WPGS

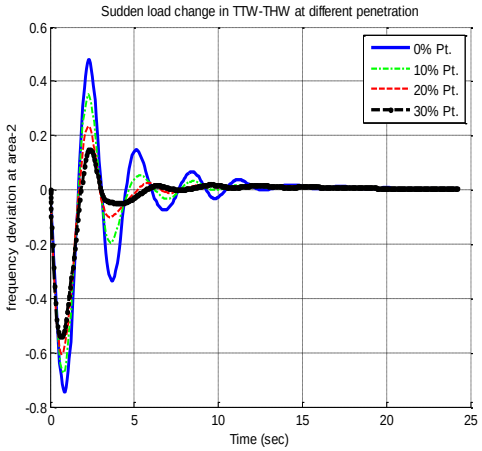

Fig. 5.23: Deviation in frequency of area-2 for TTW-THW system at different penetration level of WPGS

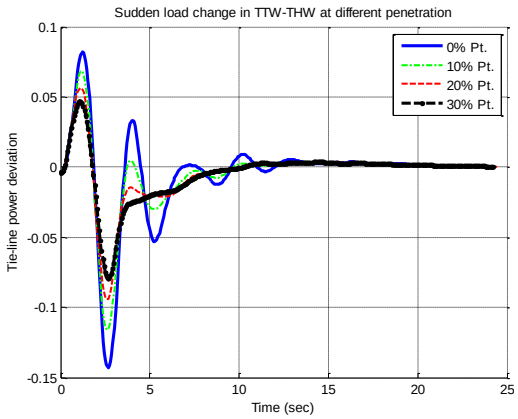

Fig. 5.24: Deviation in tie-line power for TTW-THW system at different penetration level of WPGS

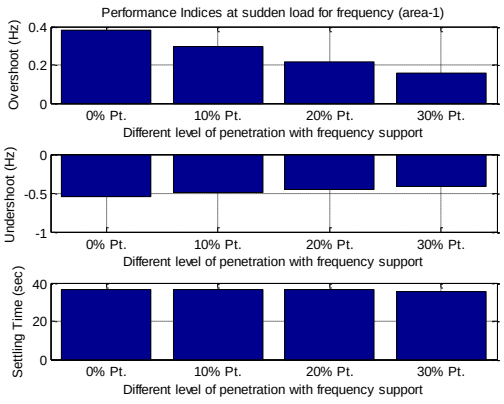

Fig. 5.25: Performance indices for deviation in frequency of area-1 for TTW-THW system

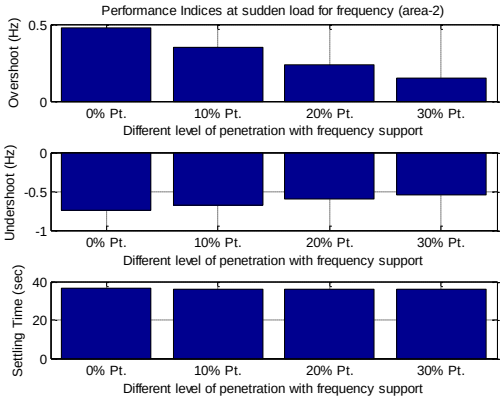

Fig. 5.26: Performance indices for deviation in frequency of area-2 for TTW-THW system

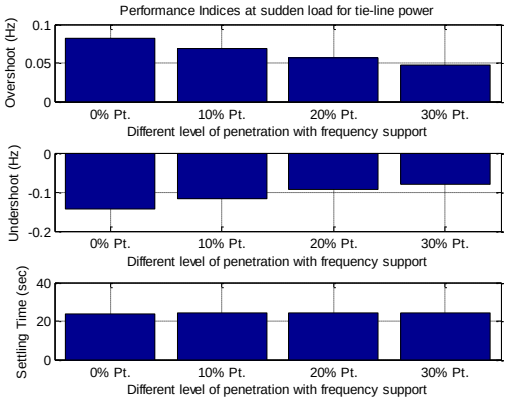

Fig. 5.27: Performance indices for deviation in tie-line power for TTW-THW system

5.3 Comparative Results of WPGS integration in different type of Systems

This section presents the detailed analysis of different sets of systems at fixed 30% penetration. Four different systems have been considered for WPGS integration with inertial support taken into consideration. These systems are,

(i) TT-TH system (No WPGS integration in any area)

(ii) TTW-TH system (WPGS integration with inertial support in area-1)

(iii) TT-THW system (WPGS integration with inertial support in area-2)

(iv) TTW-THW system (WPGS integration with inertial support in both areas)

Fig. 5.28, 5.29 and 5.30 show deviation in frequency of area-1, deviation in frequency of area-2 and deviation in tie-line power respectively. Fig. 5.31, 5.32 and 5.33 show different performance indices for deviation in frequency of area-1, deviation in frequency of area-2 and deviation in tie-line power respectively.

It is observed from these figures that WPGS penetration with inertial support is effective technique for oscillation suppression also can be concluded that WPGS is more effective

in area where a hydro generation unit exists because response time of hydro generation unit is slower as compared to thermal generating unit.

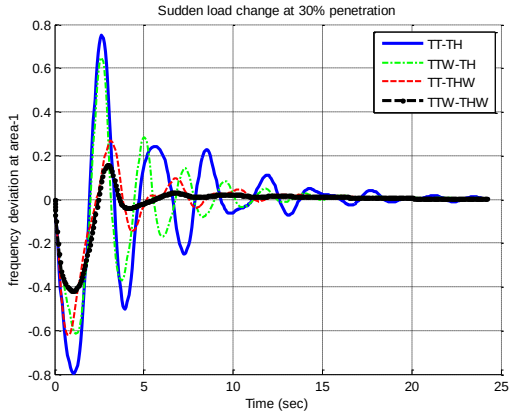

Fig. 5.28: Deviation in frequency of area-1 for different systems at 30% penetration of WPGS

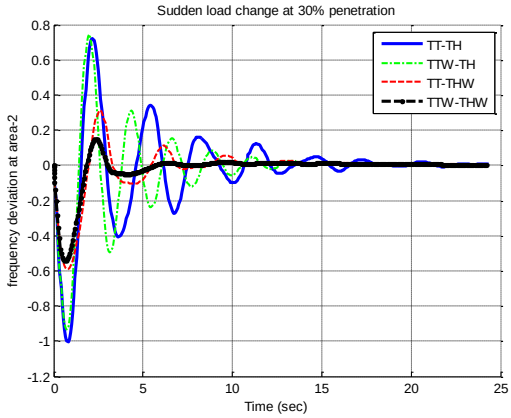

Fig. 5.29: Deviation in frequency of area-2 for different systems at 30% penetration of WPGS

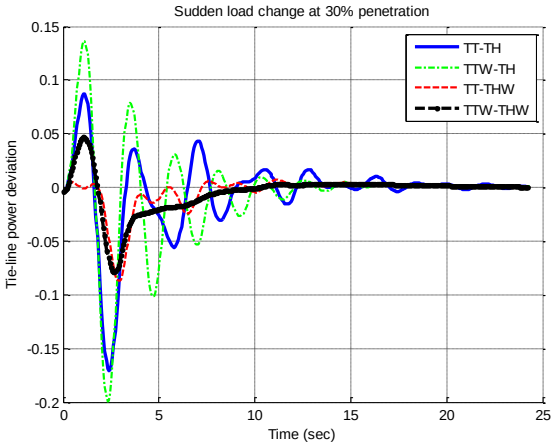

Fig. 5.30: Deviation in tie-line power for different systems at 30% penetration of WPGS

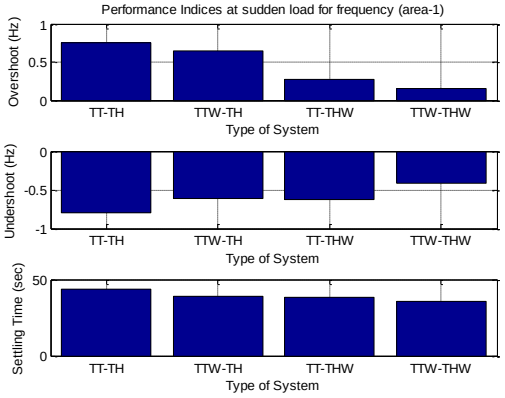

Fig. 5.31: Performance indices for deviation in frequency of area-1 for different systems at 30% penetration of WPGS

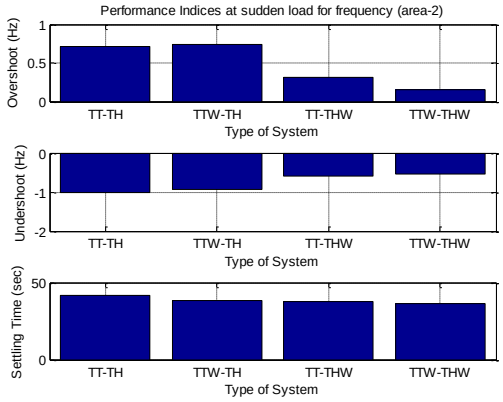

Fig. 5.33: Performance indices for deviation in frequency of area-2 for different systems at 30% penetration of WPGS

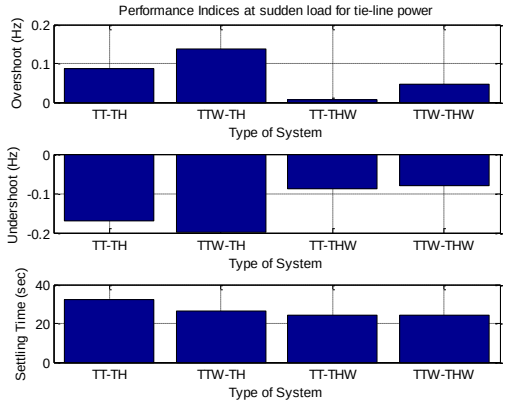

Fig. 5.34: Performance indices for deviation in tie-line power for different systems at 30% penetration of WPGS

5.4 Simulation Results with Optimized FLC in WPGS Integrated System

The Simulink model of this study is shown in Fig. 5.1. Controllers examined are, integral controller, PI Controller, PID controller, FLC and FFLC. Table 5.1 shows the gains for different controllers considered to inspect the impact of WPGS integration in TTW-THW system.

The *cpf_matrix* and DISCO demand matrix used for this study are:

$$cpf\_matrix = \begin{bmatrix} 0.25 & 0.2 & 0.15 & 0.15 \\ 0.25 & 0.25 & 0.15 & 0.2 \\ 0.3 & 0.25 & 0.35 & 0.35 \\ 0.2 & 0.3 & 0.35 & 0.3 \end{bmatrix} \text{ and } \Delta P_L = \begin{bmatrix} 0.1 \\ 0.05 \\ 0.15 \\ 0.05 \end{bmatrix}$$

Table 5.1: Different type of AGC controller's gains for TTW-THW system

	Area-1 Controller				Area-2 Controller			
ZN tuned PI Controller	K_{p1}	K_{i1}			K_{p1}	K_{i2}		
	1.0829	0.7924			1.0829	0.7924		
ZN tuned PID Controller	K_{p1}	K_{i1}	K_{d1}		K_{p1}	K_{i2}	K_{d2}	
	1.4439	1.7609	0.2960		1.4439	1.7609	0.2960	
PSO optimized Integral Controller		K_{i1}				K_{i2}		
		0.4979				2.3479		
PSO optimized PID Controller	K_{p1}	K_{i1}	K_{d1}		K_{p1}	K_{i2}	K_{d2}	
	1.1195	1.2875	0.2860		0.5650	2.2615	0.2369	
Fuzzy Logic Controller	K_{e1}	K_{ce1}	K_{p1}	K_{i1}	K_{e2}	K_{ce2}	K_{p2}	K_{i2}
	0.0998	0.0884	39.6469	65.8250	0.1667	0.0993	9.1027	23.9644
Four step optimized FLC	K_{e1}	K_{ce1}	K_{p1}	K_{i1}	K_{e2}	K_{ce2}	K_{p2}	K_{i2}
	0.0300	0.0875	33.1246	76.3125	0.0345	0.0902	4.7855	11.4962

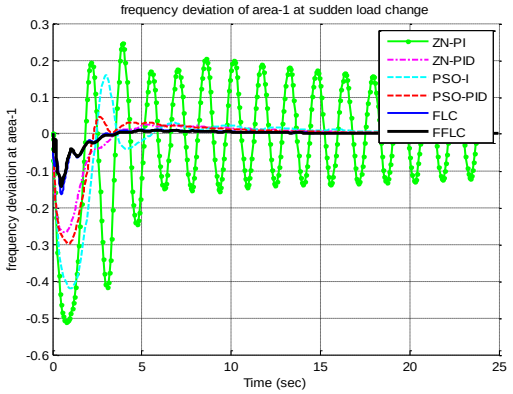

Fig. 5.34: Deviation in frequency of area-1 for TTW-THW system for different controllers at 30% penetration of WPGS

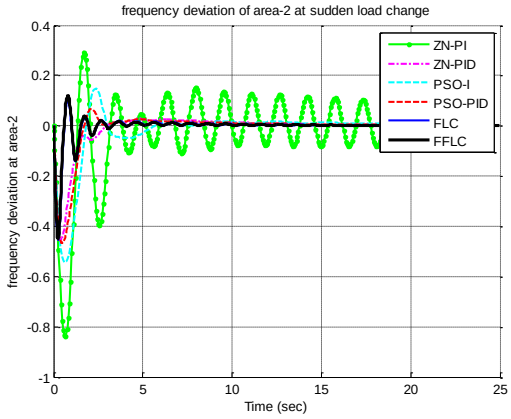

Fig. 5.35: Deviation in frequency of area-2 for TTW-THW system for different controllers at 30% penetration of WPGS

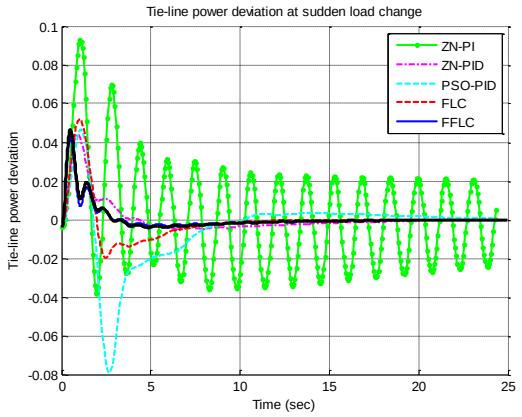

Fig. 5.36: Deviation in tie-line power for TTW-THW system for different controllers at 30% penetration of WPGS

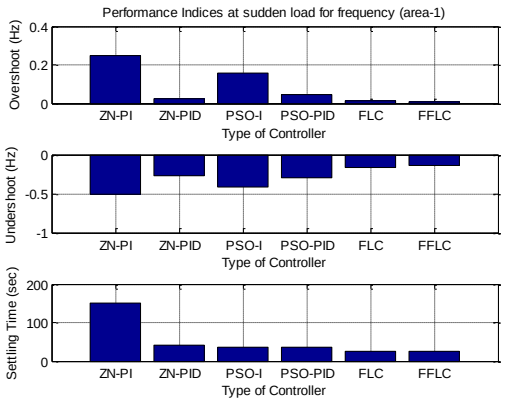

Fig. 5.37: Performance indices for deviation in frequency at area-1 for TTW-THW

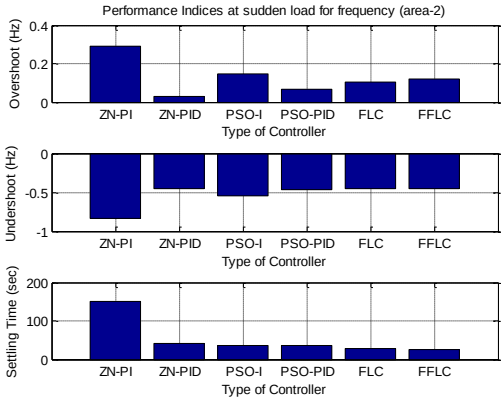

Fig. 5.38: Performance indices for deviation in frequency at area-2 for TTW-THW system

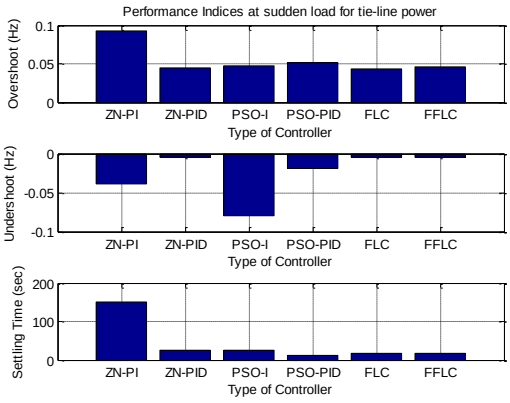

Fig. 5.39: Performance indices for deviation in tie-line power for TTW-THW system

In Fig. 5.34, 5.35 and 5.36, frequency deviation in area-1, frequency deviations in area-2 and tie-line power deviation have been shown for examined system respectively. These figures show that FFLC give better response than other controllers in terms of dynamic performance. Three different performance indices (peak undershoot, peak overshoot and settling time) have been show from these results for deviation in frequencies of both areas and deviation in tie-line power, as shown in Fig. 5.37, 5.38 and 5.39. Table 5.2 shows the numerical values of performance indices for frequency deviation in area-1, frequency deviations in area-2 and tie-line power deviation.

Table 5.2: Performance indices of Δf1, Δf2 and Δptie12 at sudden load for different controllers for TTW-THW system

	ZN PI	ZN PID	PSO I	PSO PID	FLC	FFLC
Peak Undershoot						
Δ*f1*	-0.51078	-0.26712	-0.4207	-0.2978	-0.16384	-0.14235
Δf2	-0.83632	-0.45373	-0.5416	-0.46723	-0.45206	-0.44936
Δptie12	-0.03834	-0.00482	-0.07911	-0.01969	-0.004	-0.00421
Peak Overshoot						
Δ*f1*	0.245788	0.025308	0.158897	0.045923	0.01198	0.00943
Δf2	0.289853	0.027899	0.148243	0.06673	0.102848	0.120337
Δptie12	0.093046	0.044179	0.046776	0.051946	0.042715	0.046494
Settling Time						
Δ*f1*	>150	40.57258	35.29226	35.91542	25.23268	24.6752
Δf2	>150	40.2772	36.08291	35.13223	26.97364	26.378
Δptie12	>150	24.09952	24.16262	11.86159	18.10835	17.80444

Based on these results it is concluded that FFLC can effectively suppress oscillation in comparison of other controllers.

5.5 Integration of SMES in Two Area Power System

SMES unit when integrated with system significantly improves oscillations damping. The SMES stores energy to a set value (which is less than the full state) from the utility grid during normal operation of the grid and later SMES relieves this energy when demand is

more as well as it stores the energy when generation is more than demand [3], [4]. In this study the effect of SMES is investigated. In this study, four different combinations have been taken and both areas have different sets of generating units, as considered in previous study. These combinations are differentiated based on integration of SMES unit to control area.

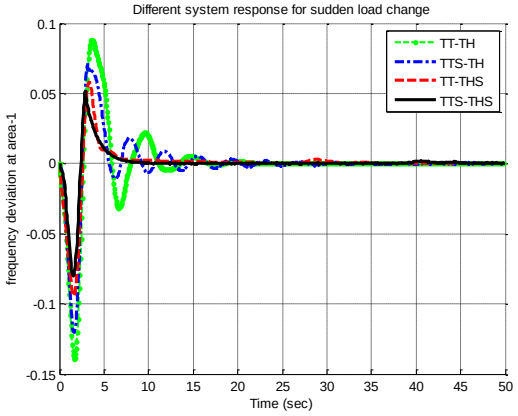

Fig. 5.40: Deviation in frequency of area-1 for different systems

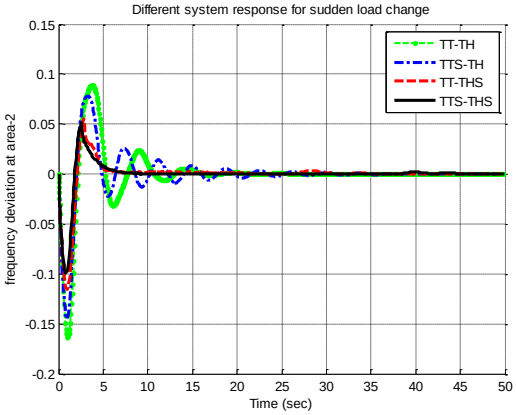

Fig. 5.41: Deviation in frequency of area-2 for different systems

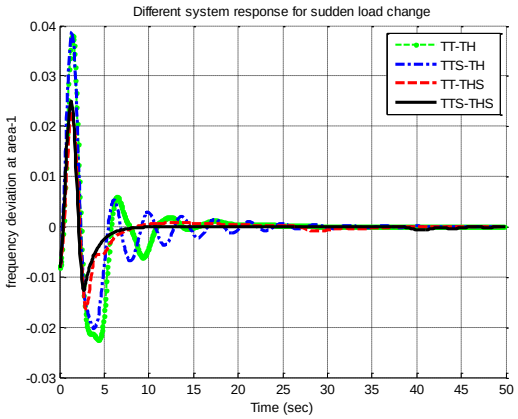

Fig. 5.42: Deviation in tie-line power for different systems

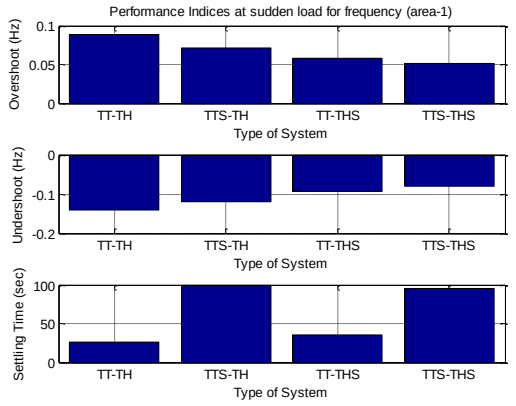

Fig. 5.43: Performance indices for deviation in frequency of area-1 for different systems

Fig. 5.40, 5.41 and 5.42 show deviation in frequency of area-1, deviation in frequency of area-2 and deviation in tie-line power respectively. These figures indicate that as SMES integration is more effective in the case where a hydro generation unit exists, when

SMES is integrated only in one control area. When SMES is integrated in both areas then it gives the better results among all different four cases.

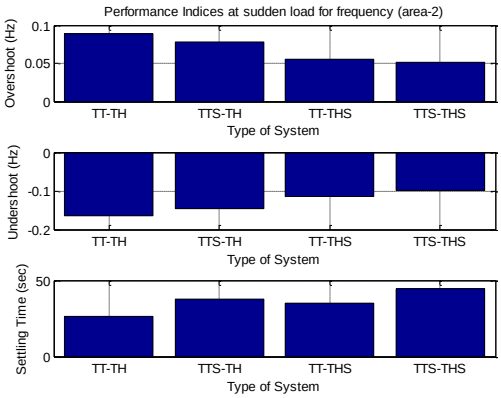

Fig. 5.44: Performance indices for deviation in frequency of area-2 for different systems

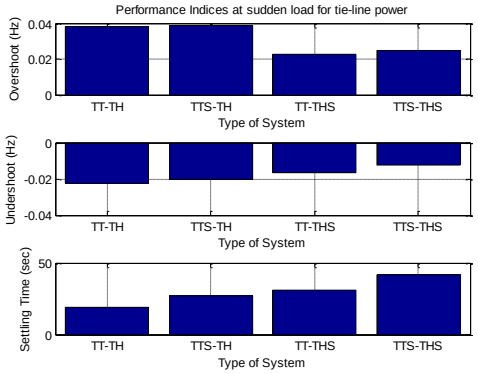

Fig. 5.45: Performance indices for deviation in tie-line power for different systems

Table 5.3: Performance indices for different types of system

		TT-TH	TTS-TH	TT-THS	TTS-THS
frequency deviation in area-1	**Peak Overshoot**	0.0882	0.0717	0.0581	0.0517
	Peak Undershoot	-0.1395	-0.1207	-0.0944	-0.0799
	Settling Time (±5%)	26.0479	99.3866	35.4253	95.1432
frequency deviation in area-2	**Peak Overshoot**	0.0889	0.0783	0.0549	0.0509
	Peak Undershoot	-0.1635	-0.1449	-0.1154	-0.0991
	Settling Time (±5%)	26.1117	37.82	34.755	44.5565
tie-line power deviation	**Peak Overshoot**	0.038	0.0388	0.0225	0.025
	Peak Undershoot	-0.0225	-0.0203	-0.0165	-0.0126
	Settling Time (±5%)	19.1988	26.9705	30.7284	41.4343

Quantified results based on three performance indices (peak undershoot, peak overshoot and settling time) for deviation in frequencies of both areas and deviation in tie-line power are shown in Fig. 5.43, 5.44 and 5.45. Table 5.3 also shows the numerical representation of these performance indices for different types of system. It is observed from analysis that SMES integration effectively suppresses oscillation but settling time is increased due to very low order oscillations.

5.6 Simulation Results with WPGS and SMES Integrated in TT-TH System

In previous section, impact of WPGS and SMES are independently studied. Now, both together are evaluated for same TT-TH system at step load perturbation from different DISCOs as per contract participation factors. To comprehensive analyze, sixteen different sets are formed in which WPGS and SMES are integrated to TT-TH system. These sets of system identified as S1 to S16 are listed below:

i. S1: TT-TH (TT-TH system with no WPGS and SMES)
ii. S2: TTS-TH (TT-TH system with SMES integration in area-1)
iii. S3: TT-THS (TT-TH system with SMES integration in area-2)
iv. S4: TTS-THS (TT-TH system with SMES integration in both areas)
v. S5: TTW-TH (TT-TH system with WPGS integration in area-1)
vi. S6: TTWS-TH (TT-TH system with WPGS & SMES integration in area-1)
vii. S7: TTW-THS (TT-TH system with WPGS in area-1 and SMES integration in area-2)
viii. S8: TTWS-THS (TT-TH system with WPGS & SMES integration in area-1 and SMES integration in area-2)
ix. S9: TT-THW (TT-TH system with WPGS integration in area-2)
x. S10: TTS-THW (TT-TH system with SMES integration in area-1 and WPGS integration in area-2)
xi. S11: TT-THWS (TT-TH system with WPGS & SMES integration in area-2)
xii. S12: TTS-THWS (TT-TH system with SMES integration in area-1 and WPGS & SMES integration in area-2)

xiii. S13: TTW-THW (TT-TH system with WPGS integration in area-1 and WPGS integration in area-2)

xiv. S14: TTWS-THW (TT-TH system with WPGS & SMES integration in area-1 and WPGS integration in area-2)

xv. S15: TTW-THWS (TT-TH system with WPGS & SMES integration in area-2)

xvi. S16: TTWS-THWS (TT-TH system with WPGS & SMES integration in both areas)

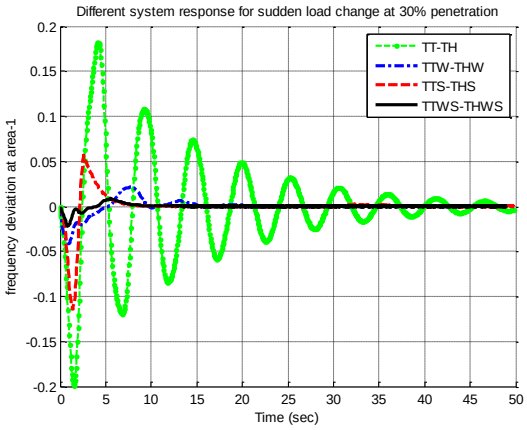

Fig. 5.46: Deviation in frequency of area-1 for different systems at 30% penetration

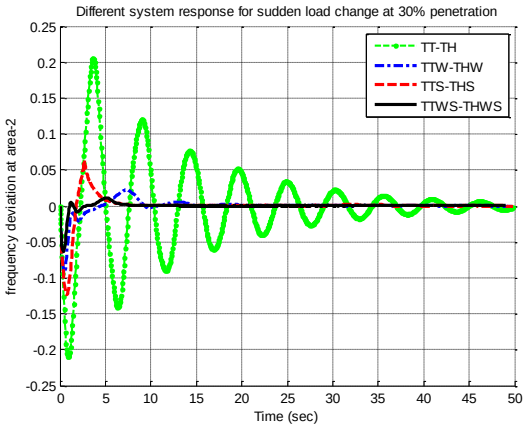

Fig. 5.47: Deviation in frequency of area-2 for different systems at 30% penetration

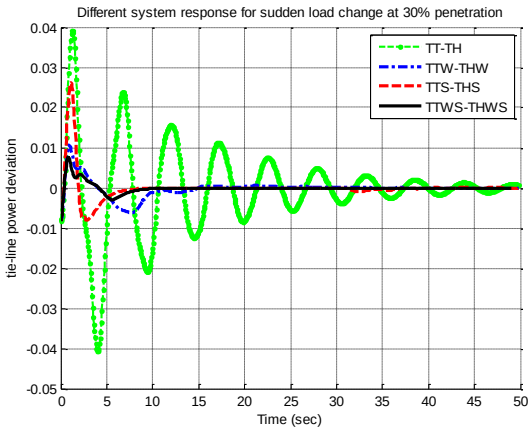

Fig. 5.48: Deviation in tie-line power for different systems at 30% penetration

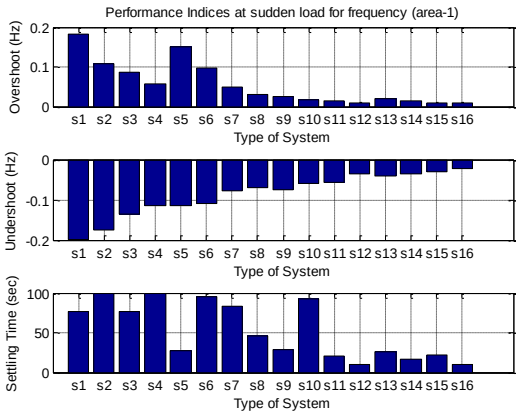

Fig.5.49: Performance indices for deviation in frequency of area-1 for different systems at 30% penetration

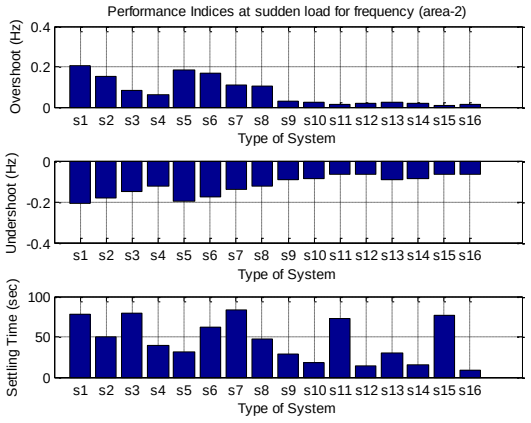

Fig. 5.50: Performance indices for deviation in frequency of area-2 for different systems at 30% penetration

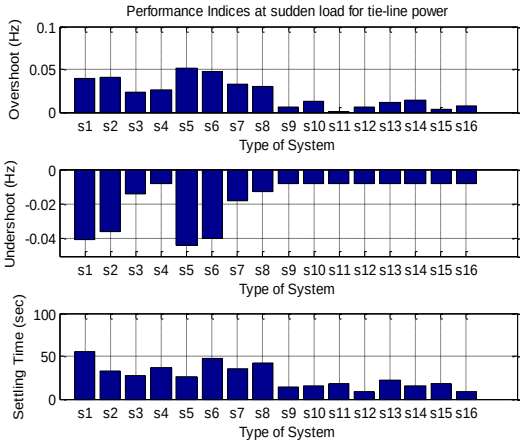

Fig. 5.51: Performance indices for deviation in tie-line power for different systems at 30% penetration

It is difficult to put frequencies and tie-line power oscillations for all these different sixteen systems in same plot so to have simplified presentation, frequencies and tie-line deviations have been shown for only four different types of systems, in which effectiveness of integration of SMES and WPGS have been examined. These four different systems are (i) TT-TH system with no WPGS inertial support and no SMES integration in any of the area, (ii) TT-TH system with WPGS inertial support for both areas & no SMES integration, (iii) TT-TH system with SMES integration for both areas & no WPGS inertial support integration in any of the area and (iv) TT-TH system with WPGS inertial support in both areas as well as SMES integration in both areas respectively. Fig. 5.46, 5.47 and 5.48 show deviation in frequency of area-1, deviation in frequency of area-2 and deviation in tie-line power for above mentioned four different types of systems. It is observed from these figures that both WPGS inertial support and SMES integration together is very effective for oscillation suppression. Three performance indices (peak undershoot, peak overshoot and settling time) for deviation in frequencies of both areas and deviation in tie-line power obtained for all these 16 different system from S1 to S16, as shown in Fig. 5.49, 5.50 and 5.51 respectively.

Results shown in Table 5.4 conclude that WPGS and SMES together may provide a viable solution for oscillation mitigation and may address issues related with AGC.

Table 5.4: Performance indices of Δf1, Δf2 and Δptie12 at sudden load for different types of systems at 30% penetration

	TT-TH	TTS-TH	TT-THS	TTS-THS	TTW-TH	TTWS-TH	TTW-THS	TTWS-THS	TT-THW	TTS-THW	TT-THWS	TTS-THWS	TTW-THW	TTWS-THW	TTW-THWS	TTWS-THWS
	S1	**S2**	**S3**	**S4**	**S5**	**S6**	**S7**	**S8**	**S9**	**S10**	**S11**	**S12**	**S13**	**S14**	**S15**	**S16**
Frequency deviation in area-1																
PO	0.1822	0.1068	0.0855	0.0562	0.1496	0.0968	0.0482	0.0318	0.0257	0.0176	0.0137	0.0097	0.0211	0.0135	0.0095	0.0083
PU	-0.1989	-0.1759	-0.135	-0.1143	-0.114	-0.1086	-0.0782	-0.0689	-0.0749	-0.0595	-0.0564	-0.0366	-0.0416	-0.0353	-0.031	-0.0217
ST	76.3611	99.9663	76.1522	99.5868	27.3782	95.8063	83.9689	45.4897	28.8918	92.0237	21.1902	10.3791	25.5232	16.4721	22.5793	10.036
Frequency deviation in area-2																
PO	0.205	0.1534	0.0809	0.0629	0.1844	0.17	0.1107	0.103	0.0278	0.0264	0.0131	0.0165	0.0221	0.0172	0.0087	0.011
PU	-0.2098	-0.1802	-0.1491	-0.1236	-0.1958	-0.1787	-0.1381	-0.1217	-0.0932	-0.088	-0.0671	-0.0635	-0.0924	-0.0879	-0.0666	-0.0634
ST	78.3525	49.6719	79.4338	39.0399	31.8165	62.4827	83.8585	47.6418	28.3695	17.8944	73.1192	13.364	29.7528	15.9376	77.0685	8.9927
Tie-line power deviation																
PO	0.0391	0.0413	0.0233	0.0262	0.0507	0.047	0.032	0.0302	0.0057	0.0124	0.0009	0.0061	0.0107	0.0145	0.0036	0.0075
PU	-0.0408	-0.0359	-0.0139	-0.0083	-0.0439	-0.0396	-0.0182	-0.013	-0.0083	-0.0083	-0.0083	-0.0083	-0.0083	-0.0083	-0.0083	-0.0083
ST	54.9217	32.5641	26.9941	36.1524	25.4446	46.838	35.6584	42.1472	14.4877	15.6396	17.4459	8.3402	21.7875	15.8097	18.3961	8.6199

Where, PO= Peak Overshoot, PU= Peak Undershoot and ST=Settling Time (±5%)

5.7 Simulation Results with Optimized FLC in WPGS and SMES Integrated System

The Simulink model of this system has been shown in Fig. 5.52. In this system, different controllers have been examined, are integral controller, PI Controller, PID controller, FLC and FFLC. In this study the gains for different controllers as mentioned above are shown in Table 5.5.

The *cpf_matrix* and DISCO demand matrix used for case are:

$$cpf\_matrix = \begin{bmatrix} 0.25 & 0.2 & 0.15 & 0.15 \\ 0.25 & 0.25 & 0.15 & 0.2 \\ 0.3 & 0.25 & 0.35 & 0.35 \\ 0.2 & 0.3 & 0.35 & 0.3 \end{bmatrix} \text{ and } \Delta P_L = \begin{bmatrix} 0.10 \\ 0.05 \\ 0.15 \\ 0.05 \end{bmatrix}$$

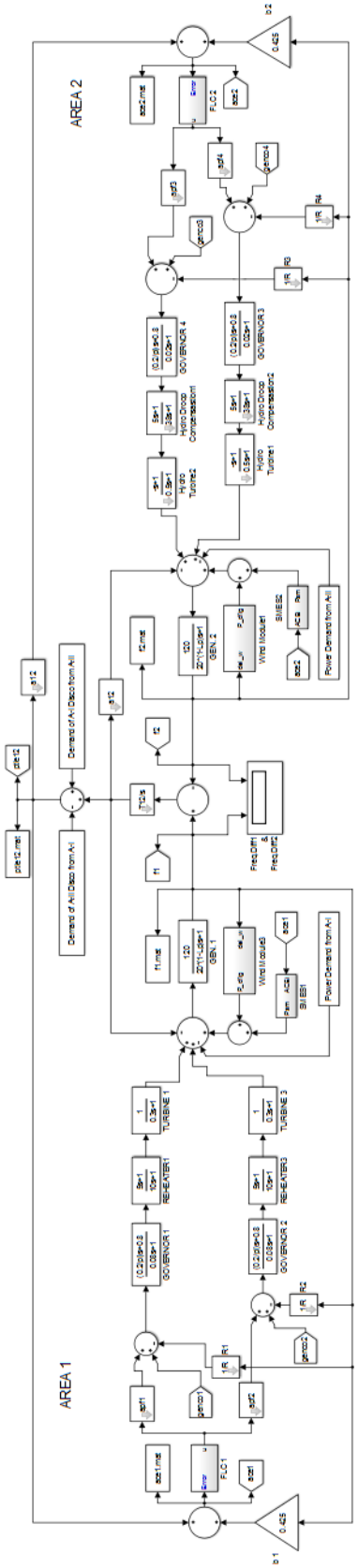

Fig. 5.52: Simulink model for TT-TH system with SMES integration in both areas and WPGS inertial support

Table 5.5: Different type of AGC controller's gains for TTWS-THWS system

	Area-1 Controller						Area-2 Controller					
ZN tuned PI Controller	K_{p1}	K_{i1}					K_{p1}	K_{i2}				
	1.6110	1.3809					1.6110	1.3809				
ZN tuned PID Controller	K_{p1}	K_{i1}	K_{d1}				K_{p1}	K_{i2}	K_{d2}			
	2.1480	3.0686	0.3759				2.1480	3.0686	0.3759			
PSO optimized Integral Controller		K_{i1}						K_{i2}				
		0.5266						2.2465				
PSO optimized PID Controller	K_{p1}	K_{i1}	K_{d1}				K_{p1}	K_{i2}	K_{d2}			
	2.2216	2.5394	0.4607				1.6591	4.6029	0.4996			
Fuzzy Logic Controller	K_{e1}	K_{ce1}	K_{p1}	K_{i1}			K_{e2}	K_{ce2}	K_{p2}	K_{i2}		
	0.1588	0.0665	38.1216	71.1617			0.1691	0.0928	8.8613	26.0029		
Four step optimized FLC	K_{e1}	K_{ce1}	K_{p1}	K_{i1}			K_{e2}	K_{ce2}	K_{p2}	K_{i2}		
	0.0178	0.0476	4.2902	17.8472			0.0375	0.0285	6.1596	11.4693		

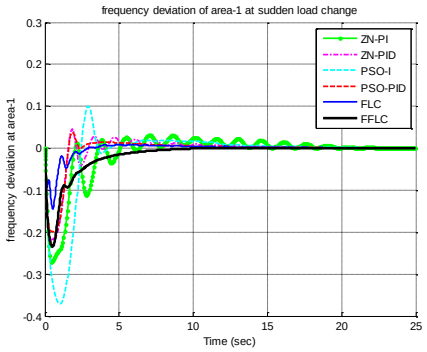

Fig. 5.53: Deviation in frequency of area-1 for TTWS-THWS system for different controllers

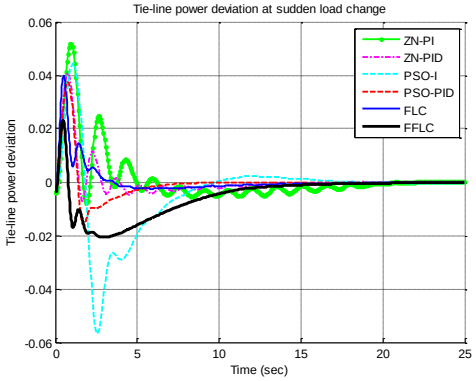

Fig. 5.54: Deviation in tie-line power for TTWS-THWS system for different controllers

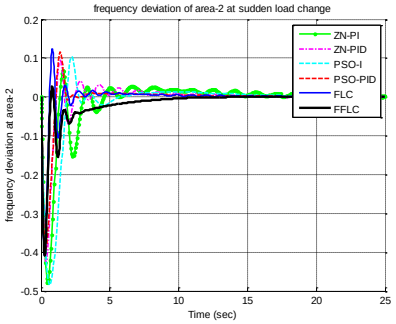

Fig. 5.55: Deviation in frequency of area-2 for TTWS-THWS system for different controllers

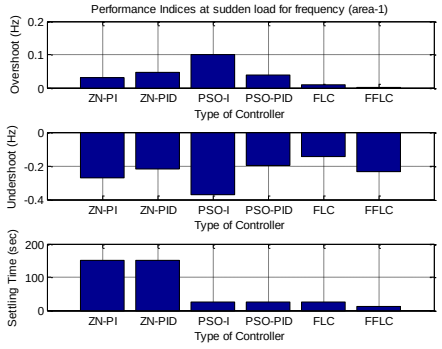

Fig. 5.56: Performance indices for deviation in frequency at area-1 for TTWS-THWS system

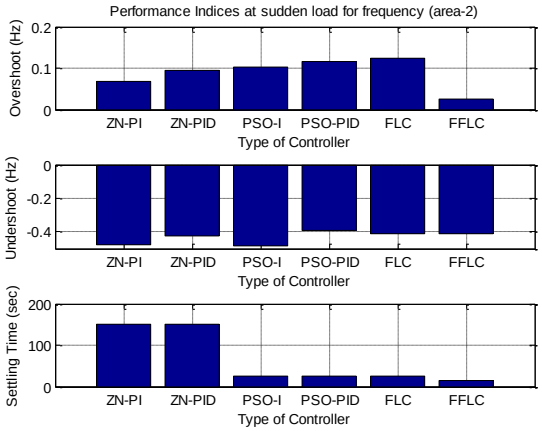

Fig. 5.57: Performance indices for deviation in frequency at area-2 for TTWS-THWS system

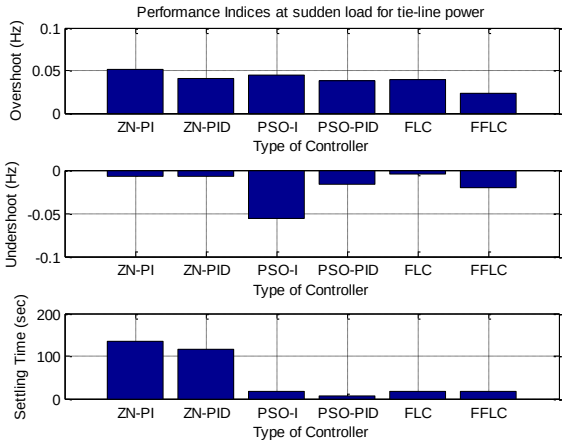

Fig. 5.58: Performance indices for deviation in tie-line power for TTWS-THWS system

Table 5.6: Performance indices of Δf1, Δf2 and Δptie12 at sudden load for different controllers for TTWS-THWS system

	ZN PI	ZN PID	PSO I	PSO PID	FLC	FFLC
Peak Undershoot						
Δf1	-0.27163	-0.21850	-0.36944	-0.19984	-0.14592	-0.23459
Δf2	-0.47862	-0.42620	-0.48445	-0.39166	-0.40961	-0.40974
Δptie12	-0.00782	-0.00717	-0.05655	-0.01604	-0.00400	-0.02056
Peak Overshoot						
Δf1	0.030908	0.045546	0.100269	0.038126	0.008569	0.000942
Δf2	0.067887	0.093654	0.102004	0.115915	0.123065	0.026313
Δptie12	0.051677	0.040777	0.044444	0.037476	0.039893	0.023125
Settling Time						
Δf1	149.9212	149.7953	26.63717	25.44194	24.17272	11.62054
Δf2	>150	149.8656	26.06514	25.04279	26.02499	13.74027
Δptie12	135.0531	117.2172	16.36825	7.833769	16.66079	18.51183

Fig. 5.53, 5.54 and 5.55 show frequency deviation in area-1, show frequency deviations in area-2 and tie-line power deviation respectively for system under study. It is observed from these figures that FFLC gives better response than other controllers in terms of dynamic performance at sudden load change. In order to enumerate these results based on

peak undershoot, peak overshoot and settling time for deviation in frequencies of both areas and deviation in tie-line power obtained as shown in Fig. 5.56, 5.57 and 5.58. Table 5.6 shows numerical results of same. It is observed that peak undershoot for deviation in frequency of area-1 and deviation in tie-line power increased, but same time settling time for deviation in frequencies of both areas decreased significantly. Thus, it can be concluded that FFLC is effective control strategy.

5.8 Summery

This chapter presents detailed simulation results on impact of integration of WPGS and SMES to AGC. Impact of WPGS firstly examined for impact of different level of penetration without inertial support where it is observed that as penetration increases oscillation in frequency and tie-line also increases while oscillation suppression is observed when WPGS equipped with inertial support mechanism is integrated. Same sets of experiments repeated for SMES integration with and without WPGS and it is concluded that SMES and WPGS with inertial support is effective techniques for oscillation suppression even for rising level of penetration also. Optimized FFLC is also tested for simulation models, where WPGS and SMES integrated model is found better in performance when compared with other controllers.

Reference

[1] G. Lalor, a. Mullane, and M. O'Malley, "Frequency Control and Wind Turbine Technologies," *IEEE Trans. Power Syst.*, vol. 20, no. 4, pp. 1905–1913, 2005.

[2] N. R. Ullah, T. Thiringer, and D. Karlsson, "Temporary Primary Frequency Control Support by Variable Speed Wind Turbines— Potential and Applications," *IEEE Trans. Power Syst.*, vol. 23, no. 2, pp. 601–612, 2008.

[3] Demirören, "Automatic Generation Control for Power System with SMES by Using Neural Network Controller," *Electr. Power Components Syst.*, vol. 31, no. May 2012, pp. 1–25, 2003.

[4] S. C. Tripathy and B. Bak-Jensen, "Automatic generation control of multi-area power system with superconducting magnetic storage unit," *2001 IEEE Porto Power Tech Proc.*, vol. 3, p. 6, 2001.

Chapter 6

Implementation of Controller as Hardware-In-Loop (CHIL)

6.1 Introduction

Designing and testing of controller for large and complex power system will be costly and time consuming. There are many challenges which make system unstable like improper selection of sampling frequency and time delay for controller. This chapter attempts to validate the performance of fuzzy logic controller developed in simulation environment in earlier chapters. The emphasis is given, if the hardware controller developed follows the simulated one. The performance parameters are not analyzed as due to limitation of hardware control circuit and interfacing issues. This work discusses a rapid prototyping procedure for controller design and proposes controller as hardware-in-the-loop (CHIL). In this process, the simulated controller is replaced by a hardware controller, which interacts with other virtual models that are simulated. First the performance of the control logic is evaluated using non real-time simulation then controller subsystem is tested with CHIL simulation. CHIL acts in faster, safer and reliable way in the model. The proposed controllers for AGC of two area deregulated power system is designed, implemented and tested.

System considered has controllers which run on a target microcontroller board, while the plant model runs on the simulation platform. The CHIL simulation results are compared with those of the fully simulated system [1], [2]. The proposed process for rapid design and testing of controller consists of following four steps as shown in Fig. 6.1, these are:

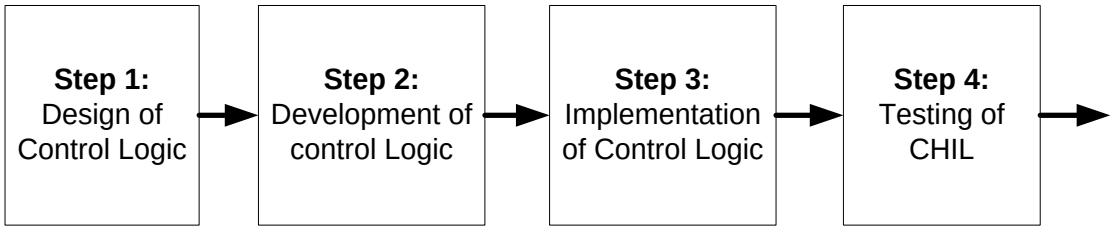

Fig. 6.1: Controller as Hardware-In-Loop

Step 1 (Design of control logic):

This first step is design of control logic for test system by understanding the requirement.

Step 2 (Development of control logic):

This step is for development and testing of control logic for test system in software environment. In this step, the plant and the controller models are defined in software based simulation environment and controller performance is verified and evaluated in software environment.

Step 3 (Implementation of control logic):

This step deals with code development of control logic and further implementation this code on suitable H/W Controller.

Step 4 (Testing of CHIL):

In this step, controller will be in real environment and plant or test system in virtual environment. The CHIL simulation provides an intermediate stage between simulation and deployment. In this process the plant and controller are separated into two subsystems, where plant model is simulated in software environment (Matlab/Simulink), and the controller runs on the actual target controller board. This approach can better

replicate the real operational condition, and hence reduces the risk and cost of the final hardware testing.

In the present work, the fuzzy logic controller is implemented in an Arduino Mega 2560. The Mega 2560 is a microcontroller board based on the ATmega2560. It has 54 digital input/output pins multiplexed with 15 channels for PWM outputs, 16 channels analog inputs and 4 channels UARTs. It runs on a 16 MHz crystal oscillator. It also has facility of hard reset. This microcontroller connects and operates for development of code in simplified way to a computer with a USB cable [3], [4].

The dSPACE 1104 works as a link between the computer modeling framework in Simulink and the hardware. Simulink model is first to be compiled and then transferred to the dSPACE board, and finally it will run in program memory. The DS1104 R&D Controller Board with CP1104 Connector Panel is used in present work. The DS1104 has a 64-bit floating-point MPC8240 processor working at 250 MHz with on-chip peripherals. The peripherals include ADC, DAC channels, digital I/O ports, serial interface and more [5]. Fig. 6.7 presents the laboratory hardware-in-the-loop setup with interface between an external controllers and the two-area power system.

For connecting the simulation model to the physical world, I/O interfaces must be added to the model and Simulink model is saved as .mdl file. The dSPACE's RTI provide interfacing blocks from external environment. Once the model is built, the Real-Time Workshop (Matlab toolbox) generates a C code from the Simulink model than cross compiler environment compiles this C code and links the object files and libraries into an executable code for the real time processor. After generating a real-time code, .sdf file can be downloaded and different types of experiments can be performed using the

ControlDesk software. ControlDesk is user-interface software of experiment environment that displays virtual instruments, inputs from sensors and reactions of actuators. From this environment, DS1104 based application can be accessed and virtual instrumentation can be configured. This software environment can be used to monitor and control experiments as well as to develop controllers [6], [7].

Fig. 6.8 and 6.9 presents the block diagram used in Simulink for FLC. In the Fig. 6.9 three blocks used for interfacing, these are DS1104 DAC_C1 & DS1104 DAC_C2 and DS1104 BIT_IN_C0. The first two blocks are for DAC channels and third one for digital input channel. On the left side of Fig. 6.9 are the blocks for DAC outputs for ACE and dACE signals and digital input is controller output that is later on averaged and further processed.

6.2 CHIL Experimental Setup

CHIL simulation setup built in the laboratory with an external hardware controller DSP and the simulation model of the two area power system. The external DSP based controller employed in the hardware-in-the loop setup, which is typically used for controlling frequency as well as tie-line power deviation. The fuzzy logic based control logic is built and compiled using the Matlab-Simulink real-time workshop (RTW). The FLC as an AGC controller is implemented in the hardware controller ATmega2560 microcontroller. The signals ACE and d(ACE)/dt from the simulated system are sent to the microcontroller through Digital-Analogue (D/A) converter card on dSPACE 1104. After the control algorithm is executed, the control signal U is sent back from the microcontroller through PWM to the simulated system through dSPACE digital input pin (IO0). In this way a closed CHIL simulation loop is implemented.

The controller is connected with Matlab/Simulink RTW in the external mode such that the internal control variables can be monitored in real-time and the control parameters can be tuned on-line.

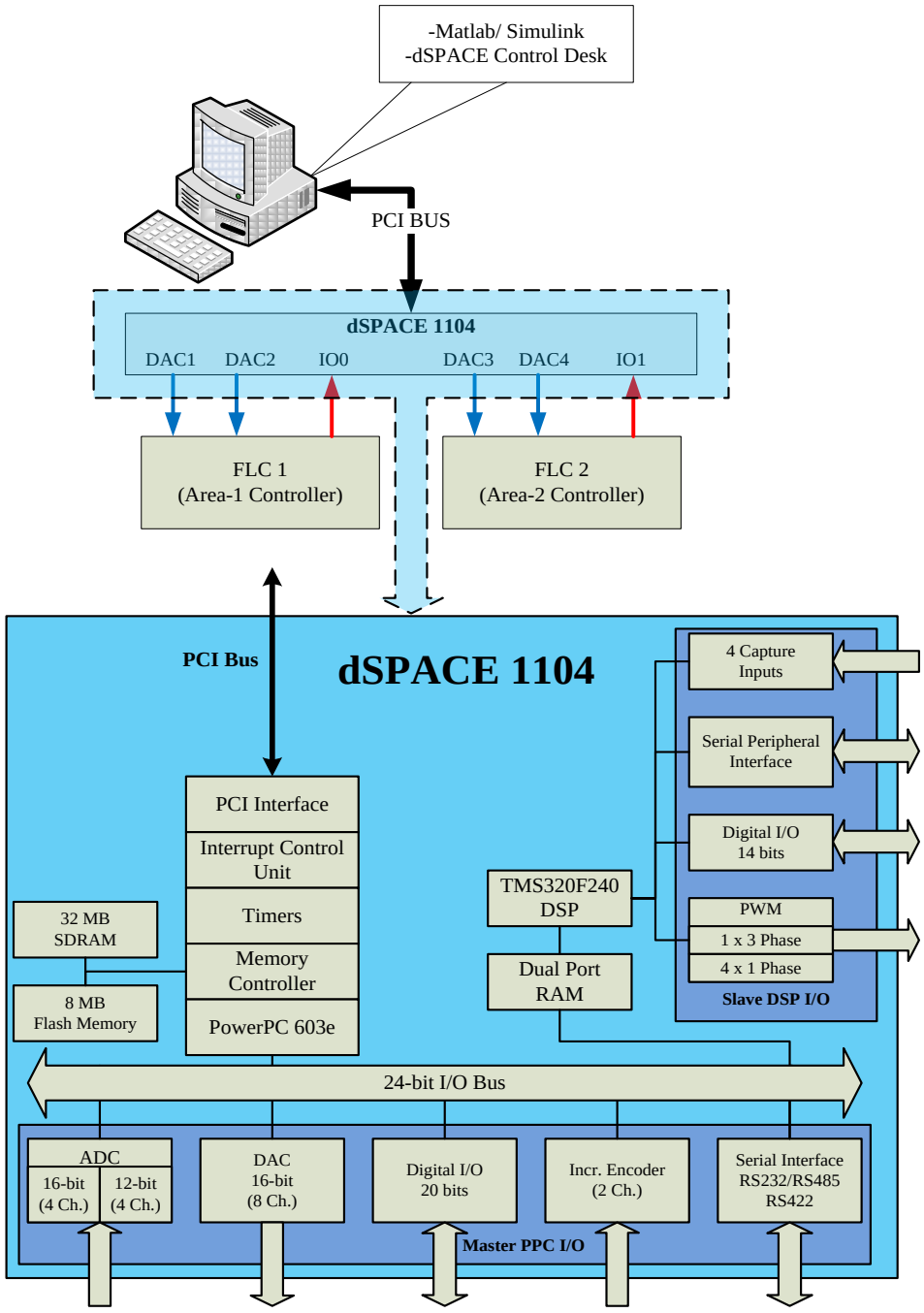

Fig. 6.2: Hardware-in-the-loop setup with FLC controllers

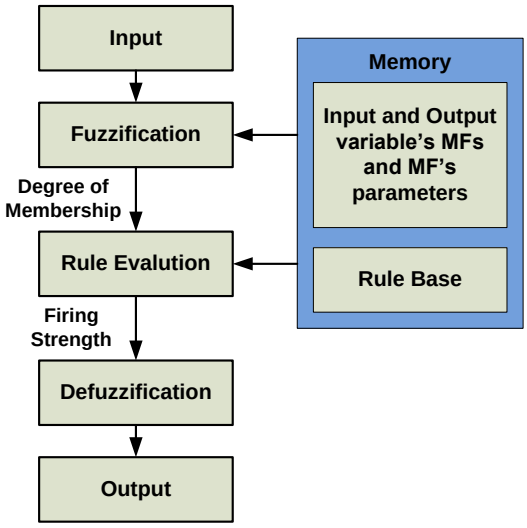

Fig. 6.3: Fuzzy logic controller system structure

Fig. 6.3 shows the structure of FLC. Inputs of FLC go through three different steps to bring FLC outputs. First step is fuzzification process that utilizes MFs of input variables, each FLC input finds degrees of membership with respect to MF's. In second step rules are evaluated by combining degrees of membership to form output strengths in the rule base. And in third step the defuzzification process computes FLC output based on strengths and membership functions of output variable. Fig. 6.4 shows a linked-list arrangement of FLC inputs and MF's as well as Fig. 6.5 shows a linked-list arrangement of FLC output and MF's. Rules can be represented by two sets of pointers, one at antecedent side and second at consequent side; see Fig. 6.6.Implementation of FLC in 'C' code is done using link list data structure design. In this following data need to be processed,

- Inputs
- Input variable's MFs
- Outputs

- Output variable's MFs
- Rules
- Antecedent values (Degree of membership)
- Consequent values (Rules firing strength)

Input node contains an input variable name, value, MF pointer, and a next input pointer. Input nodes and output node have similar data structure. MF node contains MF name, value, three points that describe a triangular membership function and MF pointer. Rule node contains three pointers in which first two indicates antecedent part (degree of membership) and another one indicates consequent part which points consequent part (rules firing strength). Finally, following steps are required for implementation of CHIL FLC:

1: Initialize input and output node;

2: Initialize input as well as output MF's parameters

3: construct input as well as output linked list

4: construct rule base linked list

5: Get inputs values from ADCs and map into appropriate range

6: Fuzzification & compute degree of membership

7: Rule Evaluation & set the firing strength of each rule

8: Defuzzification by averaging the area from fired MF's of output variable

9: Get outputs values and map into appropriate range

10: Set the duty cycle as per output value

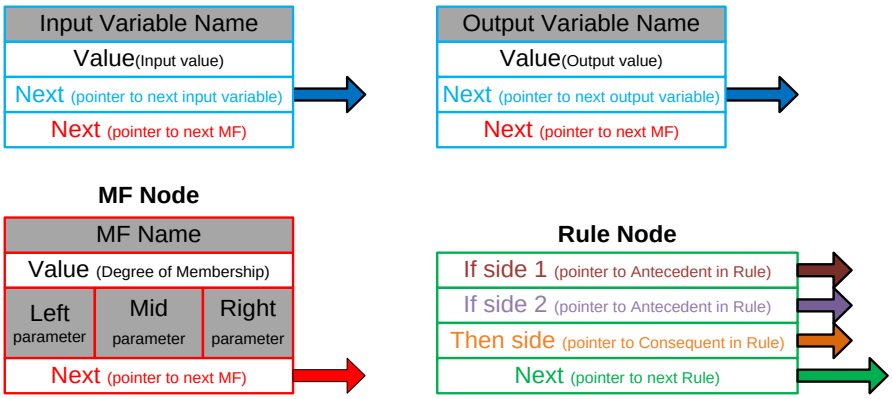

Fig. 6.4: Data structure details of input, output, MF and rule nodes

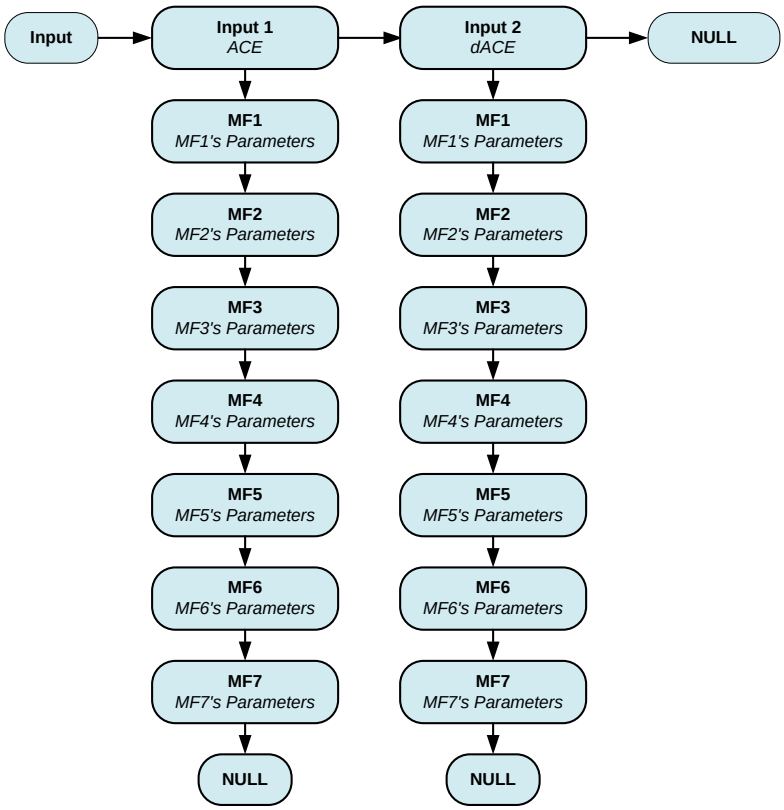

Fig. 6.5: Input data structure

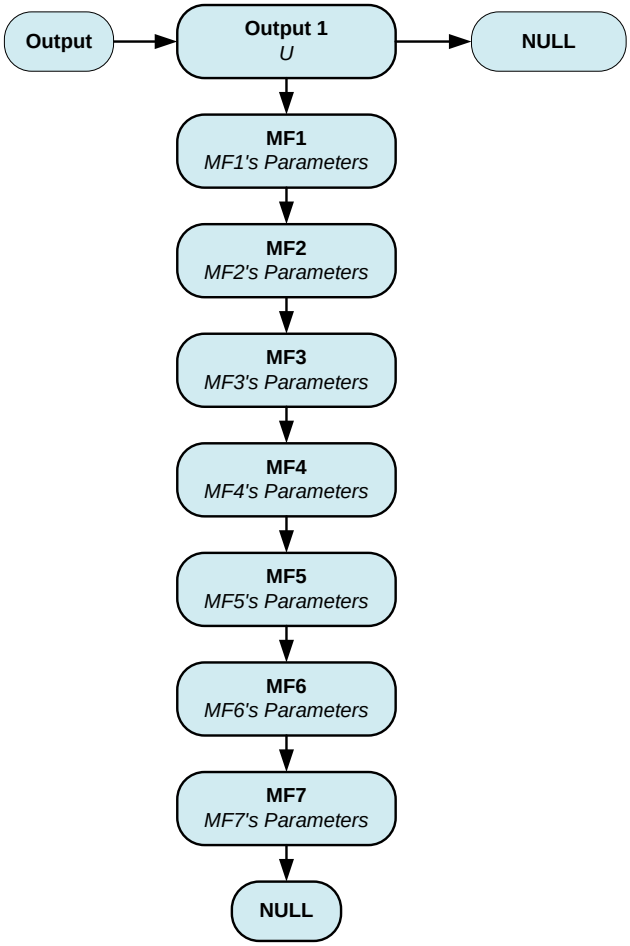

Fig. 6.6: Output data structure

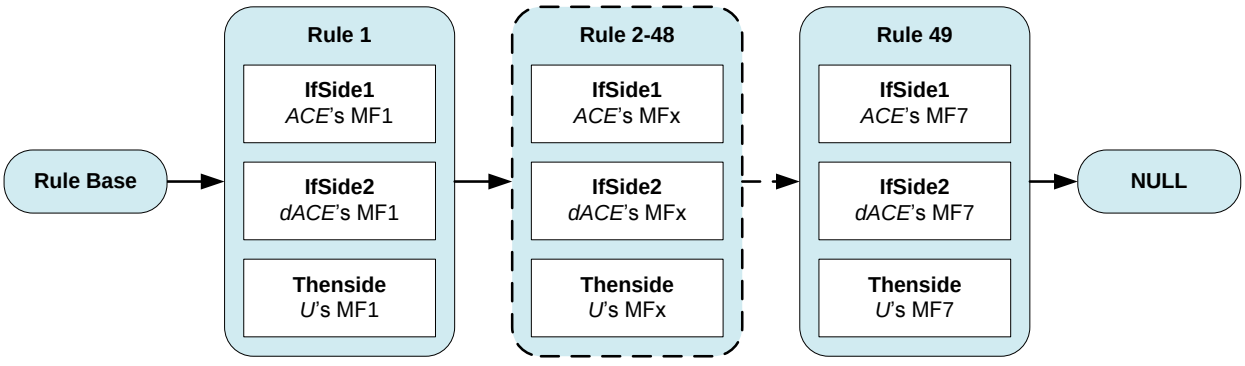

Fig. 6.7: Rule base data structure

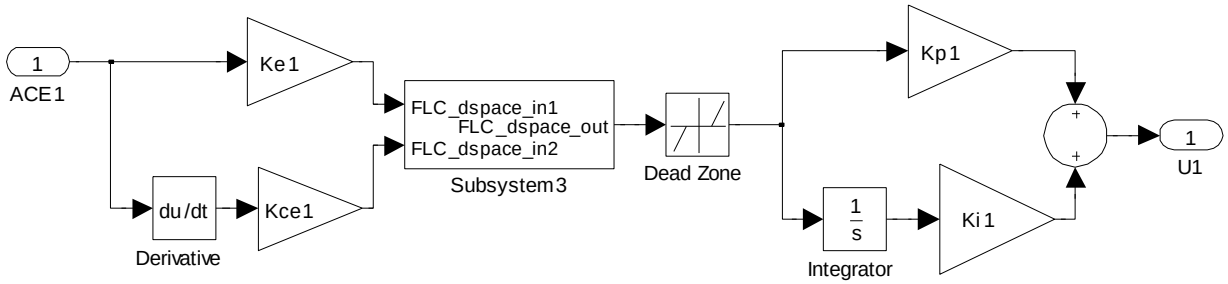

Fig. 6.8: PID type FLC in Simulink

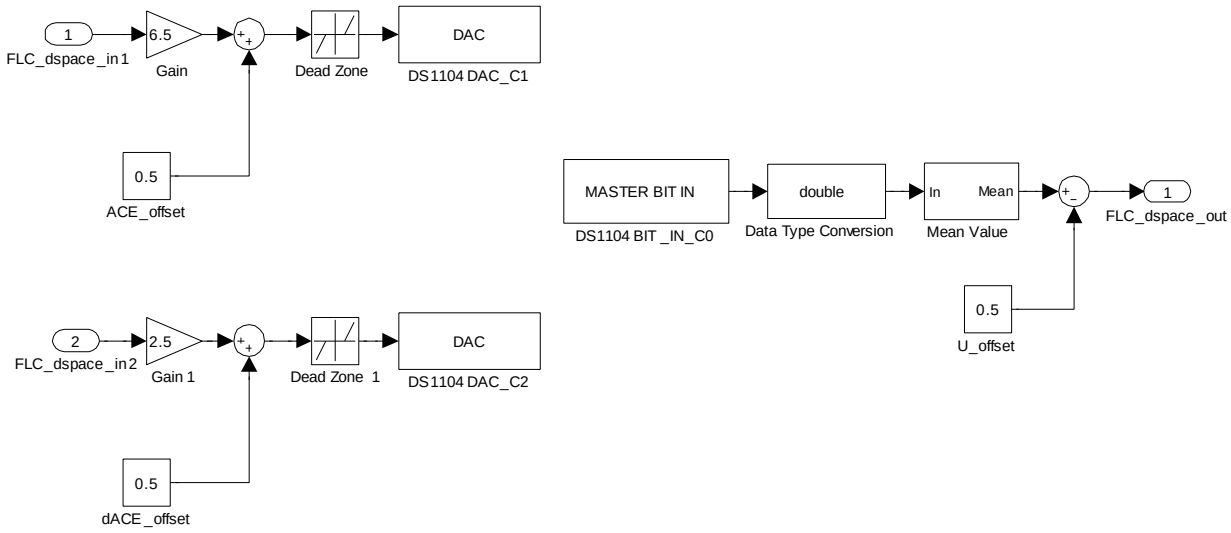

Fig. 6.9: FLC Simulink block using DS1104 interfacing blocks

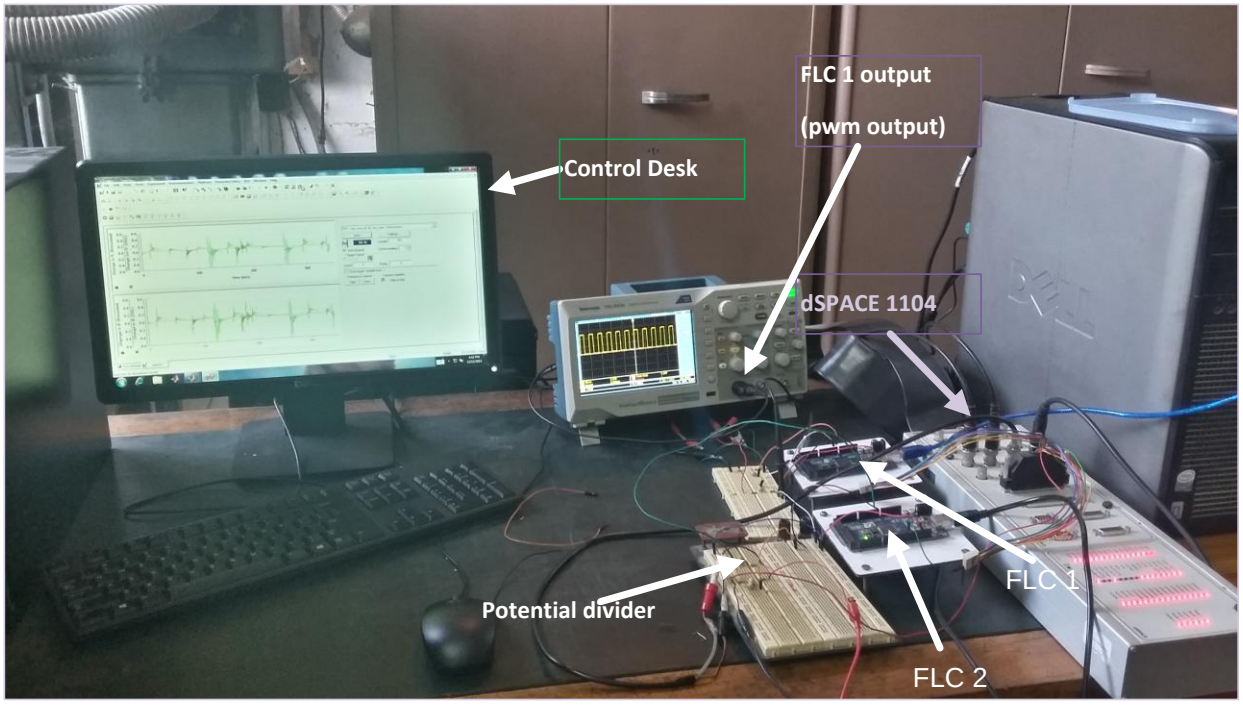

Fig. 6.10: Setup picture for FLC as CHIL

6.3 Experimental Results & Discussion

Laboratory setup for CHIL for two area interconnected deregulated system is as shown in Fig. 6.10. This CHIL is embedded with FLC and it is validated for TT-TH system, TTW-THW system and TTWS-THWS system. Results are obtained from Control Desk software for different systems as shown in Fig. 6.11, 6.12, 6.13, 6.14, 6.15, 6.15 and 6.17.

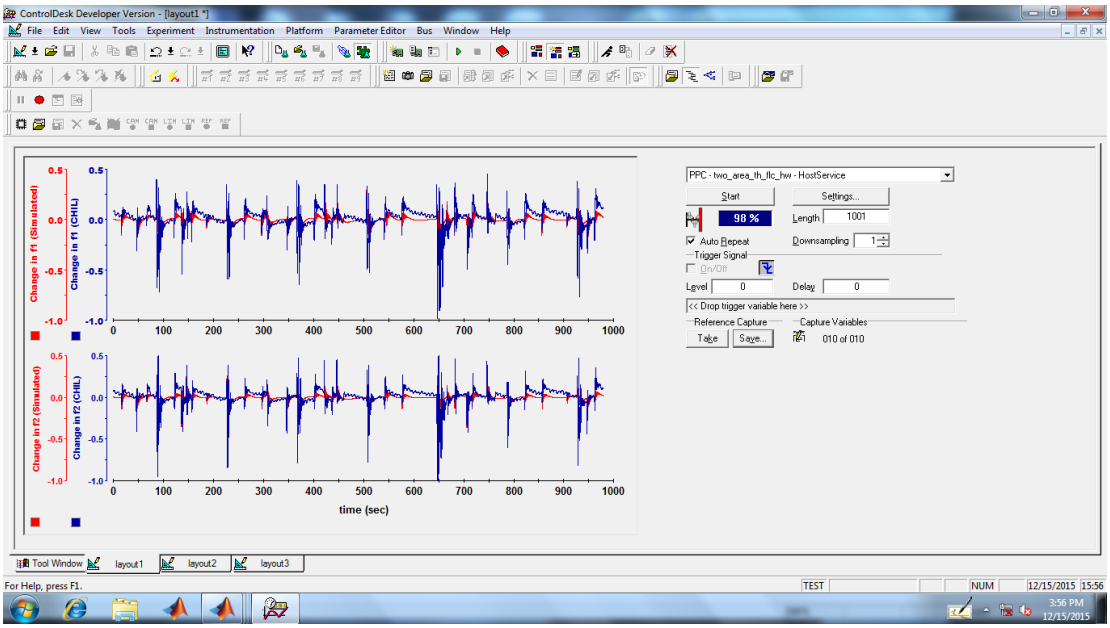

Fig. 6.11: Deviation in frequencies of both areas for TT-TH system for simulated FLC and CHIL FLC in Control Desk

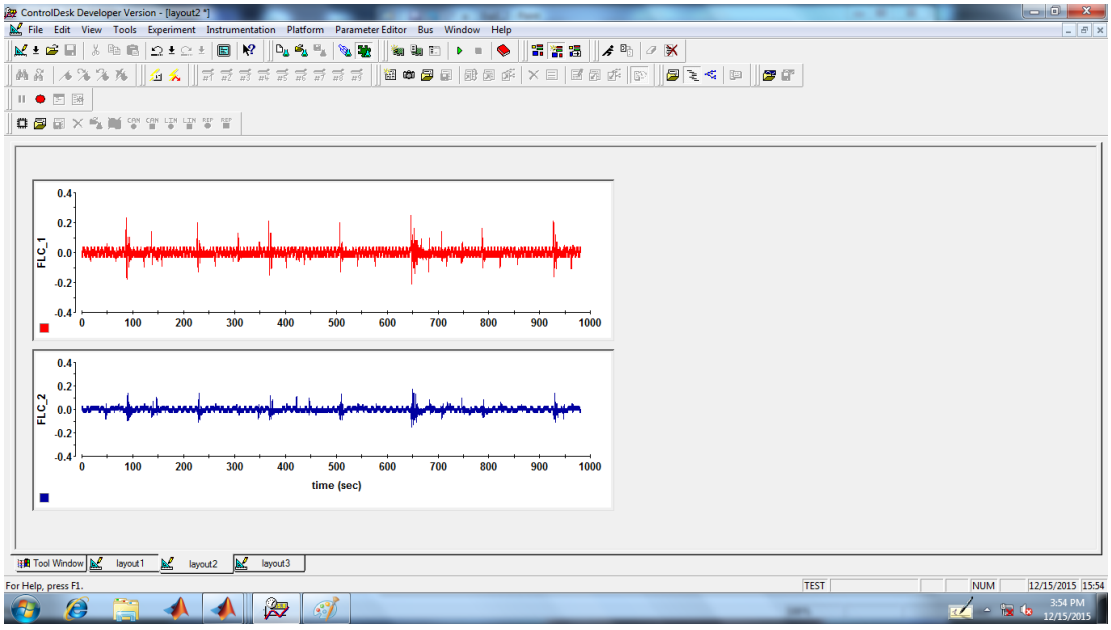

Fig. 6.12: FLCs output for both controller for TT-TH system for simulated FLC and CHIL FLC in Control Desk

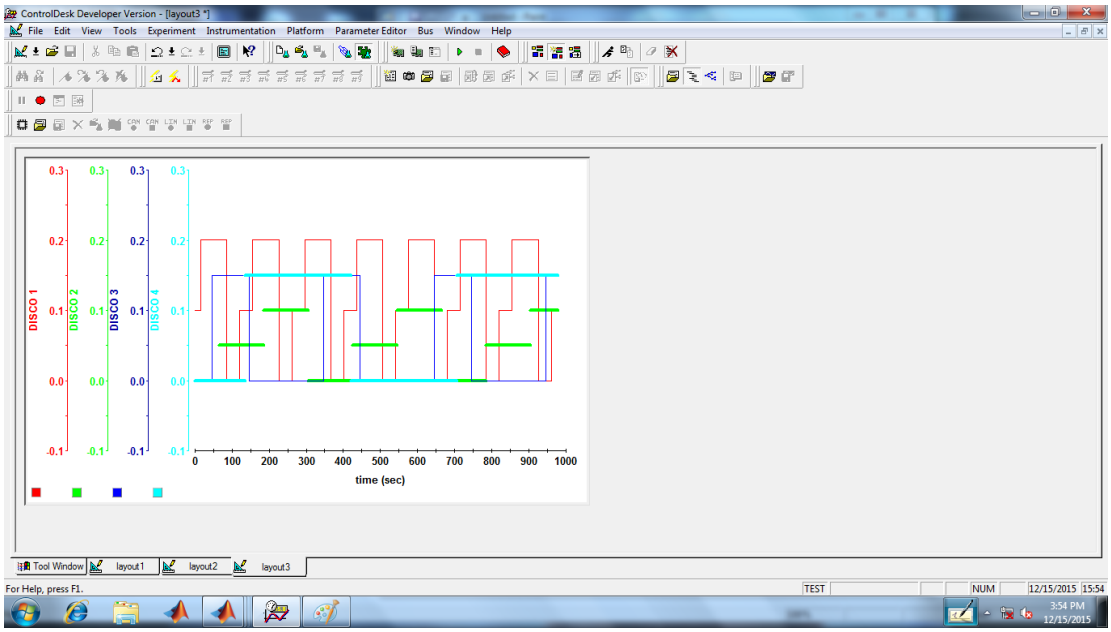

Fig. 6.13: Variable step load by different DISCOs for TT-TH system in Control Desk

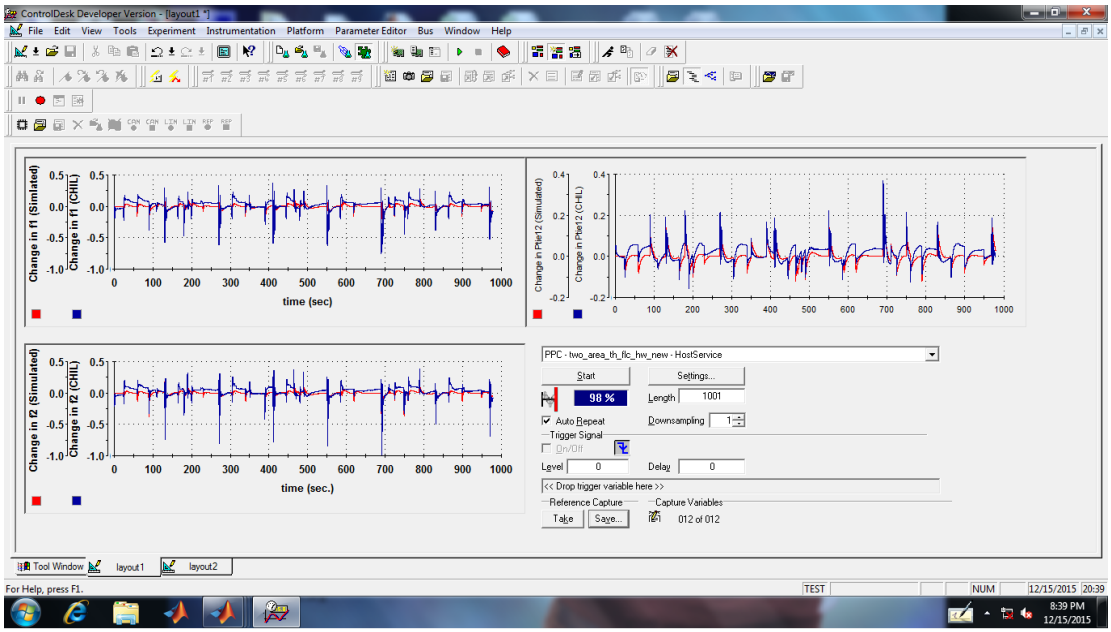

Fig. 6.14: Deviation in frequencies of both areas and deviation in tie-line power for TT-TH system for simulated FLC and CHIL FLC in Control Desk

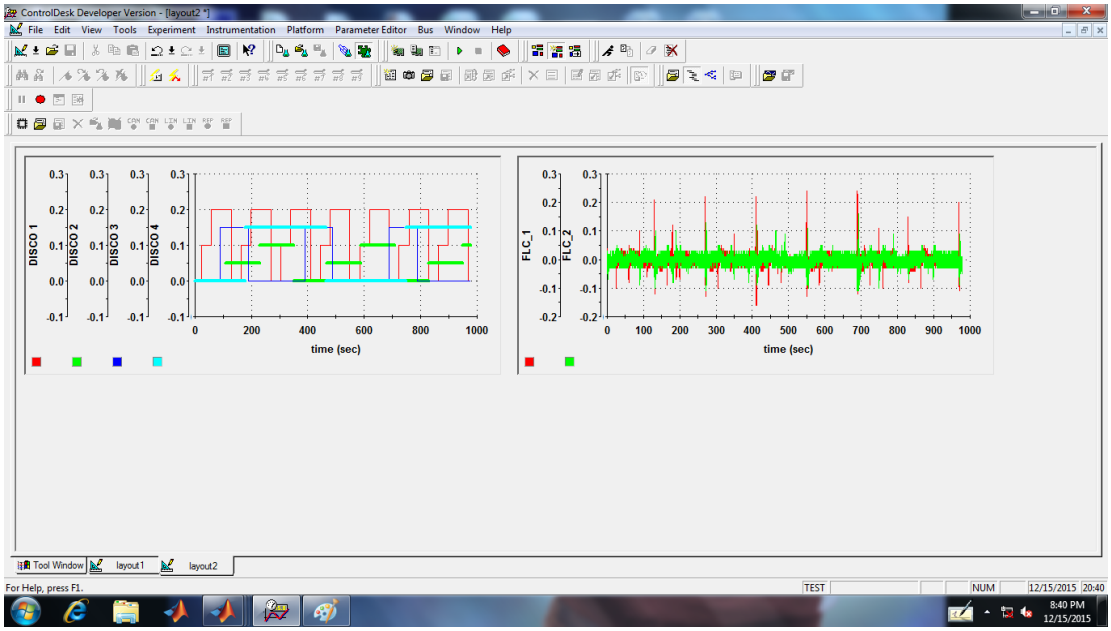

Fig. 6.15: Variable step load by different DISCOs and FLCs output for both controller for TT-TH system for simulated FLC and CHIL FLC in Control Desk

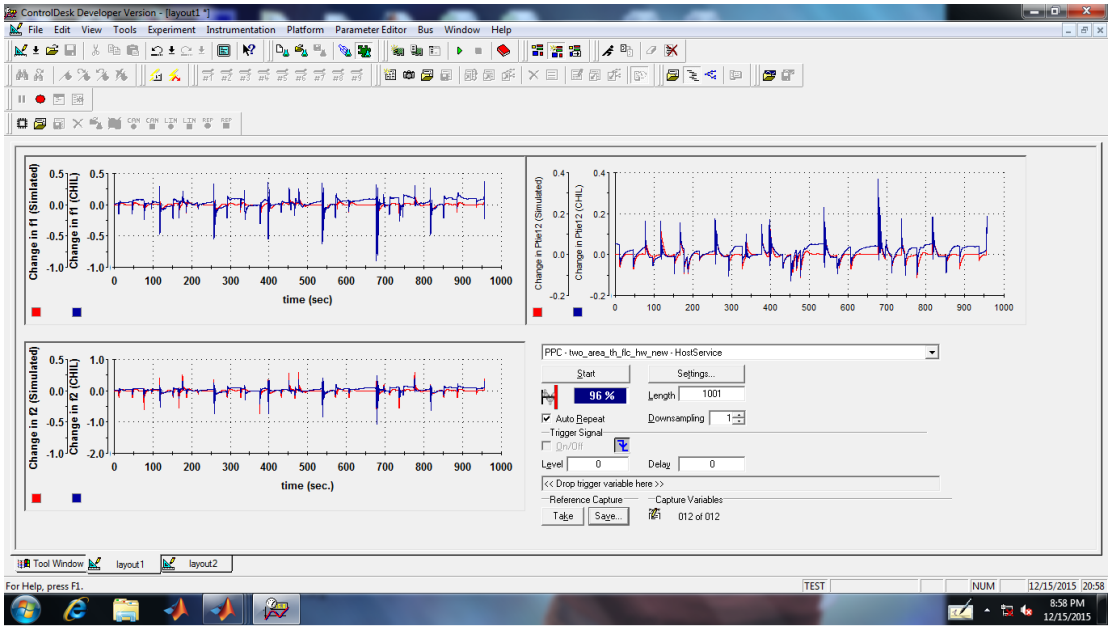

Fig. 6.16: Deviation in frequencies of both areas and deviation in tie-line power for TTWS-THWS system for simulated FLC and CHIL FLC in Control Desk

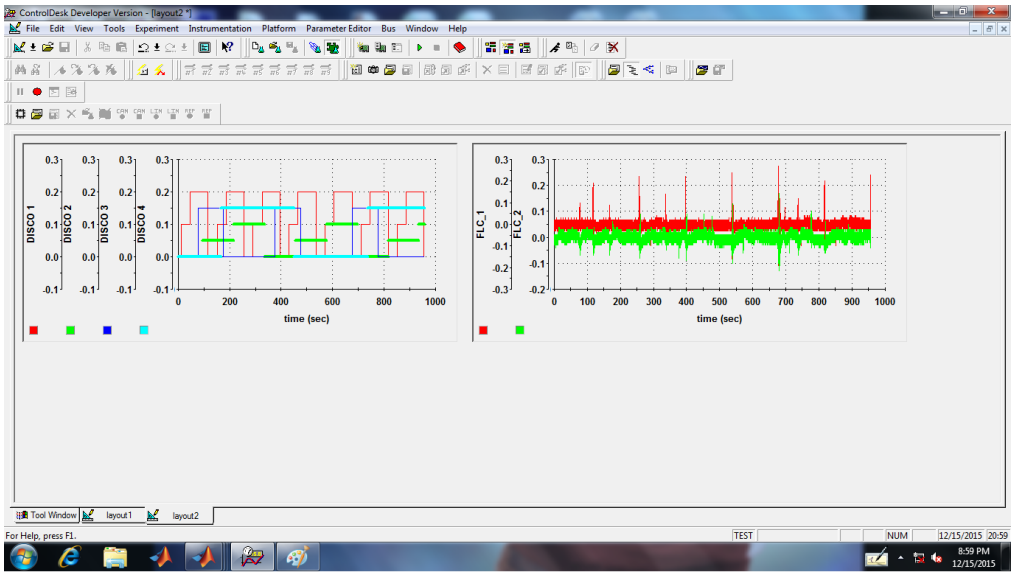

Fig. 6.17: Variable step load by different DISCOs and FLC output for TTWS-THWS system

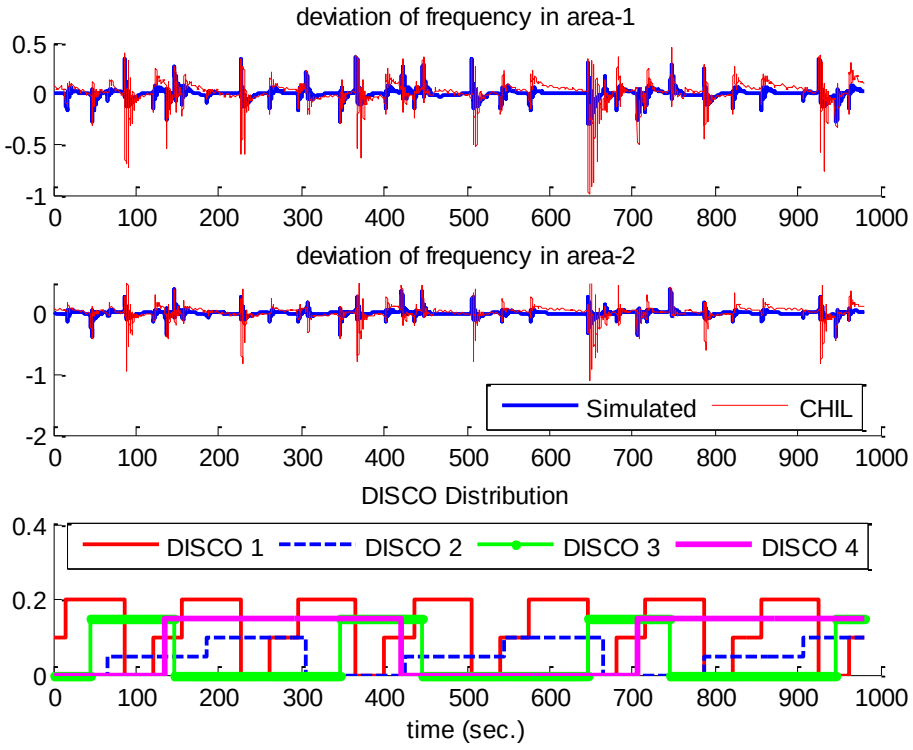

Fig. 6.18: Deviation in frequencies for TT-TH system

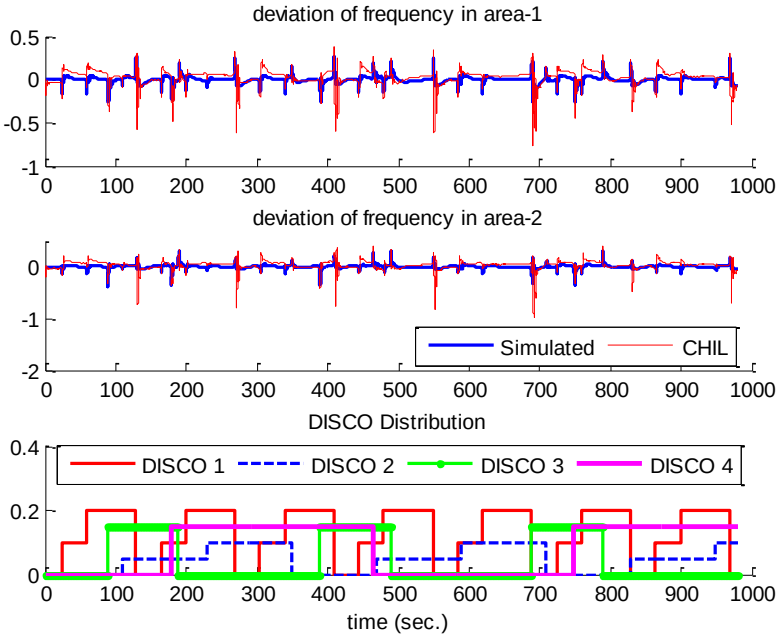

Fig. 6.19: Deviation in frequencies for TTW-THW system

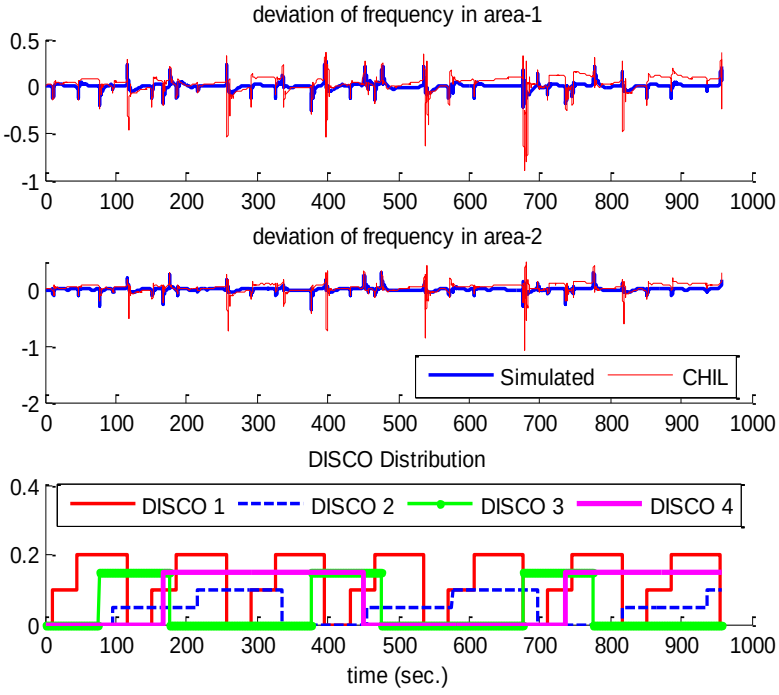

Fig. 6.20: Deviation in frequencies for TTWS-THWS system

Fig. 6.18, 6.19 and 6.20 show frequency deviation in area-1 and show frequency deviations in area-2 with respect to DISCO distribution for TT-TH system, TTW-THW system, and TTWS-THWS system respectively. It is observed from these figures that FLC based on CHIL concept following response as simulated FLC one. Simulated and experimental results have confirmed the effectiveness of the proposed FLC in the different system (TT-TH, TTW-THW and TTWS-THWS) during variable load profile.

6.4 Summary

In previous chapter it has been observed that FLC is better choice over other conventional controllers for AGC. FLC testing in hardware environment using CHIL is performed in this chapter. This FLC controller is tested for two area interconnected power system with the help of dSPACE 1104. Firstly FLC code have been developed in C language using linked list data structure then this code is dumped into Arduino Mega 2560 microcontroller. It is found that CHIL based FLC controller shows same kind of response as simulation environment in variable load profile scenario. This attempt is noticeable since it is observed that CHIL output are following simulation output but has limitation of not quantify in terms of performance parameters. This controller is also examined for two other different test models where firstly WPGS and secondly WPGS & SMES together are integrated in two area interconnected power system.

References

[1] X. Wu, H. Figueroa, and A. Monti, “Testing of Digital Controllers Using Real-Time Hardware in the Loop Simulation,” in *IEEE 35th Annual Power Electronics Specialists Conference PESC 04*, 2004, pp. 3622–3627.

[2] Y. Deng, H. Li, and S. Foo, “Controller Hardware-In-the-Loop Simulation for Design of Power Management Strategies for Fuel Cell Vehicle with Energy Storage,” *Veh. Power Propuls. Conf. VPPC’09. IEEE*, pp. 866–870, 2009.

[3] S. F. Barrett, *Arduino Microcontroller: Processing for Everyone! Part II*, vol. 5, no. 1. 2010.

[4] Y. A. Badamasi, "The working principle of an Arduino," in *Proceedings of the 11th International Conference on Electronics, Computer and Computation, ICECCO 2014*, 2014, pp. 1–4.

[5] A. Ghaffari, "dSPACE and Real-Time Interface in Simulink," 2012.

[6] M. Jemli, H. Ben Azza, and M. Gossa, "Real-time implementation of IRFOC for Single-Phase Induction Motor drive using dSpace DS 1104 control board," *Simul. Model. Pract. Theory*, vol. 17, no. 6, pp. 1071–1080, 2009.

[7] Z. A. Ghani, M. A. Hannan, and A. Mohamed, "Renewable Energy Inverter Development using dSPACE DS1104 Controller Board," in *International Conference on Power and Energy (PECon)*, 2010, pp. 69–73.

Chapter 7

Conclusions and Future Scope

7.1 Conclusions

In modern electric- power grid, to maintain grid discipline, frequency is a critical parameter to be kept within specified limits. Load perturbations in power system are inevitable and they cause frequency variation and tie-line loadings. Automatic generation control is thus important in power system operation for supplying sufficient and reliable electrical power of good quality. There are essentially two objectives of AGC. Firstly, the system frequency is to be maintained at or, very close to specified nominal value. Secondly, tie-line deviations must also be made zero as fast as possible. Complexity of present day power system pose new challenges to power engineers, where interconnections as well as integration of renewable sources of energy are on the rise. It is not an easy task to control such complex power system with simple conventional control strategy effectively and efficiently.

The research reported in thesis is an attempt to contribute towards building intelligent and optimized control schemes for automatic generation control of deregulated modern interconnected multi generation power systems. The intelligent control schemes consist of fuzzy logic approach for controller design and different optimization techniques i.e. genetic algorithm, ant colony optimization and different variants of particle swarm optimization are used to optimize controller parameters.

A number of control schemes have been developed in this thesis to control the power system of this complex nature. The complexity is further increased in this work by adding non-conventional sources of energy in two-area interconnected network. Two sources of energy considered are wind energy generating system and superconducting magnetic energy storage where both of them are used to contribute short term active power support in case of sudden load change. Conventional sources are thermal and hydro generating units with two possible combinations in area 1 and area 2. Emphasis of the work is on developing an optimized fuzzy logic controller with optimizing parameters of fuzzy controller mainly rule base, membership function parameters, scaling factors and rule's weight.

The performances of these controllers have been compared for different load disturbance in different areas as decided by contracted demand of power. A comprehensive analysis is also carried out to show impact on power frequency balance with varying wind power penetration and fixed SMES power. Optimized fuzzy controller is also compared with conventional integral, PI and PID controller and these conventional controllers are also optimized by Ziegler-Nichols and adaptive PSO.

The simulation work is validated by developing a hardware controller using Arduino Mega 2560 microcontroller. The developed optimized fuzzy controller is embedded in this microcontroller and this is integrated with PC using dSPACE 1104 controller board. dSPACE 1104 works as a link between Simulink model and hardware in external environment. Results obtained are matching with simulated cases under varying load profile from different DISCOs.

Following inferences are drawn from the results obtained with different controllers under different operating conditions in this research work.

- **Mathematical model for interconnected power system:** In this report different mathematical model for interconnected power system have been developed, deregulation in power system also been addressed in mathematical modeling. Apart from this mathematical modeling of wind power generating system (WPGS) and superconducting magnetic energy storage (SMES) also have been developed. The design and development of this mathematical model has taken into consideration of governor dead band (GDB) as nonlinearity.
- **Selection of objective function and optimization techniques for AGC:** In this thesis, nine objective functions have been examined for optimization of controllers for AGC, in which four are error based and five are performance based objective functions. In this three performance indices (peak undershoot, peak overshoot and settling time) based weighted objective function (OBJ5) was found suitable for optimization of controller as value of fitness function for it is minimum of all others. Then different stochastic optimization techniques i.e. genetic algorithm, ant colony optimization, particle swarm optimization and different variants of particle swarm optimization have been examined with selected objective function i.e. OBJ5. Successive rate based variant of PSO is adjudged best on the basis of fast convergence rate and minimum fitness value.
- **Comprehensive analysis for impact of WPGS and SMES integration to AGC:** Two non-conventional energy resources have been considered for integration with AGC, where WPGS contribute short term active power support in case of sudden load

change and SMES is used for mitigating deviations caused by sudden load change. In this thesis a comprehensive analysis for integration of WPGS and SMES has been done, where different combinations of WPGS and SMES have been considered. Apart from this impact of WPGS integration with and without frequency support on AGC performance has been analyzed for different level of penetration. Significant improvement is observed when both WPGS and SMES are connected in the system.

- **Optimization of fuzzy logic controller:** Four step optimization of fuzzy logic controller is found appropriate for interconnected power system, where rule base, membership function parameters, scaling factors and rule's weight parameters being optimized. Further this proposed optimized fuzzy controller is also compared with different types of conventional controllers and found better in performance based on performance indices.
- **Fuzzy logic controller implementation in microcontroller for AGC:** Fuzzy logic controller is implemented in microcontroller. The simulation work is validated by developing a hardware controller using Arduino Mega 2560 microcontroller. Firstly fuzzy logic controller code is developed in C language using linked list data structure then this code is dumped into Arduino Mega 2560 microcontroller.
- **Validation of embedded fuzzy logic controller using dSPACE 1104:** The embedded fuzzy logic controller in microcontroller is integrated with PC using dSPACE 1104 controller board. dSPACE 1104 works as a link between simulink model and hardware in external environment. It is found that controller as hardware-in-loop (CHIL) based fuzzy logic controller following simulated results under varying load profile for two area interconnected power system model. This controller is also

examined in two other different test models where WPGS and WPGS & SMES are integrated in two area interconnected power system respectively.

7.2 Future scopes

The work done in the thesis may be extended in the following directions:

1. The developed control strategies can also be made adaptive using ANN or other approaches.
2. The complexity of power system can further be increased by adding more sources of non-conventional energy and then power frequency balance may be studied.
3. Robust control techniques may also be integrated with developed control schemes to strengthen it further in terms of having better power system stability.
4. Real time control may also be implemented with advanced software/hardware modules.

Appendix

Mathematical Modeling of LFC:

Hydro Turbine : $\frac{(1-sT_w)}{(1+0.5sT_w)}$

Hydro Droop Compensation : $\frac{(1+sT_r)}{1+s(R_t/R_p)T_r)}$

Speed Governor : $\frac{1}{(1+sT_g)}$

Thermal Reheater : $\frac{(1+K_r sT_r)}{(1+sT_r)}$

Thermal Turbine : $\frac{1}{(1+sT_t)}$

Power System : $\frac{K_p}{(1+sT_p)}$

Table 21 Parameters of genetic algorithm

GA Parameter	Value/Type
Total number of Generation	100
Population Size	No. of Variables *5
Selection	Stochastic Uniform
Crossover Probability	0.9
Mutation Probability	0.1
Elite Count	5

Table 22 Parameters of ant colony optimization

ACO Parameter	Value/Type
No. of Ants	No. of Variables *5
Pheromone	0.05
Evaporation Parameter	0.95
Positive Pheromone	0.15
Negative Pheromone	0.30
Max Tour	100
No. of Nodes between Max and Min values	1000

Table 23 Parameters of particle swarm optimization

ACO Parameter	Value/Type
Size of Swarm	No. of Variables *5
Particle Steps	100
Cognitive Acceleration factor: C_1	1.2
Social Acceleration factor: C_2	0.2
Minimum Inertia Weight: w_{min}	0.4
Maximum Inertia Weight: w_{max}	0.9

Table 24 Parameters of SMES unit

Energy	30MJ
Nominal DC current: I_{d0}	4.5kA
Minimum DC current: I_{dmin}	4.0kA
Maximum DC current: I_{dmax}	4.9kA
Convertor Time Constant: T_{dc}	0.03sec
Superconducting Coil Inductance: L	2.5 H

Table 25 Parameters of thermal-hydro system investigated

Rated Power *(area-1 & area-2)*	P_{r1} & P_{r2}	2000MW
Transfer function gain of generator *(area-1 & area-2)*	K_{p1} & K_{p2}	120
Generator's time constant *(area-1 & area-2)*	T_{p1} & T_{p2}	20
Governor's time constant	T_{g1}	0.08
Governor's time constant	T_{g2}	0.02
Hydro droop compensation, Reset time	T_r	5
Hydro droop compensation, temporary droop	R_t	0.38
Hydro droop compensation, permanent droop	R_p	0.05
Hydro turbine's time constant	T_w	1
Steam turbine's time constant	T_t	0.3
Regulation of the governor *(area-1 & area-2)*	R_1 & R_2	2.4
Frequency bias constant	β	0.425
Synchronizing power coefficient	a_{12}	1
Synchronization coefficient	T_{12}	0.545

Data for WPGS:

WT physical parameters: H=4.64;

pAr=2*0.00159;

Kb=56.6;

Tr=0.1; Ta=0.2; Tc=0.2;

Pitch controller gains: Kp=1.5; Ki=0.15;

Droop and inertia Controller gains: Kpf=0.20/4.5; Kdf=0.15/4.5;

List of Publications

Journal Publications

[1] **Yogesh Krishan Bhateshvar**, Hitesh Datt Mathur, Houria Siguerdidjane & Surekha Bhanot, "Frequency Stabilization for Multi-area Thermal–Hydro Power System Using Genetic Algorithm-optimized Fuzzy Logic Controller in Deregulated Environment", Electric Power Components and Systems", 43:2, pp. 146-156, 2015. **(SCI Indexed)**

[2] **Y.K. Bhateshvar**, H.D. Mathur and Houria Siguerdidjane, "Study of Impact of Wind Power Generating System Integration on Frequency Stabilization in Multi-area Power System with Fuzzy Logic Controller in Deregulated Environment" Vol. 9, Issue 1, Frontiers in Energy (Springer), pp. 7-21, 2015. **(Scopus Indexed)**

[3] **Y.K. Bhateshvar** & H.D. Mathur, "Power–frequency balance with superconducting magnetic energy storage using optimized intelligent controller", Energetika, Vol. 60, No. 3, pp. 149-161, 2014. **(Scopus Indexed)**

[4] **Y.K. Bhateshvar** & H.D. Mathur, "Two Stage Optimized Fuzzy Controlled Multi-Area System for AGC in Smart Grid Age", Procedia Technology, Vol. 21, pp. 381–385,2015. **(Scopus Indexed)**

[5] **Y.K. Bhateshvar** & H.D. Mathur, "Power Frequency Oscillation Suppression using Two-Stage Optimized Fuzzy logic Controller for Multi-Generation System", *Advances in Fuzzy System*, pp. 1-13, vol. 2016, 2016. **(Scopus Indexed)**

Conference Publications

[1] **Y.K.Bhateshvar,** H.D.Mathur**,** "Four Step based ACO Optimized Fuzzy Logic Controller for Inter-area Oscillation Control in a Interconnected Power System ", National Conference on Advances in Microelectronics, Instrumentation and Communication (MICOM) , November 20-22, 2015, BITS Pilani, Pilani Campus, Pilani, India.

[2] **Yogesh Krishan Bhateshvar**, Hitesh Datt Mathur, Houria Siguerdidjane, "Power Frequency Balance in Multi-Generation Smart Grid System with V2G option" 12th IEEE India International conference Indicon-2015, 17-20 December, Jamia Millia Islamia, New Delhi.

[3] **Y.K.Bhateshvar** and H.D.Mathur, "Two Stage Optimized Fuzzy Controlled Multi-Area System for AGC in Smart Grid Age",In the proceedings of International Conference on Smart Grid Technologies, 7-8 August, 2015, Coimbatore, India.

[4] **Y.K. Bhateshvar** and H.D. Mathur, "Inter-area oscillation control with super conducting magnetic energy storage in multi-area power system using optimized intelligent controller", In the proceedings of 11th Conference of Young Scientists on Energy Issues, 29-30th May 2014, Kaunas, Lithuania.

[5] **Y.K. Bhateshvar** and H.D. Mathur, "Frequency Stabilization for Thermal-Hydro Power System with Fuzzy Logic Controlled SMES unit in Deregulated Environment", International Conference on Advanced Computing & Communication Technologies, Feb-2014, Rohtak, India

[6] L.B.F. Leite, H. Siguerdidjane, H.D. Mathur and **Y.K. Bhateshvar**, "Wind Power Inertial Support for Inter-area Oscillations Suppression with Fuzzy Controller in Varying Load Conditions" In the proceedings of IEEE International Conference on Clean Electrical Power, Alghero, Italy, June 11-13, 2013

[7] H.D. Mathur, L.B.F. Leite, H. Siguerdidjane and **Y.K.Bhateshvar**, "Study of Impact of Wind Power Penetration on Frequency Stabilizaition in Multi-area Power System" In the Proceedings of IEEE International Symposium on Advanced Topics in Electrical Engineering, Bucharest, Romania, May 23-25, 2013.

[8] **Y.K. Bhateshvar** and H.D. Mathur, "Comparative Dynamic Analysis on Frequency Stabilization for Multi-Area Power System in Deregulated Environment" In the proceedings of IEEE International Conference on. Signal Processing, Computing and Control (2012 IEEE ISPCC), March 15-17, 2012, Solan, H.P., India.

[9] **Y.K. Bhateshvar** and H.D. Mathur, "Frequency Stabilization using Fuzzy Logic based Controller for Multi-Area Power System in Deregulated Environment" In the proceedings of 2nd International Conference on Advances in Control and Optimization of Dynamical Systems (ACODS), IISc, Bangalore, India, 16-18 February' 2012.

[10] H.D. Mathur and **Y.K. Bhateshvar**,"Frequency regulation with Vehicle to grid (V2g) option in multi generation power network", accepted for Conference of Young Scientists on Energy Issues, 26-27th May 2016, Kaunas, Lithuania.

Brief Biography of the Candidate

YOGESH KRISHAN BHATESHVAR received the Bachelor of Engineering degree in electronics and communication engineering from Rajasthan University, Jaipur, India and M.Tech in automotive electronics from VIT University, Vellore, India in 2005 and 2008 respectively. He has 4 years of teaching and industrial experience. Since 2011, he is research scholar at BITS-Pilani in Department of Electrical and Electronics engineering. His research interests include intelligent control systems and their applications to automotive engineering and smart grid technologies in power systems.

Brief Biography of the Supervisor

HITESH DATT MATHUR received his B.E. in electrical engineering and his M.E. in electrical power systems from Nagpur University and Rajasthan University, India, in 1998 and 2000, respectively; he completed his Ph.D. in electrical power systems from Birla Institute of Technology and Science, Pilani, in 2007. He was post-doctoral fellow in Supelec, Gif-sur-Yvette, France, for seven months in 2013. Currently, he is an Associate Professor at Birla Institute of Technology and Science, Pilani. He is a member of IEEE, member of Institution of Engineers (India) and Life member of Indian Society of Technical Education. His research interests include automatic generation control of electrical power system, distributed generation, intelligent control applications to power systems and smart grid technologies.